MECHANICAL ENGINEERING AND SOLID MECHANICS SERIES

Materials and Structures under Shock and Impact

Patrice Bailly

ISTE WILEY

Materials and Structures under Shock and Impact

Materials and Structures under Shock and Impact

Patrice Bailly

ISTE WILEY

First published 2014 in Great Britain and the United States by ISTE Ltd and John Wiley & Sons, Inc.

ISTE Ltd
27-37 St George's Road
London SW19 4EU
UK

www.iste.co.uk

John Wiley & Sons, Inc.
111 River Street
Hoboken, NJ 07030
USA

www.wiley.com

Library of Congress Control Number: 2013951423

British Library Cataloguing-in-Publication Data
A CIP record for this book is available from the British Library
ISBN: 978-1-84821-651-8

Printed and bound in Great Britain by CPI Group (UK) Ltd., Croydon, Surrey CR0 4YY

Table of Contents

Introduction

In risk studies, engineers may be required to consider the consequences of an accident resulting in a shock on a building. This may be, for example, the impact of a vehicle or aircraft, or the effects of an explosion on an industrial site.

This book combines elements of applied mechanics from which practical and sometimes simplified methods used in such studies arise. It is aimed at Master's students or students of engineering schools with a fairly general mechanical training. It can also be used by practicing engineers who wish to enter the field of structural resistance to accidental mechanical actions. This book is an intermediary between two types of scientific literature: on the one hand, bibliographic resources on the areas of mechanics involved in studies of shocks on structures, i.e. the waves in continuous systems, behavior of materials, resistance calculations of structures, vibrations, structural dynamics, etc., and on the other hand, technical manuals devoted to practical calculation methods and design of structures to withstand shocks or explosions. These manuals may be technically very accurate, especially regarding the constructive arrangements. Just like regulations related to the calculation of reinforced concrete or metal structures, their effective use requires knowledge of the theoretical mechanical elements that led to the methods they advocate. It is also important to have a basic understanding of the physical

phenomena involved in the predicted accidental events. For example, concerning the effects of explosions on a building, the engineer responsible for the structural design must understand the physical parameters involved in the explosion process, their relationship with the extreme effect of the explosion, that is the blast wave, and the manner in which the interaction with a building leads to a dynamic load on the latter. In this book, the proposed approach is to provide the elements of fairly general and theoretical mechanics in order to develop their applications to cases of shocks and impacts. Throughout the developments, hypotheses and limitations of the models used will appear. The engineering methods discussed in this book are not based on the use of important digital codes for structure calculations.

Impact on a building is primarily a local phenomenon that causes stress and strain in the form of propagating waves in the material. The movement then extends to the entire structure. Both local and global phases of the mechanical response have different time characteristics. This book follows this chronology: Part 1 is devoted to the study of the dynamics of solids that come into play during the local phenomena. Part 2 deals with the dynamics of structures in response to a global impact on a building.

In Part 1, the propagation of movements in a continuous system is first presented in the context of linear behavior such as elasticity and viscoelasticity. Shocks on solids induce stress waves, the amplitude of which is related to impact velocity. These waves propagate and diffract and are reflected within the solids. The impact velocities during accidental events are sufficient for the level of stress to exceed the yield strength of the construction materials. It is then necessary to understand how the nonlinear aspects of behavior influence the propagation of stress and strain. A feature of shocks is to provoke pressure levels much higher than those commonly found in materials under static loads. The study of behavior, in this case, is quite specific to the field of shock.

In Part 2, the case of a simple structure (modeled by a mechanical system with one degree of freedom) is used to introduce the engineering tools of the shock response spectrum and iso-damage curves. Two types of short-term dynamic loading are then introduced:

collisions and explosions. Collisions of structures, or crashes, are discussed with the aim of clarifying the load imposed on the structure that is affected. The case of explosions is approached by defining some basic knowledge of dynamics, which is necessary to understand the phenomenon. The goal is to achieve the characteristic elements of dynamic loading that can be imposed on a structure. The basic construction element is usually a beam. A study on the evolution of stress and movements in beams during impacts is considered in order to identify the various possible levels of modeling and their areas of relevance. To study the overall response, structures of buildings or industrial buildings can be modeled by mechanical systems with several degrees of freedom, as it is customary to do in earthquake studies. The nonlinear behavior phase of structures can be achieved. In metal or reinforced concrete structures, it is most often through the formation of plastic hinges that these nonlinearities occur. The response to the shock of a structure with plastic hinges is considered.

Despite its compact size, this book covers various significant and representative aspects of problems related to studies on shocks on buildings. Not all types of materials and structures are covered in this book, for example composite materials, plates and shells are not included. Finally, it should be noted that an educational approach guided the organization of this book.

PART 1

Dynamics of Solids

Chapter 1

Motion within Solids

The concept of stress and strain waves emerges from the equations of motion in elastic continuum. Uniaxial propagation is particularly well-studied because of its practical importance. The waves can be altered within their propagation by dispersion and dissipation. For viscoelastic solids, we can address the effects of behavior sensitive to strain in a linear framework.

1.1. Representation of the medium

1.1.1. *Framework of continuum mechanics*

The problem for the engineer is to describe the position (or displacement) of solids and fluids. This mechanism is of a macroscopic scale. On this macroscopic scale, solid or fluid matter can be seen as continuous, which is not the case at the microscopic level of particles, molecules and atoms. The macroscopic scale is not the same for all materials: a fraction of a millimeter for a metal, a few inches for geomaterials such as rock or concrete.

In this book, we only refer to classical mechanical engineering knowledge of continuum mechanics and structural strength. This chapter intends to recall the basics of continuum motion when these

can be described by linear equations, such as in the context of small strains and elastic or viscoelastic material behavior.

1.1.2. *Representation of motion*

The motions in matter are identified in an affine Euclidean space. A point in matter which occupies position M_0 at time 0, defined by the vector $\underline{X}$, is in position M_t at time t, defined by the vector $\underline{x}$. A certain amount of matter that occupies the simply connected domain Ω_0 at time 0, also occupies the simply connected domain Ω_t at time t (Figure 1.1).

$$\underline{OM}^0 = \underline{X}(X_1, X_2, X_3) \qquad \underline{OM}^t = \underline{x}(x_1, x_2, x_3) \qquad \underline{U} = \underline{x} - \underline{X} \qquad [1.1]$$

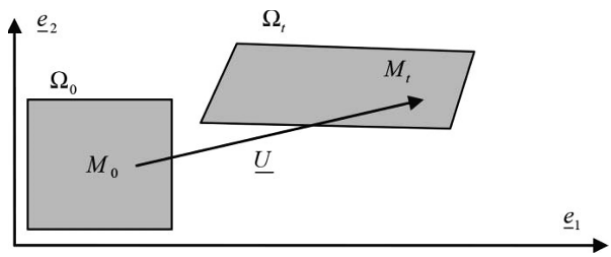

Figure 1.1. *Material field in its initial position and after transformation*

The description of these movements can be given from two points of view: one is called "Lagrangian" and the other is called "Eulerian". The Lagrangian description involves following the matter points in their motion. The current position, or displacement, is expressed depending on the initial position and t, using a continuous vector function [1.2] that defines the trajectories (this is a bijection of Ω_0 to Ω_t, due to the continuity of displacement of the system):

$$\underline{x} = \underline{\varphi}(\underline{X}, t) \qquad [1.2]$$

The Eulerian description involves the knowledge of the velocity field at each moment relative to the current position. The Eulerian

description of the velocity field involves specifying the velocity of the particle passing position $\underline{x}$ at time t [1.3]:

$$\underline{V}(\underline{x},t) \qquad [1.3]$$

If the Eulerian velocity field does not depend on time, the motion is stationary. Eulerian representation is mainly used for fluids and materials undergoing very large strains. In the remaining chapter, we use the Lagrangian point of view. The strain is characterized by the Green–Lagrange strain tensor [1.4]:

$$\begin{aligned} &\underline{\underline{E}} = \tfrac{1}{2}\left({}^{t}\underline{\underline{\nabla\varphi}}\,\underline{\underline{\nabla\varphi}} - \underline{\underline{1}} \right) \quad \underline{\underline{E}} = \tfrac{1}{2}\left(\underline{\underline{\nabla U}} + {}^{t}\underline{\underline{\nabla U}} + {}^{t}\underline{\underline{\nabla U}}\,\underline{\underline{\nabla U}} \right) \\ &E_{ij} = \tfrac{1}{2}\left(U_{i,j} + U_{j,i} + U_{k,i}U_{k,j} \right) \end{aligned} \qquad [1.4]$$

In many cases for solids, displacements and strains are very small (0.001% elongation, for example). A linearization is then performed by retaining only the first-order infinitesimal. This is called the linearized strain tensor [1.5]:

$$\underline{\underline{\varepsilon}} = \frac{1}{2}\left(\underline{\underline{\nabla U}} + {}^{t}\underline{\underline{\nabla U}} \right) \qquad \varepsilon_{ij} = \frac{1}{2}\left(U_{i,j} + U_{j,i} \right) \qquad [1.5]$$

It is this tensor that will be most widely used. Each component has a simple physical significance: ε_{ii} represents the relative elongation in direction i. ε_{ij} ($i \neq j$) represents the angular distortion relative to the two directions i and j. The tensor trace, equal to the divergence of the displacement vector, represents the relative change in volume. The partition of the strain tensor in its spherical part, which is related to the change in volume, and its deviatoric part, which is related to the change of form [1.6], is used:

$$\begin{aligned} &\theta = trace\,\underline{\underline{\varepsilon}} = div\underline{U} \qquad \underline{\underline{e}} = \underline{\underline{\varepsilon}} - \frac{\theta}{3}\underline{\underline{\mathfrak{I}}} \\ &\underline{\underline{\varepsilon}} = \frac{\theta}{3}\underline{\underline{\mathfrak{I}}} + \underline{\underline{e}} \qquad \varepsilon_{ij} = \frac{\theta}{3}\delta_{ij} + e_{ij} \end{aligned} \qquad [1.6]$$

1.1.3. *Representation of internal forces*

In a continuum, internal forces can be represented either by a scalar field, pressure ($p(\underline{x},t)$), or by a tensorial field, the Cauchy stress tensor. In an orthonormal frame, this tensor is represented by a symmetric matrix [1.7]. Figure 1.2 shows a representation of the components of the stress tensor of a material whose faces are normal to the reference axes wherein the said tensor is expressed:

$$\underline{\underline{\sigma}}(\underline{x},t) = \begin{pmatrix} \sigma_{11} & \sigma_{12} & \sigma_{13} \\ \sigma_{12} & \sigma_{22} & \sigma_{23} \\ \sigma_{13} & \sigma_{23} & \sigma_{33} \end{pmatrix} \qquad [1.7]$$

For solids, it is customary to partition the stress tensor into a so-called "spherical" or isotropic part, characterized by pressure p, and a so-called "deviatoric" part [1.8]:

$$\begin{aligned} p &= -\frac{1}{3} trace\, \underline{\underline{\sigma}} \qquad \underline{\underline{S}} = \underline{\underline{\sigma}} + p\,\underline{\underline{\Im}} \\ \underline{\underline{\sigma}} &= -p\,\underline{\underline{\Im}} + \underline{\underline{S}} \qquad \sigma_{ij} = -p\,\delta_{ij} + S_{ij} \end{aligned} \qquad [1.8]$$

The representation of internal forces by pressure concerns, *a priori*, non-viscous fluids. However, when shocks occur in solids, the pressure can become very large and the terms of the deviatoric part (shear stress) may be negligible compared to the pressure. In these cases, it is possible to retain only pressure to represent internal forces. This is a hydrodynamic model of a material.

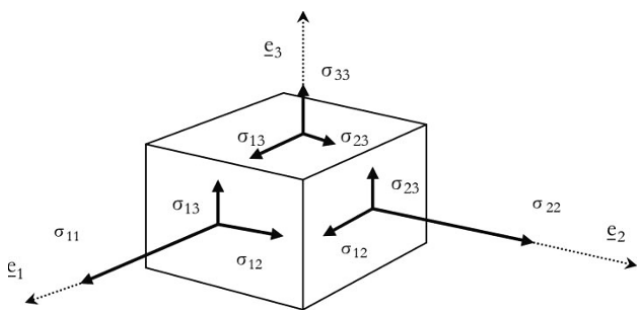

Figure 1.2. *Representation of the components of the Cauchy stress tensor on a piece of material*

Writing the behavior or resistance of a material logically involves stress tensor invariants. Besides the main constraints (σ_I, σ_{II}, σ_{III}) that are the eigenvalues of the matrix representing the stress tensor, various invariants of this tensor are used:

– The first invariant of the stress tensor, which defines the pressure [1.9]:

$$I_1 = trace\,\underline{\underline{\sigma}} = \sigma_{kk} = -3p \qquad [1.9]$$

– The second invariant of the deviator tensor, which defines the von Mises equivalent stress [1.10]:

$$J_2 = \frac{1}{2}\,\underline{\underline{S}} : \underline{\underline{S}} = \frac{1}{2} S_{ij} S_{ij} \qquad \sigma_{eq} = \sqrt{3J_2} = \sqrt{\frac{3}{2}\,\underline{\underline{S}} : \underline{\underline{S}}} = \sqrt{\frac{3}{2} S_{ij} S_{ij}} \qquad [1.10]$$

– The third invariant, and the Lode angle χ [1.11]:

$$J_3 = \tfrac{1}{3}\left(\text{trace}\left(\underline{\underline{\sigma}}^3\right)\right)^{1/3} = \tfrac{1}{3}\left(\sigma_{ij}\,\sigma_{jk}\,\sigma_{ki}\right)^{1/3} \qquad \cos(3\chi) = \frac{3\sqrt{3}\,J_3}{2J_2^{3/2}} \qquad [1.11]$$

Use of the fundamental principle of mechanics and its application to the continuum leads to equilibrium equations. We consider a continuum in a field Ω with a density ρ. We denote volume forces by $\underline{f}$. Then, the equations are as follows:

– with a pressure field [1.12]:

$$-\underline{grad}\; p + \underline{f} = \rho\,\underline{\ddot{U}} \qquad p_{,i} + f_i = \rho U_{i,tt} \qquad [1.12]$$

– or with a stress field [1.13]:

$$\underline{div}\;\underline{\underline{\sigma}} + \underline{f} = \rho\,\underline{\ddot{U}} \qquad \sigma_{ij,j} + f_i = \rho U_{i,tt} \qquad [1.13]$$

In general, these equations are insufficient to predict motion across the field from external forces data. It is necessary to involve a relationship between the internal forces and the geometric transformation (strain). This relationship, which cannot be deduced from the fundamental principles of mechanics, is called behavior. In this chapter, we consider isotropic linear elasticity and linear

viscoelasticity. Nonlinear behaviors and their consequences on motion will be discussed in Chapter 3.

1.2. Elastodynamic equations

1.2.1. *Navier equations*

To obtain the equations governing motion in a continuum, we must associate the equilibrium equations and material behavior. Elastic behavior has been widely studied [ACH 93, GRA 75]. Isotropic linear elastic behavior is reflected in the equations linking stress to strain. The stress tensor can be expressed in terms of strain and the strain tensor can also be expressed in terms of stress [1.14]:

$$\begin{aligned} &\underline{\underline{\sigma}} = \lambda\ trace\left(\underline{\underline{\varepsilon}}\right)\ \underline{\underline{\mathfrak{I}}} + 2\mu\ \underline{\underline{\varepsilon}} \qquad \sigma_{ij} = \lambda\ \varepsilon_{kk}\delta_{ij} + 2\mu\,\varepsilon_{ij} \\ &p = -K\,\theta \qquad \underline{\underline{S}} = 2G\ \underline{\underline{e}} \qquad S_{ij} = 2G\,e_{ij} \\ &\underline{\underline{\varepsilon}} = \frac{1+\nu}{E}\,\underline{\underline{\sigma}} - \frac{\nu}{E}\,trace\left(\underline{\underline{\sigma}}\right)\ \underline{\underline{\mathfrak{I}}} \qquad \varepsilon_{ij} = \frac{1+\nu}{E}\sigma_{ij} - \frac{\nu}{E}\,\sigma_{kk}\delta_{ij} \end{aligned} \qquad [1.14]$$

λ and μ are Lamé coefficients, E is the Young modulus and ν is the Poisson coefficient. K is the bulk modulus and G is the shear modulus. The relationship between these different coefficients is given in [1.15]:

$$\begin{aligned} &E = \frac{\mu(3\lambda+2\mu)}{\lambda+\mu}, \qquad \nu = \frac{\lambda}{2(\lambda+\mu)}, \qquad K = \frac{E}{3(1-2\nu)} \\ &\lambda = \frac{\nu E}{(1-2\nu)(1+\nu)}, \qquad \mu = G = \frac{E}{2(1+\nu)} \end{aligned} \qquad [1.15]$$

An elasticity problem is formulated by combining the fundamental principle of the mechanics equation and the behavior relationship [1.16]:

$$\begin{aligned} &\underline{div}\,\underline{\underline{\sigma}} + \underline{f} = \rho\underline{\ddot{U}} \qquad \sigma_{ij,j} + f_i = U_{i,tt} \\ &\underline{\underline{\varepsilon}} = \tfrac{1}{2}\left(\underline{\underline{\nabla U}} + {}^{t}\underline{\underline{\nabla U}}\right) \qquad \varepsilon_{ij} = \tfrac{1}{2}\left(U_{i,j} + U_{j,i}\right) \\ &\underline{\underline{\sigma}} = \lambda\left(trace\ \underline{\underline{\varepsilon}}\right)\underline{\underline{\mathfrak{I}}} + 2\mu\,\underline{\underline{\varepsilon}} \qquad \sigma_{ij} = \lambda\,\varepsilon_{kk}\delta_{ij} + 2\mu\,\varepsilon_{ij} \end{aligned} \qquad [1.16]$$

The Navier equations are the displacement equations obtained by eliminating stress and strain. First, we can express stress as a function of displacement, and thus obtain its gradient [1.17]:

$$\begin{matrix} \underline{\underline{\sigma}} = \lambda\left(div\,\underline{U}\right)\underline{\underline{\Im}} + \mu\left(\underline{\nabla U} + {}^{t}\underline{\nabla U}\right)\underline{\underline{\varepsilon}} & \sigma_{ij} = \lambda\, U_{i,i}\delta_{ij} + \mu\left(U_{i,j} + U_{j,i}\right) \\ \underline{div}\,\underline{\underline{\sigma}} = \left(\lambda+\mu\right)\underline{\nabla}\left(div\,\underline{U}\right) + \mu\,\underline{\Delta U} & \sigma_{ij,j} = \lambda\, U_{i,ij} + \mu\left(U_{i,jj} + U_{j,ij}\right) \end{matrix} \quad [1.17]$$

Then, we can obtain the equations governing the motion of an elastic continuum, involving only the displacement field. Two vector equations are possible, using either the Laplacian or the curve of the displacement field [1.18]:

$$\begin{matrix} \mu\,\underline{\Delta U} + \left(\lambda+\mu\right)\underline{\nabla}\left(div\,\underline{U}\right) + \underline{f} = \rho\,\underline{\ddot{U}} & \left(\mu\, U_{i,jj} + \left(\lambda+\mu\right)U_{j,ji} + f_i = U_{i,tt}\right) \\ \left(\lambda+2\mu\right)\,\underline{\nabla}\left(div\,\underline{U}\right) - \mu\,\underline{rot}\left(\underline{rot}\,\underline{U}\right) + \underline{f} = \rho\,\underline{\ddot{U}} & \end{matrix} \quad [1.18]$$

By deriving and summing equations [1.18], a scalar equation governing volume variations is obtained. This is the expansion equation [1.19]:

$$\left(\lambda+2\mu\right)\,\Delta\left(div\,\underline{U}\right) + div\,\underline{f} = \rho\, div\,\underline{\ddot{U}} \quad \left(\lambda+2\mu\right)\,U_{i,jji} + f_{i,i} = \rho\,\ddot{U}_{i,i} \quad [1.19]$$

1.2.2. *Strain waves*

1.2.2.1. *Helmholtz decomposition*

The Helmholtz decomposition theorem states that any vector field, differentiable twice, can be written in a unique manner as the sum of a gradient field and a rotational field [1.20]:

$$\exists\ \underline{U}^{P}\ \ and\ \ \underline{U}^{S}\ \ \underline{U} = \underline{U}^{P} + \underline{U}^{S} \quad \begin{cases} \underline{U}^{P} = \underline{\nabla}\,\Phi \\ \underline{U}^{S} = \underline{rot}\,\underline{\Psi} \end{cases} \quad [1.20]$$

The field $\underline{U}^{P}$ is the primary irrotational field [1.21]:

$$\underline{rot}\,\underline{U}^{P} = \underline{rot}\left(\underline{\nabla}\,\Phi\right) = 0 \quad [1.21]$$

The field $\underline{U}^S$ is the second field, which is said to be solenoid, and corresponds to motion that does not cause changes in volume [1.22]:

$$div\,\underline{U}^S = div\left(\underline{rot}\,\underline{\Psi}\right) = 0 \qquad [1.22]$$

1.2.2.2. *P-waves*

If we only consider the primary field, the equation of motion is written as [1.23]:

$$\left(\lambda + 2\mu\right)\,\underline{\nabla}\left(div\,\underline{U}^P\right) = \rho\,\underline{\ddot{U}}^P \qquad [1.23]$$

This is a propagation equation. This primary field corresponds to the propagation of P-waves [1.24]:

$$\underline{\Delta}\,\underline{U}^P = \frac{\rho}{\left(\lambda + 2\mu\right)}\,\underline{\ddot{U}}^P \qquad U^P_{i,jj} = \frac{\rho}{\left(\lambda + 2\mu\right)}\,U^P_{i,tt} \qquad [1.24]$$

The propagation velocity of these P-waves is C_p [1.25]:

$$C_P = \sqrt{\frac{\left(\lambda + 2\mu\right)}{\rho}} \qquad = \sqrt{\frac{E\left(1-\nu\right)}{\rho\left(1-2\nu\right)\left(1+\nu\right)}} \qquad [1.25]$$

Motions of P-wave propagation are extensions and compressions.

1.2.2.3. *S-waves*

If we only consider the secondary field, the equation of motion is written as [1.26]:

$$\mu\;\underline{\Delta U}^S = \rho\,\underline{\ddot{U}}^S \qquad \mu\,U^S_{i,jj} = \rho\,U^S_{i,tt} \qquad [1.26]$$

This is also a propagation equation. The propagation of this secondary field corresponds to S-waves, with a propagation velocity C_s [1.27]:

$$C_s = \sqrt{\frac{\mu}{\rho}} \qquad = \sqrt{\frac{E}{2\rho(1+\nu)}} \qquad [1.27]$$

The propagation of S-waves corresponds to shear movements without volume change. In an elastic system, the velocity ratio of P- and S-waves depends only on the Poisson coefficient [1.28]:

$$\left(\frac{C_p}{C_s}\right)^2 = \frac{\lambda + 2\mu}{\mu} = 2\frac{1-\nu}{1-2\nu} \qquad [1.28]$$

1.2.2.4. *Plane waves*

If the displacement depends on only one variable in space ($\underline{U}(x_1)$), the motion is that of plane waves. Propagation is in one direction. The equations governing the motion are [1.29]:

$$\begin{cases} \dfrac{\partial^2 U_1}{\partial {x_1}^2} = \dfrac{1}{{C_P}^2}\ddot{U}_1 \\ \dfrac{\partial^2 U_2}{\partial {x_1}^2} = \dfrac{1}{{C_S}^2}\ddot{U}_2 \\ \dfrac{\partial^2 U_3}{\partial {x_1}^2} = \dfrac{1}{{C_S}^2}\ddot{U}_3 \end{cases} \qquad [1.29]$$

The longitudinal components of displacement, along the axis of propagation, correspond to P-waves and thus propagate at velocity C_P. The transversal displacements, orthogonal to the direction of propagation, correspond to S-waves at velocity C_S. Figure 1.3 gives an illustration of the movements associated with these strain waves.

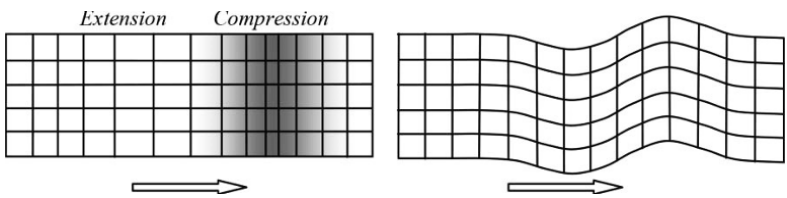

Figure 1.3. *Movements and strains associated with P-waves (left) and S-waves (right)*

1.2.2.5. *P-waves in spherical symmetry*

Consider a pressure wave emitted from a point within a large solid. This could represent the effect of an underground explosion. We naturally take the spherical coordinates, because the movement follows the symmetry [1.30]:

$$\underline{U}\begin{pmatrix} U_r = u(r) \\ U_\theta = 0 \\ U_\varphi = 0 \end{pmatrix} \qquad [1.30]$$

The propagation equation in the radial direction is then [1.31]:

$$\Delta u - \left(\frac{\rho}{\lambda + 2\mu}\right)\frac{\partial^2 u}{\partial t^2} = 0 \qquad [1.31]$$

This equation can also be written as [1.32]:

$$\frac{1}{r}\frac{\partial^2 (ru)}{\partial r^2} - \frac{1}{{C_P}^2}\frac{\partial^2 u}{\partial t^2} = 0 \qquad [1.32]$$

If we insert $z = ru$, the equation takes the form [1.33]:

$$\frac{\partial^2 z}{\partial r^2} - \frac{1}{{C_P}^2}\frac{\partial^2 z}{\partial t^2} = 0 \qquad [1.33]$$

With this change of variable, we see that the propagation occurs at P-wave velocity and the range of motion decreases in proportion to *1/r*.

1.3. One-dimensional waves

1.3.1. *Uniaxial stress state*

Uniaxial stress state is an approximation that is made when the considered solid is of slender shape (wire or bar undergoing tension or compression). The solid is then represented geometrically by a straight

line, and the displacement field depends only on the abscissa along the line (Figure 1.4). Stress and strain tensors at a point then take a simplified form [1.34]:

$$\underline{\underline{\varepsilon}} = \begin{pmatrix} \varepsilon_1 & 0 & 0 \\ 0 & \varepsilon_2 & 0 \\ 0 & 0 & \varepsilon_2 \end{pmatrix} \qquad \underline{\underline{\sigma}} = \begin{pmatrix} \sigma_1 & 0 & 0 \\ 0 & 0 & 0 \\ 0 & 0 & 0 \end{pmatrix} \qquad [1.34]$$

The equations of motion take the form of system [1.35] (note that, for the ease of writing, $x_1 = x \quad \sigma_1 = \sigma \quad \varepsilon_1 = \varepsilon \quad U_1 = U$):

$$\frac{\partial \sigma}{\partial x} = \rho \frac{\partial^2 U}{\partial t^2} \qquad \varepsilon = \frac{\partial U}{\partial x} \qquad \sigma(\varepsilon) \qquad [1.35]$$

In the case of a linear elastic medium, the propagation equation is [1.36]:

$$\frac{\partial^2 U}{\partial x^2} - \frac{1}{C_0^2} \frac{\partial^2 U}{\partial t^2} = 0 \quad \text{where} \quad C_0 = \sqrt{\frac{E}{\rho}} \qquad [1.36]$$

C_0 is the wave velocity in uniaxial stress state.

1.3.2. *Uniaxial strain state*

Uniaxial strain state corresponds to a situation where movement is in one direction only (axial). There is no radial strain (Figure 1.4). This may correspond to strain on the area near the impact in a solid. There exists a test called “impact plate” where a material is tested in a state of stress. Stress and strain tensors at a point then take a simplified form [1.37]:

$$\underline{\underline{\varepsilon}} = \begin{pmatrix} \varepsilon_1 & 0 & 0 \\ 0 & 0 & 0 \\ 0 & 0 & 0 \end{pmatrix} \qquad \underline{\underline{\sigma}} = \begin{pmatrix} \sigma_1 & 0 & 0 \\ 0 & \sigma_2 & 0 \\ 0 & 0 & \sigma_2 \end{pmatrix} \qquad [1.37]$$

Elastic behavior gives the relationship between the axial stress and radial stress [1.38]:

$$\sigma_2 = \frac{\nu}{(1-\nu)}\sigma_1 \qquad \sigma_1 = (\lambda + 2\mu)\varepsilon_1 = \frac{E(1-\nu)}{(1-2\nu)(1+\nu)}\varepsilon_1 \qquad [1.38]$$

The propagation equation is [1.39]:

$$\frac{\partial^2 U}{\partial x^2} - \frac{1}{C_P^2}\frac{\partial^2 U}{\partial t^2} = 0 \qquad [1.39]$$

Compression motion in a uniaxial strain state corresponds to P-waves.

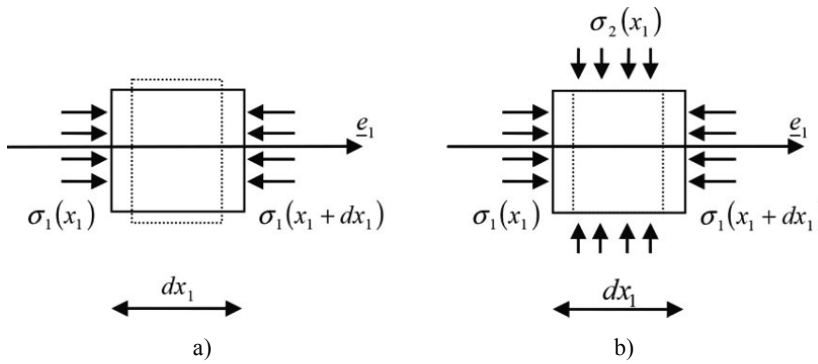

Figure 1.4. *Volume element in a state of uniaxial stress a), or in a state of uniaxial strain b)*

Table 1.1 presents the values of elastic properties, and uniaxial compression waves and P-waves propagation velocities for common building materials.

	ρ (kg/m^3)	E (GPa)	ν	C_0 (m/s)	C_P (m/s)
Steel	7,870	210	0.3	5,160	5,990
Concrete	2,200	20	0.2	3,010	3,170
Glass	2,500	69	0.18	5,250	5,470
Wood*	500	10	0.35	4,470	5,660
Brick	1,800	14	0.2	2,790	2,940

*Average characteristics of glulam.

Table 1.1. *Elastic characteristics of some building materials and velocity values for waves in uniaxial stress state and uniaxial strain state*

1.3.3. *The d'Alembert solution*

There are several ways of explaining the wave equation solutions that we have just seen. The propagation equation of type [1.36] or [1.39] can also be written as [1.40] (note the speed C):

$$\left(\frac{\partial}{\partial x}-\frac{1}{C}\frac{\partial}{\partial t}\right)\left(\frac{\partial}{\partial x}+\frac{1}{C}\frac{\partial}{\partial t}\right)U=0 \qquad [1.40]$$

It is possible to make the following change in variables [1.41]:

$$U(\xi,\varsigma),\ \xi=t-\frac{x}{C}\ \text{and}\ \varsigma=t+\frac{x}{C} \qquad [1.41]$$

In this case, equation [1.40] leads to [1.42]:

$$\frac{\partial^2 U}{\partial\xi\,\partial\varsigma}=0 \qquad [1.42]$$

The solution can be written as the sum of two functions of one variable:

$$U(\xi,\varsigma)=F(\xi)+G(\varsigma),\ U(x,t)=f\left(t-\frac{x}{C}\right)+g\left(t+\frac{x}{C}\right) \qquad [1.43]$$

Functions *f* and *g* are determined by the initial conditions. Figure 1.5 shows strain fields at two instants if the motion is described by a function of type *f*. This function is called a progressive wave, as it describes a displacement field or strain, which moves in a positive direction at speed *C*. A type function *g* is called a regressive wave, because it corresponds to a field that moves in the negative direction.

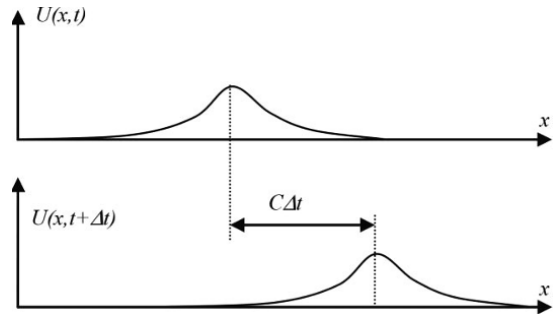

Figure 1.5. *Example of a displacement field at two instances separated by Δt, for a progressive wave represented by an f (t – x/C) function*

This form of writing can be used for spherical *P-waves*. A wave that corresponds to a movement from the origin of the coordinate can be written as [1.44]:

$$u(r,t)=\frac{1}{r}f\left(t-\frac{r}{C_P}\right) \qquad [1.44]$$

1.4. Harmonic waves

1.4.1. *Definitions*

Propagation equation solutions can also be sought in harmonic form. That is, the functions *f* and *g* from the previous section are written as sums of harmonic functions [1.45]:

$$U(x,t)=A\ \cos\left(kx-\omega t\right)=A\cos k\left(x-Ct\right)\ \text{or}$$
$$U(x,t)=A\ \Re e\left(e^{i(kx-\omega t)}\right) \qquad [1.45]$$

A number of variables associated with the propagation of the harmonic wave are defined as follows:

– phase $(kx - \omega t)$;

– phase velocity $C = \frac{\omega}{k}$;

– wavelength $\lambda = \frac{2\pi}{k}$;

– number of waves $n = \frac{1}{\lambda}$.

Generally, any function can be represented as a sum of harmonic functions via the Fourier transformation [1.46]:

$$U(x,t) = \frac{1}{2\pi}\int_{-\infty}^{+\infty} U^*(x,\omega)e^{-i\omega t}d\omega \qquad [1.46]$$

The previously seen unidirectional waves can be written as the sum of harmonic waves. Another example for writing waves in this form is that of Rayleigh waves (Figure 1.6). These waves correspond to vertical surface motion. The motion is sinusoidal at the surface and absorbed exponentially with depth [1.47]:

$$\underline{U}\begin{pmatrix} U_1 = Ae^{-x_2+ik(x_1-C_R t)} \\ U_2 = Be^{-x_2+ik(x_1-C_R t)} \\ U_3 = 0 \end{pmatrix} \qquad [1.47]$$

The speed of Rayleigh waves is calculated by expressing stress conditions on the surface as zero. This leads to equation [1.48]. The Rayleigh wave speed is slightly less than that of S-waves:

$$\left(2 - \frac{C_R^2}{C_S^2}\right)^2 - 4\sqrt{\left(1 - \frac{C_R^2}{C_P^2}\right)\left(1 - \frac{C_R^2}{C_S^2}\right)} = 0$$

$$0{,}862 < \frac{C_R}{C_S} < 0{,}955 \quad \left(\frac{C_R}{C_S} \approx \frac{0{,}862 + 1{,}14\,\nu}{1+\nu}\right) \qquad [1.48]$$

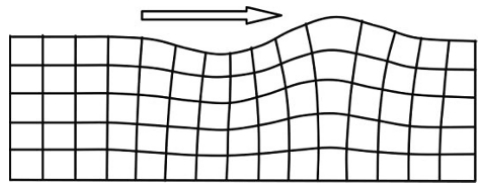

Figure 1.6. *Motion and strains associated with Rayleigh waves*

1.4.2. *Wave dispersion*

When expressed as the superposition of harmonic waves, it is possible that phase velocity is constant (as in the examples we have just seen) or that it depends on wavelength or pulse. The dispersion relation is the function that connects phase velocity to wavelength or pulse ($C(\omega)$ or $C(\lambda)$ or $k(\omega)$). The wave is then formulated according to expression [1.49]:

$$U(x,t)=\frac{1}{2\pi}\int_{-\infty}^{+\infty}U^*(x,\omega)e^{-i\omega t}d\omega \qquad U^*(x,\omega)=W^*(\omega)e^{ik(\omega)x} \qquad [1.49]$$

If the phase velocity is not constant, independent of pulse or wavelength, a movement propagates by "deforming" itself because all its harmonic components do not propagate at the same speed. This is called dispersion. As previously seen in uniaxial plane waves, there is no dispersion because wave velocity is constant. For uniaxial stress waves, we get the dispersion equation by introducing the harmonic solution [1.45] into the equation of motion [1.36]. Then, we obtain equation [1.50], which shows that the phase velocity is constant:

$$Ek^2-\rho\omega^2=0 \quad C=\frac{\omega}{k}=\sqrt{\frac{E}{\rho}} \qquad [1.50]$$

The dispersion phenomenon occurs when movements are the solutions of equations that are a little more complex than those we have already seen. These situations occur when the motion in certain solids is studied. In Chapter 8, we will see the case of beam flexion. An interesting case, important for its practical application, is the case of strain waves in rods.

1.4.3. *Dispersion of waves in a rod*

The strain wave rod model, previously seen with the uniaxial stress state hypothesis, is an approximation to the motion occurring in an actual rod. In practice, this model is widely used. The description of motion can be improved by taking into account the radial strain that occurs under the Poisson effect [BAN 41, MIN 60]. A first approach is, quite simply, the "Love-Rayleigh" wave. A detailed study of waves in rods was given by Pochhammer [POC 76] and Chree [CHR 89]. These descriptions lead to dispersed waves (Figure 1.7).

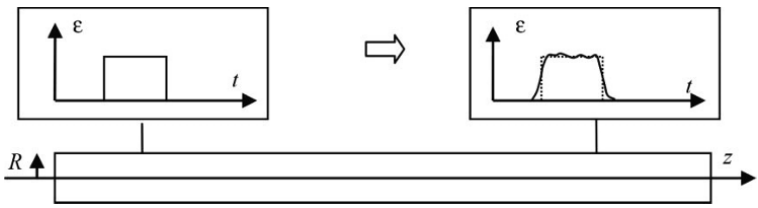

Figure 1.7. *Modifying the shape of a wave by dispersion effect. Example of two-point strain measurements, due to the propagation of a pressure wave in a rod of radius R*

1.4.3.1. *The "Love-Rayleigh" solution*

The idea is to take lateral movement into account by considering its contribution in the expression of kinetic energy. To do this, a hypothesis on the velocity field is made [1.51]. A radial displacement is associated with axial strain (along z), proportional to the radius:

$$\underline{U}\left(\underline{X},t\right)=\underline{U}\left(r,\theta,z,t\right)=\begin{pmatrix} U_r\left(r,z,t\right) \\ U_\theta=0 \\ U_z\left(z,t\right) \end{pmatrix} \qquad U_r=-\nu r\frac{\partial U_z}{\partial z} \qquad [1.51]$$

The kinetic energy of a rod section of unit length dz can be calculated by expression [1.52]:

$$E_c=\frac{1}{2}\int_0^R 2\pi\rho\left(\frac{\partial U_r}{\partial t}\right)^2 rdr+\frac{1}{2}\rho\pi R^2\left(\frac{\partial U_z}{\partial t}\right)^2 \qquad [1.52]$$

Taking the above kinetic hypothesis into account, we eliminate radial displacement of the expression and obtain the expression of energy [1.53]:

$$E_c = \frac{1}{2}\int_0^R 2\pi\rho v^2 \left(\frac{\partial^2 U_z}{\partial z \partial t}\right)^2 r^3 dr + \frac{1}{2}\rho\pi R^2 \left(\frac{\partial U_z}{\partial t}\right)^2 \qquad [1.53]$$

Integration gives expression [1.54]:

$$E_c = \frac{1}{4}\pi\rho v^2 R^4 \left(\frac{\partial^2 U_z}{\partial z \partial t}\right)^2 + \frac{1}{2}\rho\pi R^2 \left(\frac{\partial U_z}{\partial t}\right)^2 \qquad [1.54]$$

The kinetic energy theorem indicates that the power of the forces applied to the element is equal to the kinetic energy time derivative. The power of the forces on a single slice is expressed as [1.55]:

$$\Pi_e = \pi R^2 \frac{\partial \sigma}{\partial z}\frac{\partial U_z}{\partial t} = E\pi R^2 \frac{\partial^2 U_z}{\partial z^2}\frac{\partial U_z}{\partial t} \qquad [1.55]$$

The kinetic energy time derivative is expressed as [1.56]:

$$\frac{\partial E_c}{\partial t} = \frac{1}{2}\pi\rho v^2 R^4 \frac{\partial^2 U_z}{\partial z \partial t}\frac{\partial^3 U_z}{\partial z \partial t^2} + \rho\pi R^2 \frac{\partial U_z}{\partial t}\frac{\partial^2 U_z}{\partial t^2} \qquad [1.56]$$

Expression of the first term is changed by noting that we can consider relationship [1.57]:

$$\frac{\partial^2 U_z}{\partial z \partial t}\frac{\partial^3 U_z}{\partial z \partial t^2} = \int \frac{\partial^3 U_z}{\partial z^2 \partial t}\frac{\partial^3 U_z}{\partial z \partial t^2} dz + \int \frac{\partial^2 U_z}{\partial z \partial t}\frac{\partial^4 U_z}{\partial z^2 \partial t^2} dz \qquad [1.57]$$

Integration by parts of the last term of expression [1.57] leads to equation [1.58]:

$$\frac{\partial^2 U_z}{\partial z \partial t}\frac{\partial^3 U_z}{\partial z \partial t^2} = \frac{\partial U_z}{\partial t}\frac{\partial^4 U_z}{\partial z^2 \partial t^2} \qquad [1.58]$$

Taking this result into account, application of the kinetic energy theorem leads to the equation of motion [1.59]:

$$\frac{\rho\nu^2R^2}{2}\frac{\partial^4U_z}{\partial z^2\partial t^2}+\rho\frac{\partial^2U_z}{\partial t^2}=E\frac{\partial^2U_z}{\partial z^2} \qquad [1.59]$$

The equation of wave dispersion associated with this equation of motion takes the form [1.60]:

$$\frac{\rho\nu^2R^2}{2}k^2\omega^2+\rho\omega^2=Ek^2 \qquad [1.60]$$

With this modeling, there is wave dispersion, since speed depends on the number of waves according to formula [1.61]:

$$C=\frac{C_0}{\sqrt{1+\frac{\nu^2R^2k^2}{2}}} \qquad [1.61]$$

The change in velocity as a function of wave number is shown in Figure 1.7.

1.4.3.2. *The Pochhammer and Chree solution*

A solution of the Navier equation in a cylindrical domain of radius R was obtained by Pochhammer and Chree. The solution is sought as a sum of harmonics according to [1.49], but in three-dimensional space, taking into account the symmetry of revolution [1.62]. This is done using the Fourier transformation (denoted by *):

$$\underline{U}(\underline{X},t)=\frac{1}{2\pi}\int_{-\infty}^{+\infty}\underline{U}^*(r,z,\omega)e^{-i\omega t}d\omega \quad \underline{U}^*(r,z,\omega)=\underline{W}^*(r,\omega)e^{ik(\omega)z} \qquad [1.62]$$

The elastic behavior can be expressed in the frequency domain [1.63]:

$$\underline{\underline{\sigma}}^*(\omega)=\lambda\, tr(\underline{\underline{\varepsilon}}^*(\omega))\underline{\underline{1}}+2\mu\,\underline{\underline{\varepsilon}}^*(\omega) \qquad [1.63]$$

The equation of motion becomes [1.64]:

$$\mu \underline{\Delta U}^* + (\lambda + \mu)\underline{\nabla}(div\underline{U}^*) + \underline{f} = -\rho\omega^2 \underline{U}^* \qquad [1.64]$$

The Helmholtz decomposition is used [1.65]:

$$\underline{U}^*(\underline{X},\omega) = \nabla\Phi^*(\underline{X},\omega) + rot\,\underline{\Psi}^*(\underline{X},\omega) \qquad [1.65]$$

This decomposition leads to two propagation equations [1.66]:

$$\begin{aligned} &\nabla^2\boldsymbol{\phi}^*(\underline{X},\boldsymbol{\omega}) + \frac{\boldsymbol{\omega}^2}{C_1^2}\boldsymbol{\phi}^*(\underline{X},\boldsymbol{\omega}) = 0 \quad \text{and} \\ &\nabla^2\underline{H}^*(\underline{X},\boldsymbol{\omega}) + \frac{\boldsymbol{\omega}^2}{C_2^2}\underline{H}^*(\underline{X},\boldsymbol{\omega}) = 0 \end{aligned} \qquad [1.66]$$

The "potential" functions are logically formulated using a cylindrical coordinate system [1.67]:

$$\begin{aligned} &\Phi^*(\underline{X},\omega) = \varphi(r,\theta,\omega)\, e^{ikz} \\ &\underline{\Psi}^*(\underline{X},\omega) = \left(\psi_r(r,\theta,\omega)\underline{e_r} + \psi_\theta(r,\theta,\omega)\underline{e_\theta} + \psi_z(r,\theta,\omega)\underline{e_z}\right)e^{ikz} \end{aligned} \qquad [1.67]$$

Given the symmetry of the revolution problem, it is possible to simplify these expressions and write the potentials as [1.68]:

$$\begin{aligned} &\Phi^*(\underline{X},\omega) = \varphi(r,\omega)\, e^{ikz} \\ &\underline{\Psi}^*(\underline{X},\omega) = \psi_\theta(r,\omega)\, e^{ikz}\underline{e_\theta} \end{aligned} \qquad [1.68]$$

Taking the limiting factors into account (zero stress on the cylindrical surface of rod $r = R$), the resolution leads to writing the analytical expression of these functions as [1.69]:

$$\begin{aligned} &\Phi^*(\underline{X},\omega) = A(\omega)J_0(\alpha r)e^{ikz} \\ &\underline{\Psi}^*(\underline{X},\omega) = B(\omega)J_1(\beta r)e^{ikz} \end{aligned} \quad \text{where} \quad \begin{aligned} \alpha^2 &= \frac{\rho\omega^2}{\lambda + 2\mu} - k^2 \\ \beta^2 &= \frac{\rho\omega^2}{\mu} - k^2 \end{aligned} \qquad [1.69]$$

J_0 and J_1 are Bessel functions of order 0 and 1. By introducing the displacement field obtained from these functions into the Navier equation, we obtain the dispersion equation [1.70]:

$$(2\alpha / R)(\beta^2 + k^2)J_1(\alpha.R)J_1(\beta.R) - (\beta^2 - k^2)^2 J_0(\alpha.R)J_1(\beta.R) - 4k^2\alpha.\beta.J_1(\alpha.R)J_0(\beta.R) = 0 \quad [1.70]$$

Figure 1.8 shows the variation in wave speed depending on wave number and radius of the rod.

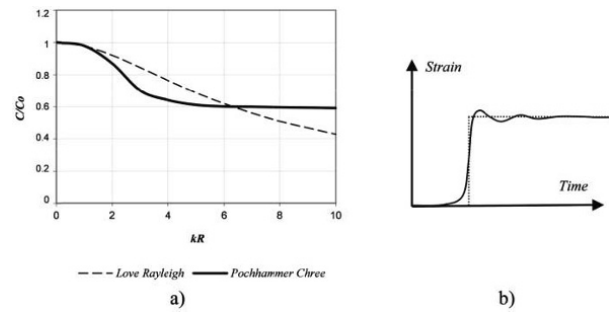

Figure 1.8. *a) Change in wave speed in a rod of radius R, according to the parameter kR, for the Love-Rayleigh model (dotted line) and for the Pochhammer Chree model (solid line); b) mapping the effect of dispersion on a strain wave that was originally a discontinuity*

Figure 1.8(b) shows, qualitatively, the effect of this dispersion. If the temporal evolution of strain at the end of a bar, subsequent to a shock, is represented by a discontinuity (dashed line). The temporal evolution of strain at another point, far from the end, is shown by the solid line.

1.5. Viscoelasticity

1.5.1. *Representation of rheological behavior*

1.5.1.1. *Representation and models*

When considering the problem of dynamics of solids, it is logical to question the possible dependence of the material behavior in physical time, through rate of strain. In this section, we discuss some

ways to take this effect into account when it exists. Linear behavior is developed using models and common tools. An application will be made in order to acquire equations of motion for viscoelastic bodies. Nonlinear effects will be discussed in Chapter 3. The functional representation of behavior is the most general way to express stress as a function of strain and the history of the material [1.71]. We can obviously express strain based on the history of stress using the inverse function:

$$\underline{\underline{\sigma}}(t) = \Re\left(\underline{\underline{\varepsilon}}(\tau)\right) \qquad \underline{\underline{\varepsilon}}(t) = \Re^{-1}\left(\underline{\underline{\sigma}}(\tau)\right) \qquad \tau \in]-\infty, t] \qquad [1.71]$$

Each variable is determined by its value at an initial time and the loading history between the initial time and time t. The material "remembers" all the stresses that have been imposed on it in the past. This memory may be tempered by progressive "oversight", meaning that stress $\sigma(\tau)$ has increasingly less influence on the current strain as τ gets further away from t. The formula should respect the principle of non-duality (or causality). That is, the stress at a given time may depend on the rate of strain at the same time. However, the strain at a given time may not depend on the stress rate at the same time. Thus, we find that a discontinuity in the rate of strain can cause a discontinuity in stress, but a discontinuity in the rate of stress cannot cause a discontinuity in strain. In practice, a functional representation of this is difficult because of the need to remember strain history. Attempts have been made to replace strain history by taking into account stress and strain derivative values at a considered time (differential equations and rheological models), or internal variables (variables of state). One idea is to write stress as a function of strain and its derivatives. Unfortunately, this does not describe some rheological aspects. More generally, it is possible to write an equation linking stress, strain and their derivatives [1.72]. This formula is less stringent than the functional formula and not all equations are able to represent a behavior:

$$L\left(\sigma, \dot{\sigma}, ..., \varepsilon, \dot{\varepsilon}, ...\right) = 0 \qquad [1.72]$$

1.5.1.2. *Construction of rheological models*

In rheological models, the material is compared to an assembly of simple mechanical elements [PER 69]. These analogous elements are only symbols and are unrelated to the constitution of the material. Figure 1.9 shows three typical rheological models to represent viscoelasticity. The purpose is to describe a phenomenological behavior by the construction of its thermodynamically relevant model. The mechanical elements may be translated by linear or nonlinear relationships. When behavior is linear, it is often useful to replace the functions of time (stress and strain) by their operational images using the Laplace–Carson transformation. The Laplace–Carson transformation is very similar to the Laplace transformation. The image of a function $f(t)$ is the Laplace transformation of the time derivative thereof [1.73]. It will be denoted by $f(p)$ (p complex):

$$\overline{f}(p) = p\int_0^{\infty} e^{-pt} f(t)\,dt \qquad [1.73]$$

This transformation has the same properties as the Laplace transformation. The Heaviside function, which is often used in rheology, has the operational image of the unit.

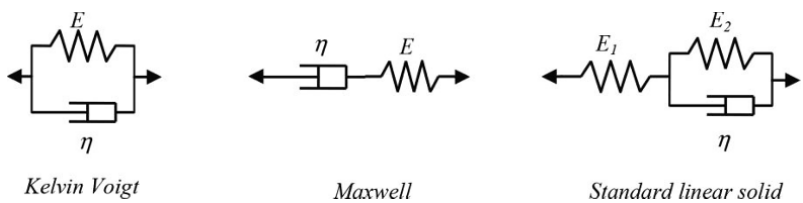

Figure 1.9. *Representation of three classical rheological models*

1.5.2. *Creep and relaxation functions*

1.5.2.1. *Formulation*

The creep function $f(t)$ is the strain response of a solicitation represented by a stress slot [1.74]:

$$f(t) = \varepsilon(t) \;\; if \;\; \sigma(t) = H(t) \qquad [1.74]$$

With operational images, creep function is expressed as a ratio [1.75]:

$$\bar{f}(p) = \frac{\bar{\varepsilon}(p)}{\bar{\sigma}(p)} \qquad [1.75]$$

Behavior can be obtained from the creep function. We obtain the Boltzmann equations [1.76] (square brackets indicate discontinuity):

$$\begin{aligned} \varepsilon(t) &= \sigma(0) f(t) + \int_0^t f(t-\tau) \frac{d\sigma}{d\tau}(\tau) d\tau + \sum_{i=1}^{n} f(t-t_i) [[\sigma(t_i)]] \\ \varepsilon(t) &= \sigma(t) f(0) + \int_0^t \sigma(t-\tau) \frac{df}{d\tau}(\tau) d\tau + \sum_{i=1}^{n} f(t-t_i) [[\sigma(t_i)]] \end{aligned} \qquad [1.76]$$

The relaxation function $r(t)$ is the stress response to a solicitation represented by a strain slot [1.77]:

$$r(t) = \boldsymbol{\sigma}(t) \quad if \quad \boldsymbol{\varepsilon}(t) = H(t) \qquad [1.77]$$

The operational image of the relaxation function is expressed by the ratio [1.78]:

$$\bar{r}(p) = \frac{\bar{\sigma}(p)}{\bar{\varepsilon}(p)} \qquad [1.78]$$

Use of the relaxation function is symmetrical to that of the creep function, and we obtain the behavioral relationships [1.79]:

$$\begin{aligned} \sigma(t) &= \varepsilon(0) r(t) + \int_0^t r(t-\tau) \frac{d\varepsilon}{d\tau}(\tau) d\tau + \sum_{i=1}^{n} r(t-t_i) [[\varepsilon(t_i)]] \\ \sigma(t) &= \varepsilon(t) r(0) + \int_0^t \varepsilon(t-\tau) \frac{dr}{d\tau}(\tau) d\tau + \sum_{i=1}^{n} r(t-t_i) [[\varepsilon(t_i)]] \end{aligned} \qquad [1.79]$$

1.5.2.2. *Three-dimensional aspect*

In the case of isotropy, the definition of relaxation (or creep) involves only two independent scalar functions. Relaxation is written as [1.80]:

$$\underline{\underline{\boldsymbol{\sigma}}}(t) = \boldsymbol{\lambda}(t) \left(trace \underline{\underline{\boldsymbol{\varepsilon}}}_0 \right) \underline{\underline{1}} + 2\boldsymbol{\mu}(t) \underline{\underline{\boldsymbol{\varepsilon}}}_0 \quad if \quad \underline{\underline{\boldsymbol{\varepsilon}}}(t) = \underline{\underline{\boldsymbol{\varepsilon}}}_0 H(t) \qquad [1.80]$$

– $2\mu(t)$ is the relaxation function in simple shear;

– $\lambda(t)+2\mu(t)$ is the relaxation function in simple extension.

Therefore, it returns to loading, regardless of formula [1.81]:

$$\begin{aligned}\underline{\underline{\sigma}}(t) &= \lambda(t)\left(trace\,\underline{\underline{\varepsilon}}(0)\right)\underline{\underline{\mathfrak{I}}} + 2\mu(t)\,\underline{\underline{\varepsilon}}(0) \\ &+ \int_0^t\left(\frac{d\lambda}{d\tau}(t-\tau)\left(trace\left(\underline{\underline{\varepsilon}}(\tau)\right)\right)\underline{\underline{\mathfrak{I}}} + 2\frac{d\mu}{d\tau}(t-\tau)\,\underline{\underline{\varepsilon}}(\tau)\right)d\tau\end{aligned} \quad [1.81]$$

This equation is much simpler when written in operational form [1.82]:

$$\overline{\underline{\underline{\sigma}}} = \overline{\lambda}\left(trace\,\overline{\underline{\underline{\varepsilon}}}\right)\underline{\underline{1}} + 2\overline{\mu}\,\overline{\underline{\underline{\varepsilon}}} \quad [1.82]$$

Independent creep functions are also two in number and we can write the inverse relationship [1.83]:

$$\overline{E}\,\overline{\underline{\underline{\varepsilon}}} = (1+\overline{\nu})\,\overline{\underline{\underline{\sigma}}} - \overline{\nu}\;trace\left(\overline{\underline{\underline{\sigma}}}\right)\underline{\underline{1}} \quad [1.83]$$

Since the definition of behavior requires data from two relaxation (or creep) functions, we can use the following two functions:

– $K(t)$ relaxation function under isotropic (hydrostatic) load;

– $G(t)$ relaxation function under split load.

The spherical part and the deviatoric part of behavior are then separately identified. K and G functions can be from different rheological models [1.84]. Generally, spherical behavior is solid-like, while deviatoric behavior can be fluid-like:

$$\begin{aligned}&\overline{p} = 3\overline{K}\,\overline{\theta} \quad \Leftrightarrow \quad p = 3\theta(0)K(t) + 3\int_0^t \frac{dK}{d\tau}(t-\tau)\,\theta(\tau)\,d\tau \quad \left(\theta = trace\underline{\underline{\varepsilon}}\right) \\ &\overline{s}_{ij} = 2\overline{G}\,\overline{e}_{ij} \quad \Leftrightarrow \quad s_{ij} = 2e_{ij}(0)\,G(t) + 2\int_0^t \frac{dG}{d\tau}(t-\tau)\,e_{ij}(\tau)\,d\tau\end{aligned} \quad [1.84]$$

1.5.3. *Rheological models*

1.5.3.1. *Kelvin–Voigt model*

This model is obtained by connecting a spring and a shock absorber in parallel (Figure 1.9). The differential equation of behavior and its operational image are immediate [1.85]:

$$\sigma(t) = E\varepsilon(t) + \eta\,\dot{\varepsilon}(t) \quad \text{and} \quad \bar{\sigma}(p) = (E + p\eta)\,\bar{\varepsilon}(p) \qquad [1.85]$$

It is easy to solve this equation to express strain as a function of stress [1.86]:

$$\varepsilon(t) = \varepsilon_0\, e^{-\frac{E}{\eta}(t-t_0)} + \frac{1}{\eta}\int_{t_0}^{t} e^{-\frac{E}{\eta}(t-\tau)}\sigma(\tau)\,d\tau \qquad [1.86]$$

In the simple model, the creep function is obtained from its operational image. A characteristic creep time τ appears [1.87]:

$$\bar{f}(p) = \frac{\bar{\varepsilon}(p)}{\bar{\sigma}(p)} = \frac{1}{E + \eta\, p}$$

$$f(t) = E\left(1 - e^{-\frac{t}{\tau}}\right) \qquad \text{where} \quad \tau = \frac{\eta}{E} \qquad [1.87]$$

We can build a generalized model with multiple creep times, which is to imagine putting several simple Kelvin–Voigt models in series, with different characteristics (E_i, η_i). The creep function can be written as [1.88]:

$$f(t) = \frac{1}{E_0} + \sum_{i=1}^{n} \frac{1}{E_i}\left(1 - e^{-\frac{t}{\tau_i}}\right) + \frac{t}{\eta_\infty} \qquad \text{with} \quad \tau_i = \frac{\eta_i}{E_i} \qquad [1.88]$$

The first term exists if there is a spring without a shock absorber in series, and the last term is present if there is a shock absorber without a spring in series (in the latter case, we get fluid-like behavior). This model is characterized by a spectrum of E_i stiffness values associated with characteristic times τ_i. A more general model can be considered

using a continuous distribution of stiffness versus creep time $j(\tau)$. The creep function takes the form [1.89]:

$$f(t) = \frac{1}{E_0} + \int_0^{+\infty} j(\tau)\left(1 - e^{-\frac{t}{\tau}}\right) d\tau + \frac{t}{\eta_\infty} \qquad [1.89]$$

The function $j(\tau)$ can be deduced from the experimental measure of $f(t)$.

1.5.3.2. *Maxwell model*

This model is obtained by connecting a spring and a shock absorber in series (Figure 1.9). The strains of the spring and shock absorber are added. The behavior is formulated as [1.90]:

$$\dot{\varepsilon}(t) = \frac{1}{E}\dot{\sigma}(t) + \frac{1}{\eta}\sigma(t) \qquad p\bar{\varepsilon}(p) = \left(\frac{p}{E} + \frac{1}{\eta}\right)\bar{\sigma}(p) \qquad [1.90]$$

It is also easy to solve and express strain depending on stress and stress as a function of strain [1.91]:

$$\varepsilon(t) = \varepsilon_0 + \frac{1}{E}\left(\sigma(t) - \sigma_0\right) + \frac{1}{\eta}\int_{t_0}^{t} \sigma(\tau)\, d\tau$$

$$\sigma(t) = \left(\sigma_0 - E\varepsilon_0\right) e^{-\frac{E}{\eta}(t - t_0)} - \frac{E^2}{\eta}\int_{t_0}^{t} e^{-\frac{E}{\eta}(t-\tau)} \varepsilon(\tau)\, d\tau \qquad [1.91]$$

The relaxation function is useful to describe the simple model [1.92]:

$$\bar{r}(p) = \frac{1}{\frac{1}{E} + \frac{1}{\eta p}} \quad \Rightarrow \quad r(t) = E e^{-\frac{t}{\tau}} \quad avec \quad \tau = \frac{\eta}{E} \qquad [1.92]$$

Let us consider placing several simple models with different features in parallel. We then get a stiffness spectrum based on relaxation time. The relaxation function takes the form [1.93]:

$$r(t) = E_\infty + \sum_{i=1}^{n} E_i e^{-\frac{t}{\tau_i}} \qquad [1.93]$$

The first term exists if we place a spring alone in parallel (we obtain solid-like behavior). A generalization of the model is obtained by considering a stiffness density continuous distribution as a function of relaxation time [1.94]:

$$r(t) = E_\infty + \int_0^{+\infty} g(\tau) e^{-\frac{t}{\tau}} d\tau \qquad [1.94]$$

1.5.3.3. *Standard linear model*

This rather general model is also called the Zener model (Figure 1.9). The behavior is written as [1.95]:

$$\begin{aligned} &(E_1 + E_2 + p\eta)\,\bar{\sigma}(p) = E_1(E_2 + p\eta)\,\bar{\varepsilon}(p) \\ &\sigma(t) + \frac{\eta}{E_1 + E_2}\dot{\sigma}(t) = \frac{E_1 E_2}{E_1 + E_2}\left(\varepsilon(t) + \frac{\eta}{E_2}\dot{\varepsilon}(t)\right) \end{aligned} \qquad [1.95]$$

This differential equation is often written as [1.96]:

$$\sigma(t) + a\dot{\sigma}(t) = E\left(\varepsilon(t) + b\dot{\varepsilon}(t)\right) \qquad [1.96]$$

But it only represents a behavior under the conditions E, a, $b > 0$ and $a < b$.

A more general linear model is represented by the linear differential equation [1.97] (with some restrictions linked to the causality condition):

$$L_1(\sigma) = L_2(\varepsilon) \quad \Leftrightarrow \quad a_0\sigma + a_1\dot{\sigma} + ...a_i\sigma^{(i)}... = E_0\varepsilon + E_1\dot{\varepsilon} + ...E_i\varepsilon^{(i)}... \qquad [1.97]$$

The behavior can be written in operational form [1.98]:

$$a(p)\,\bar{\sigma}(p) = E(p)\,\bar{\varepsilon}(p) \qquad [1.98]$$

As $a(p)$ and $E(p)$ are polynomials, we can decompose the relaxation and creep functions into simple elements [1.99]:

$$\overline{r}(p)=\frac{E(p)}{a(p)}=E_{\infty}+\sum_{i=1}^{n}E_i\frac{p}{p+\dfrac{1}{\tau_i}}+\eta_0 p$$

$$\overline{f}(p)=\frac{a(p)}{E(p)}=\frac{1}{E_0}+\sum_{i=1}^{n}\frac{1}{E_i}\frac{\dfrac{1}{\tau_i}}{p+\dfrac{1}{\tau_i}}+\frac{1}{p\eta_{\infty}} \qquad [1.99]$$

Returning to the original formulas, it can be noted that an equivalence exists between this model and that of the generalized Kelvin–Voigt and generalized Maxwell models.

1.5.4. *Complex modulus*

With linear behavior, if the stress is periodic, the response is also periodic. If the strain is harmonic, the Fourier transformation [1.100] is used:

$$\varepsilon(t)=\Re e\left(\varepsilon^{*}(t)\right) \qquad \varepsilon^{*}(t)=\varepsilon_0 e^{-i\omega t} \qquad \overline{\varepsilon}^{*}=\varepsilon_0\frac{p}{p-i\omega} \qquad [1.100]$$

If the material is a viscoelastic solid, the response is [1.101]:

$$\overline{\sigma}^{*}(p)=\varepsilon_0\left(\frac{E_{\infty}p}{p-i\omega}+\sum_{j=1}^{n}E_j\frac{p^2}{\left(p+\dfrac{1}{\tau_j}\right)(p-i\omega)}\right) \qquad [1.101]$$

This expression can easily be developed into rational fractions [1.102]:

$$\overline{\sigma}^{*}=\varepsilon_0\frac{\overline{r}(i\omega)p}{p-i\omega}+\varepsilon_0\sum_{j=1}^{n}E_j\frac{\left(\dfrac{1}{1+i\omega\tau_j}\right)p}{p+\dfrac{1}{\tau_j}} \qquad [1.102]$$

We then return to the original function [1.103]:

$$\sigma^*(t) = r(i\omega)\,\varepsilon_0\,e^{i\omega t} + \varepsilon_0 \sum_{j=1}^{n} E_j \left(\frac{1}{1+i\omega\tau_j} \right) e^{-\frac{t}{\tau_j}} \qquad [1.103]$$

The second term represents the transitional state that tends toward 0. Steady state is represented by [1.104]:

$$\sigma^*(t) = \sigma_0 e^{i\omega t} \qquad \text{where} \quad \sigma_0 = r(i\omega)\varepsilon_0 \qquad [1.104]$$

The $r(i\omega)$ function is the complex modulus E^*. It can be written as [1.105]:

$$E^*(\omega) = \tilde{E}(\omega) e^{-i\varphi(\omega)} \qquad [1.105]$$

Using harmonic tests and a frequency sweep, we can access curves representing the modulus and the complex modulus phase experimentally. We can also define the dynamic modulus E_d and the loss factor β as [1.106]:

$$E^*(\omega) = E_d(\omega)\left(1 + i\beta(\omega)\right) \qquad [1.106]$$

For the three models described above, the complex modulus parameters can be explained:

– Kelvin–Voigt model [1.107]:

$$E_d = E \qquad \beta = \frac{\eta\omega}{E} \qquad [1.107]$$

– Maxwell model [1.108]:

$$E_d = \frac{E}{1+\left(E/\eta\omega\right)^2} \qquad \beta = \frac{E}{\eta\omega} \qquad [1.108]$$

– Standard linear model [1.109]:

$$E_d = \frac{E_1\left(E_2\left(E_1+E_2\right)+\eta^2\omega^2\right)}{\left(E_1+E_2\right)^2+\eta^2\omega^2} \quad \beta = \frac{\eta\omega E_1}{E_2\left(E_1+E_2\right)+\eta^2\omega^2} \qquad [1.109]$$

1.5.5. *Waves in viscoelastic media*

1.5.5.1. *Propagation equation*

As we formulated motion in a continuous elastic medium in section 1.2, we can formulate and study motion in a continuous viscoelastic medium [SCH 63, BLA 93]. Generally, we obtain an equation of motion by linking the viscoelastic behavior equation with the dynamics equation [1.110]:

$$\sum_{i=1}^{n} a_i \frac{\partial^i \sigma}{\partial t^i} = \sum_{i=1}^{n} E_i \frac{\partial^i \varepsilon}{\partial t^i} \qquad \frac{\partial \sigma}{\partial x} = \rho \frac{\partial^2 U}{\partial t^2} \quad \varepsilon = \frac{\partial U}{\partial x} \qquad [1.110]$$

By eliminating the stress and strain variables, the equation of motion is a differential equation of partial displacement derivatives [1.111]:

$$\sum_{i=1}^{n} E_i \frac{\partial^{i+2} U}{\partial x^2 \partial t^i} = \rho \sum_{i=1}^{n} a_i \frac{\partial^{i+2} U}{\partial t^{i+2}} \qquad [1.111]$$

It is also possible to express the differential equation as a function of stress [1.112]:

$$\sum_{i=1}^{n} E_i \frac{\partial^{i+2} \sigma}{\partial x^2 \partial t^i} = \rho \sum_{i=1}^{n} a_i \frac{\partial^{i+2} \sigma}{\partial t^{i+2}} \qquad [1.112]$$

For the Kelvin–Voigt behavior model, the equations of motion are written as [1.113]:

$$E \frac{\partial^2 U}{\partial x^2} + \eta \frac{\partial^3 U}{\partial x^2 \partial t} = \rho \frac{\partial^2 U}{\partial t^2} \quad \text{and} \quad E \frac{\partial^2 \sigma}{\partial x^2} + \eta \frac{\partial^3 \sigma}{\partial x^2 \partial t} = \rho \frac{\partial^2 \sigma}{\partial t^2} \qquad [1.113]$$

For the Maxwell behavior model, the equations of motion are written as [1.113]:

$$\frac{\partial^3 U}{\partial x^2 \partial t} = \frac{\rho}{\eta} \frac{\partial^2 U}{\partial t^2} + \frac{\rho}{E} \frac{\partial^3 U}{\partial t^3} \quad \text{and} \quad \frac{\partial^2 \sigma}{\partial x^2} = \frac{\rho}{\eta} \frac{\partial \sigma}{\partial t} + \frac{\rho}{E} \frac{\partial^2 \sigma}{\partial t^2} \qquad [1.114]$$

The equations of motion can be addressed in operational form (using the Laplace transformation). The equation of behavior is written as [1.115]:

$$\sum s^i a_i \bar{\sigma} = \sum s^i E_i \bar{\varepsilon} \qquad \bar{\sigma} = \bar{E}(s)\bar{\varepsilon} \qquad \bar{E}(s) = \frac{\sum s^i E_i}{\sum s^i a_i} \quad [1.115]$$

The dynamics principle is written as [1.116]:

$$\frac{\partial \bar{\sigma}}{\partial x} = \rho s^2 \bar{U} \quad [1.116]$$

We deduce the equation of motion image [1.117]:

$$\frac{\partial^2 \bar{U}}{\partial x^2} = \frac{\rho s^2}{\bar{E}(s)} \bar{U} \quad [1.117]$$

The general solution of this equation is, in its operational form [1.118]:

$$\bar{U}(x,s) = A(s)\, e^{-sx\sqrt{\frac{\rho}{\bar{E}(s)}}} + B(s)\, e^{sx\sqrt{\frac{\rho}{\bar{E}(s)}}} \quad [1.118]$$

In Chapter 2, we will see some solutions for movement in viscoelastic solids in case of shocks. The viscoelastic properties of a material are often determined by a complex modulus; we may use a Fourier transformation of the equation of motion. Behavior and the dynamics equation can be written using expressions [1.119]:

$$\sigma^* = E^*(\omega)\varepsilon^* \qquad \frac{\partial \sigma^*}{\partial x} = -\rho \omega^2 U^* \quad [1.119]$$

Thus, the equation of motion is [1.120]:

$$\frac{\partial^2 U^*}{\partial x^2} = -\frac{\rho \omega^2}{E^*(\omega)} U^* \quad [1.120]$$

1.5.5.2. *Dispersion equation*

In viscoelastic media, movement expressed in harmonic form must contain a dissipation term, and in the frequency domain, an elementary wave is formulated according to [1.121]:

$$U^*(x,\omega) = A\, e^{\alpha x + i(kx - \omega t)} \qquad [1.121]$$

The dispersion equation, in complex form, is written as [1.122]:

$$E^*(\alpha + ik)^2 U^* = -\rho\omega^2 U^* \qquad [1.122]$$

This complex equation can also be written as a function of the dynamic modulus and loss factor [1.123]. This corresponds to two real equations [1.124]:

$$E_d(1 + i\beta)(\alpha + ik)^2 = -\rho\omega^2 \qquad [1.123]$$

$$\begin{aligned} &E_d\left(k^2 - \alpha^2 + 2\beta\alpha k\right) = \rho\omega^2 \\ &\beta\left(k^2 - \alpha^2\right) - 2\alpha k = 0 \end{aligned} \qquad [1.124]$$

The general solutions to these equations are [1.125]:

$$k = \omega\sqrt{\frac{\rho}{E_d}}\sqrt{\frac{1+\sqrt{1+\beta^2}}{2\left(1+\beta^2\right)}} \quad \alpha = \beta\omega\sqrt{\frac{\rho}{E_d}}\sqrt{\frac{1}{2\left(1+\beta^2\right)\left(1+\sqrt{1+\beta^2}\right)}} \qquad [1.125]$$

For the Kelvin–Voigt model, the dynamic modulus and loss factor are expressions [1.126]. This leads to the dispersion and dissipation relationships [1.127]:

$$E_d = E \qquad \beta = \frac{\eta\omega}{E} \qquad [1.126]$$

$$\frac{C}{C_0} = \sqrt{\frac{2\left(1+\beta^2\right)}{1+\sqrt{1+\beta^2}}} \qquad A = \frac{\alpha C_0}{\omega} = \frac{\beta}{\sqrt{2\left(1+\beta^2\right)\left(1+\sqrt{1+\beta^2}\right)}} \qquad [1.127]$$

For the Maxwell model, the dynamic modulus and loss factor are expressions [1.128]. This leads to the dispersion and dissipation relationships [1.129]:

$$E_d = \frac{E}{1+\left(E/\eta\omega\right)^2} \qquad \beta = \frac{E}{\eta\omega} \qquad [1.128]$$

$$\frac{C}{C_0} = \sqrt{\frac{2}{1+\sqrt{1+\beta^2}}} \qquad A = \frac{\alpha C_0}{\omega} = \frac{\beta}{\sqrt{2\left(1+\sqrt{1+\beta^2}\right)}} \qquad [1.129]$$

Figures 1.10 and 1.11 show the speed of waves and the absorption parameter A as a function of dimensionless pulse for Kelvin–Voigt and Maxwell models.

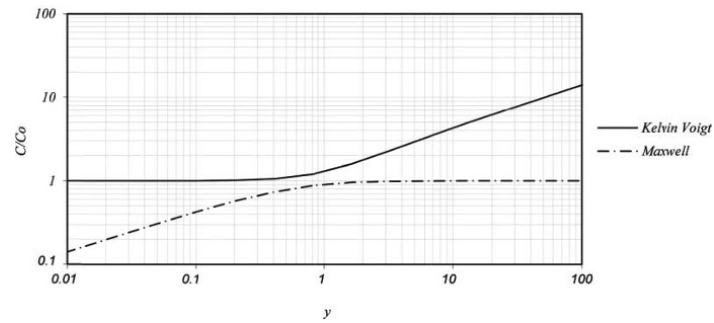

Figure 1.10. *Wave velocity as a function of dimensionless pulse ($y = \eta\omega/E$) for the Kelvin–Voigt model and the Maxwell model*

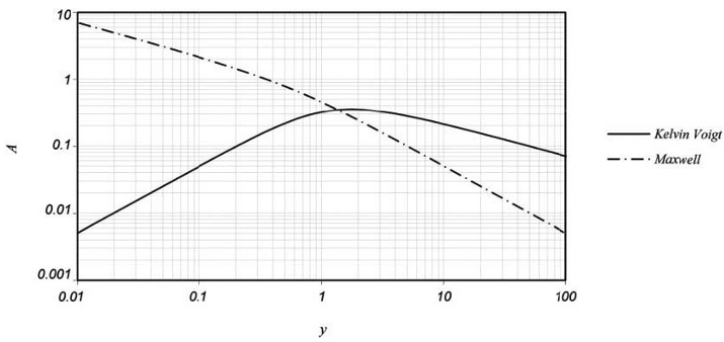

Figure 1.11. *Absorption parameter A as a function of dimensionless pulse ($y = \eta\omega/E$) for the Kelvin–Voigt model and the Maxwell model*

Chapter 2

Shocks in Solids

In Chapter 1, it was shown that transitional movements in solids can be represented by waves. When shocks occur in solids, in theory, these waves have a discontinued waveform. Therefore, it is necessary, in the first instance, to specify the equations governing the motion associated with these discontinuity waves. The application of elastic solids will be made, which leads to practical methods of evaluating stresses caused by shocks. To conclude, we will show how the presence of linear viscosity behavior of a material modifies the effects of a shock.

2.1. Discontinuity of stress and velocity

2.1.1. *Conservation equations*

2.1.1.1. *Propagation of a discontinuity*

In continuum mechanics, stress discontinuity is non-stationary and must be associated with velocity discontinuity. It is interesting to consider the physical relationships governing the states of the material when passing a discontinuity front of fixed propagation direction, as shown in Figure 2.1. The material undergoes uniaxial strain. The medium is characterized by its state at a given time (density, stress and velocity). We will consider two states: before (indexed 0) and

after (without index) passage of the discontinuity front. D is the propagation velocity of the discontinuity surface (according to propagation direction e_1) and V is the particulate or material velocity in the same direction. The scalar stress noted here is the normal stress on a normal facet in the direction of propagation (σ_{11} if the propagation direction is e_1). Similarly, the scalar strain used subsequently is the relative elongation in the direction of propagation (ε_{11}).

The three principles of conservation of mass, momentum and energy will introduce relationships that link state of matter parameters to the discontinuity front (regardless of the behavior of the material).

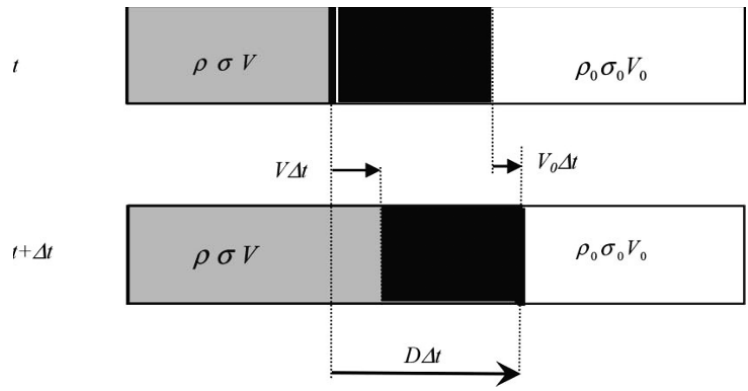

Figure 2.1. *Propagation of the velocity and stress discontinuity (index 0 affects the characteristics of the medium before passing the discontinuity front). The shaded area corresponds to an elementary mass*

2.1.1.2. *Conservation of mass*

Conservation equations are acquired by considering the motion between two instances of passage of the discontinuity front (strains and stresses of compression are positively noted). We consider a "tube" section unit (Figure 2.1). During the interval Δt, the stress jump has advanced by $D\Delta t$. The material occupying volume $(D - V_0)\Delta t$ at time t, occupies volume $(D - V)\Delta t$ at time $t + \Delta t$ (this volume corresponds to the shaded area in Figure 2.1). Then, the equation of conservation of mass is [2.1]:

$$\rho(D-V)=\rho_0(D-V_0) \qquad [2.1]$$

At the passage of the wave, longitudinal strain in the direction of wave propagation is [2.2]:

$$\varepsilon-\varepsilon_0=\frac{V-V_0}{D-V_0}=1-\frac{\rho_0}{\rho} \qquad [2.2]$$

2.1.1.3. *Conservation of momentum*

The same amount of material has a momentum of $\rho_0 V_0(D - V_0)$ at time t and a momentum of $\rho V(D - V)$ at time $t + \Delta t$. The change in momentum corresponds to the applied forces: $\sigma - \sigma_0$. The equation of conservation of momentum is [2.3]:

$$\sigma-\sigma_0=\rho V(D-V)-\rho_0 V_0(D-V_0) \qquad [2.3]$$

Given the equation of conservation of mass, this equation can also use the expression :

$$\sigma-\sigma_0=\rho(V-V_0)(D-V)=\rho_0(V-V_0)(D-V_0) \qquad [2.4]$$

2.1.1.4. *Conservation of energy*

Total energy is the sum of mass internal energy e and kinetic energy. Variations in the elementary volume energy over time (shaded area in Figure 2.1) are due to the power generated by the applied forces. This leads to the conservation formula [2.5]:

$$\rho\left(e+\frac{V^2}{2}\right)(D-V)-\rho_0\left(e_0+\frac{V_0^2}{2}\right)(D-V_0)=\sigma V-\sigma_0 V_0 \qquad [2.5]$$

The variation of internal energy at the passage of the stress jump is expressed by formula [2.6]:

$$e-e_0=\frac{1}{2}\left(V^2-V_0^2\right)+\frac{\sigma V-\sigma_0 V_0}{\rho_0(D-V_0)} \qquad [2.6]$$

This formula can be expressed differently, taking into account the relationships for conservation of mass [2.1] and momentum [2.3]:

$$e - e_0 = \frac{1}{2}(\sigma + \sigma_0)\frac{\left(V^2 - V_0^2\right)}{\rho_0 (D - V_0)} \qquad [2.7]$$

Taking into account relationship [2.2], we obtain the most common formula for internal energy variation at the jump discontinuity:

$$e - e_0 = \frac{1}{2}(\sigma + \sigma_0)\left(\frac{1}{\rho_0} - \frac{1}{\rho}\right) \qquad [2.8]$$

2.1.2. *State diagram*

Equations in the previous section provide the relationships between state parameters before and after the passage of the wave. It is possible to represent the state of matter in a diagram, retaining state parameters for particle or material velocity and stress. If the material behavior is elastic, the speed of the wave is known ($D = C$) and the relationship of conservation of momentum [2.3] is written, for a material initially at rest, as [2.9]. Quantity Z is the impedance:

$$\Delta\sigma = \rho_0 C\, \Delta V \quad (Z = \rho_0 C) \qquad [2.9]$$

There is a good reason to specify the configuration of the strain in the medium, as discussed in section 1.3. In uniaxial stress state, impedance will have the speed C_0. In uniaxial strain state, impedance will have the wave velocity P, C_P [2.10]:

$$\begin{aligned} &"\sigma 1D" \quad Z = \rho_0 C_0 = \sqrt{\rho_0 E} \\ &"\varepsilon 1D" \quad Z = \rho_0 C_P = \sqrt{\frac{\rho_0 E(1-\nu)}{(1-2\nu)(1+\nu)}} \end{aligned} \qquad [2.10]$$

Figure 2.2 shows a state of matter diagram. For an elastic material, initially at rest, the point corresponding to the state after the passage of a jump is located at (A), with a slope Z, in accordance with equation [2.9]. If at state (A) another wave passes, the point representing the state after the passage will be located at another point.

If we imagine a reference centered on (A), this point will be located on a straight line passing through (A) of slope $\pm Z$ [2.11]:

$$\pm\Delta\sigma = \pm Z\,\Delta V \qquad [2.11]$$

Figure 2.2 and Table 2.1 show the four possible situations and four directions in which point B can be searched, depending on the type of wave that is propagated. Using notations mentioned in Chapter 1, when we formulate waves using the d'Alembert solution, the waves propagating in the positive direction of the axis are known as "progressive waves" and are represented by a function $f\ (t - x/C)$. Waves propagating in the negative direction of the axis are called "retrogressive" and are represented by a function $g\ (t - x/C)$. If compressive stress increases when a wave passes, it is a compression wave. If compressive stress decreases when a wave passes, it is an expansion wave.

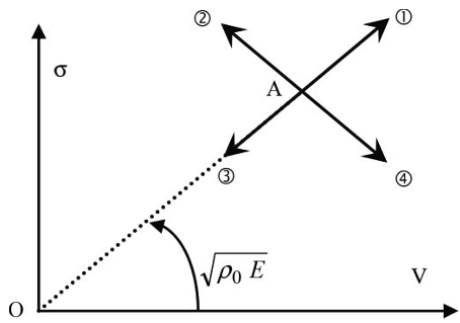

Figure 2.2. *"Stress-particle velocity" diagram; point A represents the state of matter and the arrows indicate the four possible evolutions of this state at the passage of a discontinuity wave*

	Progressive wave	Retrogressive wave
	$f(t-x/C)$	$g(t+x/C)$
	$\Delta\sigma = Z\,\Delta V$	$\Delta\sigma = -Z\,\Delta V$
Compression	(1) $\Delta\sigma > 0 \quad \Delta V > 0$	(2) $\Delta\sigma > 0 \quad \Delta V < 0$
Expansion	(3) $\Delta\sigma < 0 \quad \Delta V < 0$	(4) $\Delta\sigma < 0 \quad \Delta V > 0$

Table 2.1. *The four possible situations for the passage of a discontinuity wave*

2.2. Wave course

2.2.1. *Lagrange diagram*

The Lagrange representation has the goal of visualizing the "course diagram" of waves in a plane with two axes: space and time. The ideal wave that we represent is characterized by a steep jump in the strain field. A displacement imposed at $x = 0$, at a constant velocity, creates a strain wave. The diagram shows the position of the steep jump (Figure 2.3):

$$U(x,t) = a\left(t - \frac{x}{C}\right) H\left(t - \frac{x}{C}\right) \quad V(x,t) = a\, H\left(t - \frac{x}{C}\right)$$

$$\varepsilon(x,t) = -\frac{a}{C} H\left(t - \frac{x}{C}\right) \quad \sigma(x,t) = \sigma_a\, H\left(t - \frac{x}{C}\right) \quad \left(\sigma_a = a\sqrt{E\rho}\right) \qquad [2.12]$$

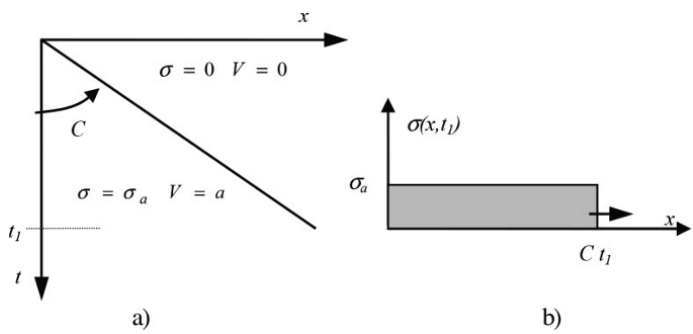

Figure 2.3. *Diagram of the course of a wave: a) position of the wave jump in the space–time diagram; b) stress field at a time t_1 (the arrow indicates the direction of discontinuity displacement)*

If the displacement at $x = 0$ ceases, there will be an expansion wave and a strain slot will propagate within the solid (Figure 2.4):

$$U(x,t) = a\left(t - \frac{x}{C}\right)\left(H\left(t - \frac{x}{C}\right) - H\left(t - \theta - \frac{x}{C}\right)\right)$$
$$\varepsilon(x,t) = -\frac{a}{C}\left(H\left(t - \frac{x}{C}\right) - H\left(t - \theta - \frac{x}{C}\right)\right) \qquad [2.13]$$

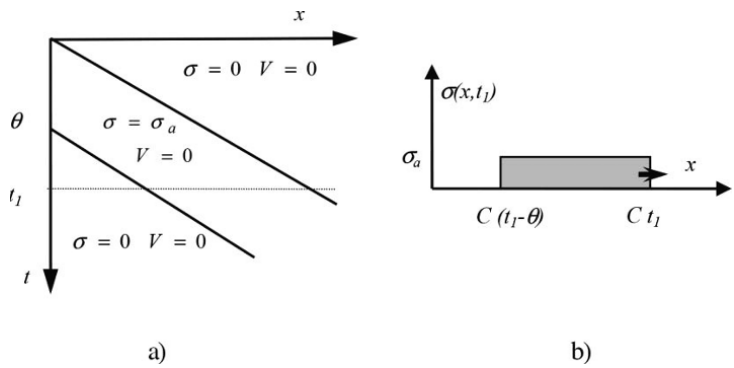

Figure 2.4. *Course diagram of a stress slot: a) position of the slot in the space–time diagram; b) stress field at time $t_1 > \theta$*

2.2.2. *Reflection on a free extremity*

Let us consider a rod of length L whose extremity is free of stress. Stress, and therefore strain, is always zero at the extremity. For the d'Alembert solution, it is written as [2.14]:

$$U(x,t) = f\left(t - \frac{x}{C}\right) + g\left(t + \frac{x}{C}\right)$$
$$\forall\, t \quad \varepsilon(L,t) = -\frac{1}{C} f'\left(t - \frac{L}{C}\right) + \frac{1}{C} g'\left(t + \frac{L}{C}\right) = 0 \qquad [2.14]$$

The free edge condition imposes relationships [2.15]:

$$g'\left(t + \frac{x}{C}\right) = f'\left(t - \frac{x}{C} + \frac{2L}{C}\right) \text{ and therefore } g\left(t + \frac{x}{C}\right) = -f\left(t - \frac{x}{C} + \frac{2L}{C}\right) \quad [2.15]$$

This means that the arrival of a compression wave at a free extremity, propagating in the positive direction, generates through its reflection an expansion wave propagating in the opposite direction (Figure 2.5).

The reflection of a strain slot on a free extremity leads to the Lagrange diagram (Figure 2.6). Therefore, a strain wave reflects itself, at a free extremity, changing sign.

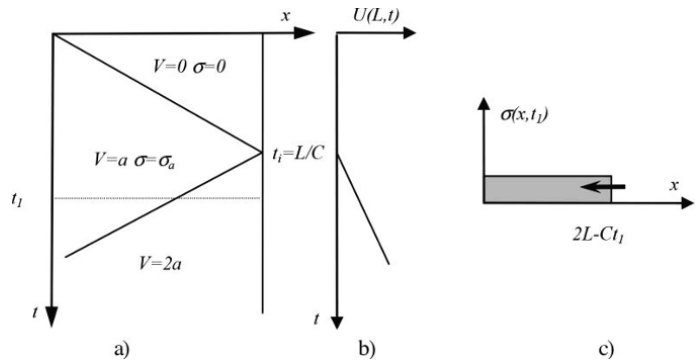

Figure 2.5. *Diagram of wave course with its reflection on a free extremity: a) the jump of the wave in the space–time diagram; b) displacement of the free extremity; c) stress field at time* $t_1 > L/C$

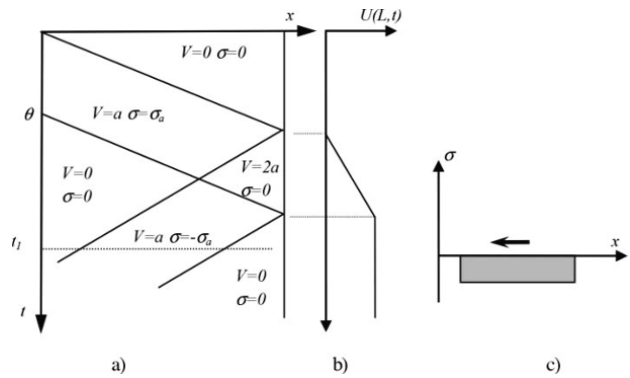

Figure 2.6. *Course diagram of a slot with its reflection on a free extremity: a) position of the jump of a wave in the space–time diagram; b) displacement of the free extremity; c) a stress field at time* t_1

2.2.3. *Reflection on a fixed extremity*

Let us consider a rod of length L with a fixed extremity. Displacement is always zero at the extremity. For the d'Alembert solution, this condition is written as [2.16]:

$$\forall t \quad U(L,t) = f\left(t - \frac{L}{C}\right) + g\left(t + \frac{L}{C}\right) = 0 \qquad [2.16]$$

This condition imposes relationship [2.17]:

$$g\left(t+\frac{x}{C}\right)=f\left(t-\frac{x}{C}+\frac{2L}{C}\right) \qquad [2.17]$$

This means that the arrival of a compression wave at a fixed extremity, traveling in a positive direction, generates through its reflection a compression wave of the same amplitude propagating in the opposite direction (Figure 2.7).

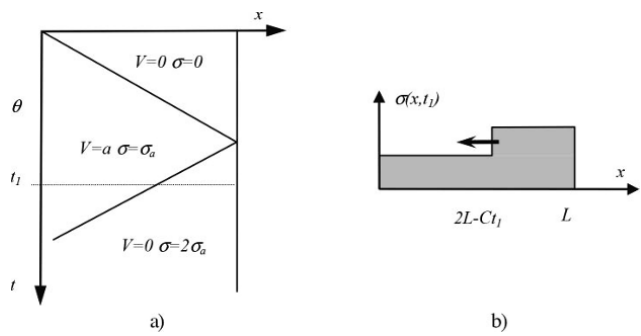

Figure 2.7. *Diagram of wave course with its reflection at a fixed extremity: a) position of the jump of the wave in the space–time diagram; b) stress field at time t_1*

The reflection of a strain slot on a fixed extremity leads to the Lagrange diagram in Figure 2.8. A strain wave is therefore reflected, on a fixed extremity, by a wave of the same sign.

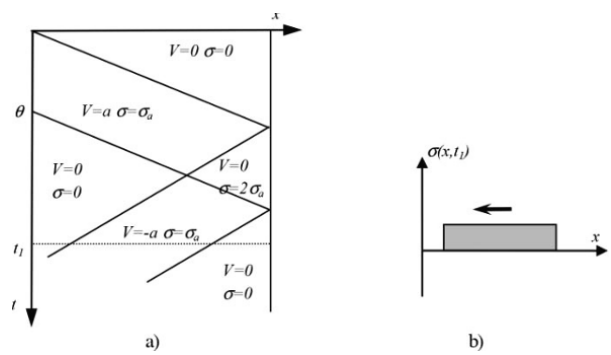

Figure 2.8. *Course diagram of a slot with its reflection on a fixed extremity: a) slot position in the space–time diagram; b) stress field at time t_1*

2.2.4. *Diffraction at an interface*

Let us consider two rods in contact. These rods can be made up of different materials and consist of different sections (S_1 ρ_1 E_1 and S_2 ρ_2 E_2). We expect a strain wave to arrive at this interface. At the interface, a reflected wave and a transmitted wave will be generated (Figure 2.9). Using the d'Alembert solutions, the displacements and strains in rods 1 and 2 have expressions [2.18]:

$$U_1 = f_1 + g_1 \qquad U_2 = f_2$$
$$\varepsilon_i = -\frac{f_1'}{C_1} \qquad \varepsilon_r = \frac{g_1'}{C_1} \qquad \varepsilon_t = -\frac{f_2'}{C_2} \qquad [2.18]$$

Two conditions must be verified at the interface if there is no loss of contact:

– equal forces [2.19]:

$$E_1 S_1 (\varepsilon_i + \varepsilon_r) = E_2 S_2 \varepsilon_t \qquad [2.19]$$

– equal velocities [2.20]:

$$f_1' + g_1' = f_2' \quad or \quad C_1 \varepsilon_r - C_1 \varepsilon_i = - C_2 \varepsilon_t \qquad [2.20]$$

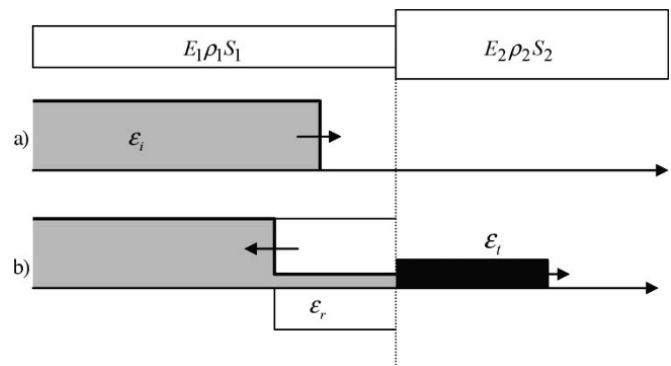

Figure 2.9. *Diffraction of a strain wave at the interface of two solids with different impedances: a) incident wave prior to arrival at the interface; b) reflected and transmitted wave after diffraction*

The reflection and transmission coefficients are defined as [2.21]:

$$\varepsilon_r = R\,\varepsilon_i \quad \varepsilon_t = T\,\varepsilon_i \qquad [2.21]$$

Both conditions are expressed by system [2.22]:

$$\begin{cases} E_1 S_1 (1+R) = E_2 S_2 T \\ C_1 (R-1) = -C_2 T \end{cases} \qquad [2.22]$$

The values of the coefficients can be calculated as [2.23]:

$$T = \frac{2C_1 E_1 S_1}{C_2 E_1 S_1 + C_1 E_2 S_2} \qquad R = \frac{C_1 E_2 S_2 - C_2 E_1 S_1}{C_2 E_1 S_1 + C_1 E_2 S_2} \qquad [2.23]$$

We should note that the transmission coefficient is always positive. The sign of the reflection coefficient depends on two quantities that are the impedances of the rods [2.24]:

$$R > 0 \;\; if \;\; S_2\sqrt{E_2\rho_2} > S_1\sqrt{E_1\rho_1} \qquad [2.24]$$

2.2.5. *Waves and modes*

In this section, a link is made between the representation of motion in a solid by waves and representation of motion by vibration modes. When vibrations in a mechanical structure are studied, we seek a solution to the equation of motion in the form [2.25]:

$$U(x,t) = \psi(t)\,\phi(x) \qquad [2.25]$$

The equation of motion [2.26] takes the form [2.27]:

$$\frac{\partial^2 U}{\partial x^2} - \frac{1}{C^2}\frac{\partial^2 U}{\partial t^2} = 0 \qquad [2.26]$$

$$\phi''\psi - \frac{1}{C^2}\ddot{\psi}\,\phi = 0 \text{ or } \frac{\ddot{\psi}}{\psi} = C^2\frac{\phi''}{\phi} = const = -\omega^2 \qquad [2.27]$$

Then, we can separately examine the space and time functions [2.28]:

$$\begin{cases} \ddot{\psi} + \omega^2 \psi = 0 \\ \phi'' + \dfrac{\omega^2}{C^2}\phi'' = 0 \end{cases} \quad \begin{cases} \psi = A \sin \omega t + B \cos \omega t \\ \phi = a \sin \dfrac{\omega x}{C} + b \cos \dfrac{\omega x}{C} \end{cases} \qquad [2.28]$$

The ϕ space function must verify the boundary conditions. Let us consider, for example, a rod of length L fixed at both extremities. The boundary conditions for the rod are [2.29]:

$$\phi(0) = 0 \quad \text{and} \quad \phi(L) = 0 \qquad [2.29]$$

This implies relationships [2.30]:

$$b = 0 \quad \text{and} \quad \frac{\omega L}{C} = n\pi \quad n \in IN \qquad [2.30]$$

The constant ω can only take certain values, called eigenfrequencies, which are associated with space functions [2.31]:

$$\omega_n = \frac{n\pi C}{L} \quad n \in IN \quad \phi_n = a \sin \frac{n\pi x}{L} \qquad [2.31]$$

Motion can be written as the superposition of normal modes [2.32]:

$$U(x,t) = \sum_{n=1}^{\infty} \psi_n(t)\ \phi_n(x) = \sum_{n=1}^{\infty} \sin \frac{n\pi x}{L} \left(A \cos \omega_n t + B \sin \omega_n t \right) \qquad [2.32]$$

This type of solution is interesting, for example in acoustics, for a vibrating string. The first natural frequency is the fundamental frequency and subsequent frequencies correspond to harmonics. Regarding structure vibrations, this type of solution is useful if the sum of the first few modes gives a good representation of motion. However, this type of solution may seem different from the d'Alembert solution. It is possible to show that this is the same

motion, but observed at different time scales. We take the above example with the d'Alembert solution [2.33]:

$$U(x,t) = f\left(t - \frac{x}{C}\right) + g\left(t + \frac{x}{C}\right) \qquad [2.33]$$

The boundary conditions [2.34] impose relationships [2.35]:

$$U(0,t) = 0 \quad \text{and} \quad U(L,t) = 0 \qquad [2.34]$$

$$\begin{cases} \forall t \quad f(t) + g(t) = 0 \\ \forall \tau \quad f\left(\tau - \frac{L}{C}\right) + g\left(\tau + \frac{L}{C}\right) = 0 \end{cases} \qquad [2.35]$$

It is possible to choose $\tau = t + L/C$. We show that function g is periodic [2.36]:

$$g(t) = g\left(t + \frac{2L}{C}\right) \qquad [2.36]$$

The same is true for function f. These functions can be decomposed into a Fourier series [2.37]:

$$\begin{cases} f(t) = a_0 + \sum_{n=1}^{\infty} a_n \cos\frac{Cn\pi t}{L} + b_n \sin\frac{Cn\pi t}{L} \\ g(t) = a_0' + \sum_{n=1}^{\infty} a_n' \cos\frac{Cn\pi t}{L} + b_n' \sin\frac{Cn\pi t}{L} \end{cases} \qquad [2.37]$$

Boundary conditions impose that $a_n' = -a_n$ and $b_n' = b_n$. It follows that motion can be written as [2.38] and [2.39]:

$$\begin{aligned} U(x,t) = \sum_{n=1}^{\infty} a_n & \left[\cos\frac{n\pi C}{L}\left(t - \frac{x}{C}\right) - \cos\frac{n\pi C}{L}\left(t + \frac{x}{C}\right)\right] \\ & + b_n\left[\sin\frac{n\pi C}{L}\left(t - \frac{x}{C}\right) + \sin\frac{n\pi C}{L}\left(t + \frac{x}{C}\right)\right] \end{aligned} \qquad [2.38]$$

$$U(x,t)=\sum_{n=1}^{\infty}2\sin\left(\frac{n\pi x}{L}\right)\left(a_n\sin\left(\frac{n\pi Ct}{L}\right)+b_n\cos\left(\frac{n\pi Ct}{L}\right)\right) \quad [2.39]$$

Thus, motion is written as the superposition of normal modes, and eigenfrequencies characteristic of the solid exist.

2.3. Shocks of solids

2.3.1. *Shocks of two solids*

Interactions between impacting solids depend on the shape of the solids. In the following references, we can find studies integrating this aspect [GOL 01, ARC 04, ZUK 90]. The study of shocks will here be addressed in a very simple configuration. We consider shock of two solids that are two rods of same section. Solid 1 is at rest and solid 2 arrives with an impact velocity V_2 (Figure 2.10).

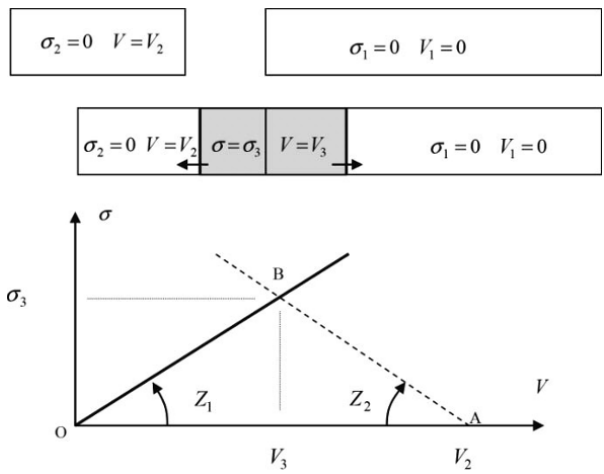

Figure 2.10. *Shocks of two solids. Solid 1 is initially at rest and solid 2 arrives with velocity V_2*

To determine the impact of the shock, we consider the state of matter in both solids at the area of impact. Figure 2.11 shows the state diagram. In this diagram, the state of matter in solid 1 is represented

by point O, and the state of matter in solid 2 is represented by point A. Upon impact, the stress in solid 1 (in the impact zone) will grow and the representative point changes along slope Z_1. In solid 2, velocity will decrease and state, near the point of contact, will change along the line going from A of slope $-Z_2$, as shown in Figure 2.2 and Table 2.1. The diagram shows that at the moment of impact, the balance of stresses at the interface can only be for values V_3 and σ_3 (Figure 2.11).

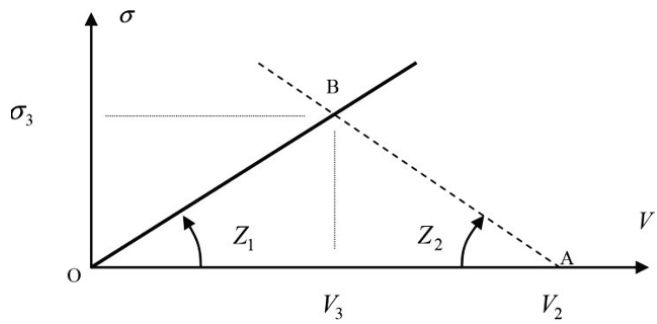

Figure 2.11. *Evolutions of representative states of solids in the "stress-particle velocity" diagram. The behavior of solid 1 is shown by a solid line and that of projectile 2 by a dashed line*

Changes in states of matter are given by formulas [2.40]. The state in the impact zone is characterized by V_3 and σ_3 [2.41]. After impact, compression waves will propagate through the solid at velocity C:

$$\begin{aligned}\sigma_3 - \sigma_1 &= Z_1\left(V_3 - V_1\right)\\ \sigma_3 - \sigma_2 &= Z_2\left(V_2 - V_3\right)\end{aligned} \qquad [2.40]$$

$$\sigma_3 = \frac{Z_1 Z_2}{Z_1 + Z_2} V_2 \qquad V_3 = \frac{Z_2}{Z_1 + Z_2} V_2 \qquad [2.41]$$

In the shock diagram, if solids are from different sections, to the extent that an approach using one-dimensional waves is valid, we can replace stress by force in the section. The relationship at the passing of a wave becomes [2.42]:

$$\Delta F = \pm S Z \Delta V \qquad [2.42]$$

A second example is shown in Figure 2.12. The solids do not have the same properties. We can call them the projectile and the target. The target is initially at rest and its state is represented by point *O* in the diagram. In the same diagram, the state of the projectile is represented by point *A*. After impact, the state (represented by point *B*) is spread in both solids. In the projectile, the compression wave reaches the extremity and is reflected as an expansion wave (as seen in section 2.2.2), and the state behind the latter is represented by point *C*. This expansion wave makes contact after time *2Li/Ci*. This produces a diffraction and the states B and C pass to state E according to the rules as shown in Figure 2.2 and Table 2.1. At the right extremity of the target, the compression wave is reflected and generates a retrogressive expansion wave. The target extremity passes into the state represented by point *D*. Finally, when the retrogressive expansion wave resulting from the reflection meets the progressive expansion wave from the states represented by *E* and *D*, we move on to the state represented by point *G*. In this latter state, the target material is under tension. This is a situation where there is a risk of cracking, i.e. tensile rupture. This risk exists for materials with a tensile strength lower than that in compression. Thus, the target can withstand, without damage, the state represented by B, but break before reaching state G.

It is interesting to note that to determine motion after a shock leads to a result different from that commonly accepted from basic mechanical considerations, with the assumption of rigid body.

The basic situation is shown in Figure 2.13. A mass m_1 of velocity V impacts a mass m_2 at rest. After the impact, masses m_1 and m_2, respectively, have velocities V_1 and V_2. Between the two instants, we can express conservation of momentum and, assuming (wrongly) that the shock occurred without energy dissipation, conservation of kinetic energy [2.43]:

$$\begin{aligned} m_1 V &= m_1 V_1 + m_2 V_2 \\ \frac{1}{2} m_1 V^2 &= \frac{1}{2} m_1 V_1^2 + \frac{1}{2} m_2 V_2^2 \end{aligned} \qquad [2.43]$$

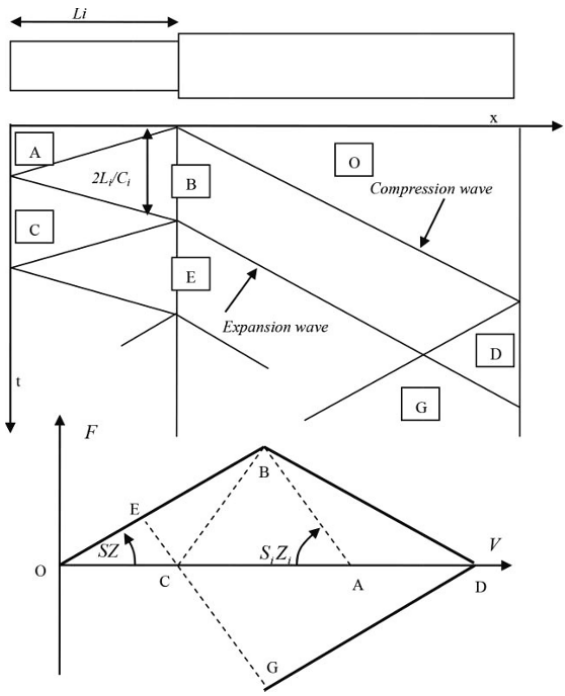

Figure 2.12. *Shock of two solids, course diagram of waves generated by shock and diagram of states of matter in the solid (the solid line is relative to the target and the projectile line is dashed)*

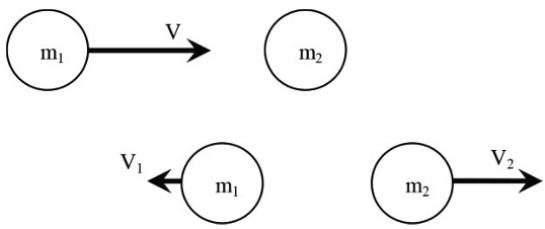

Figure 2.13. *Shock of two solids, situations before and after impact*

We then obtain velocities after the shock, given as [2.44]:

$$V_1 = \frac{\alpha - 1}{1 + \alpha} V \qquad V_2 = \frac{2\alpha}{1 + \alpha} V \qquad \alpha = \frac{m_1}{m_2} \qquad [2.44]$$

Unfortunately, this "simple" physics translates into reality with difficulty. It can only be confirmed by experiments in rare cases, such as a bowler's "tile" ($\alpha = 1 \quad V_1 = 0 \quad V_2 = V$). Momentum is always conserved but energy balance must include the strain energy of the solid (elastic energy) and, optionally, the dissipated energy if there is damage, breakage or yielding of solids. However, except in the case of two identical solids where, through geometrical singularity, elastic strain energy is zero after impact, this elastic strain energy is not negligible compared to kinetic energy, regardless of the stiffness of the material. To show this, in Figure 2.14, we consider the example of impact of two rods of the same material and same diameter. The target is double the length of the projectile. A Lagrange diagram shows the course of the waves and a state diagram specifies the velocities and stresses. For energy balance, the kinetic energy and the elastic strain energy per unit length must be specified [2.45]:

$$dE_C = \frac{1}{2}\rho S V^2$$

$$dE_e = \frac{1}{2}\frac{\sigma^2}{E} S \left(= \frac{1}{2}\rho S V^2 \; if \; \sigma = \sqrt{E\rho}\, V \right) \qquad [2.45]$$

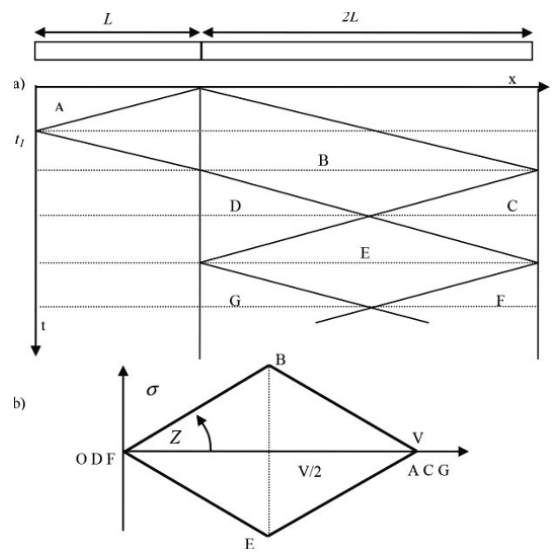

Figure 2.14. *Shock of two solids: a) wave course diagram; b) state matter diagram*

Energies calculated at different times are presented in Table 2.2. We note that there is conservation of total energy and momentum. After impact, the target's elastic energy has the same value as the kinetic energy, the latter being regardless of the Young's modulus of the material. We also note that after impact, the projectile is stationary $V_1 = 0$ and the target moves at an average velocity $V_2 = V/2$. Experiments confirm this result. The conservation of kinetic energy hypothesis would have led to the incorrect estimates $V_1 = -V/3$ and $V_2 = 2V/3$.

	Projectile		Target	
	E_c	E_e	E_c	E_e
$t = 0$	$\frac{1}{2}\rho SLV^2$	0	0	0
t_1	$\frac{1}{8}\rho SLV^2$	$\frac{1}{8}\rho SLV^2$	$\frac{1}{8}\rho SLV^2$	$\frac{1}{8}\rho SLV^2$
$2t_1$ and so on	0	0	$\frac{1}{4}\rho SLV^2$	$\frac{1}{4}\rho SLV^2$

Table 2.2. *Kinetic and elastic energies involved during a collision*

2.3.2. *Successive shocks*

It is possible that the target is composed of several layers of materials. The stress wave generated by an impact will be diffracted at each change of material properties. The state diagram is used to determine the conditions of this diffraction. Let us consider the case of a target consisting of two solids (Figure 2.15). The state diagram is shown in Figure 2.16. The behavior of solid 1 is shown by a thick line, solid 2 by a thin line and solid 3 by a dotted line. Solid 2, launched at velocity V_2, will hit solid 1 that is itself in contact with solid 3. After the impact of solid 2 on solid 1, the state is denoted as A in the state diagram, and after transition of the shock wave from solid 1 to solid 3, the state is denoted as B. States A and B can be determined from the known impedances Z_1, Z_2 and Z_3. Figure 2.16

shows two possible cases according to the respective impedances of solids 1 and 3.

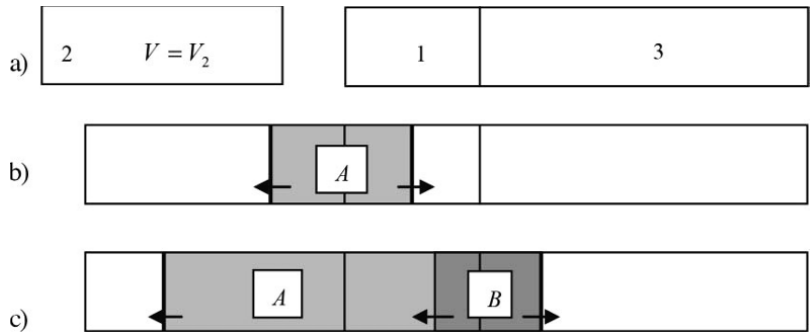

Figure 2.15. *Successive shocks in three solids: a) situations before impact; b) after impact of solid 1 on solid 2; c) after the passage of the compression wave in solid 3*

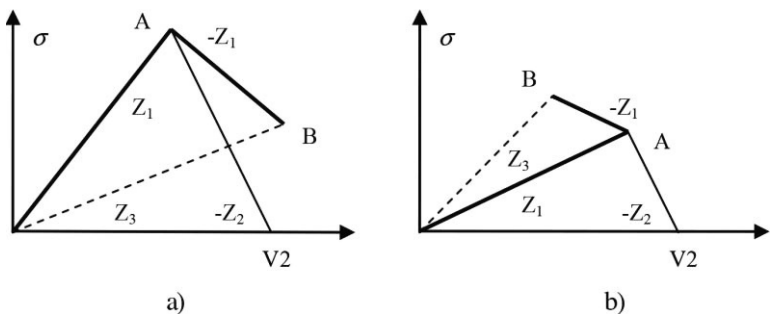

Figure 2.16. *State diagram in three solids: a) where solid 1 has higher impedance than solid 3; b) where it has lower impedance*

2.3.3. *Wave trapping and cracking*

An impact such as dynamic loading generates a compression wave such as the one discussed earlier. The duration of this compression corresponds to a round trip of the projectile waves. Then, if the impactor and target have the same impedance, the stress level is reset to 0 and a discharge wave propagates through the material. Moreover, when the compression wave reaches a face free of stresses, an

expansion wave propagating in the opposite direction is issued to comply with the condition of 0 stress at the extremity. The meeting of these two expansion waves leads to a tensile stress, the amplitude of which is equal to that of the initial compressive wave. From this general case, we evoke two particular situations. If the target consists of two solid multiples, and the meeting of the two expansion waves occurs at the exact location of the interface between the two solids, then there will be a separation of the two solids and no stress will be propagated (Figure 2.17).

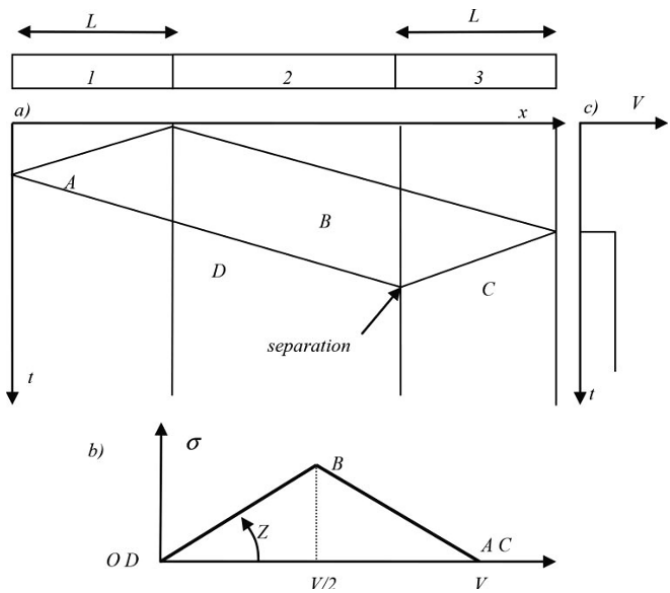

Figure 2.17. *Successive shocks in three solids case of the "trapping wave": a) course diagram; b) state diagram in three solids; c) velocity of the right side of solid 3*

In practice, this situation may be desirable. It is, particularly, observed if the solid at the free extremity has the same dimensional and material characteristics as the impactor. It is called a "trapping wave" and leaves at a velocity equal to that of the impactor, which itself remains stationary.

Another situation is rupture by cracking. Rupture by cracking occurs in materials with a tensile strength lower than compressive strength, such as in concrete. If two expansion waves meet, the material becomes tensioned (for example Figures 2.12 and 2.14). The intensity of this tension cannot be supported by the material and a rupture occurs. Figure 2.18 shows this situation.

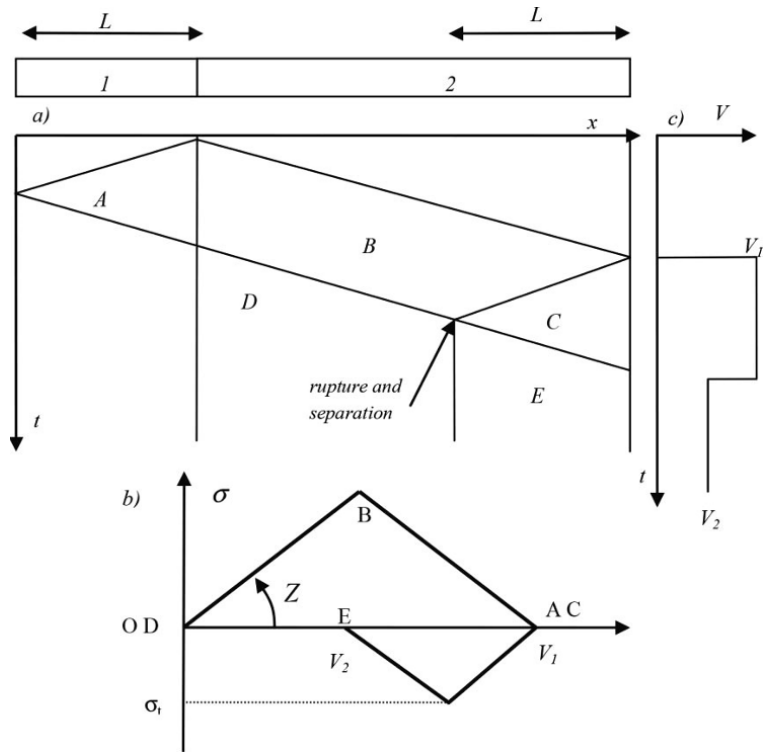

Figure 2.18. *Shocks of two solid with rupture by tension through cracking: a) course diagram; b) states in three solids; c) velocity of the right side of solid 2*

Upon arrival of the compression wave on the free surface, the latter gains a velocity equal to the velocity V_1 of impact (point C in Figure 2.18(b)). At the intersection of the two expansion waves, stress decreases up to the tensile strength and then returns to zero (point E; if there were no rupture, E would return to O). The right side gains the

velocity V_2. Measurement of velocity on the front of the ejected part, more specifically the "velocity jump", can be used to estimate the tensile strength (formula [2.46] called the "Novikov formula"):

$$\sigma_t = \frac{1}{2}(V_1 - V_2)\sqrt{E\rho} \qquad [2.46]$$

2.4. Shocks on viscoelastic solids

The study of viscoelastic solids is of practical significance. Many materials have more or less significant viscoelastic properties. In some cases, they are even used intentionally for absorption. In this section, some basic results on the behavior of shocks on viscoelastic solids are given [KOL 56, HUN 60, GOL 01].

2.4.1. *Conditions at the interface*

At the interface between two solids, velocity and stress equalities are imposed on the two solids in contact. To determine the states that will be generated during the impact of the two solids, we must know the relationship between velocity and stress at the edge of the solids. For elastic solids, the latter relationship is linear and the ratio of velocity to stress is called impedance. For viscoelastic solids, this relationship is less straightforward. If displacements are described as harmonics, they are expressed using the Fourier transformation [2.47]:

$$U^*(x,\omega) = A\, e^{\alpha x + i(kx - \omega t)} \qquad [2.47]$$

We can deduce velocity and strain as [2.48]:

$$V^*(x,\omega) = -i\omega\, U^*(x,\omega) \quad \varepsilon^*(x,\omega) = (\alpha + ik)\, U^*(x,\omega) \qquad [2.48]$$

Using the behavior relationship with a complex modulus, we obtain the relationship between stress and velocity at the extremity of the solid (x = 0) [2.49]:

$$\sigma^*(0,\omega) = \frac{(-k + i\alpha)\, E^*}{\omega} V^*(0,\omega) \qquad [2.49]$$

Using the Laplace transformation, it is also possible to formulate the operational images of these conditions at one extremity. The image of the equation of motion (and its solution) is shown in [2.50] (the one-dimensional solid is represented by the "half-line" of origin 0 and positive abscissa; conditions at the extremity are written as $x = 0$):

$$\frac{\partial^2 \bar{U}}{\partial x^2} = \frac{\rho s^2}{\bar{E}(s)} \bar{U} \quad \bar{U}(x,s) = A(s)\, e^{-sx\sqrt{\frac{\rho}{\bar{E}(s)}}} \qquad [2.50]$$

The operational image of behavior is written as [2.51]:

$$\sum_{i=1}^{n} s^i a_i \,\bar{\sigma} = \sum_{i=1}^{n} s^i E_i \,\bar{\varepsilon} \quad \bar{\sigma} = \bar{E}(s)\bar{\varepsilon} \qquad \bar{E}(s) = \frac{\sum_{i=1}^{n} s^i E_i}{\sum_{i=1}^{n} s^i a_i} \qquad [2.51]$$

We can deduce velocity, strain and stress at the origin as [2.52]:

$$\bar{V}(0,s) = s\bar{U}(0,s) \qquad \bar{\varepsilon}(0,s) = \left(\frac{\partial \bar{U}}{\partial x}\right)_0 = -s\,A(s)\sqrt{\frac{\rho}{\bar{E}(s)}} \qquad [2.52]$$
$$\bar{\sigma} = \bar{E}(s)\bar{\varepsilon} = -sA(s)\sqrt{\rho \bar{E}(s)}$$

Then, the relationship between stress and velocity at the origin is [2.53]:

$$\bar{\sigma}(s) = -\bar{V}(s)\sqrt{\rho \bar{E}(s)} \qquad [2.53]$$

This relationship can be explained with particular models.

2.4.1.1. *Kelvin–Voigt*

The relationship at the interface for a Kelvin–Voigt solid is written in the operational form [2.54]:

$$\bar{V}(s) = -\frac{\bar{\sigma}(s)}{\sqrt{\rho(E + \eta s)}} \qquad [2.54]$$

This gives the condition [2.55] as time functions of stress and velocity (* denoting the convolution product):

$$V(t) = -\frac{\sigma(t)}{\sqrt{\rho\eta}} * \frac{e^{-Et/\eta}}{\sqrt{\pi t}} \qquad [2.55]$$

If the solid is loaded at its extremity, by applying a compressive stress of intensity σ_0, the velocity of this extremity is given by formula [2.56] (*erf* is the "error" function):

$$\bar{V}(s) = \frac{\sigma_0}{s\sqrt{\rho(E+\eta s)}} \quad V(t) = \frac{\sigma_0}{\sqrt{\rho E}}\, erf\left(\sqrt{\frac{Et}{\eta}}\right) \qquad [2.56]$$

This result can be formulated with dimensionless variables [2.57]:

$$v = \frac{V\sqrt{\rho E}}{\sigma_0} = erf\sqrt{\tau} \quad \left(\tau = \frac{Et}{\eta}\right) \qquad [2.57]$$

If the solid is solicited at its extremity, with an imposed velocity V_0, the stress at that extremity is given by formula [2.58]. This may correspond to a shock against a very rigid obstacle:

$$\bar{\sigma}(s) = \frac{V_0}{s}\sqrt{\rho(E+\eta s)}$$
$$\sigma(t) = V_0\sqrt{E\rho}\left(erf\sqrt{\frac{Et}{\eta}} + \sqrt{\frac{\eta}{Et}}\frac{e^{-Et/\eta}}{\sqrt{\pi}}\right) \qquad [2.58]$$

The same result can be formulated with dimensionless variables [2.59]:

$$S = \frac{\sigma}{V_0\sqrt{E\rho}} = erf\sqrt{\tau} + \frac{e^{-\tau}}{\sqrt{\pi\tau}} \qquad [2.59]$$

Time evolutions in dimensionless velocity and stress as a function of dimensionless time τ are shown in Figure 2.19.

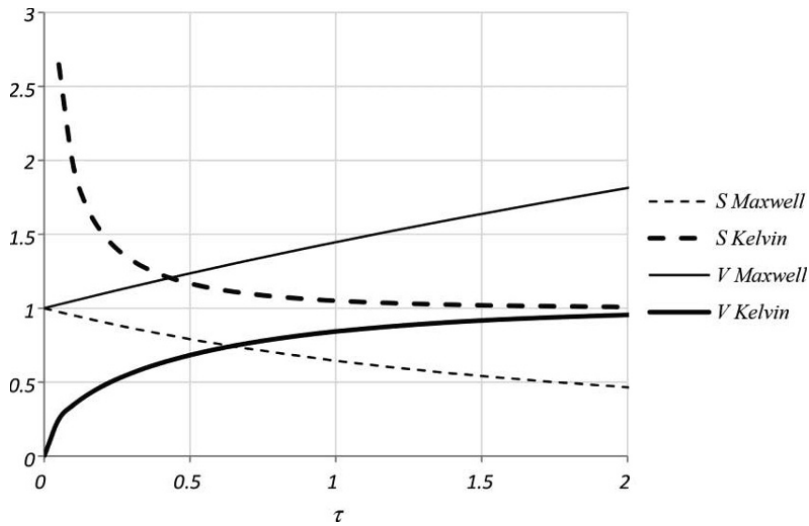

Figure 2.19. *Evolutions at the extremity of a viscoelastic solid: solid line (V Maxwell, V Kelvin): time evolution of dimensionless velocity at the extremity of a solid where a stress slot is imposed; dashed line (S Maxwell, S Kelvin): time evolution of dimensionless stress at the extremity of a solid where a velocity slot is imposed*

2.4.1.2. *Maxwell*

The relationship at the interface for a Maxwell solid is written in the operational form [2.60]:

$$\bar{\sigma}(s) = -\bar{V}(s)\sqrt{\rho E}\sqrt{\frac{s}{s + E/\eta}} \qquad [2.60]$$

This gives condition [2.61] on time functions of stress and velocity (I_0 and I_1 are modified Bessel functions of the first kind of order 0 and 1):

$$V(t) = -\frac{\sigma(t)}{\sqrt{\rho E}} * \frac{E}{2\eta} e^{-Et/2\eta}\left(I_0\left(\frac{Et}{2\eta}\right) + I_1\left(\frac{Et}{2\eta}\right)\right) \qquad [2.61]$$

If the solid is solicited at its extremity, by applying a compressive stress of intensity σ_0, the velocity of this extremity is given by formula [2.62]:

$$\bar{V}(s)=\frac{\sigma_0}{s\sqrt{\rho E}}\sqrt{\frac{s+E/\eta}{s}}$$
$$V(t)=\frac{\sigma_0}{\sqrt{\rho E}}e^{-Et/\eta}\left(\left(\frac{Et}{\eta}+1\right)I_0\left(\frac{Et}{2\eta}\right)+\frac{Et}{\eta}I_1\left(\frac{Et}{2\eta}\right)\right) \quad [2.62]$$

This can be formulated with dimensionless variables [2.63]:

$$v=\frac{V\sqrt{\rho E}}{\sigma_0}=e^{-\tau}\left((\tau+1)I_0\left(\frac{\tau}{2}\right)+\tau\, I_1\left(\frac{\tau}{2}\right)\right) \quad [2.63]$$

If the solid is solicited at its extremity by an imposed velocity V_0, the stress at that extremity is given by formula [2.64]:

$$\bar{\sigma}(s)=\frac{V_0\sqrt{\rho E}}{\sqrt{s(s+E/\eta)}} \qquad \sigma(t)=V_0\sqrt{\rho E}\; e^{-Et/2\eta}\; I_0\left(\frac{Et}{2\eta}\right) \quad [2.64]$$

In the dimensionless form, this becomes [2.65]:

$$S=\frac{\sigma}{V_0\sqrt{\rho E}}=e^{-\tau}I_0\left(\frac{\tau}{2}\right) \quad [2.65]$$

Time evolutions in velocity and stress as a function of dimensionless time τ are shown in Figure 2.19. Note that the initial behavior of the Maxwell solid is that of an elastic body ($v = 1$, $S = 1$) and tends toward a fluid. A Kelvin–Voigt solid has a very rigid initial behavior and tends toward an elastic behavior.

2.4.2. *Impact of an elastic solid on a viscoelastic solid*

Let us consider the impact of an elastic solid, featuring E_e and ρ_e, arriving with velocity V_i at a viscoelastic solid. The shock conditions [2.40] and [2.41] are reflected in operational form by formulas [2.66]:

$$\begin{cases}\bar{\sigma}=\sqrt{\rho_e E_e}\left(\bar{V}_i-\bar{V}\right)\\ \bar{\sigma}=\bar{V}\sqrt{\rho\bar{E}}\end{cases} \qquad \bar{\sigma}=\frac{V_i\sqrt{\rho_e E_e}\sqrt{\rho\bar{E}}}{s\left(\sqrt{\rho_e E_e}+\sqrt{\rho\bar{E}}\right)} \quad [2.66]$$

We can explain the solution in a Kelvin–Voigt solid. We denote the impedance ratio of the elastic solid to the viscoelastic solid as z:

$$\bar{\sigma} = \frac{V_i \sqrt{\rho_e E_e}\sqrt{\rho(E+\eta s)}}{s\sqrt{\rho_e E_e} + s\sqrt{\rho(E+\eta s)}} \qquad z = \sqrt{\frac{E_e \rho_e}{E\rho}} \qquad [2.67]$$

The stress at the interface is formulated with the dimensionless parameters [2.68]:

$$S = \frac{\sigma}{V_i\sqrt{E_e\rho_e}} = H(t) + \frac{z}{z-1}\left(e^{\tau(z-1)}\,erfc\sqrt{\tau z} - 1\right) + \frac{\sqrt{z}}{z-1}\,erf\sqrt{\tau} \qquad [2.68]$$

This result is shown in Figure 2.20. Impact stress is obtained from the shock of elastic solid upon a rigid body. Stress tends toward the value that would give formula [2.41] if there were no viscosity.

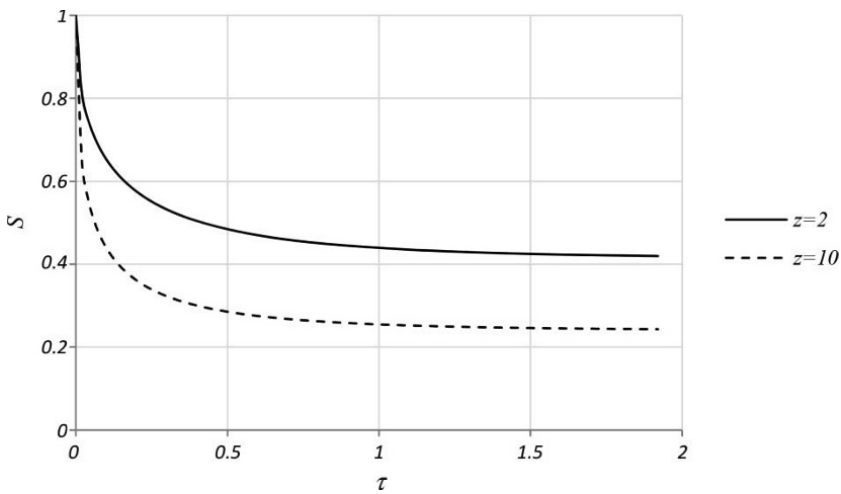

Figure 2.20. *Evolution of stresses at the interface during impact of an elastic solid on a viscoelastic solid (Kelvin Voigt) for two impedance contrasts*

2.4.3. *Shock of two viscoelastic solids*

The case of two viscoelastic solids is not generally easy to explain. Let us take the example of two identical Kelvin–Voigt solids. If a stationary solid is hit by another solid arriving at velocity V_i, from relationship [2.41], stress at the interface is formulated by operation [2.69]:

$$\bar{\sigma} = \frac{V_i \rho (E + \eta s)}{2s\sqrt{\rho (E + \eta s)}} \qquad [2.69]$$

The time formula is given by formula [2.70]. This expression is similar to that obtained with an imposed velocity:

$$\sigma(t) = \frac{V_i \sqrt{E\rho}}{2}\left(erf\sqrt{\frac{Et}{\eta}} + \sqrt{\frac{\eta}{Et}}\frac{e^{-Et/\eta}}{\sqrt{\pi}} \right) \qquad [2.70]$$

2.4.4. *Propagation of shock in a Maxwell solid*

The propagation of a wave in a viscoelastic solid is not generally easy to explain. An interesting case (that will be discussed in Chapter 3) is that of the propagation of a stress wave generated by an imposed velocity at one end in a Maxwell solid. The wave equation in a Maxwell solid is recalled in [2.71]. Displacement or stress formulas are similar:

$$\frac{\partial^3 U}{\partial x^2 \partial t} = \frac{\rho}{\eta}\frac{\partial^2 U}{\partial t^2} + \frac{\rho}{E}\frac{\partial^3 U}{\partial t^3} \qquad [2.71]$$

If the solid is geometrically modeled as a "half-line" with its origin at 0 and positive abscissa, the solution is written in operational form [2.72]. The term containing the exponential of x does not exist due to the zero stress condition when x tends to infinity:

$$\bar{\sigma}(x,s) = D(s)\, e^{-\frac{x}{C_0}\sqrt{s(s+E/\eta)}} \qquad [2.72]$$

The imposed velocity condition is [2.73]:

$$\bar{V}(0,s) = -\frac{V_0}{s} \qquad [2.73]$$

Given the behavior relationship, we can entirely explain the stress image [2.74]:

$$\bar{\sigma}(x,s) = \frac{V_0\sqrt{\rho E}}{\sqrt{s(s+E/\eta)}}\, e^{-\frac{x}{C_0}\sqrt{s(s+E/\eta)}} \qquad [2.74]$$

The stress field is then explained by [2.75]:

$$\sigma(x,t) = V_0\sqrt{\rho E}\; e^{-Et/2\eta}\; I_0\left(\frac{E}{2\eta}\sqrt{t^2-\frac{x^2}{C_0^2}}\right) H\left(t-\frac{x}{C_0}\right) \qquad [2.75]$$

This field can be expressed in terms of dimensionless variables [2.76]:

$$S = \frac{\sigma}{V_0\sqrt{\rho E}} = e^{-\tau/2}\; I_0\left(\frac{1}{2}\sqrt{\tau^2-X^2}\right) H(\tau - X) \quad \left(X = \frac{xE}{C_0\eta}\right) \qquad [2.76]$$

Figure 2.21 shows the shape of the stress field at different times. The stress discontinuity amplitude decreases exponentially with distance from the point of impact.

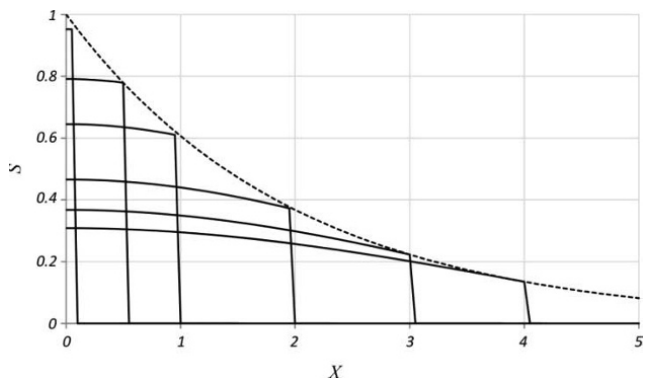

Figure 2.21. *Spatial distribution of stresses in a Maxwell solid at different times after impact (τ = 0.1, 0.5, 1, 2, 3, 4); dotted line: envelope of successive positions on the jump*

Chapter 3

Waves and Shocks in a Nonlinear Medium

The purpose of this chapter is to show how nonlinear and irreversible behaviors of materials that are highly stressed during impacts have consequences on movements and waves in solids.

3.1. Irreversible phenomena

3.1.1. *Impact velocity*

The stress generated in a solid upon impact depends on impact velocity. According to the considered phenomena, this velocity can vary from a few centimeters per second to a few kilometers per second. Mechanical and thermodynamic phenomena occurring in materials can be different depending on the range of impact velocities. Table 3.1 presents the ranges of impact velocity. Two dimensionless parameters characterize the relative kinetic energy (π_1) and relative stress (π_2) (the values were calculated using average values for building materials such as steel or concrete). Accidental shocks are in the range of 1–50 m/s, which is sufficient to exceed the yield strength of building materials. Impact velocities above the kilometer per second are related to projectiles of weapons. Hypervelocity shocks may involve impacts on satellites in space. Impact velocity is greater than wave velocity in the material and, in this case, the study of

material behavior is beyond the scope of this book, which is limited to accidental shocks.

$\pi_1 = \frac{\rho V^2}{\sigma_e}$	$\pi_2 = \frac{V\sqrt{E\rho}}{\sigma_e}$	V (m/s)	Type of shock
10^{-5}	5×10^{-2}	5×10^{-1}	Quasi-static
10^{-3}	5×10^{-1}	5	Slow shock
10^{-1}	5	5×10^{1}	Shock (accidental)
10	5×10^{1}	5×10^{2}	Fast shock (weapons)
10^{3}	5×10^{2}	5×10^{3}	Hypervelocity impact

Table 3.1. *Range of impact velocities and magnitudes of dimensionless parameters for concrete or steel solids*

3.1.2. *Load paths*

Impacts of solids generate very high stresses, as has been discussed in Chapter 2. These stress states can reach and exceed the limits of the elastic or viscoelastic behavior of the material. Figure 3.1 shows the different stress states leading to irreversible phenomena in material behavior. The different paths corresponding to different areas of load are schematically shown in terms of two invariants of the stress tensor: pressure and the equivalent von Mises stress (the dotted line shows the limits of the elastic domain). Yield can be achieved in three different areas, each corresponding to a type of irreversible mechanism in the behavior of the material. Fissures and fractures can occur in extension (A), especially when cracking. In other areas, slipping phenomena can occur under high shear stress (B). A more specific characteristic of impact loads is the generation of high pressure to levels that are rarely achieved under static loading, which can irreversibly compact the material (C). These three types of irreversible behavior are well known and specific models exist. Breakage in extension can be brittle [BUI 78] or more or less ductile. Damage models can be used to describe material degradation under this type of loading [LEM 09]. Description of the slipping phenomena is usually done in the context of plasticity or viscoplasticity models. Finally, the phenomenon of compaction modeling can use the formalism of

plasticity, with volumetric plastic strains, or use more specific formalisms. We will discuss the models associated with these mechanisms and see their consequences in the movements of such waves in solids.

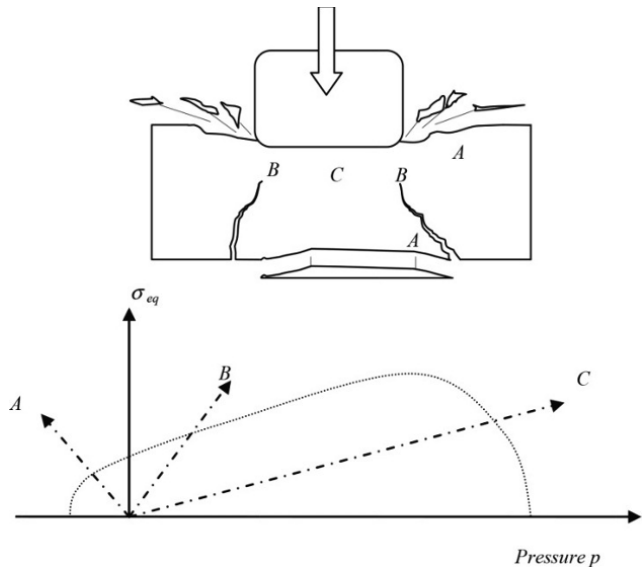

Figure 3.1. *Different areas in a solid support impact and schematic loading paths, represented in terms of two invariants (p and σ_{eq})*

3.1.3. *Strain velocity*

Another characteristic of impacts is to produce dynamic loading and thus impose a certain strain velocity on the material. The question may arise as to whether the nonlinear behavior and strength of the material show dependence on the rate of strain. This question makes sense because dependence on strain rate in linear viscoelastic behavior has been observed. Experimental observations often point in this direction. The apparent strength of many materials, metal or concrete, depends on the strain rate [TAN 92, BIS 91]. Experimental results relative to resistance, in uniaxial stress state, are usually represented by a graph, as a function of strain rate on a logarithmic scale. It appears that at certain velocity ranges, strength varies nearly linearly with the logarithm of the strain rate. This finding suggests empirical

models. Strength appears to be related to strain rate by a relation of type [3.1]:

$$\sigma = K\left(\dot{\varepsilon}\right)^{\beta} \text{ or } \beta = \left(\frac{\partial \sigma}{\partial \ln \dot{\varepsilon}}\right) \qquad [3.1]$$

We can provide a physical basis to this observation. In crystalline materials, plastic strain has its origin in the movement of dislocations. For metals, in conditions of high strain rate, flow is sensitive to temperature and strain rate, and this sensitivity can be expressed by an Arrhenius-type law [3.2]:

$$\dot{\varepsilon}_p = \dot{\varepsilon}_0 \, e^{-\frac{\Delta G}{kT}} \qquad [3.2]$$

$\Delta G(\tau, T)$ is the change in Gibbs free energy and $\dot{\varepsilon}_0$ is a reference strain rate. The Gibbs free energy depends on the shear stress τ according to expression [3.3]:

$$\Delta G = \Delta G_0 - \upsilon\left(\tau - \tau_a\right) - (\upsilon \text{ is an activation volume}) \qquad [3.3]$$

Expression of shear stress becomes [3.4]:

$$\tau = \tau_a + \Delta G_0 + \left(\frac{kT}{\upsilon}\right) \ln\left(\frac{\dot{\varepsilon}_p}{\dot{\varepsilon}_0}\right) \qquad [3.4]$$

In a situation of uniaxial stress, $\sigma = \tau\sqrt{3}$ and we obtain the approximate expression [3.5]:

$$\left(\frac{\partial \sigma}{\partial \ln \dot{\varepsilon}_p}\right)_{T,\varepsilon_p} \approx \frac{4kT}{\upsilon} \qquad [3.5]$$

In a fairly general manner and in order to cover a wide range of strain rates, we often use the Cowper–Symonds model [3.6] for metal materials, which expresses the ratio of the resistance at a certain rate of strain relative to static resistance:

$$Ad = \frac{\sigma_d}{\sigma_s} = 1 + \left(\frac{\dot{\varepsilon}}{C}\right)^{1/P} \qquad [3.6]$$

For structural steel, the parameters of the Cowper–Symonds model have the average values of $C = 40\ s^{-1}$ and $P = 5$. The change in relative resistance as a function of the strain rate is shown in Figure 3.2.

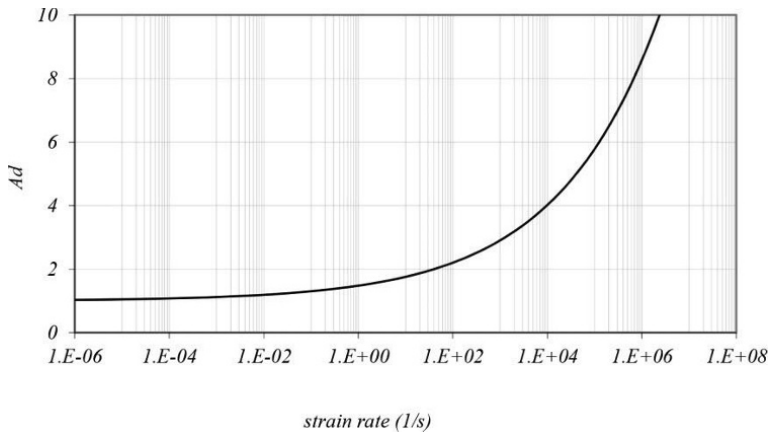

Figure 3.2. *Change in the apparent relative resistance of structural steel relative to strain rate*

The approach used for metals can be extended to other materials. For example, for polymers, a multiplicative model "power law" has been proposed, which takes into account the role of temperature [3.7]:

$$\sigma = A\ \varepsilon^n\ \dot{\varepsilon}^m\ e^{w(T-T_0)^\alpha} \qquad [3.7]$$

For brittle or quasi-brittle materials such as concrete, it seems that better phenomenological descriptions are obtained by taking into account the inertial effects linked to cracking and scaling effects. Modeling can be based on the heterogeneous and random nature of the material on a microscopic level [SUA 84, DEN 00, LAM 07].

3.1.4. *Shear and plasticity*

3.1.4.1. *Plasticity and dynamics*

The use of elastoplastic behavior models for materials is very common for the calculation of structures. These models are based on

the definition of a standard yield or plastic flow threshold. This criterion is a function of stress (more precisely, its invariants) and, possibly, other internal parameters characterizing the state of the material. Plastic flow is then defined by the laws of evolution linking an increment of plastic strain to an increment of stress [LEM 09, FRA 95]. For the remainder of the study, we only consider simple models that we consolidate into two categories. The Tresca and von Mises criteria do not involve pressure (mean stress) and are instead used for metallic materials. Coulomb and Drücker Prager criteria [DRU 52] are used for "cohesive and friction" materials such as concrete or rock [DAR 95, MAZ 04]. The formulas of the four criteria are presented in Table 3.2.

Tresca criterion	Coulomb criterion $\left(\sigma_i > \sigma_j\right)$
$\sup_{i \neq j} \left\lvert \sigma_i - \sigma_j \right\rvert - Y = 0$	$\sup_{i \neq j} \left\{ \sigma_i \left(1 + \sin\varphi\right) - \sigma_j \left(1 - \sin\varphi\right) - 2C\cos\varphi \right\} = 0$
von Mises criterion	Drücker Prager criterion
$\sigma_{eq} - Y = 0$	$\sigma_{eq} + \alpha\left(trace\underline{\underline{\sigma}} - Y_h\right) = 0$

Table 3.2. *Plasticity criteria. Formulas as a function of the main stresses for the Tresca and Coulomb criteria, and as a function of the equivalent von Mises stress and the first invariant for the Drücker Prager and von Mises criteria*

Many authors have tried to take into account the experimental observation mentioned above, noting that resistance, or more precisely the maximum stress reached during a test, was dependent on strain rate. We show formula [3.8], following the Holmquist, Johnson and Cook model [HOL 93], involving strain rate in the expression of yield point (ABCN are constants and D is a damage parameter). In this scalar expression, stress and strain are taken in the sense of von Mises criterion. Variants of this model exist [STE 89, MIM 96]:

$$\frac{\sigma_{eq}}{\sigma_s} = \left(A\left(1 - D\right) + B\left(\frac{p}{\sigma_s}\right)^N \right)\left(1 + C\ln\left(\frac{\dot{\varepsilon}}{\dot{\varepsilon}_0}\right)\right) \qquad [3.8]$$

3.1.4.2. *Viscoplasticity*

Experimental observations suggest that we can write stress as the sum of a strain function, which reflect the quasi-static behavior, and a term dependent on the rate of the plastic strain [3.9]:

$$\sigma = f(\varepsilon) + C\ln\left(1 + b\dot{\varepsilon}_p\right) \qquad [3.9]$$

This amounts to considering that the plastic strain depends on the difference between the current stress and the stress corresponding to static evolution. From the above formula, we get expression [3.10]:

$$\dot{\varepsilon}_p = \frac{1}{b}\left(e^{\left(\frac{\sigma - f(\varepsilon)}{C}\right)} - 1 \right) \qquad [3.10]$$

More generally, we can write that plastic strain rate is a function of the state of stress and strain, which is the definition of viscoplasticity [3.11]:

$$E\dot{\varepsilon}_p = g(\sigma,\varepsilon) \quad \dot{\varepsilon}_p = \dot{\varepsilon} - \frac{\dot{\sigma}}{E} \quad \rightarrow \quad \dot{\sigma} = E\dot{\varepsilon} - g(\sigma,\varepsilon) \qquad [3.11]$$

A fairly simple viscoplastic model, which will be discussed later, is the Bingham model, represented by a rheological model in Figure 3.3 and corresponding to formula [3.12]:

$$\dot{\sigma} = E\dot{\varepsilon} - \frac{E}{\eta}(\sigma - Y) \qquad [3.12]$$

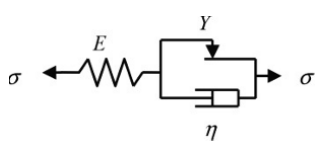

Figure 3.3. *Representation of viscoplastic rheological Bingham model*

In these scalar expressions, stress and strain are taken in the sense of von Mises criterion. More generally, the three-dimensional

aspect can be obtained from a formula based on a dissipation potential [3.13]:

$$\dot{\underline{\underline{\varepsilon}}}_p = \frac{\partial \varphi}{\partial \underline{\underline{\sigma}}} \qquad [3.13]$$

Many authors have rigorously formalized viscoplastic behavior laws [MAL 51, PER 63, BOD 75]. For metallic materials, the plastic strain rate is often "proportional" to deviatoric stress, as in Norton's viscoplastic law [3.14]:

$$\dot{\underline{\underline{\varepsilon}}}_p = \frac{3}{2\sigma_{eq}} \left(\frac{\sigma_{eq} - Y}{k} \right)^N \underline{\underline{S}} \qquad [3.14]$$

3.1.5. *Behavior under high pressure*

Shocks in solids can generate very high pressure levels (several hundred megapascals). These levels can result in irreversible volume changes in materials, which we call compaction. This situation is rather rare in quasi-static loading, as many models representating this phenomenon have been developed in the scope of dynamic applications. One behavior construction method is to separate the stress and strain tensors into their spherical and deviatoric parts [3.15]:

$$\begin{aligned} \underline{\underline{\sigma}} &= -p\,\underline{\underline{1}} + \underline{\underline{S}} \qquad \left(\sigma_{ij} = -p\,\delta_{ij} + S_{ij}\right) \\ \underline{\underline{\varepsilon}} &= \frac{\theta}{3}\underline{\underline{1}} + \underline{\underline{e}} \qquad \left(\varepsilon_{ij} = \frac{\theta}{3}\delta_{ij} + e_{ij}\right) \end{aligned} \qquad [3.15]$$

We can then separately define the relationship between the spherical parts (pressure and volume change), which is called isotropic behavior, and the relationship between the deviatoric parts, as mentioned in the previous paragraph. Of course, there can be coupling between these two relationships. This approach to describing behavior has a lot of significance if we consider that there is no coupling between the two terms of volume and deviatoric behavior, as formulated in [3.16] (the second expression often taking a scalar form

with the use of the equivalent von Mises stress). This assumption is realistic for metals since the deviatoric behavior, plasticity, is independent of pressure and does not generate volume changes:

$$p(\theta) \quad \text{and} \quad \underline{\underline{S}}\left(\underline{\underline{e}}\right) \qquad [3.16]$$

However, this hypothesis of decoupling of the two parts of behavior is not valid for geomaterials and materials that contain porosity, such as concretes. First, the plastic flow threshold depends on pressure and flow that causes volume change; second, the presence of shear promotes compaction. Modeling irreversible volume phenomena can use the formalism of plasticity models. One approach is to consider yield surfaces, closed on the hydrostatic axis, and formulate the laws of evolution including volumetric plastic strains. This method was used to model concrete under high pressure with a Willam–Warnke model [HAN 85] or Gurson model [GUR 77, BUR 01]. A second method is to consider two threshold surfaces, one for the slipping mechanism and the other for the compaction mechanism. This is the case of the "Cap" surface model [SAN 76]. The two plasticity mechanisms may be interdependent [LOR 87].

For very high intensity dynamic loading, for example when solid explosives come into contact, the main element of behavior is the relationship between pressure and volume change. This means that the magnitude of shear stress is small compared to that of pressure. If we only consider pressure, we must use a hydrodynamic model. The volumic relationship of behavior can be confused with law of state. This may consist of the relationship between pressure and porosity, and possibly other thermodynamic variables such as temperature and phase states [3.17]:

$$p(\mu, T, ...) \qquad \mu = \frac{\rho}{\rho_0} - 1 \qquad [3.17]$$

The relationship between pressure and density is often written in polynomial. In numerical codes, an example of this kind of law is the "p-α model", α being a porosity index [HER 69]. We will revisit this notion of law of state to describe the compaction of a material by shock wave.

3.2. Adiabatic shear

3.2.1. *Dynamic and thermal*

When solids are quasi-statically loaded, it is customary to consider that during loading the material undergoes an isothermal thermodynamic transformation. Indeed, irreversible mechanical phenomena cause heat, but it is assumed that heat is diffused in this material fast enough to maintain the isothermal assumption. It is assumed that the characteristic time for heat diffusion in a solid is very short compared to the characteristic time of mechanical stress. If strain rate increases, this assumption may be impaired. To decide, we consider the heat equation in a solid [3.18]. In this equation, the heat source is the energy dissipated by the irreversible phenomena from the mechanical behavior of the material. Mean values for common building materials are presented in Table 3.3:

$$\lambda \Delta T = \rho C \frac{\partial T}{\partial t} - \varphi \qquad [3.18]$$

where

– T is the temperature;

– λ is the thermal conductivity;

– ρ is the density;

– C is the specific heat (notation for this section only);

– φ is the heat source;

– $\alpha = \lambda / \rho C$ is the thermal diffusion coefficient.

	ρ (kg/m^3)	C (J/kg·K)	λ (W/m·K)	α (10^{-6}m^2/s)
Steel	7,870	452	80	15
Concrete	2,400	880	2.1	0.54
Glass	2,500	700	0.87	0.50
Wood	420	2,720	0.14	0.12
Brick	1,800	840	0.5	0.30

Table 3.3. *Thermal characteristics of some building materials*

Energy provided by irreversible mechanical phenomena can be diffused into the material or used as a source of heat, depending on the relative importance of the two terms in the heat equation. The dimensionless number that allows us to judge the relative importance of these two terms, and thus the relative importance of diffusion, is the Fourier number. Expression of this number is given in [3.19]. In this formula, L_c is the characteristic length of a solid and t_c is the characteristic time of the phenomenon:

$$Fo = \frac{\rho C L_c^{\,2}}{\lambda t_c} \qquad [3.19]$$

If this number is small compared to 1, the diffusion phenomenon is dominant. The temperature in the solid is almost uniform, and if it is not isolated from the outside, the transformation can be considered isothermal. If the Fourier number is large compared to 1, diffusion is negligible and the energy is used to heat the material locally. The transformation can then be regarded as adiabatic. For dynamic stresses, a characteristic time is the time needed to achieve a critical level of strain relative to irreversible phenomena [3.20]:

$$t_c = \frac{\varepsilon_c}{\dot{\varepsilon}} \qquad [3.20]$$

The condition of adiabatic transformation is [3.21]:

$$\dot{\varepsilon} >> \frac{\lambda \varepsilon_c}{\rho C L_c^2} \qquad [3.21]$$

For example, for a test on steel, the characteristic values $\varepsilon_c \approx 10^{-2}$ $L_c \approx 10^{-3}$ m can be selected. The strain rate from which changes can be considered as adiabatic is $\dot{\varepsilon} >> 10^{-1}\ \mathrm{s}^{-1}$.

Dynamic loading conditions are such that the adiabatic transformation assumption is often more realistic than the isothermal transformation. If the behavior of a material is sensitive to temperature, the dynamic rupture conditions can then be different to those usually obtained in quasi-staticity, as in isothermal conditions. This also holds if the behavior of the material is not sensitive to strain

rate. To study this situation simply, let us consider a behavior where stress depends on strain and temperature [3.22]:

$$\underline{\underline{\sigma}}\left(\underline{\underline{\varepsilon}},T\right) \qquad [3.22]$$

The change in internal energy in the material is a function of the change in temperature [3.23]:

$$de = \rho\, C\, dT \qquad [3.23]$$

In a material undergoing adiabatic transformation, we can write the following result [3.24]. The strain that comes into play in this equation is the one related to heat source mechanisms (usually, plastic strain). The Taylor–Quinney β coefficient can be less than 1. This reflects the fact that all the energy is dissipated as heat. Some of this energy can be "blocked" in the material:

$$\varphi = \beta\, \underline{\underline{\sigma}} : \underline{\underline{\dot{\varepsilon}}}^{p} \qquad [3.24]$$

3.2.2. *Adiabatic shear condition*

For the rest of our demonstration, let us consider a one-dimensional case, or that of a radial load, in which the stress parameter and strain are denoted as σ and ε (in general, it is shear and plastic distortion). Relationship [3.24] can be written as [3.25] (taking a Taylor–Quinney coefficient equal to 1):

$$\frac{de}{dt} = \varphi \quad \rightarrow \quad \frac{dT}{d\varepsilon} = \frac{\sigma}{\rho\, C} \qquad [3.25]$$

Differentiation of the behavior relationship gives expression [3.26]:

$$\frac{d\sigma}{d\varepsilon} = \left(\frac{\partial\sigma}{\partial\varepsilon}\right)_{T} + \left(\frac{\partial\sigma}{\partial T}\right)_{\varepsilon} \frac{dT}{d\varepsilon} \qquad [3.26]$$

The first term represents the slope of the stress–strain curve in isothermal transformation (quasi-static case). This term is generally positive. The second term represents the expansion of stress, at constant strain, when temperature rises. This term is generally negative [3.27]:

$$\left(\frac{\partial\sigma}{\partial\varepsilon}\right)_T > 0 \quad \left(\frac{\partial\sigma}{\partial T}\right)_\varepsilon < 0 \qquad [3.27]$$

The instability condition (rupture) in the material, as a condition of adiabatic loading, takes the form [3.28]:

$$\frac{d\sigma}{d\varepsilon} \le 0 \quad \rightarrow \quad \left|\left(\frac{\partial\sigma}{\partial T}\right)_\varepsilon\right| \frac{\sigma}{\rho\, C} \ge \left(\frac{\partial\sigma}{\partial\varepsilon}\right)_T \qquad [3.28]$$

Table 3.4 gives, for three models of isothermal behavior, the expression of critical strain for which adiabatic shear may appear. The stresses here are shears and plastic strain distortions $(\sigma \to \tau, \varepsilon \to \gamma)$.

	Culver model	Pomey model	Bai model
Isothermal behavior	$\tau = B\gamma^n$	$\tau = A + B\ln\gamma$	$\tau = Y + b\gamma$
Critical strain	$\gamma_c = \dfrac{-n\rho C}{\left(\dfrac{\partial\tau}{\partial T}\right)_\gamma}$	$\gamma_c = \dfrac{B\rho C}{\tau\left\lvert\dfrac{\partial\tau}{\partial T}\right\rvert_\gamma}$	$\gamma_c = \dfrac{\rho C}{\left\lvert\dfrac{\partial\tau}{\partial T}\right\rvert_\gamma} - \dfrac{Y}{b}$

Table 3.4. *Critical strain distortions in adiabatic conditions for three models of isothermal behavior*

If the material is sensitive to strain rate, stress can be represented by $\sigma(\varepsilon, \dot{\varepsilon}, T)$. Then, the differential is written as [3.29]:

$$d\sigma = \left(\frac{\partial\sigma}{\partial\varepsilon}\right)_{\dot{\varepsilon},T} d\varepsilon + \left(\frac{\partial\sigma}{\partial\dot{\varepsilon}}\right)_{\varepsilon,T} d\dot{\varepsilon} + \left(\frac{\partial\sigma}{\partial T}\right)_{\varepsilon,\dot{\varepsilon}} dT \qquad [3.29]$$

which can also be written as [3.30]:

$$\frac{d\sigma}{d\varepsilon} = \left(\frac{\partial\sigma}{\partial\varepsilon}\right)_{\dot{\varepsilon},T} + \left(\frac{\partial\sigma}{\partial\dot{\varepsilon}}\right)_{\varepsilon,T} \frac{\ddot{\varepsilon}}{\dot{\varepsilon}} + \left(\frac{\partial\sigma}{\partial T}\right)_{\varepsilon,\dot{\varepsilon}} \frac{dT}{d\varepsilon} \qquad [3.30]$$

The additional term that appears has a sign that is dependent on the acceleration of strain. The instability condition becomes [3.31]:

$$\left|\left(\frac{\partial\sigma}{\partial T}\right)_{\varepsilon,\dot{\varepsilon}}\right|\frac{\sigma}{\rho C_p}-\left(\frac{\partial\sigma}{\partial\dot{\varepsilon}}\right)_{\varepsilon,T}\frac{\ddot{\varepsilon}}{\dot{\varepsilon}}\geq\left(\frac{\partial\sigma}{\partial\varepsilon}\right)_{T,\dot{\varepsilon}} \qquad [3.31]$$

For example, an isothermal behavior model using power laws and the application of the stability criterion leads to the critical strain expression [3.33]:

$$\tau = A\gamma^n\dot{\gamma}^m \quad \gamma_c = \frac{n}{\frac{1}{C}\left|\frac{\partial\tau}{\partial T}\right|_{\gamma,\dot{\gamma}}-\frac{m}{\dot{\gamma}}\frac{d\dot{\gamma}}{d\gamma}} \qquad [3.32]$$

3.3. Propagation in uniaxial stress state

3.3.1. *Elastoplastic material*

In Chapter 2, we discussed shock in elastic solids in uniaxial state of stress or strain. We will extend this study to the case where the elastic limit of the material is reached. First, let us consider uniaxial stress state. According to formula [2.40], if solid 1 impacts on solid 2 at velocity V_i, the induced compressive stress depends on the velocity and impedances of the two materials. A certain velocity can reach yield stress [3.33]:

$$V_i = \sigma_e\frac{Z_1+Z_2}{Z_1Z_2} \qquad [3.33]$$

If the impact velocity is greater than this value, yielding will occur. We will study motion and waves that are propagated in this case. Generally, in uniaxial stress state, the equations of motion take the form [3.34]:

$$\frac{\partial\sigma}{\partial x}=\rho\frac{\partial^2 u}{\partial t^2} \qquad \varepsilon=\frac{\partial u}{\partial x} \qquad [3.34]$$

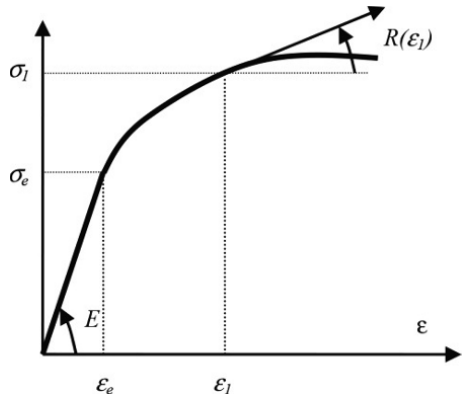

Figure 3.4. *Stress–strain relationship in uniaxial state for an elastoplastic material*

To treat monotonic loading, we assume that stress is a simple function of the current strain [3.35]. Figure 3.4 shows the evolution of the stress versus strain:

$$\sigma(\varepsilon) \quad \text{and} \quad K(\varepsilon) = \frac{d\sigma}{d\varepsilon} \qquad [3.35]$$

Motion is then described by the partial differential equation [3.36]:

$$R\frac{\partial^2 u}{\partial x^2} = \rho\frac{\partial^2 u}{\partial t^2} \qquad [3.36]$$

If R is constant, the elastic wave propagation equation solutions are known. We propose to solve this equation through the simple case as shown in Figure 3.5.

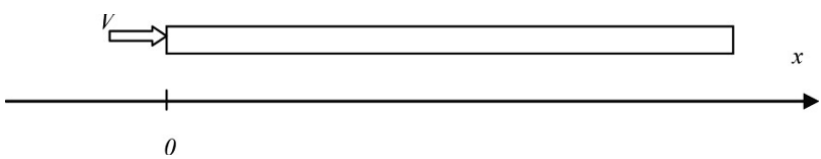

Figure 3.5. *Long rod undergoing velocity discontinuity at the origin*

The domain is the half-line and the boundary conditions are given in [3.37]:

$$x \in [0,\infty[\quad u(0,t) = -Vt \quad \text{and} \quad u(\infty,t) = 0 \qquad [3.37]$$

To solve this problem, which was addressed by Taylor and von Karman, we determined variable α [3.38]:

$$\alpha = \frac{x}{t} \qquad (dx = t\ d\alpha) \qquad [3.38]$$

We suppose that strain is a function of α [3.39]:

$$\varepsilon = f(\alpha) \qquad \text{and} \quad u(x,t) = \int_{\infty}^{x} f(\alpha)\, dx = t\int_{\infty}^{\alpha} f(\beta)\, d\beta \qquad [3.39]$$

We deduce the displacement derivatives with respect to time [3.40] and in relation to space [3.41]:

$$\frac{\partial u}{\partial t} = \int_{\infty}^{\alpha} f(\beta)d\beta + t f(\alpha)\frac{d\alpha}{dt} = \int_{\infty}^{\alpha} f(\beta)d\beta - \alpha f(\alpha)$$

$$\text{as } \frac{d\alpha}{dt} = -\frac{x}{t^2} = -\frac{\alpha}{t}$$

$$\frac{\partial^2 u}{\partial t^2} = f(\alpha) - \alpha f'(\alpha)\frac{d\alpha}{dt} - f(\alpha)\frac{d\alpha}{dt} = \frac{\alpha^2}{t} f'(\alpha) \qquad [3.40]$$

$$\frac{\partial u}{\partial x} = \frac{du}{d\alpha}\frac{d\alpha}{dt} = f(\alpha) \text{as} \frac{d\alpha}{dx} = \frac{1}{t}$$

$$\frac{\partial^2 u}{\partial x^2} = \frac{1}{t} f'(\alpha) \qquad [3.41]$$

The propagation equation [3.36] imposes one of the two equalities from [3.42]:

$$\rho\alpha^2 = K \quad \text{or} \quad f'(\alpha) = 0 \qquad [3.42]$$

Respecting the boundary conditions of the problem, the solution will come in three different forms in three different areas as presented in Table 3.5. The associated strain field is shown in Figure 3.6, as a function of the variable *x/t*.

$0 < x < Ct$	$u(x,t) = -Vt + \varepsilon_1 x$	Area of uniform strain
$Ct < x < C_0 t$	$\frac{x^2}{t^2} = \frac{R}{\rho}$	Area where plastic strains progress
$C_0 t < x$	$u(x,t) = 0$ and $\varepsilon = 0$	Area not yet reached by the waves

Table 3.5. *Displacement fields in an elastoplastic impacted rod*

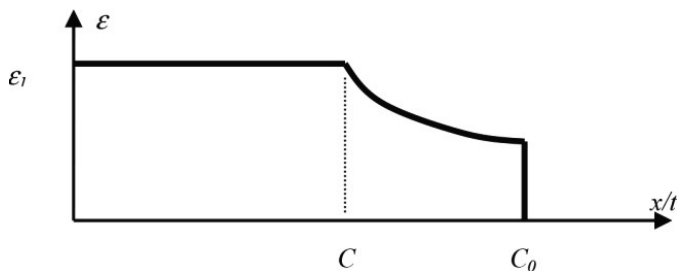

Figure 3.6. *Strain field in an impacted elastoplastic rod*

In the intermediate area, we understand that each strain increment propagates at a velocity that depends on the value of *R* for the level of strain. We investigate the relationship between velocity at the origin, strain ε_1 and behavior $R(\varepsilon)$. To do this, we can write the displacement at the origin with expression [3.43]:

$$u(0,t) = -Vt = t\int_{\infty}^{0} f(\alpha)\, d\alpha \qquad [3.43]$$

We deduce the velocity at the origin [3.44]:

$$V = \int_{0}^{\infty} f(\alpha)\ d\alpha \qquad [3.44]$$

This expression corresponds to the calculation of the area under the curve as shown in Figure 3.6. Velocity can also be expressed by the integral along the other axis [3.45]:

$$V = \int_0^{\varepsilon_1} \alpha \; d\varepsilon = \int_0^{\varepsilon_1} \sqrt{\frac{R}{\rho}} \; d\varepsilon \qquad [3.45]$$

If function $R(\varepsilon)$ is known, we can find a relationship between ε_1 and V. The speed of the "plastic" wave jump can be calculated using formula [3.46]:

$$C = \left(\sqrt{\frac{R}{\rho}} \right)_{\varepsilon_1} = \sqrt{\frac{R(\varepsilon_1)}{\rho}} \qquad [3.46]$$

We can illustrate the propagation of a plastic wave with the example of an elastoplastic material with linear hardening. The behavior of the material is represented by the curve as shown in Figure 3.7.

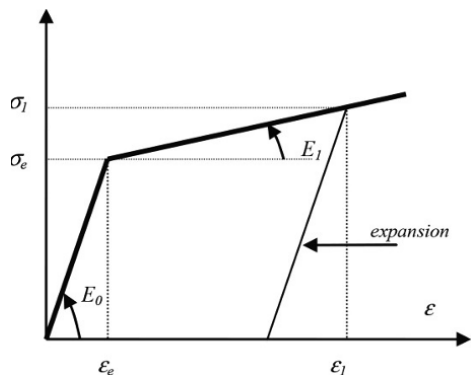

Figure 3.7. *Elastoplastic relationship with linear hardening*

The strain field is shown in Figure 3.8(a). The relationship between velocity at the origin (impact velocity) and maximum strain is given by formula [3.47]:

$$V = \int_0^{\varepsilon_0} \sqrt{\frac{E_0}{\rho}} \, d\varepsilon + \int_{\varepsilon_0}^{\varepsilon_1} \sqrt{\frac{E_1}{\rho}} \, d\varepsilon \qquad [3.47]$$

The calculation gives relationship [3.48]:

$$V = \varepsilon_1 \sqrt{\frac{E_1}{\rho}} + \varepsilon_0 \left(\sqrt{\frac{E_0}{\rho}} - \sqrt{\frac{E_1}{\rho}} \right) \qquad [3.48]$$

The velocity of a "plastic" wave jump, therefore, has expression [3.49]:

$$C_1 = \sqrt{\frac{E_1}{\rho}} \qquad [3.49]$$

The relationship between impact velocity and maximum strain can be written as [3.50]:

$$V = C_1 \, \varepsilon_1 + \left(C_0 - C_1 \right) \varepsilon_0 \qquad [3.50]$$

If the condition of the imposed velocity ceases after time θ, an expansion wave will propagate in the solid at speed C_0 through elastic waves. In Chapter 2, we saw that the duration of a shock was related to the size and characteristics of the impactor.

Figure 3.8(b) shows a diagram of the course of waves. We see the elastic compression wave jump (A) that propagates at speed C_0. The plastic compression wave jump (B) leaves at the same instant, but propagates more slowly, at speed C_1. From time θ, an expansion wave (C) propagates at speed C_0. The expansion wave joins the plastic compression wave at time θ_1. After this time, no more areas are yielded in the solid. The length of the area that has been yielded is given by formula [3.51]:

$$Lp = \theta \frac{C_0 C_1}{C_0 - C_1} \qquad [3.51]$$

3.3.2. *Viscoplastic material*

The propagation of a yield wave in a viscoplastic solid has been studied by [SOK 48] and [MAL 51]. Here, we take the example of a

simple Bingham viscoplasticity model to show how plastic strain waves propagate in a medium whose behavior is sensitive to the rate of strain. Beyond the elastic limit, the behavior of the material is consistent with the expression [3.52]:

$$\sigma = Y + \eta\left(\dot{\varepsilon} - \frac{\dot{\sigma}}{E}\right) \qquad [3.52]$$

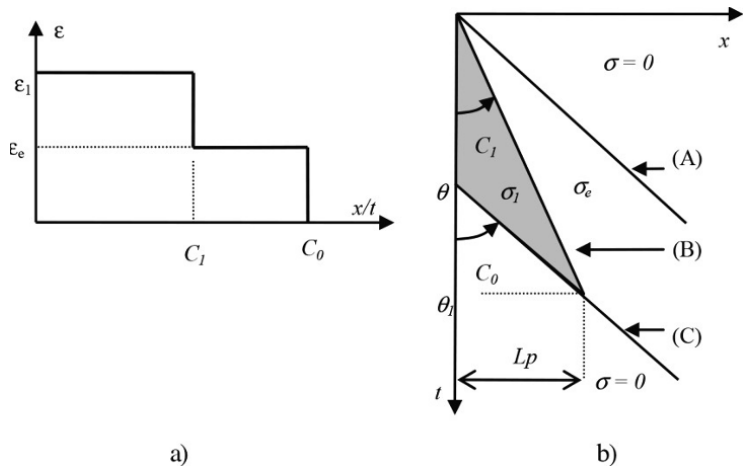

Figure 3.8. *a) The strain field of an impacted elastoplastic rod; b) course diagram of elastic and plastic waves*

We consider the same geometric configuration and the same boundary conditions as in the previous section [3.37]. We will change the variables in order to only consider what happens beyond the plasticity threshold. This threshold is characterized by a stress threshold Y and an impact velocity associated with [3.53]:

$$V_e = \frac{Y}{\sqrt{E\rho}} \qquad [3.53]$$

The change of variable is the following [3.54]:

$$\sigma_v = \sigma - Y \quad V_v = V - V_e \qquad [3.54]$$

In the area where the elastic limit is exceeded, the equation of motion can be expressed in terms of "viscoplastic" stress [3.55]:

$$\frac{\partial^2 \sigma_v}{\partial x^2} = \frac{\rho}{\eta}\frac{\partial \sigma_v}{\partial t} + \frac{\rho}{E}\frac{\partial^2 \sigma_v}{\partial t^2} \qquad [3.55]$$

There is a similarity with the equation of motion in a viscoelastic Maxwell medium, and the operational image of the solution is [3.56]:

$$\bar{\sigma}_v(x,s) = D(s)\, e^{-\frac{x}{C_0}\sqrt{s(s+E/\eta)}} \qquad [3.56]$$

The imposed velocity condition is formulated in operational form [3.57]:

$$\bar{V}_v(0,s) = -\frac{V_v}{s} \qquad [3.57]$$

Given the behavior relationship, we can completely explain the image of the stress [3.58]:

$$\bar{\sigma}_v(x,s) = \frac{V_v\sqrt{\rho E}}{\sqrt{s(s+E/\eta)}}\, e^{-\frac{x}{C_0}\sqrt{s(s+E/\eta)}} \qquad [3.58]$$

Returning to time functions, the stress field is then explained with formula [3.59]:

$$\sigma_v(x,t) = V_v\sqrt{\rho E}\; e^{-Et/2\eta}\; I_0\left(\frac{E}{2\eta}\sqrt{t^2 - \frac{x^2}{C_0^2}}\right) H\left(t - \frac{x}{C_0}\right) \qquad [3.59]$$

Returning to the initial variables, the stress field obtained in the yielded area is given by [3.60]:

$$\sigma(x,t) = \left(Y + \left\langle V\sqrt{\rho E} - Y\right\rangle e^{-Et/2\eta}\; I_0\left(\frac{E}{2\eta}\sqrt{t^2 - \frac{x^2}{C_0^2}}\right)\right) H\left(t - \frac{x}{C_0}\right) \qquad [3.60]$$

This field can be expressed in terms of dimensionless variables [3.61]:

$$\tau = \frac{Et}{\eta} \quad X = \frac{xE}{C_0\eta}$$

$$S = \frac{\sigma(x,t)}{Y} = \left(1 + \left\langle \frac{V\sqrt{\rho E}}{Y} - 1 \right\rangle e^{-\tau/2}\, I_0\left(\frac{1}{2}\sqrt{\tau^2 - X^2}\right)\right) H(\tau - X) \qquad [3.61]$$

Figure 3.9 shows the stress field at different moments ($\tau = 1$, $\tau = 2$, $\tau = 3$ and $\tau = 4$) in a viscoplastic solid. The dotted line shows the exponential decay of amplitude as it tends toward the yield limit.

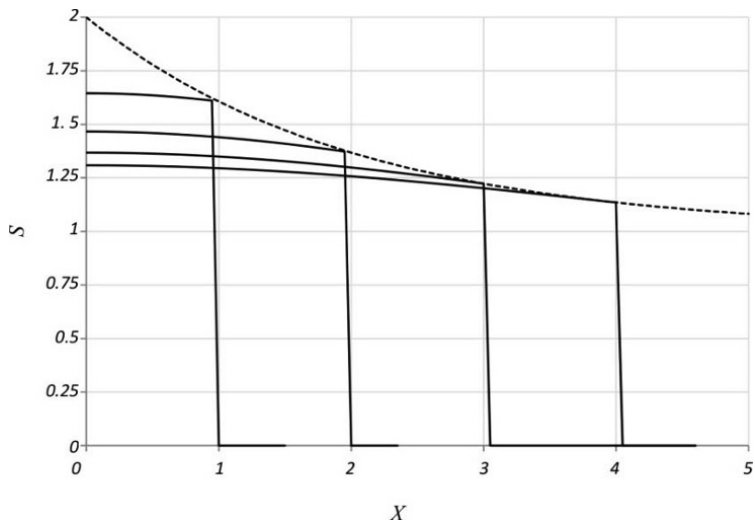

Figure 3.9. *Stress field at different moments ($\tau = 1$, $\tau = 2$, $\tau = 3$, $\tau = 4$) in a viscoplastic solid. The dotted line shows the exponential decay of the amplitude as it tends toward the elastic limit*

3.4. Uniaxial strain state

3.4.1. *Metallic material*

In some shock situations, the movement of a solid can be properly represented in a uniaxial strain state (see Chapter 1). We will study the

consequences of yield in this situation. We distinguish between two types of plasticity criteria, first considering a criterion independent of pressure, such as the Tresca and the von Mises criteria commonly used for metallic materials. In a uniaxial strain state, which may correspond to certain impact conditions, the strain and stress tensors are of the forms [3.62]:

$$\underline{\underline{\varepsilon}} = \begin{pmatrix} \varepsilon_1 & 0 & 0 \\ 0 & 0 & 0 \\ 0 & 0 & 0 \end{pmatrix} \qquad \underline{\underline{\sigma}} = \begin{pmatrix} \sigma_1 & 0 & 0 \\ 0 & \sigma_2 & 0 \\ 0 & 0 & \sigma_2 \end{pmatrix} \qquad [3.62]$$

To study such a stress state, the most common assumption is that the material is described by perfect elastoplastic behavior. We then make a partition between elastic and plastic strain [3.63]:

$$\underline{\underline{\boldsymbol{\varepsilon}}} = \underline{\underline{\boldsymbol{\varepsilon}}}^e + \underline{\underline{\boldsymbol{\varepsilon}}}^p \quad \Leftrightarrow \quad \boldsymbol{\varepsilon}_i^e + \boldsymbol{\varepsilon}_i^p = 0 \left(i = 2,3\right) \qquad [3.63]$$

Plastic flow is incompressible, which implies the relationship [3.64]:

$$\text{trace } \underline{\underline{\varepsilon}}^p = 0 \qquad \Leftrightarrow \qquad \varepsilon_1^p + 2\varepsilon_2^p = 0 \qquad [3.64]$$

The plastic flow criterion is of von Mises or Tresca type, which in this case is translated through equation [3.65]:

$$\sigma_1 - \sigma_2 = Y = \sigma_e \qquad [3.65]$$

In the elastic phase, the relationships between stress and strain are [3.66]:

$$\begin{aligned} \sigma_1 &= \left(\lambda + 2\mu\right)\varepsilon_1 = \frac{E\left(1-\nu\right)}{\left(1-2\nu\right)\left(1+\nu\right)}\varepsilon_1 = \left(K + \frac{4}{3}G\right)\varepsilon_1 \\ \sigma_2 &= \frac{\nu}{1-\nu}\sigma_1 \end{aligned} \qquad [3.66]$$

Then, we can express the stress state at the plasticity threshold [3.67]:

$$\sigma_1 - \sigma_2 = \left(1 - \frac{\nu}{1-\nu}\right)\sigma_1 = Y$$
$$\sigma_1 = \frac{1-\nu}{1-2\nu} Y = \left(\frac{K}{2G} + \frac{2}{3}\right) Y \qquad [3.67]$$

The yield in a uniaxial strain state is also called the Hugoniot elastic limit (HEL). We can deduce the value of the strain threshold [3.68]:

$$\varepsilon_1 = \frac{1+\nu}{E} Y = \frac{Y}{2G} \qquad [3.68]$$

Beyond the yield threshold, the equations that remain valid are those of perfect plasticity and incompressible flow [3.69]:

$$\sigma_1 = Y + \sigma_2$$
$$\text{trace } \underline{\underline{\varepsilon}} = \text{trace } \underline{\underline{\varepsilon}}^e \quad \Leftrightarrow \quad \varepsilon_1 = \varepsilon_1^e + 2\varepsilon_2^e \qquad [3.69]$$

The change in volume is solely due to elastic strains. We can deduce the relationship, after yielding, between stress and strain in direction 1 [3.70]:

$$\text{trace } \underline{\underline{\sigma}} = 3K \text{ trace } \underline{\underline{\varepsilon}}^e \quad \Leftrightarrow \quad \sigma_1 + 2\sigma_2 = 3K\varepsilon_1$$
$$\sigma_1 = K\varepsilon_1 + \frac{2}{3}Y \qquad [3.70]$$

This behavior is shown in Figure 3.10(c), as well as the behavior under hydrostatic stress state (b) and uniaxial stress state (simple compression) (a).

Once the elasticity threshold is crossed, we see that the behavior curve in uniaxial strain (c) is parallel to the behavior in hydrostatic stress state (b). It is often assumed, through extrapolation, that behavior obtained in uniaxial strain state, when near the elastic threshold, is the same as the relationship between pressure and volume changes under hydrostatic conditions. However, we must not forget that this result is based on assumptions of the von Mises criterion and incompressibility of plastic strain.

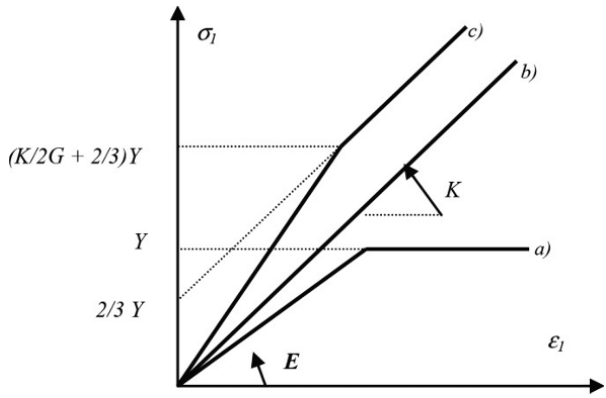

Figure 3.10. *Stress–strain relationship for an elastoplastic material: a) in uniaxial stress state, b) in isotropic state and c) in uniaxial strain state*

In uniaxial strain state, elastic waves propagate with the velocity C_{el}, which is equal to C_P of P-waves, and plastic waves propagate at velocity C_{pl} [3.71]:

$$c_{el} = \sqrt{\frac{K + \frac{4G}{3}}{\rho}} = \sqrt{\frac{H}{\rho}} c_{pl} = \sqrt{\frac{K}{\rho}} \qquad [3.71]$$

If the shock is of limited duration, stress at the origin becomes zero and an expansion wave is created. During the expansion, σ_1 decreases and the material returns to the elastic range. Therefore, first there is an elastic expansion. Then, σ_1 becomes smaller than σ_2 and the plasticity criterion can again be achieved. At this point, the relationships between the stresses then become [3.72]:

$$\sigma_2 - \sigma_1 = Y \text{ and } \sigma_1 = \frac{\nu}{1-\nu}\sigma_2 \qquad [3.72]$$

Then, there is a plastic expansion, or release, in the material. During this phase the stress σ_1 follows the law [3.73].

Figure 3.11 shows a loading and unloading cycle in uniaxial strain state. There is a residual strain at the end of the cycle and the final stress state does not coincide with the initial state.

$$\sigma_1 = K\varepsilon_1 - \frac{2}{3}Y \qquad [3.73]$$

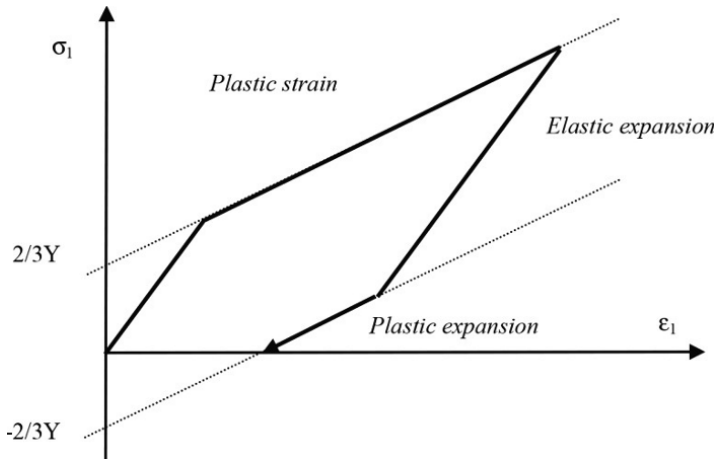

Figure 3.11. *The loading and unloading cycle in uniaxial strain state*

From the viewpoint of waves in a solid, the expansion is composed of an elastic wave and a plastic wave. Figure 3.12(a) shows the graph of the course of the waves. Two compression waves, one elastic and the other plastic, leave at the initial time. At the end of loading time θ, two waves also leave: one elastic and one plastic. Figure 3.12(b) shows the stress field in a solid shortly after loading. We distinguish between, from right to left, the elastic compression wave, the plastic compression wave, which progresses more slowly, the expansion elastic wave, which will catch up the previous wave, and, finally, the plastic expansion wave.

3.4.2. *Geomaterial*

For cohesive and friction materials such as concrete, the criterion associated with the onset of irreversible strain from internal slip depends on pressure. We will consider the Drücker Prager criterion. This criterion is obtained by adding sensitivity to the spherical part of the stress tensor to the von Mises criterion. In the space of main

stresses, this criterion is represented by a cone whose axis is the trisection and the summit is the abscissa Y_h [3.74]:

$$f\left(\underline{\underline{\sigma}}\right) = \sigma_{eq} - \alpha\left(I_1 + Y_h\right) \qquad [3.74]$$

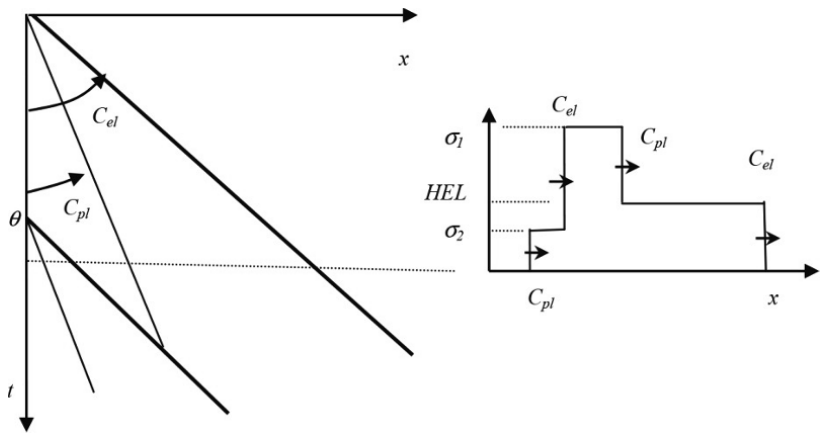

Figure 3.12. *Course diagram of waves in an elastoplastic solid in a) uniaxial strain state and b) stress field at a time*

As before, we consider uniaxial strain state [3.62]. In these conditions, the invariants are expressed as [3.75]:

$$\sigma_{eq} = \sigma_1 - \sigma_2 \quad I_1 = \sigma_1 + 2\sigma_2 \qquad [3.75]$$

The plasticity criterion is formulated as [3.76]:

$$\sigma_1\left(1-\alpha\right) - \sigma_2\left(1+2\alpha\right) - \alpha Y_h = 0 \qquad [3.76]$$

At the elasticity limit, the main constraints are in the ratio [3.77]:

$$\sigma_2 = \frac{\nu}{1-\nu}\sigma_1 \qquad [3.77]$$

Under uniaxial strain load, the yielding threshold (HEL) appears for the stress level [3.78]:

$$\sigma_1 = \frac{\alpha(1-\nu)Y_h}{(1-2\nu)-\alpha(1+\nu)} \quad [3.78]$$

We must note that this threshold only exists if condition [3.79] is verified. Thus, for materials with a Poisson coefficient close to 0.5 and a sufficient angle of internal friction, the criterion will never be reached. This means that for these materials, irreversible phenomena in uniaxial strain state will be of compaction type rather than internal slipping type.

$$\alpha < \frac{1-2\nu}{1+\nu} \quad [3.79]$$

We continue the study as if the criterion is met. When σ_1 exceeds the threshold [3.78], the criterion [3.76] is verified and lateral stress can be calculated [3.80]:

$$\sigma_2 = \frac{1-\alpha}{1+2\alpha}\sigma_1 - \frac{\alpha Y_h}{1+2\alpha} \quad [3.80]$$

If we retain the assumption of incompressible plastic flow, formulas [3.69] and [3.70] remain valid. Then, we can express the relationship of stress as a function of strain [3.81]:

$$\sigma_1 = K(1+2\alpha)\varepsilon_1 + \frac{2\alpha}{3}Y_h \quad [3.81]$$

In this case, we see that the conclusion made earlier through considering the von Mises criterion is no longer valid. The pressure–volume relationship cannot be deduced from the stress–strain relationship under the oedometer path by a simple translation. However, if the deviatoric behavior is well known, deduction is still possible with the assumption of incompressible plastic flow. Here, we have considered perfect plasticity models. If there is hardening and if plastic expands or contracts, although in principle this is not impossible, producing the pressure–volume relationship from the stress–strain relationship can get quite complicated.

3.5. Shock waves

3.5.1. *Origin of the phenomenon*

In section 3.3.1, we saw that when nonlinear behavior is exhibited, a stress and strain level is propagated at a velocity that depends on the slope of the stress–strain curve corresponding to this point [3.46]. In uniaxial stress state, this slope is a decreasing function, and therefore, as stress is increased at the extremity of a solid, strain waves propagate increasingly slowly as shown in Figure 3.6. In uniaxial strain, the material can compact itself and the curvature of changes in the stress versus strain may become positive. Therefore, the slope of this curve can increase. If we imagine that stress is increased at the extremity of a solid, then strains could propagate faster from a certain threshold level than at lower levels. There is a discrepancy that reflects the fact that a continuous description of propagation of stresses and strains according to their amplitude is no longer possible. If an impact causes a level of stress in a solid that belongs in a region of positive curvature in stress–strain law, it will propagate the stress level by shock wave.

To understand the propagation of this shock wave, we take the equations for conservation of mass and momentum formulated in Chapter 2 for a discontinuity wave (see equations [2.1]–[2.4]). The material is, before passage of the wave, in the "0" state (density ρ_0, particle velocity V_0, strain ε_0 and stress σ_0) and, after passage of the wave, in the "1" state (density ρ_1, particle velocity V_1, strain ε_1 and stress σ_1). Conservation equations are used to write the variation in strain and stress as a function of material velocity and shock wave velocity D [3.82]. If we express volume decreases and compressions positively, we see that the ratio between stress change and strain change can only be positive:

$$\begin{cases} \Delta\varepsilon = \dfrac{V - V_0}{D - V_0} = 1 - \dfrac{\rho_0}{\rho} \\ \Delta\sigma = \rho_0 \left(D - V_0\right)\left(V - V_0\right) \end{cases} \quad \rightarrow \quad \frac{\Delta\sigma}{\Delta\varepsilon} = \rho_0 \left(D - V_0\right)^2 \qquad [3.82]$$

Assuming that before the shock, particle velocity being zero, we can deduce the velocity of the shock wave from this ratio [3.83].

Figure 3.13 shows the stress–strain curve at the two states before and after passage of the shock wave:

$$S = \frac{\Delta\sigma}{\Delta\varepsilon} = \rho_0 D^2 \qquad D = \sqrt{\frac{S}{\rho_0}} \qquad [3.83]$$

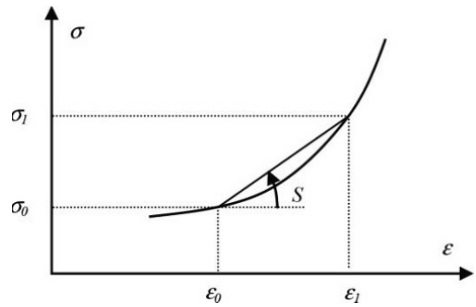

Figure 3.13. *Stress–strain curve in uniaxial state with compaction jumping from state 0 to state 1 at the passage of a shock wave*

Upon impact on a solid, two different situations can occur (see Figure 3.14). If the shock is not too strong, the matter will go from state "0" to state "*i* ", and the shock wave will be preceded by a wave, called "elastic precursor", because the velocity of the shock wave jump is less than that of the elastic waves. If the shock is very violent, the material will go from state "0" to state "*ii*", velocity may exceed that of the elastic waves and there is no precursor.

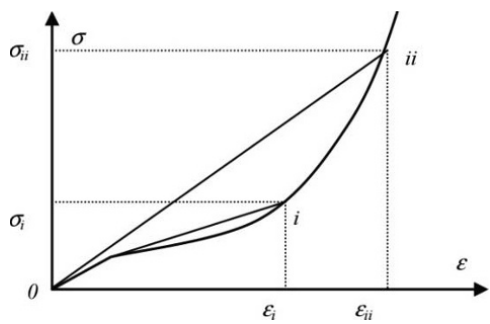

Figure 3.14. *Stress–strain curve in uniaxial state with compaction: from state 0 to state i: shock wave with elastic precursor; from state 0 to state ii: shock wave without elastic precursor*

3.5.2. *Compaction at the passage of a shock wave*

At the beginning of this chapter (section 3.1.4), we looked at behaviors such as compaction. If these behaviors are studied in dynamics, in uniaxial strain state, different descriptions exist [3.84]. If, when static, it is customary to consider a curve showing stress as a function strain, then other representations are possible in dynamics. It is possible to represent the relationship between stress jump and particle velocity jump at the passage of a shock in the material. In Chapter 2, we saw the great practical value of such a description for the study of shocks in elastic solids. The interest of this description remains for compactable solid. A third representation is possible by giving the change in the velocity of a shock wave through a material as a function of particle velocity after the shock (the material is initially at rest). This third method is useful for very violent shocks where both D and V values are directly accessible by experimentation.

$$\sigma(\varepsilon) \quad \leftrightarrow \quad \sigma(V) \quad \leftrightarrow \quad D(V) \qquad [3.84]$$

For example, if compaction is described by a stress–strain relationship of "power" type, other relationships can be deduced using the laws of conservation of mass and momentum [3.85]:

$$\sigma = A\varepsilon^n \quad \leftrightarrow \quad \sigma = A^{\frac{1}{n+1}} \rho_0^{\frac{n}{n+1}} V^{\frac{2n}{n+1}} \quad \leftrightarrow \quad D = \left(\frac{A}{\rho_0}\right)^{\frac{1}{n+1}} V^{\frac{n-1}{n+1}} \qquad [3.85]$$

Figure 3.15 shows an example of using the state diagram from the law $\sigma(V)$ to find the level of stress σ_C created by impact on a compactable material, with solid impedance Z arriving at velocity V_i.

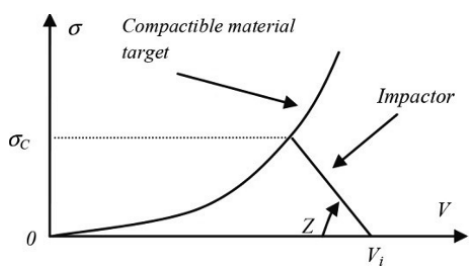

Figure 3.15. *Using the state diagram to determine the stress created by the impact of a solid of impedance Z on a compactable material*

Figure 3.16 shows the correspondence between the stress–strain relationship and the shock velocity–material velocity relationship for three basic behaviors: elasticity, plasticity and compaction. In the latter case, the model often takes the form of the McQueen formula [MCQ 70] given in [3.86]:

$$D = A + BV^n \qquad [3.86]$$

As a first approximation, $n = 1$, we present three materials in Table 3.6.

Quartz	$D = 6{,}319 + 1.41\ V \quad (\text{m/s})$
Water	$D = 1{,}460 + 2.2\ V \quad (\text{m/s})$
Air	$D = 241 + 1.06\ V \quad (\text{m/s})$

Table 3.6. *Behavior of three materials when under shock*

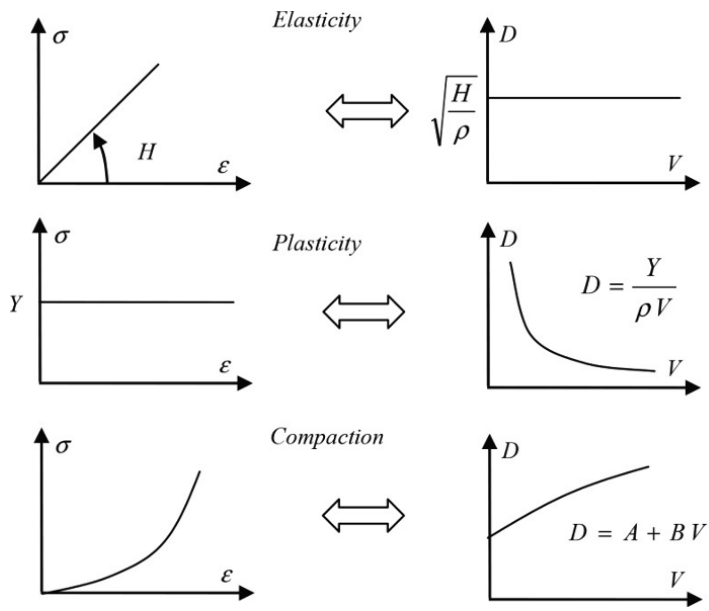

Figure 3.16. *Correspondence between the stress–strain relationship and the shock velocity–material velocity relationship for three basic behaviors*

Figure 3.17 shows the correspondence between the stress–strain relationship and shock velocity–material velocity relationship for a material with compactable elastoplastic behavior.

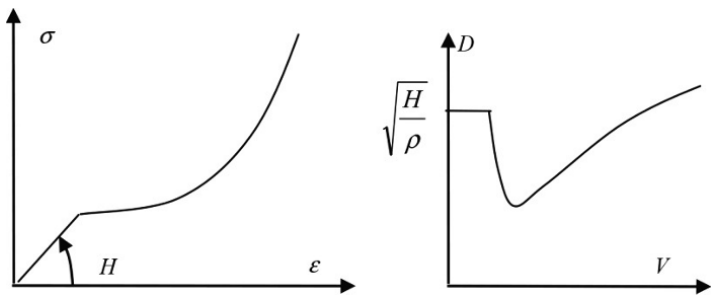

Figure 3.17. *Correspondence between stress–strain relationship and shock velocity–material velocity relationship for a compactable elastoplastic material*

3.5.3. *Notion of state law*

We have seen (section 3.1.4) that there are several ways to model compaction. In the case of very high intensity dynamic loading in contact with solid explosives or under very strong impacts, it is customary to separate the internal forces into an isotropic part (average pressure or stress) and a deviatoric part (shear) [3.15]. Pressure reaches very high values, in the order of tens of gigapascals, while shear stresses are of limited value due to the plastic flow, in the order of hundreds of megapascals. It is assumed that very high pressure can be described separately from the laws of evolution for the two components of internal forces. The limitations of this hypothesis are still questionable for materials where compaction and flow mechanisms are coupled, such as concrete. The relationship between shear and distortion is called the behavior law. The relationship between pressure and volume change is called state law in a thermodynamic sense. This state law obtains its formula by expressing pressure as a function of the internal energy and specific volume [ZUK 90] [3.87]:

$$p(e,v) \qquad \left(v=\frac{1}{\rho}\right) \qquad [3.87]$$

It is generally assumed that in this law, there is no dependence on strain rate. Differentiation of the law gives the expression [3.88]:

$$dp = \left(\frac{\partial p}{\partial v}\right)_e dv + \left(\frac{\partial p}{\partial e}\right)_v de \qquad [3.88]$$

We therefore pass from a "0" state to a current state by formula [3.89]:

$$p = p_0 + \int_{v_0}^{v} \left(\frac{\partial p}{\partial v}\right)_e dv + \int_{e_0}^{e} \left(\frac{\partial p}{\partial e}\right)_v de \qquad [3.89]$$

The last term represents the change in pressure at constant volume. To calculate this term, we determine the Gruneisen parameter, assumed to depend only on the specific volume [3.90]:

$$\Gamma(v) = v\left(\frac{\partial p}{\partial e}\right)_v \qquad [3.90]$$

The pressure change at constant volume can be expressed in terms of this parameter [3.91]:

$$\int_{e_0}^{e} \left(\frac{\partial p}{\partial e}\right)_v de = \frac{\Gamma(v)}{v}(e - e_0) \qquad [3.91]$$

The state law is generally determined by an impact test in uniaxial strain state. The relationship between stress and change in volume is called the Hugoniot relationship. We can deduce pressure, p, in isotropic state from pressure p_H, the Hugoniot relation, by formula [3.92]:

$$p = p_H + \frac{\Gamma}{v}(e - e_H) \qquad [3.92]$$

where e_H is the internal energy in the "Hugoniot" state and can be calculated, as already seen in [2.8], using formula [3.93]:

$$e_H = \frac{1}{2}P_H\left(\frac{1}{\rho_0} - \frac{1}{\rho}\right) = \frac{1}{2}P_H\frac{\mu}{\rho} \qquad \left(\mu = \frac{\rho}{\rho_0} - 1\right) \qquad [3.93]$$

This allows us to deduce the state law through experiments in uniaxial strain state [3.94]:

$$p = p_H\left(1-\frac{\Gamma\mu}{2}\right)+\frac{\Gamma}{v}e \qquad [3.94]$$

Often, the Hugoniot relationship is expressed as a polynomial [3.95]:

$$p_H = c_1\mu + c_2\mu^2 + c_3\mu^3 \qquad [3.95]$$

Figure 3.18 shows a relationship between pressure and specific volume for a compactable solid. At the passage of a shock wave, the state abruptly changes from an initial state to a compacted state following a "Rayleigh" line, which corresponds to formula [3.83]. Then, if there is an expansion that brings the solid back to its initial pressure, compaction being an irreversible process, the path will be different. We show by the dashed–dotted line the behavior of the completely compacted solid, in which all porosity was closed. The shaded area indicates energy supplied to the material to achieve this compaction.

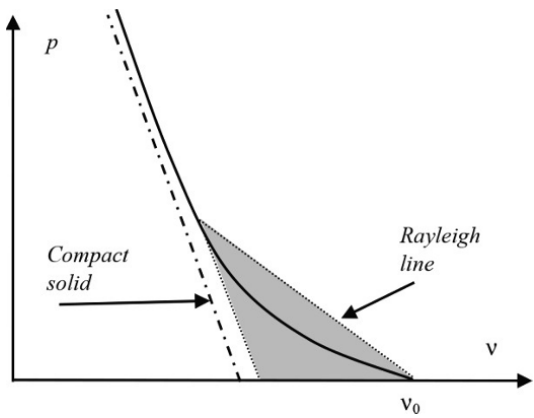

Figure 3.18. *Compacting a solid in the pressure–volume diagram, compression by shock wave and expansion showing the energy supplied for compaction*

Chapter 4

Dynamic Materials Testing

This chapter aims to show how knowledge of movements in solids, as seen in previous chapters, is used for the construction and analysis of tests to characterize the behavior of materials under a high rate of strain. The Hopkinson pressure bar technique is presented. Technical aspects of measurements are not addressed. There are specific and comprehensive works on testing techniques (for example [FRA 01]).

4.1. Dynamic testing

4.1.1. *Testing means*

The most conventional testing means are electromechanical or hydraulic machines that make it possible to submit a sample of material to tensile stress or compression. Various devices are used to create stress states. It is customary to speak of materials testing if load leads to a state of homogeneous stress and strain in the test body. If load leads to a state of non-homogeneous stress or strain, we refer to it as structure testing. Flexion tests are of the second type. Strain rate in the test body is related to the velocity of the movable portion (the crosshead) of the testing machine. For electromechanical machines, the maximum velocity is in the order of millimeters per second. This value may be higher for hydraulic machines. Test specimens are of a

size in the order of centimeters or tens of centimeters. "Quasi-static" tests are usually made with strain rates from 10^{-5} to 10^{-3} s^{-1}. To achieve velocities of a much higher order of magnitude, specific experimental means are required. High strain rates can be achieved subsequent to the impact of a solid upon the test body. Hydraulic machines have been designed for velocities in the order of 1 m/s. In these machines, a cylinder pushes a crosshead that impacts the test body. Strain rates from 10 to 100 s^{-1} can then be achieved. A simpler idea is to drop a mass on the test body (chute). The purpose of a test material is to perform measurements that allow an estimation of the stress and strain, assumed to be homogeneous, in a sample of matter. To access these variables, specific devices have been developed. The device most commonly used for dynamic tests is the "Hopkinson pressure bar", which will be described in section 4.2.

With this device, we can easily perform compression tests on the test body, or specimen, by imposing a strain rate from 100 to 1,000 s^{-1}. In practice, the velocity range is limited to its minimum and maximum values. Even for higher strain rates, a real impact test can be done by studying the impact of a very rigid solid on the test body, or by projecting it onto a rigid target (Taylor test). From a certain impact velocity, the concept of strain rate loses its meaning. This is the case with violent impacts, as seen in Chapter 3, which generate shock waves in solids. The material then passes almost instantaneously from a state of stress and strain to another state (strain rate tends to infinity). Tests, called plate impact tests, are present for studying the behavior of materials at the passage of shock waves. For a more complete vision of dynamic testing, refer to [LAT 01].

4.1.2. *Specific difficulty*

A test aiming to characterize the behavior of a material must allow the estimation of stresses and strains. In quasi-static tests, this estimate is made by measuring forces and displacements on the contour, or part of the contour, of the test body. In simple tests, we seek to obtain homogeneous states. With the assumption of homogeneity, the estimation of stresses and strains can be based on the measurements. For example, in a simple compression test, stress is estimated by

dividing the compressive force by the section of the test specimen; strain is estimated by the ratio of specimen shortening relative to length. The experimental reality is that this homogeneity is, in practice, an approximation (for example friction at the specimen–machine interface). Loading velocity can have an impact on this homogeneity assumption. In Chapter 1, we saw that the homogeneous evolution of stress or strain in a solid is not possible. Any change is reflected through wave propagation. It is therefore necessary to consider the validity limit of the homogeneity assumption. To illustrate this, we consider a simple compression test on a concrete specimen (L = 0.1 m). Time Δt taken for a wave to make a round trip in the test body is calculated in [4.1]:

$$\Delta t = \frac{2L}{C_0} \qquad \left(C_0 = \sqrt{\frac{E}{\rho}} \approx 3{,}000 \text{ m/s} \right) \qquad [4.1]$$

If the crosshead velocity is V, the machine will impose a displacement $\delta = V\Delta t$ during this time, which corresponds to a strain of amplitude specified in [4.2]

$$\Delta \varepsilon = \frac{2V\,L}{C_0} \qquad [4.2]$$

At any given time, the difference in strain between two points on the test body can have this value. If this value is very small compared to the magnitude of the strain characteristic of the material (for example, strain at yield point), the usual quasi-static assumption of homogeneity is relevant and may be considered. For the example of concrete, while the crosshead speed is V = 1 mm/s, the difference in strain $\Delta\varepsilon$ is in the order of 10^{-7}. This value is very small compared to the strain at yield point, which is in the order of 10^{-3}. If the speed is V = 10 m/s, the difference in strain is in the same order of magnitude as strain at the elastic limit. The assumption of homogeneity or quasi-equilibrium cannot be assumed *a priori*.

For a dynamic test, we can classify the methods into two categories. If, during the test, we can make measurements that show that, although dynamic, the specimen is in a state of

quasi-equilibrium, we can easily estimate the stresses and strains. This situation is often sought for the Hopkinson pressure bar test. If this is not the case, analysis of the test can become very difficult. Advanced metrics exist (field measurements) to support the operation of a test. More generally, we can proceed using an inverse method based on a choice, *a priori*, of the type of material behavior.

4.2. Hopkinson pressure bars

4.2.1. *Device*

The original device invented by Hopkinson used only one bar [HOP 14]. The current device, consisting of two bars, was developed by Kolsky [KOL 49]. This device is shown in Figure 4.1. It consists of a compressed air canon projecting an impactor and two bars, between which a sample of the test material is placed. The basic metrology of this device consists of recording strain in the bars using resistive gauges. It is possible to complete this metrology, for example with a camera.

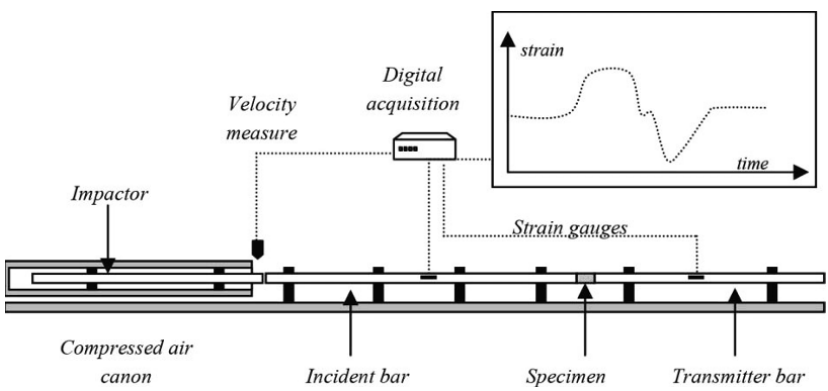

Figure 4.1. *A Hopkinson pressure bars device*

4.2.2. *Principle of the test*

The test body, or specimen, to be subjected to compression is placed between the two bars. A compressed air canon sends a

projectile from the end of the first bar, called the incident bar. The shock induces a compression slot, as shown in Chapter 2, which propagates through the bar. If the compressional wave reaches the other end of the incident bar, it compresses the test body. The latter is then crushed and a reflected wave goes back into the incident bar, and a wave is transmitted to the transmitter bar. The characteristics of these two waves are related to the behavior of the test body. Figure 4.2 shows the wave course diagram in the device. Upon impact, the projectile has velocity V_i. If the impactor and the incident bar have the same diameter and are made of the same material (which is not a requirement), the value of the amplitude of the compression wave is shown in [4.3] (ρ_B is the density of the material constituting the bars, E_B is Young's modulus and C_B is the wave velocity in the bars):

$$\sigma = \frac{1}{2}\rho_B C_B \qquad [4.3]$$

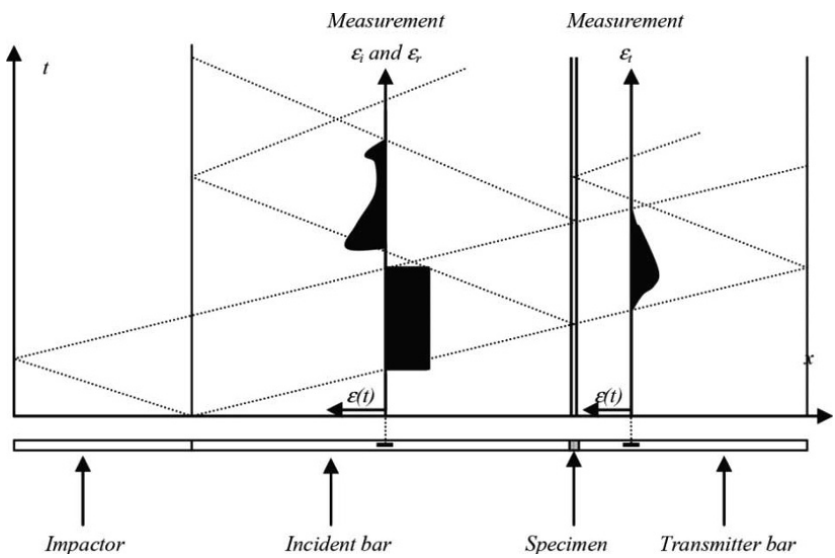

Figure 4.2. *Wave course diagram in a Hopkinson pressure bar and strain measurements in the bars*

The duration of the compression slot is that of a round trip of the waves in the impactor. The strain gauge placed on the incident bar allows for the measurement of this slot. If the compressional wave reaches the end of the incident bar, which is in contact with the sample material to be tested, diffraction occurs. A part of this wave is reflected. The gauge placed on the incident bar allows the measurement of the reflected wave. Part of the wave is transmitted and can be measured with the gauge placed on the transmitter bar. As analysis of the test is based on the knowledge of the three waves (*incident*, *reflected* and *transmitted*), it is necessary to measure them in a place where they do not overlap. Thus, a gauge needs to be placed in the middle of the incident bar, with a length greater than twice that of the impactor. For the same reasons, the transmitter bar must also be longer than the impactor. The development of strains measured by gauges, an example of which is shown in Figure 4.3, is recorded and is the raw test result. The purpose of the test is to deduce, from these measurements, the stress and strain in the sample of tested material.

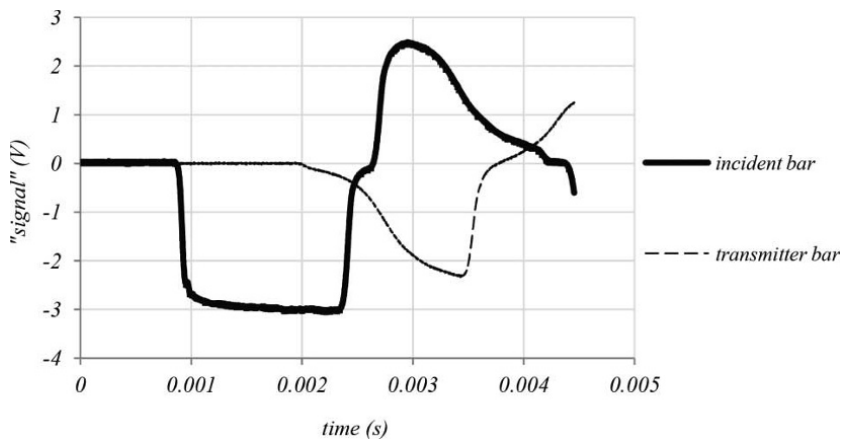

Figure 4.3. *Recording example: incident and reflected waves in the incident bar (solid line) and transmitted wave in the transmitter bar (thin line)*

We can study in more detail how the waves will compress the test body. Figure 4.4 shows the wave course diagram. The specimen generally has an inferior impedance than the bars, and velocity of the

waves is lower. Multiple successive diffractions can be observed at the interfaces between the bars and the sample.

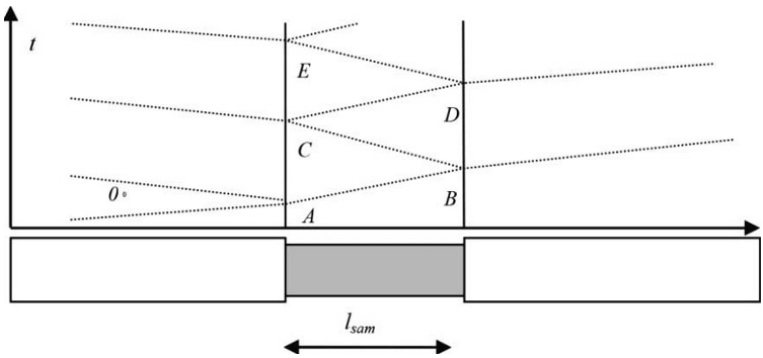

Figure 4.4. *Diagram of wave course in the test body*

Figure 4.5 shows the evolution of stress and the state diagram in the test body. The impactor shock has imposed a "0" state in the incident bar. When this wave comes into contact with the sample, it passes from rest to state "A" (Z_B is the impedance of the bars and Z_{sam} is that of the sample).

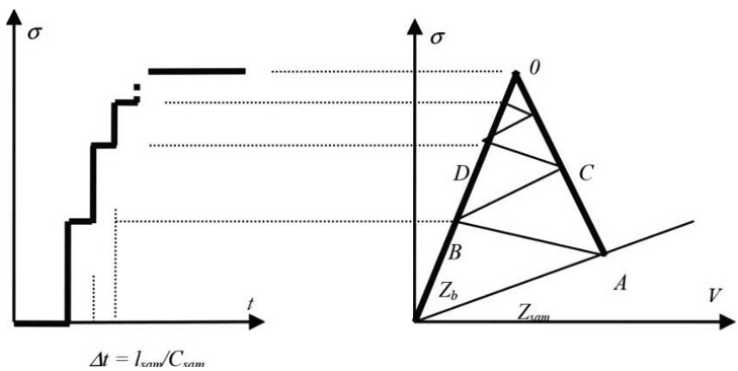

Figure 4.5. *Evolution of stress and state diagram in the test body*

A number of round trips occur in the specimen, which result in an increase in the stress state in the latter and completion of the compression test.

4.2.3. *Analysis of the test*

Test analysis methods have been extensively studied (for example [DAV48, DAV 63, FOL 83, MAL 86]). The estimation of stresses and strains in the test body requires a determination of forces and displacements at the extremities of the test body that are assumed to be in a state of simple compression (Figure 4.6).

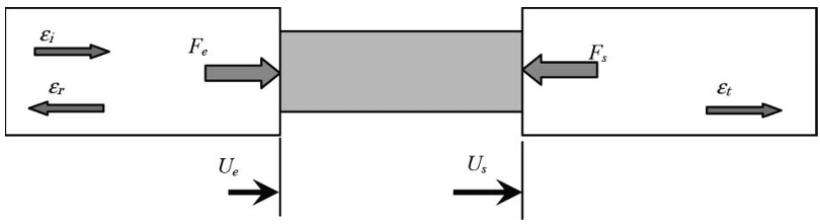

Figure 4.6. *Test body conditions at the boundaries*

The diffraction conditions mentioned in Chapter 2 are used to calculate the forces and velocities at the interfaces as a function of waves.

Incident and transmitted waves are progressive and the reflected wave is retrogressive. The corresponding formulas are given in [4.4]:

$$\begin{cases} V_e = C_B\left(\varepsilon_i(t) - \varepsilon_r(t)\right) \\ V_s = C_B\,\varepsilon_t(t) \end{cases} \quad \begin{cases} F_e = S_B E_B\left(\varepsilon_i(t) + \varepsilon_r(t)\right) \\ F_s = S_B E_B\,\varepsilon_t(t) \end{cases} \qquad [4.4]$$

These formulas are expressed by strain waves at the end of the bars. However, these formulas are measured at points far from the said ends. So, measured waves have to be transported in time. The incident wave must be “moved forward” in time and the reflected and transmitted waves must be moved “backward”. As we know how waves propagate in the bars, it is possible to perform this operation. The calculation is very simple if we plan to model the wave bars in uniaxial stress state. We can search for a more accurate result by taking wave dispersion in the bars into account, as was discussed in Chapter 1 [GON 90, ZHA 96]. Formula [4.4] shows that we must calculate the sum and difference of the waves. In practice, this

calculation will be significant if the amplitudes of these waves are in the same order of the magnitude. This depends on the ratio of impedance of the bars and the sample. In fact, if the tested material is of very low impedance compared to bars, the reflected wave will be almost opposite to the incident wave as a reflection on a fixed edge, and the transmitted wave will be very small. It will be very difficult to deduce the strength from the measurements of strain waves. It is therefore necessary to adapt the device to the material being tested. Steel bars are used to test high-performance metallic materials. To test materials such as concrete, aluminum bars would be used instead. If test materials of lower impedance are to be tested, such as wood or polymers, bars made of a material with impedance in the same order as nylon must be used. Such materials generally exhibit a viscoelastic behavior and the transport of waves, as mentioned above, must take into account the dispersion and dissipation of waves in the medium [ZHA 95, GAR 97].

The forces and velocities estimated in [4.4] are the result of an analysis of measurements. As mentioned in section 4.1.2, it is necessary to consider the state of stress and strain in the test body and its homogeneity. Knowing the force at each end is important. If both F_e and F_s forces are substantially equal, we can assume that the stress state is homogeneous in the sample. Assuming that the state of strain is homogeneous, we can use formulas [4.5]:

$$e_1 - e_0 = \frac{1}{2}(\sigma_1 + \sigma_0)\left(\frac{1}{\rho_1} - \frac{1}{\rho_0}\right) \quad e_1 - e_0 = \frac{1}{2}(\sigma_1 + \sigma_0)\left(\frac{1}{\rho_1} - \frac{1}{\rho_0}\right)$$
$$e_1 - e_0 = \frac{1}{2}(\sigma_1 + \sigma_0)\left(\frac{1}{\rho_1} - \frac{1}{\rho_0}\right). \qquad [4.5]$$

If homogeneity, or quasi-equilibrium, in the test body cannot be verified, the forces and velocities at the extremities provide useful data to try a behavior search by an inverse method [GAR 93].

4.2.4. *Types of loads*

The device described above concerns compression tests. The principle of this test has been exploited to create additional stress states in the tested specimen. Torsion and traction bars exist. It is also possible to get other loads with the compression system. Instead of directly placing the test body in contact with the bars, we can insert an intermediate device that will put, by confined compression, shear or bending tension on the material to be tested (for example [YOK 93]).

4.3. Testing by direct impact

4.3.1. *Device*

The direct impact device is simpler than the Kolsky device described previously. An impactor is projected directly onto the test body. There is only a "transmitter" bar with a gauge to measure the strain wave crossing it. Figure 4.7 illustrates this device. It is essential to measure the projectile impact velocity V_i on the test body.

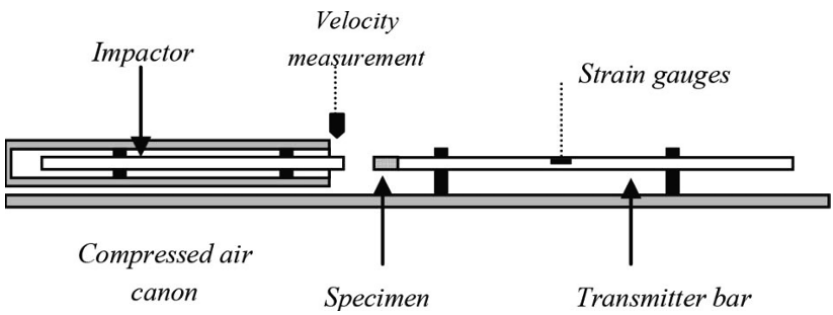

Figure 4.7. *Direct impact device*

4.3.2. *Analysis of the test*

The primary measurement is of the strain in the bar $\varepsilon_i(t)$. This strain is produced by the propagation of a compression wave

generated at the extremity. We deduce, as before, force and velocity at this extremity [4.6]:

$$\begin{aligned} F_s(t) &= S_B E_B\, \varepsilon_t(t) \\ V_s(t) &= C_B\, \varepsilon_t(t) \end{aligned} \qquad [4.6]$$

The velocity of the projectile, at any time, is then determined by the balance of momentum [4.7]:

$$V(t) = V_i - \frac{1}{M}\int_0^t F_s(\tau)d\tau \qquad [4.7]$$

If we assume a uniform strain state on the test body, the strain is then determined as [4.8]:

$$\varepsilon(t) = \frac{1}{L_e}\int_0^t \left(V(\tau) - V_s(\tau)\right)d\tau \qquad [4.8]$$

The analysis of this test is done, *a priori*, with the assumption of quasi-equilibrium in the test body. With only impact velocity measurements and measurements of wave in the bar, this hypothesis cannot be verified. It is therefore necessary to be careful or to complete the metrology, for example with a camera, to reinforce the assumptions of the analysis of this test.

4.4. Taylor impact test

4.4.1. *Principle of the test*

The Taylor impact test involves projecting a cylindrical test body onto a very stiff target. If the impact velocity is sufficient (see Chapter 2), the projectile will be yielded. A yield wave is propagated through the test body, starting from the face of contact with the target, until the initial kinetic energy of the projectile is dissipated. Figure 4.8 shows the test body at the instant of impact ($t = 0$) and an instant t where a part of the cylinder has plasticized. When the test is completed, the test body has zero velocity and a certain area is yielded ($x = X_R$).

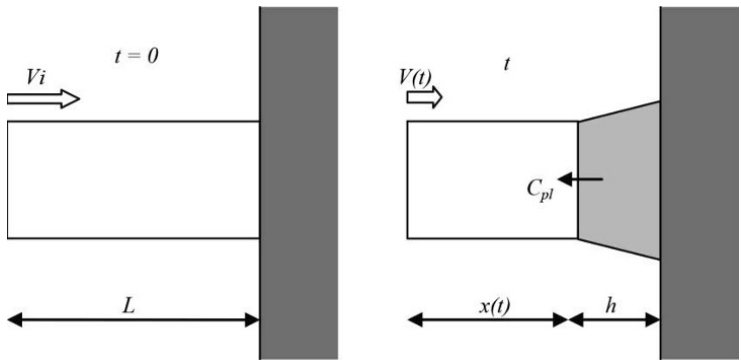

Figure 4.8. *Taylor impact device*

4.4.2. *Simplified analysis*

Analysis of the Taylor test is generally quite complex because the impact causes large strains [ZUK 90]. It is difficult to simply deduce a law of behavior. This test is often used to make a comparison with the result of a calculation that uses the finite element method and a model behavior law, in a law validation process. To understand the basic phenomena involved in this test, we propose a very simple analysis for the case where the material is assumed to be elastoplastic without hardening and without dependence on strain rate. Upon impact, an elastic wave with amplitude Y (yield) returns through the solid, at velocity C_0. A plastic wave starting at the same time also goes into the solid at velocity C_{pl}. Assuming that the plasticized zone is at rest, the relationship between stress and particle velocity is [4.9]:

$$Y = \rho C_0 V \qquad [4.9]$$

With each reflection of the elastic wave on the fixed end, the projectile velocity decreases by a quantity indicated by [4.10]:

$$dV = -\frac{2Y}{\rho C_0} \qquad \frac{1}{C_0} = -\frac{\rho dV}{2Y} \qquad [4.10]$$

A return of elastic waves in the non-plastic part of the cylinder will last for the value shown in [4.11]:

$$dt = \frac{2x}{C_0} \qquad [4.11]$$

the length dx going from the elastic to plastic state is [4.12]:

$$dx = -\left(V + C_{pl}\right) dt = -\left(V + C_{pl}\right) \frac{2x}{C_0} \qquad [4.12]$$

We then deduce the differential equation that governs the evolution of the plasticized zone [4.13]:

$$\frac{dx}{x} = -\frac{2\left(V + C_{pl}\right)}{C_0} = -\frac{\rho\left(V + C_{pl}\right)}{Y} dV \qquad [4.13]$$

By integration, we obtain the equation governing the evolution of the plastic zone [4.14]:

$$\ln x = \frac{\rho}{Y}\left(\frac{V^2}{2} + C_{pl} V\right) \qquad [4.14]$$

By integrating this equation between time $t = 0$, where $x = L$, and the final time where $V = 0$ and $x = X_R$, we obtain a formula indicating the size of the zone plasticized during the test [4.15]:

$$\ln\left(\frac{L}{X_R}\right) = \frac{\rho}{Y}\left(\frac{V_i^2}{2} + C_{pl} V_i\right) \quad \frac{L}{X_R} = e^{-\frac{\rho}{Y}\left(\frac{V_i^2}{2} + C_{pl} V_i\right)} \qquad [4.15]$$

4.5. Plate impact

4.5.1. *Devices*

The plate impact test aims to characterize the behavior of a material during the passage of a shock wave, as seen in Chapter 3. The test principle is to generate a shock wave in a test specimen by applying a relatively high strain rate on one side of a test body. This

imposed speed may result from the impact of a plate, projected from a canon. The test may also be done by propelling a plate in contact with the test specimen. This propelling is the result of an explosion of energetic material behind the plate. Figure 4.9 shows these two types of devices. It is recognized that, in the test body, the state is close to the uniaxial strain state. The basic instrumentation of this test is for measuring the velocity of the plate and the velocity of the rear face of the test body. The magnitude of the stresses referred to in this type of test is gigapascal or greater.

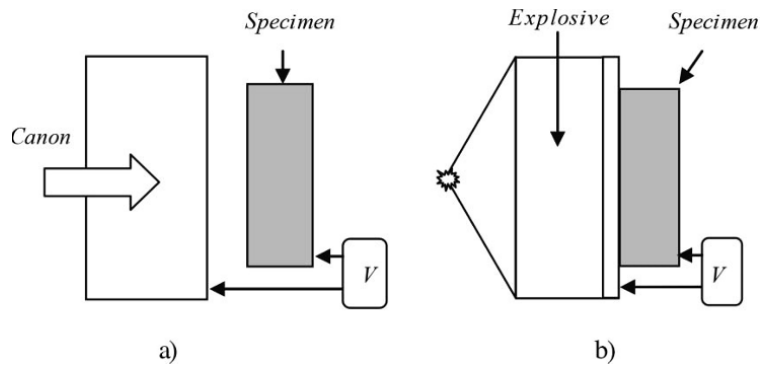

Figure 4.9. *Plate impact devices: a) plate powered by a canon; b) plate propelled by an explosive*

4.5.2. *Analysis elements*

In this test, a shock wave is created in the material for which we wish to know the behavior under very high pressure. We can estimate velocity D of the shock wave in the material by measuring the time delay between the velocity of the plate (and thus the front side) and the velocity of the rear face of the sample. Velocity of the rear face is also measured and the particulate velocity V behind the shock wave can thus be deduced. Then, we have a pair of values (D, V) associated with the behavior of the material under shock. It is therefore necessary to carry out several tests with different stress levels to approximate the shape of the relationship between velocity D and particle velocity V. In Chapter 3, we saw the duality between relationship $D(V)$ and the behavior $\sigma(\varepsilon)$ in uniaxial strain state.

PART 2

Dynamic of Structures

Chapter 5

Impact on a Simple Structure

From the mechanical response of a simple system to short-term stress, we introduce specific tools such as the shock response spectrum and iso-damage curves. These methods allow us to model a real structure through a simple system.

5.1. Basic structure

5.1.1. *Linear system with one degree of freedom*

Dynamic modeling of a simple mechanical system is an oscillator with one degree of freedom. The construction of more complex models is often based on this basic element. We first recall the characteristic parameters and properties of the system with one degree of freedom, which is used in the study of vibrations. Then, tools to assist the engineer for short-term loads will be discussed. A structure with one degree of freedom is represented by a single position parameter $x(t)$ and, therefore, a single load parameter $f(t)$. This model, often called single degree of freedom (SDOF), has been the subject of many studies [GER 96, AXI 01a]. The mathematical representation of such a system in the time domain is a differential equation where each term has a physical significance (Figure 5.1).

The equation governing the mechanical response of a structure with one degree of freedom is [5.1]:

$$m\ddot{x}(t) + c\dot{x}(t) + k\,x(t) = f(t) \qquad [5.1]$$

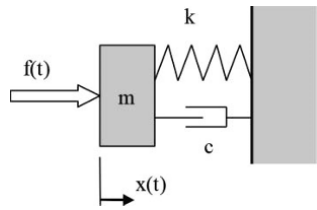

Figure 5.1. *Model of a structure with one degree of freedom*

The general problem is finding response *x(t)* if the load, or excitation, is known *f(t)*. A characteristic of oscillators, as used in the field of vibrations, is the frequency response function. In this context, if excitation (and therefore response) is periodic, we can use the Fourier transformations of force and displacement, which give an image in the frequency domain [5.2]:

$$\begin{aligned} TF\left(x(t)\right) &= x^*(\omega) & TF\left(f(t)\right) &= f^*(\omega) \\ TF\left(\dot{x}(t)\right) &= i\omega x^*(\omega) & TF\left(\ddot{x}(t)\right) &= -\omega^2 x^*(\omega) \end{aligned} \qquad [5.2]$$

Given the properties of the Fourier transformation, the differential equation is then written as [5.3]:

$$\left(-m\omega^2 + ic\omega + k\right) x^*(\omega) = f^*(\omega) \qquad [5.3]$$

The (complex) frequency response function is defined as the ratio, in the frequency domain, of the response to excitation. In the one degree of freedom example, this function is expressed as [5.4]:

$$H(\omega) = \left|H(\omega)\right| e^{i\varphi(\omega)} = \frac{x^*(\omega)}{f^*(\omega)} = \frac{1}{k - m\omega^2 + ic\omega} \qquad [5.4]$$

$H(\omega)$ has amplitude $|H(\omega)|$ and phase $\varphi(\omega)$. This means that a sinusoidal excitation produces a sinusoidal response of the same frequency. The amplitude of the response is that of excitation multiplied by $|H(\omega)|$ and the response is dephased with $\varphi(\omega)$ with respect to solicitation. If excitation is not sinusoidal, we try to describe it as the sum of harmonic functions. We can also write the frequency response function as [5.5]:

$$H(\omega) = \frac{R}{i\omega - p} + \frac{\hat{R}}{i\omega - \hat{p}} \qquad [5.5]$$

Other complex oscillator features are then defined. p is the pole and R is the residue ($\hat{p}$ and $\hat{R}$ are their conjugates). These characteristics are related to the physical parameters of the oscillator by the relationships [5.6]:

$$R = \frac{-i}{2m\omega_d} \qquad p = -\sigma + i\omega_d$$
$$\omega_d{}^2 = \omega_0{}^2 - \sigma^2 \qquad \omega_0 = \sqrt{\frac{k}{m}} \qquad \sigma = \frac{c}{2m} \qquad [5.6]$$

Figure 5.2 gives the graphical representation of the frequency response function. Paths drawn are, on the one hand, the module relative to pulsation and, on the other hand, the dephasing relative to pulsation. The oscillator characteristics are the parameters of these curves (2σ is the peak width at a level of −3dB relative to the maximum).

The elements defined here are the basic tools for general use, and in particular for studying the response of a structure to vibrational excitation [CLO 75]. We now address more specific tools for studying the effects of impacts – short-term loads.

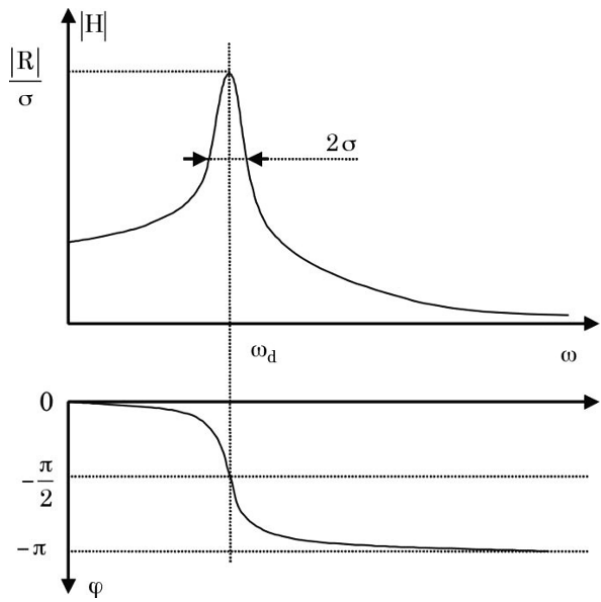

Figure 5.2. *Frequency response of a structure with one degree of freedom, amplitude and dephasing of the response*

5.1.2. *Short-term loads*

It is necessary, first, to clarify the concept of short-term as it is relative. Shocks and explosions impose loads on structures, which are modeled by *f(t)* functions. In Chapter 2, we discussed impacts of solids, and in Chapters 6 and 7, we will discuss the modeling of impacts of structures and explosions. These *f(t)* functions become zero after a certain period.

The concept of short-term refers to the natural period of the system with one degree of freedom that represents the structure ($T = 2\pi / \omega_d$).

"Short-term loading" is that which induces force on a structure, the application duration of which is less than or in the order of the natural period of the structure. It is a field of study quite different from that of forced vibrations, where excitation is considered permanent in models, that is to say, in practice, of long duration compared to the

natural period of the structure. If we study the dynamic transient response to a short-term stress, the maximum amplitude of the response, which is the main object of interest to an engineer, is reached during the first oscillations. The effect of absorption is usually negligible on these first oscillations. We, therefore, consider an equation of motion without absorption of type [5.7]:

$$m\ddot{x} + k\,x = f(t) \quad or \quad \ddot{x} + \omega^2\,x = \frac{1}{m} f(t) \qquad [5.7]$$

The first tool that we define is the impulse response. This response is the displacement caused by a load *f(t)*, represented by the Dirac delta function *δ(t)*. The Laplace transformation will be used to search for solutions to the equation of motion. The operational image of $x(t)$ is $\overline{x}(s)$. The equation of motion under impulsion is [5.8]:

$$\ddot{x}_\delta + \omega^2\,x_\delta = \frac{1}{m}\delta(t) \qquad [5.8]$$

Its operational image with the Laplace transformation is [5.9]:

$$s^2\overline{x}_\delta + \omega^2\,\overline{x}_\delta = \frac{1}{m} \qquad [5.9]$$

Under operational form, the solution is [5.10]:

$$\overline{x}_\delta = \frac{1}{m\left(s^2 + \omega^2\right)} \qquad [5.10]$$

Going back to the time domain gives solution [5.11]:

$$x_\delta(t) = \frac{1}{m\omega}\sin\omega t \qquad [5.11]$$

The interest of this impulse response is to enable the calculation of response to any *f(t)* load. Indeed, any load can be written in the operational domain as the product of itself with the image of the Dirac delta function (which is the unit). The image of the response to this

load is written in the operational domain as the product of the load image with the impulse response. Returning to the time domain, response is then represented by a convolution product which is called the Duhamel integral [5.12]:

$$\bar{x} = \bar{f}.\bar{x}_\delta \quad x = f * x_\delta \quad x = \frac{1}{m\omega}\int_0^t f(t-\tau)\sin\omega\tau\, d\tau \qquad [5.12]$$

5.2. Shock response spectrum

5.2.1. *"Slot" impulse*

The response spectrum is an evaluation tool for the effect of an action. If the action, load *f(t)*, is given (for example, the impact of a projectile or the effect of a determined explosion), the aim of the spectrum is to give the response of a basic structure to that load. The variable parameter is the eigenfrequency of the proposed structure. The response spectrum is the maximum amplitude of displacement that a basic structure will undergo, under a given load, according to its own eigenfrequency [AFN 98, LAL 99, MOR 06].

To begin, we will build the response spectrum to short-term, "rectangular" pulse-type or "slot" load as shown in Figure 5.3. Although simple, this load is realistic for some situations such as the impact of solids. In Chapter 2, we saw that these are reflected in the application of a force that remains constant for a certain period (due to the size and the velocity of the wave). The load parameters are its amplitude *P*, duration θ and pulse, which is the integral of *f(t)* [5.13]:

$$i = \int_0^\theta f(t)\, dt \qquad [5.13]$$

This load and operational image are formulated as [5.14]:

$$f(t) = P\big(H(t) - H(t-\theta)\big) \quad \bar{f}(s) = \frac{P}{s}\left(1 - e^{-\theta s}\right) \qquad [5.14]$$

The image of the response to this load is as follows [5.15]:

$$\overline{x} = \frac{P}{m}\left(\frac{1}{s\left(s^2+\omega^2\right)} - \frac{e^{-\theta s}}{s\left(s^2+\omega^2\right)} \right) \qquad [5.15]$$

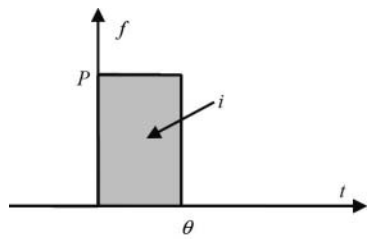

Figure 5.3. *Short-term load of "slot" or "rectangular pulse" type*

In the time domain, the result is [5.16]:

$$x = \frac{P}{m\omega^2}\left(\left(1-\cos\omega t\right) - H\left(t-\theta\right)\left(1-\cos\omega\left(t-\theta\right)\right) \right) \qquad [5.16]$$

This response takes two different expressions, depending on time [5.17]:

$$\begin{aligned} t<\theta \quad & x = \frac{P}{m\omega^2}\left(1-\cos\omega t\right) \\ t>\theta \quad & x = \frac{P}{m\omega^2}\left(\cos\omega t\cos\omega\theta + \sin\omega t\sin\omega\theta - \cos\omega t\right) \end{aligned} \qquad [5.17]$$

We will seek the maximum amplitude in both domains. To generalize the results, dimensionless variables are introduced [5.18]:

$$w^* = \frac{\omega\theta}{\pi} \quad x^* = \frac{k x_{\max}}{2P} \qquad [5.18]$$

The maximum amplitude reached during loading gives the initial spectrum [5.19]:

$$x_i{}^*\left(w^*\right) = \frac{k}{2P}\max_{t\in[0,\theta[}\left\{\left|x\left(t\right)\right|\right\} \qquad [5.19]$$

The expression of this initial spectrum is given by formulas [5.20]:

$$\begin{aligned} x_i{}^*(w^*) &= \frac{1}{2}\left|1-\cos w^*\right| \quad if\ w^* < \pi \\ x_i{}^*(w^*) &= 1 \qquad\qquad\qquad\quad if\ w^* > \pi \end{aligned} \qquad [5.20]$$

The maximum amplitude reached after loading is called the residual spectrum [5.21]:

$$x_r{}^*(w^*) = \frac{k}{2P}\max_{t\in[\theta,\infty[}\left\{\left|x(t)\right|\right\} \qquad [5.21]$$

Expression of the residual spectrum is given by formula [5.22]:

$$x_r{}^*(w^*) = \frac{1}{2}\min\left\{\sqrt{(\cos w^*-1)^2+\sin^2 w^*}\,;\left|1-\cos w^*\right|\right\} \qquad [5.22]$$

These two spectra are shown in Figure 5.4. The total spectrum is the maximum amplitude of displacement over time, regardless of the period. The total spectrum is the envelope of the initial spectrum and the residual spectrum [5.23]:

$$x^*(w^*) = \max\left\{\, x_i{}^*(w^*);\, x_r{}^*(w^*)\,\right\} \qquad [5.23]$$

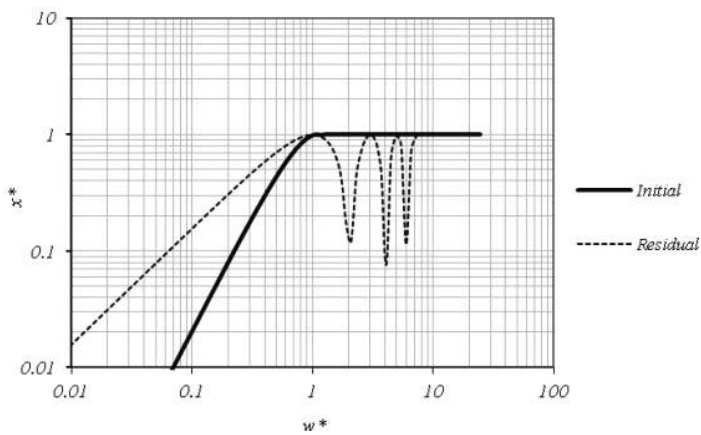

Figure 5.4. *Response spectra to a "rectangular pulse" load type: initial spectrum (solid line) and residual spectrum (dotted line)*

The total spectrum is shown in Figure 5.5. We clearly define two areas in this spectrum. If w^* is greater than *1*, the spectrum equals the unit. If w^* is less than *1*, the spectrum tends toward a line in the log-log scale. These two situations correspond to different practical cases.

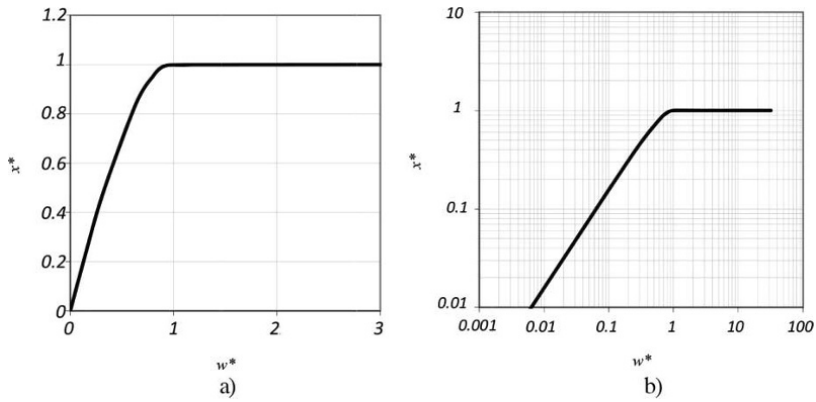

Figure 5.5. *Total spectrum of response to "rectangular pulse" load type: a) linear scale and b) logarithmic scale*

The mechanical response of the structure represented by formulas [5.17] and [5.18] can be simplified in two cases. If the loading time is small compared to the natural period of the system, it is called a pulsed load. The maximum amplitude is reached after loading. Simplifications are given in [5.24]:

$$\theta << \frac{2\pi}{\omega} \quad \cos\omega\theta \approx 1 \quad \sin\omega\theta \approx \omega\theta \qquad [5.24]$$

This leads to the response [5.25]:

$$x = \frac{P\theta}{m\omega}\sin\omega t = \frac{i}{\sqrt{km}}\sin\omega t \qquad [5.25]$$

The maximum displacement only depends on pulse i:

$$x_{\max} = \frac{i}{\sqrt{km}} \qquad [5.26]$$

It should be noted that the loading pulse is used to give the system an initial velocity. The response corresponds to free vibrations within the system. The velocity condition can be found by expressing the change in momentum during loading (between $t = 0$ and $t = \theta$) as equal to the pulse delivered to the system such that its displacement is still negligible [5.27]:

$$m\left(\dot{x}(\theta)-\dot{x}(0)\right)=i=\int_0^{\theta} f(t)\,dt \qquad [5.27]$$

In this case, only pulse determines the amplitude of the response.

However, if, load time is large compared to the natural period of the system, the maximum displacement is reached during loading and other simplifications can be made [5.28]:

$$\theta >> \frac{2\pi}{\omega} \quad x=\frac{P}{k}(1-\cos\omega t) \qquad [5.28]$$

The maximum displacement only depends on the amplitude of loading, $x_{max} = 2P/k$. If the load was static, displacement would be P/k. In this case, the structure oscillates around this value and tends toward it if there is absorption.

5.2.2. *Various types of pulses*

Short-term loading may take a different form than that of a constant force applied for a certain period. Among the different pulses, we retain those of the "triangle" and "sine" (or "half-sine") which are shown in Figure 5.6.

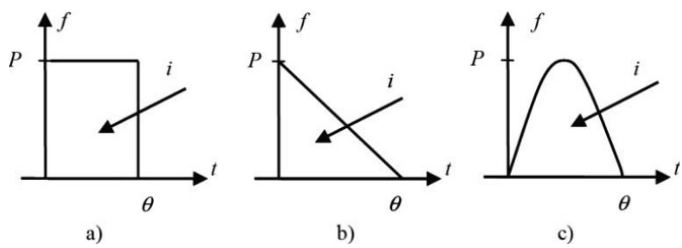

Figure 5.6. *Different shapes of impulsive loads: a) rectangle, b) triangle and c) sine*

Impulsive loading of "triangle" type may be the model of a load imposed by an explosion, as discussed in Chapter 7. This load consists of a force of intensity P applied instantly that decreases linearly until it vanishes after time θ. Its formula and operational image are shown in [5.29]:

$$\begin{aligned} f(t) &= P\left(\left(1-\frac{t}{\theta}\right)H(t)+\frac{t-\theta}{\theta}H(t-\theta)\right) \\ \overline{f}(s) &= \frac{P}{s}+\frac{P}{\theta s^2}\left(e^{-\theta s}-1\right) \end{aligned} \qquad [5.29]$$

The image of the basic system response to this load is as follows:

$$\overline{x} = \frac{P}{m\left(s^2+\omega^2\right)}\left(\frac{1}{s}+\frac{e^{-\theta s}-1}{\theta s^2}\right) \qquad [5.30]$$

In the time domain, the response to the triangular pulse is [5.31]:

$$x = \frac{P}{m\omega^2}\left((1-\cos\omega t)-\frac{(\omega t-\sin\omega t)}{\theta\omega}+\frac{\left(\omega(t-\theta)-\sin\omega(t-\theta)\right)}{\theta\omega}H(t-\theta)\right) \qquad [5.31]$$

"Sine"-type loading corresponds to a force that sinusoidally changes during a half-period. This loading may represent the result of impact on an elastic structure, as will be discussed in Chapter 6. The expression of force and its operational image are shown in [5.32]:

$$\begin{aligned} f(t) &= P\left(\sin\frac{\pi t}{\theta}H(t)+\sin\frac{\pi(t-\theta)}{\theta}H(t-\theta)\right) \\ \overline{f}(s) &= \frac{P\pi}{\theta\left(s^2+(\pi/\theta)^2\right)}\left(1+e^{-\theta s}\right) \end{aligned} \qquad [5.32]$$

The image of the response to this load is [5.33]:

$$\overline{x} = \frac{P\pi\left(1+e^{-\theta s}\right)}{m\theta\left(s^2+\omega^2\right)\left(s^2+(\pi/\theta)^2\right)} \qquad [5.33]$$

In this time domain, the result is [5.34]:

$$x = \frac{P}{m\omega\left(\omega^2 - (\pi/\theta)^2\right)} \left\{ \begin{array}{l} \left(\omega \sin\dfrac{\pi t}{\theta} - \dfrac{\pi}{\theta}\sin\omega t\right) H(t) \\ -\left(\omega \sin\dfrac{\pi(t-\theta)}{\theta} - \dfrac{\pi}{\theta}\sin\omega(t-\theta)\right) H(t-\theta) \end{array} \right. \quad [5.34]$$

From formulas [5.31] and [5.34], the response spectra of these two types of loads have been calculated. They are shown in Figure 5.7 with the rectangular load spectrum.

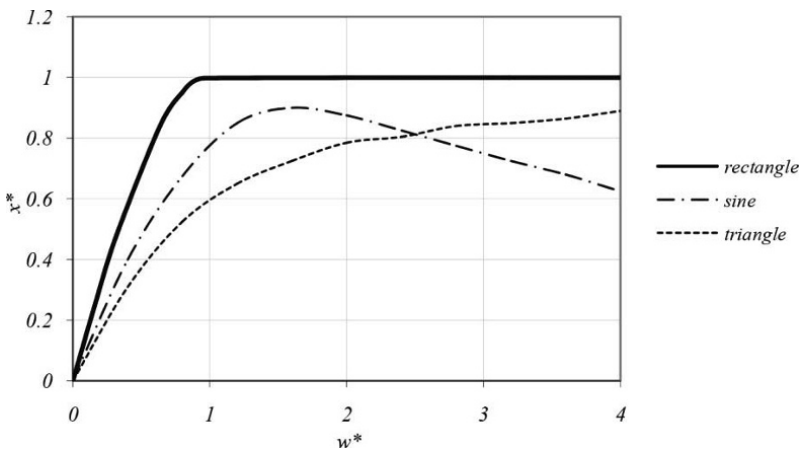

Figure 5.7. *Response spectra for three types of impulsive loads: "rectangle", "triangle" and "sine"*

5.2.3. *Alternating loading*

Transient loading does not necessarily represent a pulse as defined above. Although for a short time, there may be a sign change for the force. The impacts of solids or structures will lead to impulsive loads where the force is always positive. These loads will be detailed in Chapter 6. However, loading a structure by a blast wave after an explosion may have a phase of positive force, a consequence of overpressure, followed by a phase of negative force, a consequence of depression. The load will be detailed in Chapter 7. To understand the

effects of an alternating load, as a typical example, we take the load shown in Figure 5.8. The load is written, along with its image, by formulas [5.35]:

$$f(t)=\frac{P}{m}\sin\left(\frac{\pi t}{\theta}\right)\left(H(t)-H(t-2\theta)\right)\quad \overline{f}(s)=\frac{\pi P}{\theta m}\frac{\left(1-e^{-2\theta s}\right)}{\left(s^2+\frac{\pi^2}{\theta^2}\right)} \qquad [5.35]$$

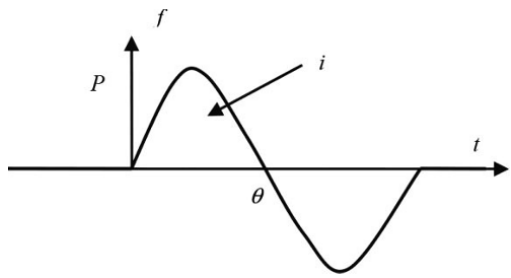

Figure 5.8. *Short-term alternating load of "sine" type*

The operational response is expressed as [5.36]:

$$\overline{x}=\frac{P}{m}\left(\frac{1-e^{-2\theta}}{\left(s^2+\frac{\pi^2}{\theta^2}\right)\left(s^2+\omega^2\right)}\right) \qquad [5.36]$$

The basic structure response to an alternating load is [5.37]:

$$x=\frac{P}{m\omega\left(\frac{\pi^2}{\theta^2}-\omega^2\right)}\left(\begin{array}{l}\frac{\pi}{\theta}\sin\omega t-\omega\sin\frac{\pi t}{\theta}+\\ H(t-2\theta)\left(\omega\sin\frac{\pi(t-2\theta)}{\theta}-\frac{\pi}{\theta}\sin\omega(t-2\theta)\right)\end{array}\right) \qquad [5.37]$$

It then becomes possible to calculate the response spectrum of such a load, still using the same dimensionless parameters. This spectrum is shown in Figure 5.9. In this figure, we remind the reader of the

rectangular pulse response spectrum. For the positive load response spectrum (section 5.2.2), we distinguish between two areas: one for relatively short-term loads, for which response amplitude depends on pulse, and the other, for longer loading durations (the relative duration w^* is always the ratio of duration of loading to the natural half-period of the structure).

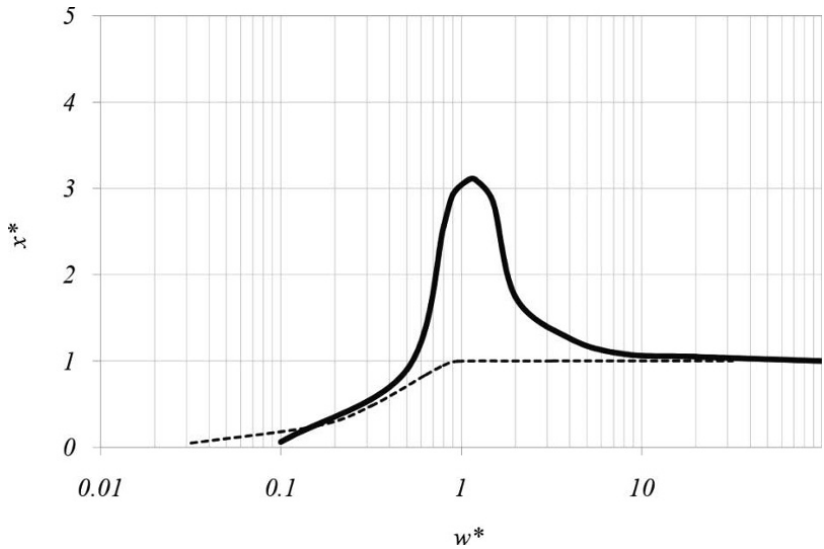

Figure 5.9. *Response spectrum to a short-term alternating load of "sine" type (solid line) compared to that of a rectangular pulse (dotted line)*

In the spectrum of an alternating load, there are three areas:

– $w^*<0.5$: the stress is of short duration for the structure. For low frequencies, the response is of very low amplitude because it depends on the total pulse, which in this case is zero.

– $0.5<w^*<5$: the loading time is in the same order of magnitude as the natural period of the structure. There is amplification of the response ($x^*>1$). This can be interpreted as the beginning of resonance of the structure.

– $5<w^*$: the load is applied slowly.

5.2.4. *Dynamic amplification factor*

For the engineer, another way of assessing the effects of a dynamic load on a structure is by determining the static load that would cause the same maximum displacement. If the amplitude of the load is P, we look for the *Daf* coefficient (dynamic amplification factor) by which we must multiply amplitude P to achieve the same maximum displacement [5.38]:

$$x_{\max} = x^{static}\left(P.Daf\right) \qquad [5.38]$$

Obviously, the dynamic load response spectrum determines this coefficient. If the eigenfrequency of the structure is ω and load time is θ, the *Daf* coefficient is deduced from the spectrum by formula [5.39]:

$$Daf = 2x^{*}\left(\omega\theta/\pi\right) \qquad [5.39]$$

If the load is always a positive force, the coefficient is less than 2. If the load is alternating, it can take larger values (up to about 7 as in the example shown in Figure 5.8). A common example for using the *Daf* is that of a long-term load with rapid implementation as shown in Figure 5.10.

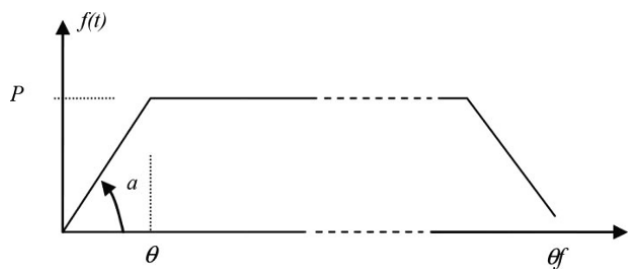

Figure 5.10. *Long-term load applied at a certain velocity*

The load is long compared to the natural period of the structure [5.40]:

$$\theta f >> \frac{2\pi}{\omega} \qquad [5.40]$$

The movement of the structure will be governed by equation [5.41]:

$$\ddot{x} + \omega^2 x = \frac{a}{m}\left(tH(t) - (t-\tau)H(t-\tau)\right) \quad [5.41]$$

The response of the structure, in operational form, is [5.42]:

$$\overline{x} = \frac{a\left(1-e^{-\theta s}\right)}{ms^2\left(s^2+\omega^2\right)} \quad [5.42]$$

The response as a function of time is expressed as [5.43]:

$$x = \frac{a}{m\omega^3}\left(\left(\omega t - \sin\omega t\right)H(t) - \left(\omega(t-\theta) - \sin\omega(t-\theta)\right)H(t-\theta)\right) \quad [5.43]$$

For times $t>\theta$, during which the maximum is reached, this expression takes the form [5.44]:

$$x = \frac{P}{k}\left(1 - \frac{1}{\omega\theta}\left(\sin\omega t - \sin\omega(t-\theta)\right)\right) \quad [5.44]$$

The desired coefficient is then determined by expression [5.45]:

$$Daf = \max_{t\in[\theta,\infty[}\left(1 - \frac{1}{\omega\theta}\left(\sin\omega t - \sin\omega t\cos\omega\theta + \cos\omega t\cos\omega\theta\right)\right) \quad [5.45]$$

It is possible to calculate this factor analytically, and we obtain formula [5.46]:

$$\begin{aligned} Daf &= 1 + \frac{1}{\omega\theta}\left(\left(1-\cos\omega\theta\right)\sin\xi + \sin\omega\theta\cos\xi\right) \\ \xi &= \arctan\left(\frac{1-\cos\omega\theta}{\sin\omega\theta}\right) \end{aligned} \quad [5.46]$$

The value of this coefficient is represented as a function of the relative time in Figure 5.11. This coefficient varies between 1 and 2.

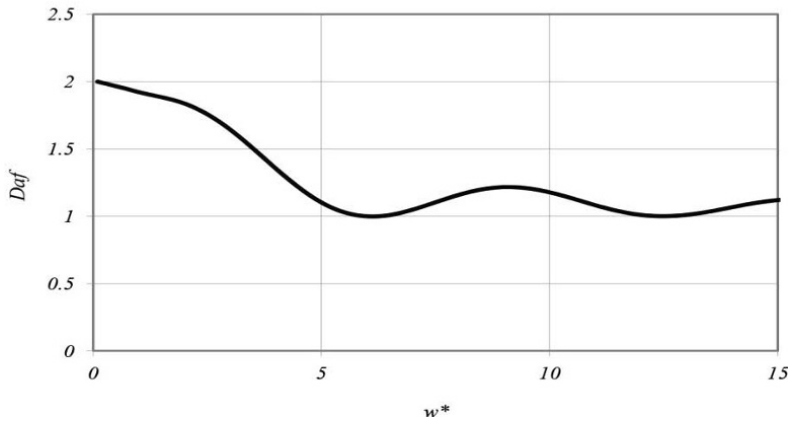

Figure 5.11. *Dynamic amplification factor as a function of the relative duration of time scalability*

5.3. Iso-damage curves

5.3.1. *Impulsive loading*

The response spectrum is a useful tool for the engineer if loading is determined and if we want to estimate the response of any structure. The practical question may arise in a different form. If a structure is known (an existing building, for example), what are the dynamic loads it is able to bear? This approach assumes that the shape of the dynamic stress is known and defined by two parameters. We take the example of a rectangular pulse, defined by two parameters, amplitude P and pulse i. The resistance of the structure is linked in order not to exceed a certain displacement amplitude, denoted by x_{max}.

The question is then formulated as the search for pairs of values (P, i) that allow x_{max} to be achieved. To make quite a general approach, dimensionless parameters are used [5.47]:

$$I^* = \frac{i}{x_{\max}\sqrt{km}} \quad P^* = \frac{2P}{kx_{\max}} \qquad [5.47]$$

As the mechanical response is known (equations [5.17]–[5.23]), it is possible to calculate the points on this iso-damage curve, also known as a P–I curve, as shown in Figure 5.12. This iso-damage curve resembles a hyperbola for which the asymptotes correspond, horizontally, to the load pulse and, vertically, to the long-term load. The use of such a graph is simple. If the parameters of the load correspond to a point below or to the left of the curve, the structure will be able to resist. If the load is of the "triangle" or "half-sine" type, the iso-damage curve looks the same. The iso-damage curve can be deduced from the response spectrum, as shown in Figure 5.13. Point i in the spectrum corresponds to a load of duration $\theta_i = \pi w_i * / \omega$. The dimensionless amplitude of the load is 1 and produces the displacement x_i. Reaching a critical displacement of 1 requires a load of amplitude $P_i = 1/x_i$. With knowledge of P_i and θ_i, we can calculate $I_i(P_i, \theta_i)$ according to a formula that depends on the shape of the signal. We then have a point on the iso-damage curve.

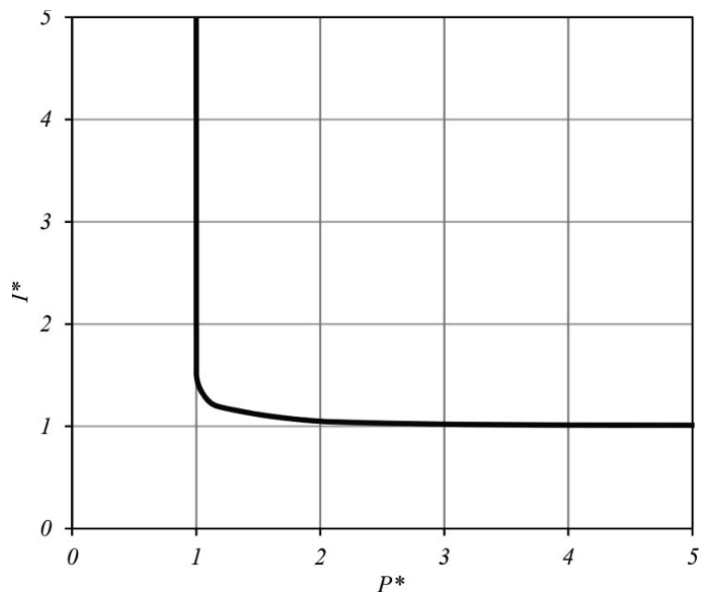

Figure 5.12. *Iso-damage curve, or "pressure-pulse" graph, for a structure with one degree of freedom solicited by a rectangular pulse*

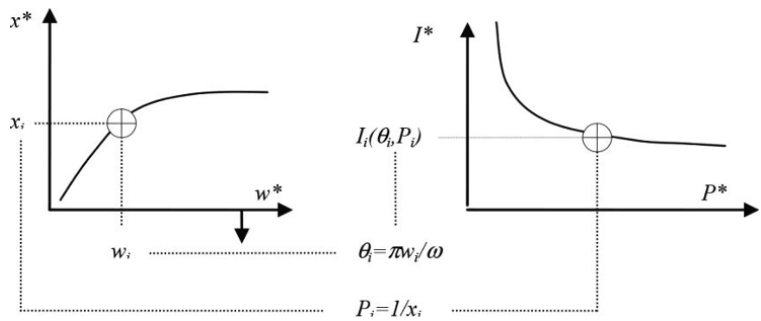

Figure 5.13. *Correspondence between a response spectrum and iso-damage curve*

5.3.2. *Alternating load*

Determination of the iso-damage curve was done in the case of an alternating load of type as in Figure 5.8. The result, derived from the spectrum, is shown in Figure 5.14. We note that in this case, the appearance of a hyperbole is not conserved and the "safety" area has a very different border. Thus, we must be very careful when there is stress accompanied by change in force direction before using tools that were originally developed for impulsive loads close to the "rectangle".

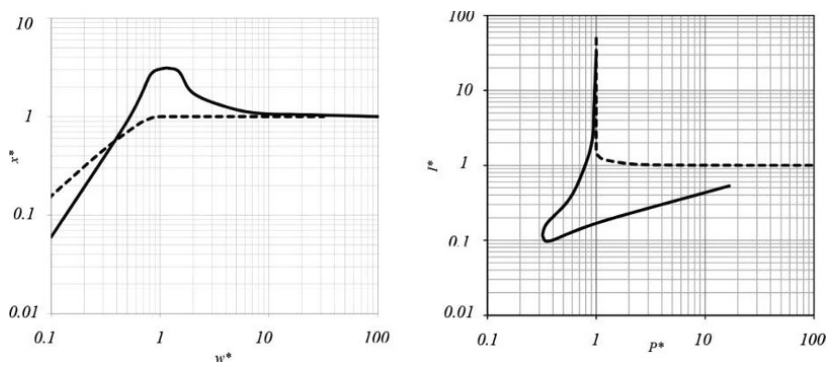

Figure 5.14. *Response spectra curves and iso-damage curve for a rectangular pulse (dotted line) and an alternating pulse (solid line)*

5.4. Modeling a real structure

5.4.1. *Definition of an equivalent system*

There are some cases where modeling a structure as a highly rigid mass, connected to a foundation via a link with easily identifiable rigidity, is quite obvious. In general, a real structure does not present itself as a mass connected to a spring. A significant work is structure modeling and the choice of mass and equivalent stiffness [BIG 64, TIL 86, PAU 05, WEE 07]. Below, we present the so-called Rayleigh method. This method is formally presented in order to demonstrate the principle and generality. In subsequent sections, typical examples of structures are modeled.

In general, a structure *(S)* is solicited by a load $Q(x, t)$ which causes displacement $\underline{U}(x,t)$. These two quantities are, *a priori*, vector fields. This structure has a mechanical model (bending beam, for example) which allows calculation of stresses and strains under static load.

The first step in modeling is to choose scalar variables to represent the load and the mechanical response:

– choice of scalar $F_e(t)$ representing the load;

– choice of scalar $X_e(t)$ representing the displacement.

There are no special restrictions to make this choice. Generally, the resultant force load is chosen for F_e and the largest structure displacement is chosen for X_e. A structural mechanics static calculation can find the ratio of this force to the displacement, which we call the equivalent stiffness [5.48]:

$$K_e = \frac{F_e}{X_e} \qquad [5.48]$$

The second step consists of determining the equivalent mass in order to give the system to one degree of freedom. This is based on the Rayleigh method for approximate determination of a specific frequency structure. We must first choose the displacement mode [5.49]. This choice may be based on intuition and must verify the

kinematic boundary conditions that are imposed on the structure. It is customary to take static strain, or the first mode of vibration of the structure, as the displacement mode if these are known:

$$\underline{U}(\underline{x},t) = \psi(t)\underline{\phi}(\underline{x}) \quad [5.49]$$

In the absence of load, we consider the free oscillations of the structure and the temporal function is harmonic [5.50]:

$$\psi(t) = \alpha e^{i\omega t} \quad [5.50]$$

It is then possible to estimate the kinetic energy of the structure that oscillates depending on the selected mode [5.51] (the integral is over the entire structure):

$$E_c = \frac{1}{2}\int \rho(\underline{x})\dot{\underline{U}}^2(\underline{x},t)\,dv = -\frac{1}{2}\omega^2\alpha^2 e^{2i\omega t}\int \rho(\underline{x})\underline{\phi}^2(\underline{x})\,dv \quad [5.51]$$

Moreover, it is also possible to determine the elastic strain energy in the structure. The elastic strain energy is explained from a calculation under static loading. Examples will be discussed in the following sections. We write this energy from the strain field associated with the chosen displacement field by formula [5.52]:

$$\underline{\underline{\varepsilon}}(\underline{U}) = \alpha e^{i\omega t}\,\underline{\underline{\varepsilon}}(\underline{\phi}) \quad [5.52]$$

The elastic energy is then written as formula [5.53]. This is a formal expression to explain the method principle. In practice, the elastic energy formula will be adapted to the mechanical model of the structure. Examples will be developed in the following sections:

$$E_e = \frac{1}{2}\int \underline{\underline{\varepsilon}}(\underline{U}) : \underline{\underline{\sigma}}\left(\underline{\underline{\varepsilon}}(\underline{U})\right) dv = \frac{1}{2}\alpha^2 e^{2i\omega t}\int \underline{\underline{\varepsilon}}(\underline{\phi}) : \underline{\underline{\sigma}}\left(\underline{\underline{\varepsilon}}(\underline{\phi})\right) dv \quad [5.53]$$

During free oscillations, these energies vary with time. Kinetic energy is at a maximum when velocity is greatest, that is to say, when the structure passes through the static equilibrium position. At this same instant, elastic strain energy is zero. Elastic energy is at its

maximum when the amplitude of strain in the structure is at its maximum. At this point, the velocities are cancelled out and the kinetic energy is zero. These maximum energies are expressed as formulas [5.54]:

$$E_c^{\max} = \frac{1}{2}\omega^2\alpha^2 \int \rho \underline{\phi}^2 dv \quad E_e^{\max} = \frac{1}{2}\alpha^2 \int \underline{\underline{\varepsilon}}\left(\underline{\phi}\right) : \underline{\underline{\sigma}}\left(\underline{\underline{\varepsilon}}\left(\underline{\phi}\right)\right) dv \quad [5.54]$$

As the sum of the two energies remains constant, and if one is at its maximum, then the other is zero, the maximum elastic energy is equal to the maximum kinetic energy. This allows us to find an expression for the eigenfrequency of the oscillating structure depending on the selected mode [5.55]:

$$\omega^2 = \frac{\int \underline{\underline{\varepsilon}}\left(\underline{\phi}\right) : \underline{\underline{\sigma}}\left(\underline{\underline{\varepsilon}}\left(\underline{\phi}\right)\right) dv}{\int \rho \underline{\phi}^2 \, dv} \quad [5.55]$$

The value of the pulsation, using the Rayleigh method, is still estimated by excess. The best choice of mode ϕ is the one that minimizes this value. Determining the eigenfrequency can determine the value to be given to the equivalent mass [5.56]:

$$M_e = \frac{K_e}{\omega^2} \quad [5.56]$$

5.4.2. *Beams in flexion*

We can explain formulas [5.54] and [5.55] if the structure is a beam in flexion. The beam in question is straight (x-axis), of length L, made up of a material with elasticity module E and density ρ. The section of the beam is S, and the second moment of area is I. Displacement of the structure corresponds to the transverse displacement field of the beam $U(x,t)$. These displacements are proportional to the chosen mode $\phi(x)$. Kinetic energy is related to the

transverse displacements of the beam [5.57]. Neglecting the kinetic energy associated with the rotation of beam sections:

$$E_c^{\max} = \frac{1}{2}\int_0^L \rho S \dot{U}^2 \, dx = \frac{\omega^2 \rho S}{2}\int_0^L \phi^2(x)\, dx \qquad [5.57]$$

In a beam, the elastic strain energy can be expressed in terms of the internal forces [5.58], where *Mf* is the bending moment, *V* is shear force and *N* is the normal force (*G* is the shear modulus and *S′* is the corrected sheared section):

$$E_e = \frac{1}{2}\int_0^L \left(\frac{Mf^2}{EI} + \frac{V^2}{GS'} + \frac{N^2}{ES} \right) dx \qquad [5.58]$$

As strains due to flexion are generally much greater than those caused by normal force and shear force, it is customary to only consider the term at the bending moment in the expression of energy. As the beam is elastic, the bending moment is proportional to the curve [5.59]:

$$E_e^{\max} = \frac{1}{2}\int_0^L \frac{Mf^2}{EI} dx = \frac{EI}{2}\int_0^L \left(\frac{\partial^2 \phi}{\partial x^2} \right)^2 dx \quad \left(\frac{Mf}{EI} = \frac{\partial^2 \phi}{\partial x^2} \right) \qquad [5.59]$$

We then deduce the expression of the eigenfrequency associated with the selected strain mode [5.60]:

$$\omega^2 = \frac{EI \int_0^L \left(\frac{\partial^2 \phi}{\partial x^2} \right)^2 dx}{\rho S \int_0^L \phi^2 dx} \qquad [5.60]$$

5.4.3. *Shock on a beam*

We address the problem of an object falling onto a beam deformed by flexion. The impact results in a point force *F(t)* applied in the middle of the beam. The beam is made up of a material with elasticity module *E* and density ρ. The beam section is *S*, and the second moment of area is *I* (Figure 5.15).

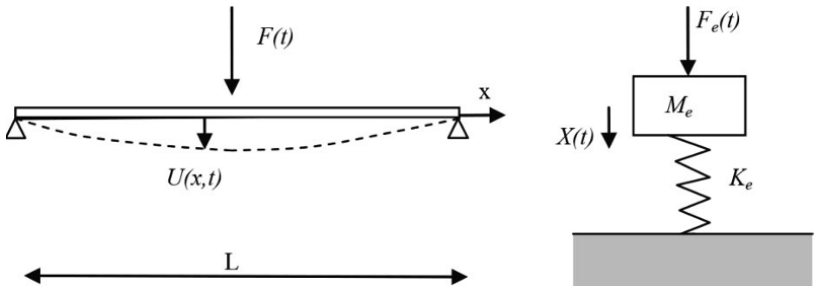

Figure 5.15. *Flexion beam undergoing an impact at its center and an equivalent system to one degree of freedom*

We try to use a system with one degree of freedom to model the mechanical response of the beam. The transverse displacement of the beam is *U(x,t)*. We choose the parameters for the model. Displacement of the center of the beam is the variable characterizing the displacement and, in this case, the equivalent force is identical to the real load [5.61]:

$$X_e(t) = U\left(\frac{L}{2}, t\right) \quad F_e(t) = F(t) \qquad [5.61]$$

Using beam theory, we can know the expression of the bending moment along the beam and the equation of the deformed line. As the structure is symmetrical, the bending moment and the strain are also symmetrical. The formula is expressed in the half-beam [5.62]:

$$Mf(x) = \frac{Fx}{2} \qquad U(x) = \frac{F}{EI}\left(\frac{x^3}{12} - \frac{L^2 x}{16}\right) \quad x \in \left[0, \frac{L}{2}\right] \qquad [5.62]$$

From these expressions, we deduce the value of the equivalent stiffness K_e of the system [5.63]:

$$K_e = \frac{F_e}{X_e} = \frac{F}{U(L/2)} = \frac{48EI}{L^3} \qquad [5.63]$$

For the beam strain mode, we will take three hypotheses to compare the results [5.64]:

– Mode ϕ_1 is proportional to the static deformed line of the beam.

– Mode ϕ_2 is the first mode of vibration on the beam.

– Mode ϕ_3 is a parabola.

These three modes satisfy the kinematic conditions imposed on the beam extremities (the third hypothesis does not verify the dynamic condition of the support because the moment and, therefore, the curvature should be zero):

$$\phi_1(x) = \frac{L^2 x}{4} - \frac{x^3}{3} \quad \left(x \in [0, L/2]\right)$$
$$\phi_2(x) = \sin\frac{\pi x}{L} \quad \phi_3(x) = x(L-x) \quad \left(x \in [0, L]\right) \qquad [5.64]$$

For mode ϕ_1, we estimate kinetic and elastic energy [5.65]:

$$E_c^{\max} = \omega^2 \rho S \int_0^{L/2} x^2 \left(\frac{x^4}{9} - \frac{x^2 L^2}{6} + \frac{L^4}{16}\right) dx = \frac{37\,\omega^2 \rho S L^7}{20160}$$
$$E_e^{\max} = EI \int_0^{L/2} 4x^2\, dx = \frac{L^3 EI}{6} \qquad [5.65]$$

We deduce the eigenfrequency associated with this mode and the equivalent mass M_e to be attributed to the equivalent system [5.66]. M is the total mass of the beam:

$$\omega^2 = \frac{3360}{37}\frac{EI}{\rho S L^4} = 90.8\frac{EI}{\rho S L^4} \quad M_e = \frac{37}{70}\rho S L = 0.529\,M \qquad [5.66]$$

Similarly, for mode ϕ_2, we estimate the kinetic and elastic energies [5.67]:

$$E_c^{\max} = \frac{\omega^2 \rho S}{2} \int_0^L \sin^2 \frac{\pi x^2}{L}\, dx = \frac{\omega^2 \rho S L}{4}$$
$$E_e^{\max} = \frac{EI}{2} \int_0^L \frac{\pi^4}{L^4} \sin^2 \frac{\pi x}{L} dx = \frac{\pi^4 EI}{4L^3} \qquad [5.67]$$

We deduce the eigenfrequency associated with mode ϕ_2 and the equivalent mass M_e to be attributed to the equivalent system [5.68]:

$$\omega^2 = \frac{\pi^4 EI}{\rho SL^4} = 97\frac{EI}{\rho SL^4} \quad M_e = \frac{48}{\pi^4}\rho SL = 0.493M \qquad [5.68]$$

Finally, for mode ϕ_3, we estimate kinetic and elastic energy [5.69]:

$$\begin{aligned} E_c^{\max} &= \frac{\omega^2 \rho S}{2}\int_0^L x^2 (L-x)^2 dx = \frac{\omega^2 \rho S L^5}{60} \\ E_e^{\max} &= \frac{EI}{2}\int_0^L 4\,dx = 2EIL \end{aligned} \qquad [5.69]$$

We deduce the eigenfrequency associated with mode ϕ_3 and the equivalent mass M_e which must then be assigned to the equivalent system [5.70]:

$$\omega^2 = 120\frac{EI}{\rho SL^4} \quad M_e = \frac{2}{5}\rho SL = 0.4M \qquad [5.70]$$

In this case, it is assumed that mode ϕ_1, proportional to strain under static loading, is the best approximation for the strain mode as it is with this mode that the lowest eigenfrequency is obtained. This optimum concept is relative because the system with one degree of freedom is already an approximation for which we will discuss the limitations in Chapter 8. We note that even a rough estimate of the mode (ϕ_3) allows us to assess the order of magnitude of the eigenfrequency.

5.4.4. *Blast on a beam*

We will now consider the action of a blast on a structure that can result in the application of a uniformly distributed load upon a beam. The beam is made up of a material with elasticity module E and density ρ. The beam section is S, and the second moment of area is I (Figure 5.16). We try to use a system with one degree of freedom to model the mechanical response of the beam. The transverse

displacement of the beam is *U(x,t)*. As in the previous example, we choose the displacement of the center of the beam as a variable characterizing the displacement. As the force parameter, we choose the resulting load distributed on the beam [5.71]:

$$X_e(t) = U\left(\frac{L}{2}, t\right) \quad F_e(t) = L\,p(t) \qquad [5.71]$$

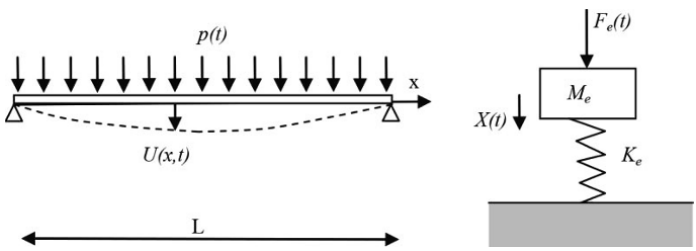

Figure 5.16. *Beam subjected to a load from a blast and the equivalent associated system*

We always know the expression of the bending moment along the beam and the equation of the deformed line [5.72]:

$$Mf(x) = \frac{pLx}{2} - \frac{px^2}{2} \quad U(x) = \frac{p}{EI}\left(\frac{Lx^3}{12} - \frac{L^3x}{24} - \frac{x^4}{24}\right) \quad x \in [0, L] \qquad [5.72]$$

From these expressions, we can deduce the value of the equivalent stiffness K_e of the equivalent system [5.73]:

$$K_e = \frac{F_e}{X_e} = \frac{pL}{U(L/2)} = \frac{384EI}{5L^3} \qquad [5.73]$$

For the mode of strain on the beam, we will use the three assumptions from the previous example [5.74]. Mode ϕ_1 is only changed by that which is proportional to the static strain on the beam because the latter is different with a distributed load:

$$\begin{aligned} &\phi_1(x) = 2Lx^3 - L^3x - x^4 \quad (x \in [0, L]) \\ &\phi_2(x) = \sin\frac{\pi x}{L} \quad \phi_3(x) = x(L - x) \quad (x \in [0, L]) \end{aligned} \qquad [5.74]$$

For the new ϕ_1 mode, we estimate kinetic and elastic energy [5.75]:

$$E_c^{\max} = \frac{\omega^2 \rho S}{2} \int_0^L \left(2Lx^3 - L^3 x - x^4\right)^2 dx = \frac{31\omega^2 \rho S L^9}{1260}$$
$$E_e^{\max} = \frac{EI}{2} \int_0^L \left(12Lx - 12x^2\right)^2 dx = \frac{12L^5 EI}{5} \quad [5.75]$$

We deduce the eigenfrequency associated with this mode and the equivalent mass M_e to be attributed to the equivalent system [5.76]:

$$\omega^2 = \frac{3024}{31} \frac{EI}{\rho S L^4} = 97.5 \frac{EI}{\rho S L^4} \quad M_e = \frac{248}{315} \rho S L = 0.787 M \quad [5.76]$$

We can calculate the eigenfrequency and the equivalent mass for mode ϕ_2, proportional to the vibration mode [5.77]:

$$\omega^2 = \frac{\pi^4 EI}{\rho S L^4} = 97 \frac{EI}{\rho S L^4} \quad M_e = \frac{384}{5\pi^4} \rho S L = 0.788 M \quad [5.77]$$

The same eigenfrequency and equivalent mass calculation is performed for mode ϕ_3 [5.78]:

$$\omega^2 = 120 \frac{EI}{\rho S L^4} \quad M_e = \frac{16}{25} \rho S L = 0.64 M \quad [5.78]$$

In this case, we note that calculations with static deformed line and calculations using the first mode of vibration give very similar results. This example also illustrates that the equivalent mass depends not only on the structure, but also on the load and choice of representative variables.

5.4.5. *Shock on a mass supported by a mast*

A structure may be composed of beams and other elements representable by non-deformable solids. We then combine beam theory and the mechanics of rigid solids. A representative example of this is a flexible mast supporting a structure similar to a rigid solid as

shown in Figure 5.17. The mast is a beam; it consists of a material with elasticity module E and density ρ. The section of the beam is S and the second moment of area is I.

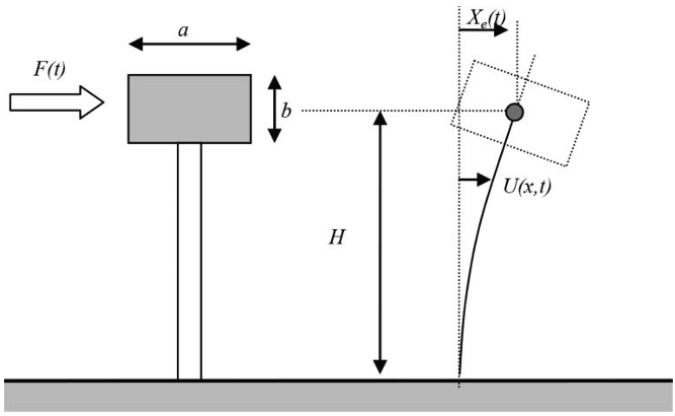

Figure 5.17. *Structure consisting of a rigid beam and a mass subjected to an impact. Modeling of deformation is shown on the right*

The rigid element has a mass M_S and a moment of inertia $\Im_S$ [5.79] (with respect to its center of gravity and the perpendicular axis to the figure). Its dimensions a and b are small compared to the height H:

$$\Im_S = \frac{M_S\left(a^2 + b^2\right)}{12} \qquad [5.79]$$

The mechanical model of the structure is shown the right part of Figure 5.17. Some simplifications are made by considering a beam of length H and estimating that the displacement of the rigid solid is characterized by the displacement and rotation of the extremities of this beam. We search for a system, equivalent to one degree of freedom, to represent the oscillating motion under the action of an impact represented by a horizontal force F acting on the rigid body. We choose the displacement of the top of the beam and the horizontal force as the parameters of the equivalent system [5.80]:

$$X_e(t) = U(H,t) \quad F_e(t) = F(t) \qquad [5.80]$$

Beam theory is used to find the bending moment and the deformed line under the action of a static force F [5.81]:

$$Mf(x) = -F(H-x) \quad U(x) = \frac{F}{EI}\left(\frac{x^3}{6} - \frac{Hx^2}{2}\right) \quad x \in [0,H] \text{ [5.81]}$$

This static calculation allows us to determine the equivalent stiffness K_e of the system [5.82]:

$$K_e = \frac{F_e}{X_e} = \frac{F}{U(H)} = \frac{3EI}{H^3} \quad \text{[5.82]}$$

We choose a strain mode proportional to strain under static load [5.83]:

$$\phi(x) = x^3 - 3Hx^2 \quad (x \in [0,H]) \quad \text{[5.83]}$$

Kinetic energy calculation is achieved by adding the term for transverse displacements of the beam to the terms from the translation and rotation of the rigid solid [5.84]. In the selected mode, mass M_s undergoes translation $\phi(H)$ and a rotation equal to the rotation at the end of the beam:

$$\begin{aligned} E_c^{\max} &= \frac{\omega^2}{2}\left(\rho S\int_0^H \phi^2(x)dx + M_S\phi^2(H) + \Im_S\left(\frac{d\phi}{dx}\right)_H^2\right) \\ E_c^{\max} &= \frac{\omega^2}{2}\left(\frac{33}{35}\rho S H^6 + 4M_S H^6 + 9\Im_S H^4\right) \end{aligned} \quad \text{[5.84]}$$

The elastic energy is only due to the strain on the beam [5.85]:

$$E_e^{\max} = \frac{EI}{2}\int_0^H \left(6(x-H)\right)^2 dx = 6EIH^3 \quad \text{[5.85]}$$

This allows the estimation of eigenfrequency [5.86]:

$$\omega^2 = \frac{12EI}{(33/35)\rho S H^3 + 4M_S H^3 + 9\Im_S H} \quad \text{[5.86]}$$

We then deduce the equivalent mass to give the system to one degree of freedom, representative of the motion of this structure depending on the strain mode [5.87]:

$$M_e = \frac{33}{140}\rho SH + M_S + \frac{9}{4}\frac{\Im_S}{H^2} \qquad [5.87]$$

The system to one degree of freedom is simple to study, but it corresponds to an assumption about the shape of displacements. The assumption made here on the shape is valid if the rigid body moment of inertia is not too large. The system to one degree of freedom is the most basic of models. The type of structure in this example can be modeled by a system with two degrees of freedom. For example, it is possible to consider the displacement and rotation of the rigid body as two degrees of freedom. The corresponding methods will be discussed in Chapter 9.

5.4.6. *Shock on a structure*

This last example concerns a building of two levels for which we want to estimate the effect of a horizontal impact (Figure 5.18). The floors are considered as rigid solids of mass M (reinforced concrete). Flexibility of the structure subjected to a horizontal force is provided by the metal studs whose mass is negligible compared to the floors. K is the stiffness provided by the set of poles for one level.

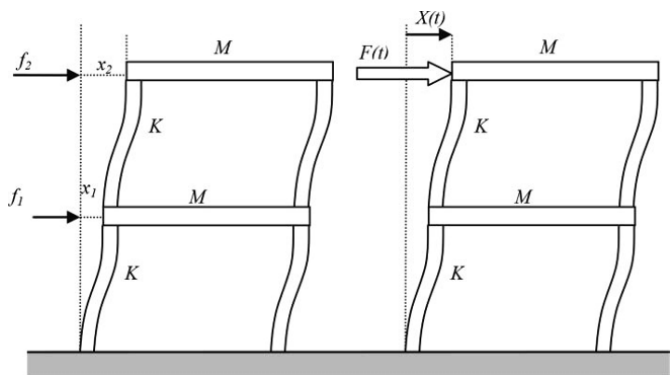

Figure 5.18. *Two-level structure: on the left, the mechanical model; on the right, the impact force and the displacement identified as parameters*

The mechanical modeling of the structure can be written in matrix form [5.88]:

$$\begin{pmatrix} f_1 \\ f_2 \end{pmatrix} = \begin{pmatrix} M & 0 \\ 0 & M \end{pmatrix} \begin{pmatrix} \ddot{x}_1 \\ \ddot{x}_2 \end{pmatrix} + \begin{pmatrix} 2K & -K \\ -K & K \end{pmatrix} \begin{pmatrix} x_1 \\ x_2 \end{pmatrix} \quad [5.88]$$

Thus, the mass and stiffness matrices are defined as [5.89]:

$$\underline{\underline{M}} = \begin{pmatrix} M & 0 \\ 0 & M \end{pmatrix} \quad \underline{\underline{K}} = \begin{pmatrix} 2K & -K \\ -K & K \end{pmatrix} \quad [5.89]$$

It is possible to consider the displacements of floors as two degrees of freedom. This will be discussed in Chapter 9. A simpler and faster but less accurate method may be to look for a system with one degree of freedom equivalent to the structure under the load. As parameters of this elementary system, we choose the displacement from level 2, *X(t)(X = x₂)* and the impact force *F(t)*. The search for equivalent stiffness is done by solving the static problem [5.90]:

$$\begin{pmatrix} 0 \\ F \end{pmatrix} = \begin{pmatrix} 2K & -K \\ -K & K \end{pmatrix} \begin{pmatrix} x_1 \\ x_2 \end{pmatrix} \quad K_e = \frac{X}{F} = \frac{K}{2} \quad [5.90]$$

We also have the static strain mode [5.91]:

$$\underline{\phi} \begin{pmatrix} 1 \\ 2 \end{pmatrix} \quad [5.91]$$

By choosing this method of static strain mode for the oscillation of the structure as a result of impact, we can calculate the kinetic energy and the elastic strain energy [5.92]:

$$E_c = \frac{\omega^2}{2} {}^t\underline{\phi}\,\underline{\underline{M}}\,\underline{\phi} = \frac{5}{2}\omega^2 M \quad E_e = \frac{1}{2} {}^t\underline{\phi}\,\underline{\underline{K}}\,\underline{\phi} = K \quad [5.92]$$

It is easy to deduce the eigenfrequency of the structure in this strain mode and the equivalent mass to give the system with one degree of freedom [5.93]:

$$\omega^2 = \frac{{}^t\underline{\phi}\,\underline{\underline{K}}\,\underline{\phi}}{{}^t\underline{\phi}\,\underline{\underline{M}}\,\underline{\phi}} = \frac{2K}{5M} \quad M_e = \frac{K_e}{\omega^2} = \frac{5}{4}M \qquad [5.93]$$

To define an equivalent system with one degree of freedom for a structure allows the use of the tools mentioned at the beginning of this chapter. However, this method should be used with caution. Indeed, equivalence is based on the choice of the shape of displacements. Intuition and simplicity guide this choice toward the static mode and the first mode of vibration. We should check that the load *F(t)* leads to strain of this type. For example, it is necessary that its duration is greater than or equal to the natural half-period of the chosen model. Otherwise, a very short load could cause displacements of a very different shape than in the selected mode. The most comprehensive study of beams (Chapter 8) and that of systems with multiple degrees of freedom (Chapter 10) will critically examine this method.

Chapter 6

Collisions of Structures

In an accident, shock on a structure may be caused by another deformable structure. The force then imposed can be estimated first in the case of elastic behavior and then by considering the crushing of the projectile.

6.1. Shocks on elastic structures

6.1.1. *Equations of motion*

Shocks on structures differ from shocks on bulk solids. The projectile and the target structure are deformable (Figure 6.1). One approach is to model the projectile and target as linear elastic systems, each with one degree of freedom [CEB 88] (Figure 6.2).

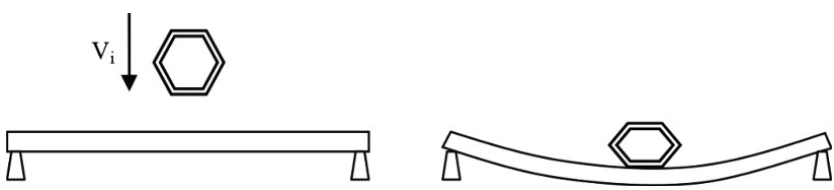

Figure 6.1. *Shock of one structure on another structure*

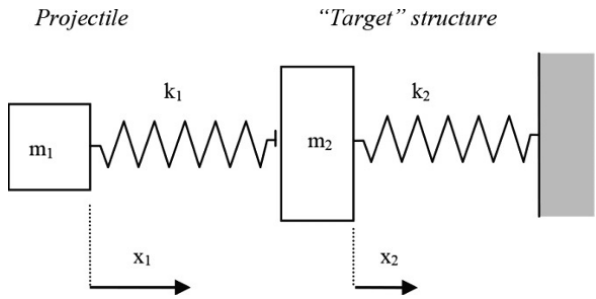

Figure 6.2. *Impact of a projectile on an elastic structure*

Let us consider the initial moment of contact between the projectile and the target structure. After this instant, and as long as the two structures are in contact, the ensemble behaves as a system with two degrees of freedom. The equations governing motion are given in [6.1]. There are no external forces applied to the system. Motion is caused by the fact that at the initial moment, the projectile mass m_1 is driven by velocity V_i. The study of this system will be used to determine the force applied to the structure during the shock:

$$\begin{cases} m_1\ddot{x}_1 + k_1(x_1 - x_2) = 0 \\ m_2\ddot{x}_2 - k_1(x_1 - x_2) + k_2 x_2 = 0 \end{cases} \qquad [6.1]$$

6.1.2. *Impact of a relatively flexible projectile*

In practice, it may occur that the mass and stiffness of the structure are much greater than those of the projectile. Displacement x_1 of the projectile is then also much larger than displacement x_2 of the structure. We can consider a decoupling of these equations by considering the approximation $k_1(x_1 - x_2) \approx k_1 x_1$. Then, it is easy to estimate the impact force and the system can be written as [6.2]:

$$\begin{cases} m_1\ddot{x}_1 + k_1 x_1 = 0 \\ m_2\ddot{x}_2 + k_2 x_2 = F(t) \end{cases} \qquad F(t) = k_1 x_1 \quad x_1 >> x_2 \qquad [6.2]$$

The resolution is then very simple and we obtain expression [6.3] for the impact force:

$$F(t) = V_i\sqrt{k_1 m_1}\sin\omega_1 t \qquad t \in \left[0, \frac{\pi}{\omega_1}\right] \qquad i = 2m_1 V_i \qquad [6.3]$$

The evolution of the impact force is shown in Figure 6.3 with characteristic values of duration, amplitude and pulse. Force cannot be negative and contact stops after time π/ω_1. This is the projectile rebound.

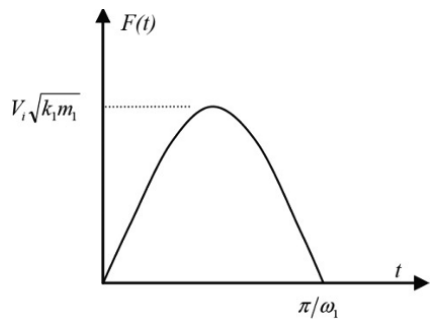

Figure 6.3. *Impact force of a structure on a rigid target, based on the elastic characteristics of the structure comprising the projectile*

6.1.3. *Coupling in a collision of two structures*

In general, motion of the projectile and the structure are coupled by equations [6.1] and determination of force requires resolution thereof. The system of equations [6.1] can be solved using the operational images from the Laplace transformation [6.4]. The initial velocity of mass m_1 is taken into account in the transformation:

$$\begin{cases} m_1\left(s^2\overline{x}_1 - V_i\right) + k_1\left(\overline{x}_1 - \overline{x}_2\right) = 0 \\ m_2 s^2\overline{x}_2 - k_1\left(\overline{x}_1 - \overline{x}_2\right) + k_2\overline{x}_2 = 0 \end{cases} \qquad [6.4]$$

This system can be rewritten as [6.5]:

$$\begin{cases} \left(s^2 + \omega_1^2\right)\overline{x}_1 - \omega_1^2\overline{x}_2 = V_i \\ \alpha\omega_1^2\overline{x}_1 - \left(s^2 + \alpha\omega_1^2 + \omega_2^2\right)\overline{x}_2 = 0 \end{cases} \qquad \alpha = \frac{m_1}{m_2} \qquad [6.5]$$

The solutions to this system are [6.6]:

$$\begin{cases} \overline{x}_1 = \dfrac{\left(s^2 + \alpha\omega_1^2 + \omega_2^2\right) V_i}{\left(s^2 + \omega_1^2\right)\left(s^2 + \alpha\omega_1^2 + \omega_2^2\right) - \alpha\omega_1^4} \\ \overline{x}_2 = \dfrac{\alpha\omega_1^2 V_i}{\left(s^2 + \omega_1^2\right)\left(s^2 + \alpha\omega_1^2 + \omega_2^2\right) - \alpha\omega_1^4} \end{cases} \quad [6.6]$$

The denominator of these expressions is a polynomial that always has two negative roots; it can thus be written as [6.7]:

$$\begin{cases} \overline{x}_1 = \dfrac{\left(s^2 + \alpha\omega_1^2 + \omega_2^2\right) V_i}{\left(s^2 + \Omega_1^2\right)\left(s^2 + \Omega_2^2\right)} \\ \overline{x}_2 = \dfrac{\alpha\,\omega_1^2 V_i}{\left(s^2 + \Omega_1^2\right)\left(s^2 + \Omega_2^2\right)} \end{cases} \quad [6.7]$$

This, by inversion, leads to temporal evolutions of both masses [6.8]:

$$\begin{cases} x_1 = \dfrac{V_i}{\left(\Omega_2^2 - \Omega_1^2\right)} \left(\begin{array}{c} \dfrac{\alpha\omega_1^2 + \omega_2^2 - \Omega_1^2}{\Omega_1} \sin \Omega_1 t \\ - \dfrac{\alpha\omega_1^2 + \omega_2^2 - \Omega_2^2}{\Omega_2} \sin \Omega_2 t \end{array} \right) \\ x_2 = \dfrac{\alpha\omega_1^2 V_i}{\left(\Omega_2^2 - \Omega_1^2\right)} \left(\dfrac{1}{\Omega_1} \sin \Omega_1 t - \dfrac{1}{\Omega_2} \sin \Omega_2 t \right) \end{cases} \quad [6.8]$$

We then deduce the force applied by the projectile onto the structure [6.9]:

$$F(t) = \frac{k_1 V_i}{\left(\Omega_2^2 - \Omega_1^2\right)} \left(\frac{\omega_2^2 - \Omega_1^2}{\Omega_1} \sin \Omega_1 t - \frac{\omega_2^2 - \Omega_2^2}{\Omega_2} \sin \Omega_2 t \right) \quad [6.9]$$

Expressions [6.8] and [6.9] are valid as long as the force is positive. It may be noted that the rate of application of this force, at

the initial time, is always the same and equals $k_1 V_i$. To represent this force, dimensionless parameters [6.10] are introduced:

$$f = \frac{F}{V_i \sqrt{k_1 m_1}} \quad \tau = \frac{\omega_1 t}{\pi} \quad \alpha = \frac{m_1}{m_2} \quad \beta = \frac{k_1}{k_2} \qquad [6.10]$$

Figure 6.4 shows four examples of impact forces for particular values of coefficients α and β. Curve A corresponds to the impact on a rigid structure as discussed in the previous section. The impact force may differ from the "half-sine" shape if we take flexibility of the structure into account.

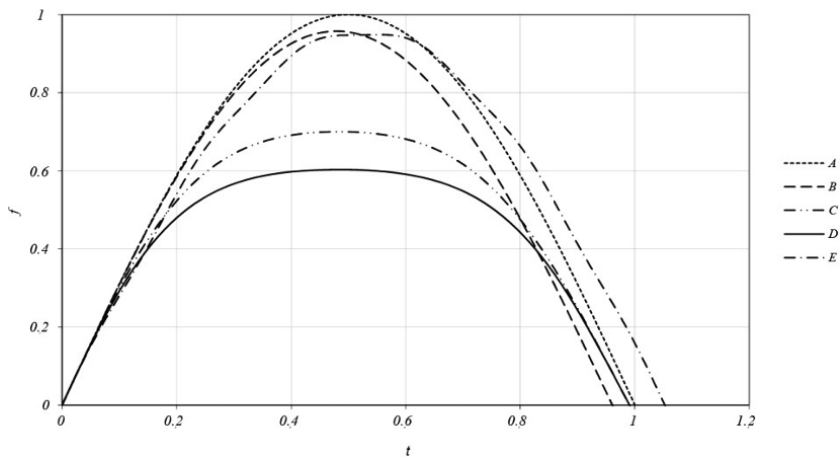

Figure 6.4. *Impact force during the collision of two structures: (A) rigid target; (B) $\alpha = 0.1$, $\beta = 1$; (C) $\alpha = 1$, $\beta = 1$; (D) $\alpha = 1$, $\beta = 0.1$; (E) $\alpha = 10$, $\beta = 0.1$*

6.1.4. *Fall of a rigid body onto a flexible structure*

A practical case for which we can ignore coupling is a rigid body falling onto a deformable structure. Take the example of a rock falling onto a structure covering a road in the mountains [ZHA 06]. To illustrate this, we consider an object falling in the middle of a beam that deforms by bending. The beam is made of a material of elasticity module E and density ρ. The beam section is S, and the second moment of area is I. This beam is modeled as a system with one

degree of freedom. The variable characterizing displacement is displacement of the center of the beam (Figure 6.5).

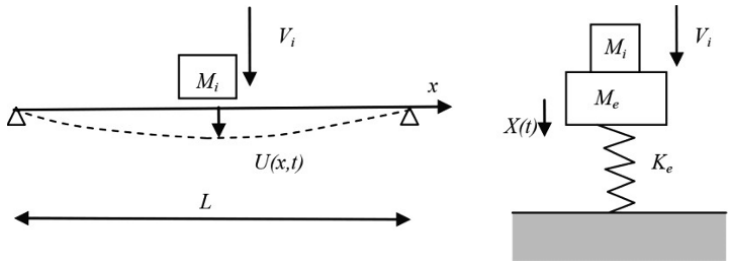

Figure 6.5. *A rigid body falling onto an elastic structure*

Stiffness K_e and equivalent mass M_e are determined by the Rayleigh method described in Chapter 5 [6.11]:

$$K_e = \frac{48EI}{L^3} \quad M_e \approx 0.5\,M \qquad [6.11]$$

A shock results in a point force $F(t)$ applied to the middle of the beam [6.12] ($\delta(t)$ is the Dirac delta function and $H(t)$ is the Heaviside function):

$$F(t) = M_i V_i\,\delta(t) + M_i\,g\,H(t) \qquad [6.12]$$

After impact, the block remains in contact with the beam and it is the ensemble of two masses that oscillate. The response of the beam is then [6.13]:

$$X(t) = \frac{M_i g}{K_e}(1-\cos\omega t) + \frac{M_i V_i}{\sqrt{K_e(M_e+M_i)}}\sin\omega t \quad \left(\omega = \sqrt{\frac{K_e}{M_i+M_e}}\right) \qquad [6.13]$$

This expression is valid as long as the two masses are fixed, i.e. if the acceleration does not exceed that of gravity. If this condition is always satisfied, there is no rebound. The condition for non-rebound can be explained by formula [6.14]:

$$M_i V_i\,\omega < g\sqrt{M_e(M_e+2M_i)} \qquad [6.14]$$

6.2. Shock with crushing

6.2.1. *Crushing phenomena*

Impacts of structures can lead to an impact force that exceeds the elastic resistance capacity of one of them. For the projectile, we talk of its crushing on the structure. Later in the classification of shocks, we will see that this qualifies as "soft". If one is interested in projectile crushing mechanisms, the phenomena that occur beyond the elastic phase can be more or less complex, but they generally reflect the fact that the force that a structure can withstand is limited. We denote force by *Fp*. This force can be estimated by theoretical or experimental study of the bearing capacity of the structure of the projectile under static conditions. This force *Fp* can be the result of plasticizing in compression, as discussed in Chapter 3, but more frequently, it is the buckling mechanism that characterizes crushing. We will first look at the mechanism of elastic buckling of a bar upon impact. In this case, the buckling length does not depend on the boundary conditions as when static, but depends on the impact velocity. Figure 6.6 shows a bar impacting, at velocity V_i, a structure we will consider as rigid.

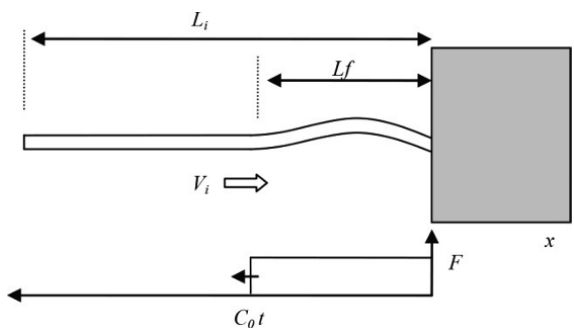

Figure 6.6. *Initiation of buckling of a bar upon impact*

The force caused by the shock can be determined according to the principles discussed in Chapter 2, and its expression is given by [6.15]:

$$F = S\sqrt{E\rho}\,V_i \qquad [6.15]$$

Section S, the Young modulus E and density ρ are the characteristics of the projectile bar. The Euler critical force that causes the elastic buckling of the bar is given by expression [6.16]:

$$F_c = \frac{\pi^2 E I}{Lf^2} \qquad [6.16]$$

During buckling of a static bar, buckling length Lf is known and determined by the conditions at the extremities. We then make the compressive force grow until it reaches the value F_c at which buckling occurs. During a shock, the compressive force is determined by the conditions of shock [6.15] and the compressed zone propagates in the bar at velocity C_0. Buckling may initiate if the length of the compressed zone corresponds to the buckling length associated with the compression force [6.17]:

$$Lf = \pi \sqrt{\frac{I C_0}{S V_i}} \qquad [6.17]$$

Buckling can only initiate if the buckling length is less than the length of the bar. This condition is reflected in the impact velocity by [6.18]:

$$V_i > \frac{\pi^2 I C_0}{S L_i^2} \qquad [6.18]$$

The critical buckling length therefore decreases as impact velocity increases according to [6.17]. To illustrate this, we consider an impactor that is a steel bar of 10 mm in diameter with impact velocities in the range of those of accidental impacts, around 10 m/s.

Figure 6.7 shows the critical buckling length depending on the impact velocity. This is the initiation of buckling. In dynamics, the compressive force may continue to propagate through the rest of the bar, and can even grow if the extremity on the left of the bar is not free but connected to a solid element. The study of this dynamic buckling will be discussed at the end of Chapter 8.

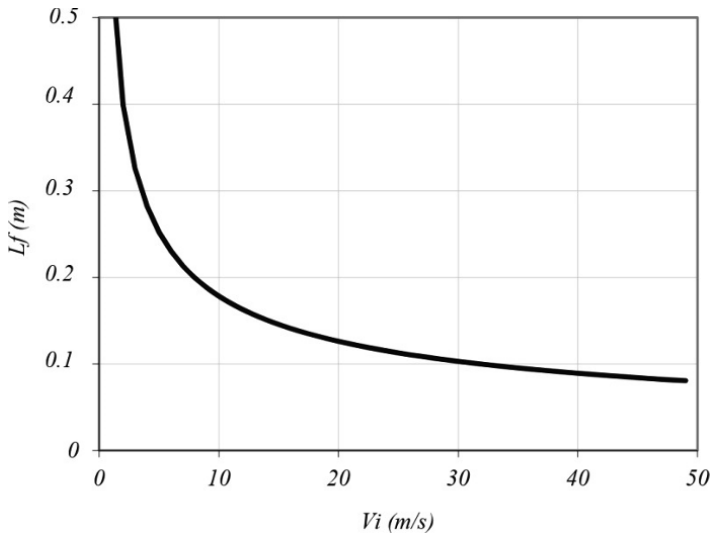

Figure 6.7. *Buckling length as a function of impact velocity for a steel bar 10 mm in diameter*

The projectiles can have more complex geometries than a simple bar. A fairly common situation is characterized by the fact that a "local" buckling length exists, linked to the geometry of the structure and which can be determined statically, i.e. less than the defined "global" buckling length, as we have just discussed under shock conditions. Another feature is that crushing corresponds to large plasticizing in the structure. In these cases, the maximum force that the projectile *Fp* can support can be determined in a static state. A typical example of this situation is that of the projectile consisting of a metal tube.

Figure 6.8 shows a tube crushing against a rigid target. Experiments show that the compressive force supported by the tube is limited by plastic buckling manifested by the tube's "accordion" folding. Upon impact, this folding appears at the extremity that is in contact with the target. A local buckling length (2λ) is observed. To determine the limiting force, we can proceed by experimentation. We can also estimate the amount of plastic work in the folding mechanism [JON 89]. Figure 6.8 shows a model for the folding mechanism. This

is a simplified view of the actual mechanism. A fold is supposed to respect the cylindrical symmetry and be composed of three annular plastic hinges. Two of them, denoted (1), remain on the circumference of the tube. The fold is formed outwardly by two cones that plasticize, denoted (3), and an annular plastic hinge, denoted (2), with a circumference that increases.

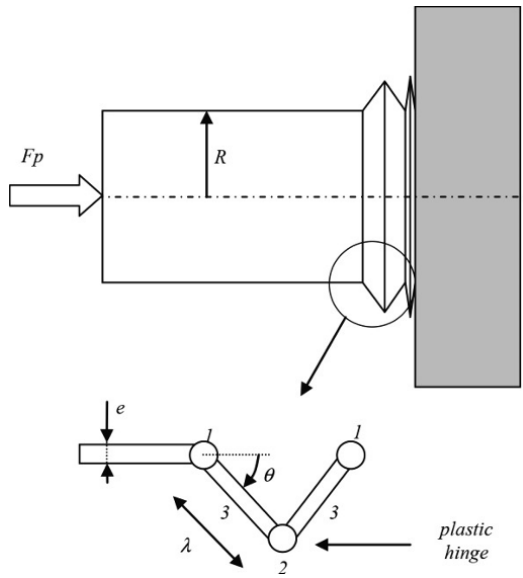

Figure 6.8. *Crushing of a cylindrical tube against a rigid target. Overview and detail of the folded area with plastic hinges*

We can successively estimate the energy dissipated by these three elements during folding if the angular parameter θ passes from 0 to $\pi/2$. The material is assumed to be perfectly plastic with yield σ_e. Elastic strains are neglected when it comes to plastic strain. We first calculate the energy dissipated by the hinges (1). It can be assumed that plasticizing occurs during flexion in a state close to the strain plane. The plastic moment per unit length is estimated by formula [6.19]:

$$Mp = \frac{e^2}{2\sqrt{3}}\sigma_e \qquad [6.19]$$

Thus, the work done is equal to the time unit length multiplied by the circumference and rotation of $\pi/2$. For both hinges (1), this work is equal to W_1 [6.20]:

$$W_1 = 2\pi^2 RMp \qquad [6.20]$$

For hinge (2), the expression should take into account that the length of the circumference increases progressively with folding. In a given state, characterized by the position parameter θ, a rotation increment of $d\theta$ produces elementary work dW_2 as indicated by formula [6.21]:

$$dW_2 = 4\pi\left(R + \lambda\sin\theta\right)Mp\,d\theta \qquad [6.21]$$

Integrating between 0 and $\pi/2$, we obtain the work done by hinge (2), for which expression W_2 is given by [6.22]:

$$W_2 = 2\pi\left(R\pi + 2\lambda\right)Mp \qquad [6.22]$$

For elements (3), the work comes from the extension that occurs by increasing the radius that passes from R to $R+x$ as x ranges from 0 to λ. The estimate of work W_3 is given by formula [6.23]:

$$W_3 = 2e\sigma_e\int_0^{\lambda} 2\pi x\,dx = 2\pi e\sigma_e\lambda^2 \qquad [6.23]$$

During this folding phase, the cylinder is shortened from length 2λ, and the plastic work is therefore equal to the work done by force Fp, which leads to formula [6.24]:

$$W = 2Fp\lambda = W_1 + W_2 + W_3 \qquad [6.24]$$

We obtain an expression for crushing force through formula [6.25]:

$$Fp = \pi e\sigma_e\left(\frac{e}{\sqrt{3}}\left(\frac{\pi R}{\lambda}+1\right)+\lambda\right) \qquad [6.25]$$

Expression of this force involves the length parameter λ. There may be projectiles where this length is determined by the geometry and structure, for example, if there are reinforcement rings. In the

"smooth" tube that we study, this length will "naturally" be defined as one that is consistent with the lowest crushing force possible. This leads to expression [6.26]:

$$\frac{\partial Fp}{\partial \lambda} = \pi e \sigma_e \left(1 - \frac{e\pi R}{\lambda^2 \sqrt{3}} \right) = 0 \qquad \lambda = \frac{\sqrt{e\pi R}}{\sqrt[4]{3}} \qquad [6.26]$$

By introducing this length into expression [6.25], we obtain an expression of the crushing force according to the dimensional and material characteristics of the projectile [6.27]:

$$Fp = \pi e \sigma_e \left(\frac{e}{\sqrt{3}} \left(\sqrt[4]{3} \sqrt{\frac{\pi R}{e}} + 1 \right) + \frac{\sqrt{e\pi R}}{\sqrt[4]{3}} \right) \qquad [6.27]$$

Other hypotheses can be made to estimate the crushing shape. For example, the manual [DNA 83] uses a mechanism modeled by the diagram in Figure 6.9. The wavelength of the folding mechanism is set empirically from many experimental results using formula [6.28]:

$$\lambda = 2.8e + \frac{R}{4} \qquad [6.28]$$

Rotation during folding takes the thickness of the tube into account. The work put in then has expression [6.29]:

$$W = Fp(2\lambda - 3e) \qquad [6.29]$$

The estimation of plastic work then leads to the formulation of the crushing force explained in [6.30]:

$$Fp = \frac{\pi e \sigma_e}{2\lambda - 3e} \left(\lambda \sqrt{4\lambda^2 - 9e^2} + eR \arccos \frac{3e}{2\lambda} \right) \qquad [6.30]$$

The crushing of tubes of different shapes has been extensively studied, both theoretically and experimentally [JON 89]. Rectangular section tubes have been particularly well studied because they give a good representation of the crushing of motor vehicle parts, which we call "spars", that plasticize during frontal impact in the same manner as described here. Force *Fp* is not necessarily constant throughout the

crushing process. The geometric characteristics of the projectile, like the section, may vary along the length. This will give a force $Fp(x)$, where x is the reference position of the zone that plastically deforms.

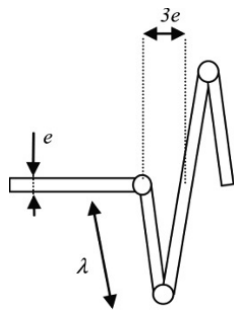

Figure 6.9. *Crushing of a cylindrical tube on a rigid target. Detail of a folding mechanism with plastic hinges*

6.2.2. *Impact force*

During a shock, the force applied to the target structure is from two sources: on the one hand, there is the projectile crushing force, as discussed in the previous section; on the other hand, there is the impulsion that the structure must provide to cancel out or absorb the motion of the mass being crushed. A rather general determination of the impact force was proposed by Riera [RIE 68]. The projectile is an elongated structure that behaves like a beam or a tube in compression that has just been crushed against the target (Figure 6.10).

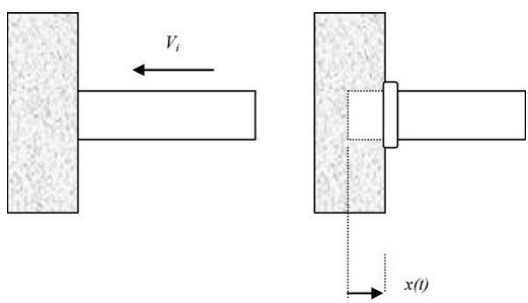

Figure 6.10. *Impact of a projectile against a target; definition of the crushed length*

The projectile has a mass per unit length $\mu(x)$ and the force that it can withstand during compression is limited to a value $Fp(x)$, which corresponds to plasticizing or buckling. x is the longitudinal abscissa in the projectile and $x(t)$ is the length that is crushed at time t as shown in Figure 6.10. We want to determine the force $F(t)$ between the target and the projectile. To do this, we must consider dynamic equilibrium at all times. We denote $V(t)$ as the velocity of the uncrushed part of the projectile. This velocity decreases monotonically. Between two instants separated by dt, a projectile section of length dx is crushed and passes from velocity $V(t)$ to 0 as shown in Figure 6.11.

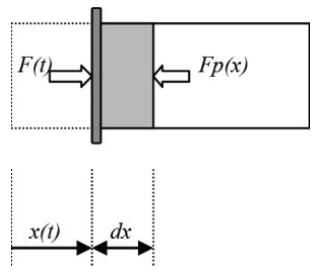

Figure 6.11. *Projectile element dx crushed during a time increment dt*

During the time interval dt, the change in momentum is $\mu(x)dxV(t)$. At time t, the section supports $F(t)$ on the target side and always $Fp(x)$ on the projectile side. The impulse is thus: $F(t)\ dt - Fp(x)dt$. This leads to equation [6.31]:

$$\mu(x)dxV(t) = F(t)\,dt - Fp(x)\,dt \qquad [6.31]$$

We deduce the impact force by formula [6.32], called the "Riera formula":

$$F(t) = Fp(x) + \mu(x)\,V^2(t) \qquad [6.32]$$

Some authors have proposed considering a coefficient α that takes the notion of "effective mass" ($0.5 < \alpha < 1$) into account, which slightly modifies the expression and gives [6.33]:

$$F(t) = Fp(x) + \alpha\mu(x)V^2(t) \qquad [6.33]$$

Using this formula to find $F(t)$ requires the calculation of the projectile velocity after the initiation of impact until it stops. We then write the equation of motion of the non-crushed part of the projectile, of length $L - x$. This equation is given in [6.34]:

$$\dot{V}(t)\int_x^L \mu(\varsigma)\,d\varsigma + Fp(x) + \mu(x)V^2(t) = 0 \qquad [6.34]$$

We can also write this equation for position $x(t)$, which gives formula [6.35]:

$$\ddot{x}\int_x^L \mu(\varsigma)\,d\varsigma + Fp(x) + \mu(x)\dot{x}^2 = 0 \qquad [6.35]$$

This equation is nonlinear and must be solved numerically (using finite differences). Thus, we can solve the equation if the projectile is a thin and light tube of constant section. In [6.36], we give the useful characteristics of this projectile:

$$\mu = 10\ \text{kg/m} \qquad L = 1\ \text{m} \qquad Fp = 100\ \text{N} \qquad [6.36]$$

Calculation was performed by taking, successively, initial velocity $V_i = 5\ \text{m/s}$ and then $V_i = 10\ \text{m/s}$. The results of these calculations are shown in Figure 6.12.

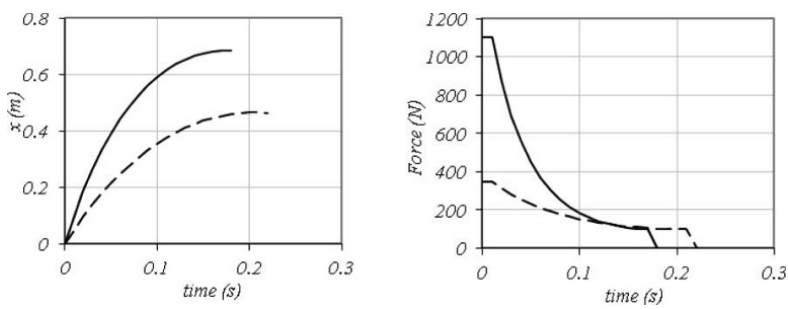

Figure 6.12. *Impact force determined by the Riera formula: solid line $V_i = 5\ m/s$, dotted line $V_i = 10\ m/s$*

During the compression phase, velocity decreases and the projectile ceases to apply a force on the structure when its velocity becomes zero. For a given projectile, the duration of the shock is

shorter if the impact velocity is higher. We note that at the beginning of a shock, the kinetic term μV^2 is preponderant, and more so with increasing impact velocity. As the projectile slows down, the force tends, logically, toward the value of the static crushing force. The Riera formula [6.32] is the basis for the general determination of the impact force models. In Figure 6.13, we give the example of a model to represent the impact force when an airliner *crashes* against a building. We can observe several phases:

– Force is stable (approximately 20 Nm), which corresponds to the crushing force of the cabin, the kinetic term has little influence because linear mass is low.

– The force peak (approximately 90 Nm) corresponds to the contact of large masses that are the motors and reservoirs.

In [BAN 09], we can find the impact forces corresponding to many aircrafts.

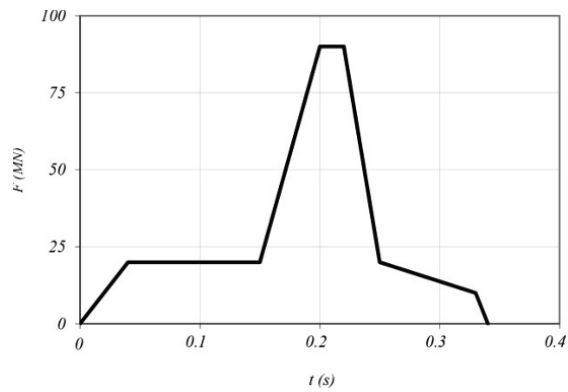

Figure 6.13. *Example of impact force model for a commercial airliner at a velocity of 100 m/s*

6.3. Classification of shocks

6.3.1. *Hard shock and soft shock*

The aim here is to qualify an accidental impact as “hard” or “soft”. A formalization of the classification of shocks was established by Koechlin [KOE 07] from the elements previously defined in this

chapter and in Chapter 2. This classification is done by considering the behaviors of the projectile and target in the first moments of impact. To classify the different types of shock, we consider the resistance of the target, denoted *Fc*. This limit force may be due to plasticizing or another mode of rupture. In the first moments of the shock, the projectile applies maximum impact force, if there is crushing, given by formula [6.37]; V_i is the impact velocity:

$$Fp + \mu V_i^2 \qquad [6.37]$$

This allows us to define a hard shock, for which the target ruptures. Hard shock is written as [6.38]:

$$Fc < Fp + \mu V_i^2 \qquad [6.38]$$

Soft impact is when there is a rupture of the projectile, which is expressed by [6.39]:

$$Fc > Fp + \mu V_i^2 \qquad [6.39]$$

The boundary between these two types of shock is represented by equation [6.40]:

$$\frac{Fp}{Fc} + \frac{\mu V_i^2}{Fc} = 1 \qquad [6.40]$$

By defining the dimensionless parameters that are the relative resistance *R* and the relative kinetic force *K*, this equation can be written more simply as [6.41]:

$$\frac{Fp}{Fc} = R \qquad \frac{\mu V_i^2}{Fc} = K \qquad R + K = 1 \qquad [6.41]$$

Relative kinetic force is called impact factor *I* by some authors. Another expression of this factor is [6.42]:

$$I = \frac{NmV_i^2}{d^3\sigma_c} \qquad [6.42]$$

N is a dimensionless parameter, *m* is the mass of the projectile, *d* is its diameter and σ_c is the resistance to compression from the target.

6.3.2. *Shock with rebound or crushing*

Another classification criterion can be considered by looking at the conditions in which the projectile is not crushed. The study of the impact of solids in Chapter 2 indicates that the maximum force a projectile can transmit, as an elastic solid, to the target is given by formula [6.43]:

$$Fp_{\max} = V_i S\sqrt{E_p \rho_p} \qquad [6.43]$$

If the force of impact is greater than this value, the projectile will be crushed, as indicated by [6.44]:

$$Fp > V_i S\sqrt{E_p \rho_p} \qquad [6.44]$$

Crushing can be written as [6.45]:

$$Fp^2 > V_i^2 S^2 E_p \rho_p \qquad [6.45]$$

If we consider that the force a projectile can transmit is limited by plasticizing, it can be written as [6.46]. If it is another phenomenon that limits force, we consider an equivalent fictional strain ε_p:

$$Fp = S E_p \varepsilon_p \qquad [6.46]$$

The two previous formulas lead to crushing [6.47]:

$$Fp > \frac{V_i^2 S^2 E_p \rho_p}{S E_p \varepsilon_p} \qquad [6.47]$$

We can also write this in form [6.48], by using the relative resistance parameters R and the relative kinetic force K:

$$\frac{Fp}{Fc} > \frac{\mu V_i^2}{\varepsilon_p Fc} \qquad R\varepsilon_p < K \qquad [6.48]$$

If the maximum force that the projectile can transmit is greater than the resistance of the target, the target will be crushed, resulting in [6.49]:

$$Fc^2 < V_i^2 S^2 E_p \rho_p \qquad [6.49]$$

Crushing of the projectile thus finally results in [6.50]:

$$\frac{Fc}{Fp} > \frac{\mu V_i^2}{\varepsilon_p Fc} \qquad KR < \varepsilon_p \qquad [6.50]$$

All these conditions can be drawn together onto the same diagram as shown in Figure 6.14. The different areas determine the types of shocks.

– Zone A: this is an elastic shock with projectile rebound as discussed in section 6.1.

– Zone B: this is an elastic shock for the target, but with no rebound because the projectile is crushed.

– Zone C: this is the area of soft shocks.

– Zone D: this is the area of hard shocks.

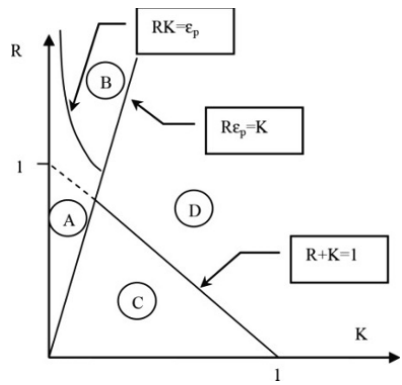

Figure 6.14. *Diagram of shock classification depending on the relative resistance and the relative kinetic force*

In crash studies, cases A and B are quite rare. For example, a land vehicle or an aircraft crashing into a reinforced or prestressed concrete structure generally corresponds to a situation as in zone C (soft impact) [SAA 07]. (Warning: this classification is based on what happens in the first moments of shock.) A shock classified as "soft" first leads to the collapse of the projectile, but the impact force produced can then lead to the destruction of the impacted structure.

Chapter 7

Explosions and Blasts

This chapter is devoted to the study of the load that a structure supports if an accidental explosion occurs in the environment. An explosion of gaseous mixture in free space is predominartly considered in order to highlight the parameters and elements of understanding of the thermodynamic explosion phenomenon. Modeling pressure waves generated by explosions and their interaction with structures are considered in simple geometrical configurations.

7.1. Accidental explosions

7.1.1. *Importance of the risk of explosion*

On industrial sites, accidental explosions are relatively frequent. These are mainly gas explosions and, to a lesser extent, dust explosions. The number of explosions with significant and serious consequences is in the order of 10 per year worldwide. Following an incident or an accident, flammable products in the gaseous or liquid phase may be released into the atmosphere. This type of accident can happen during the implementation phase of hazardous products in an industrial process or during the storage or transportation of these products. For some activities, the risk of explosion cannot be eliminated (rocket engine test bench, for example). It is then necessary to take this solicitation into account for the design of protective structures or

buildings to ensure the safety of equipment and people. It should be noted that the term "explosion" covers phenomena for which physicochemical processes may be different. The first meaning of the term refers to a rapid combustion generating a pressure wave. We must then distinguish detonation and deflagration. Explosion can also be physical, where the pressure wave is due to a phenomenon other than rapid combustion. For example, this is the case for the BLEVE case, where spontaneous vaporization in a large amount of fluid creates a pressure jump. BLEVE is an acronym for the term *boiling liquid expanding vapor explosion*. BLEVE is produced by spontaneous vaporization in a liquid. This phenomenon can occur in a liquefied gas tank if there is a major leak or following heating. Modeling the effects of shock waves is based on quantification of the energy available in the tank at the time of its rupture. Explosions can occur in free space (*unconfined vapor cloud explosion*) or in confined spaces. Dust explosions are most likely to occur in confined spaces. There are numerous studies in the literature that deal with the study of accidental explosions (for example, [BAK 83, SIM 94, LAN 84]).

7.1.2. *Gas explosion process*

This section is intended to provide the basic knowledge necessary for understanding the thermodynamic phenomena that lead to a pressure wave. An explosion is a combustion process in a reactive gas mixture. After an initiation process, a combustion jump combined with a pressure discontinuity jump is propagated [LEE 65]. "Fresh" gases, which have not yet reacted, are located upstream of the jump, and combusted gases are located downstream. Figure 7.1 shows the jump propagating in a monodimensional manner, with the thermodynamic variables associated with fresh gas (index 0) and combusted gas (respectively, particle velocity, pressure, density, internal energy, enthalpy).

To understand the basic patterns of explosive combustion, we must consider the three principles of conservation: mass, momentum and energy. These three principles bring about the relationship between the parameters of the gas state and discontinuity jump. These equations are similar to those already seen in Chapter 2.

7.1.2.1. *Conservation of mass*

The conservation equations can be found by considering the motion between two moments at the passage of the discontinuity jump (we denote the strains and stresses of compression positively). We consider a "tube" of unitary section (in Figure 7.1). The equation for the conservation of mass is expressed by formula [7.1]:

$$\rho(D-V)=\rho_0(D-V_0) \qquad [7.1]$$

The change in specific volume at the passage of the wave is shown in [7.2]:

$$v-v_0=\frac{1}{\rho}-\frac{1}{\rho_0}=-\frac{1}{\rho_0}\frac{V-V_0}{D-V_0} \qquad [7.2]$$

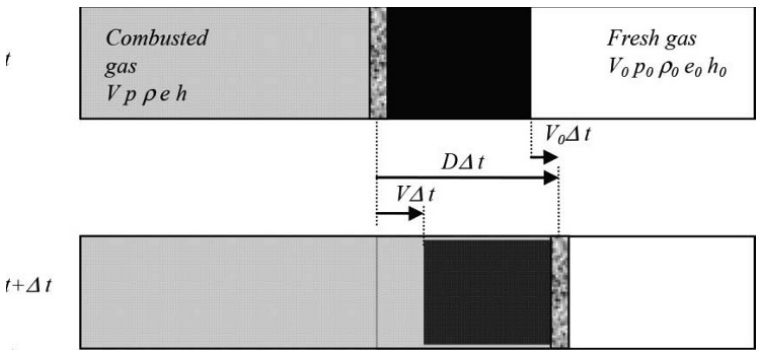

Figure 7.1. *Propagation of a combustion jump associated with a velocity and stress discontinuity (index 0 affects the characteristics of the medium before the passage of the jump). Shaded area: combusted gas; white area: fresh gas; and blotted area: volume occupied by a basic mass*

7.1.2.2. *Conservation of momentum*

The equation of conservation of momentum is expressed by formula [7.3]:

$$p-p_0=\rho V(D-V)-\rho_0 V_0(D-V_0) \qquad [7.3]$$

Given the equation of conservation of mass, this equation can also be written as [7.4]:

$$p - p_0 = \rho(V - V_0)(D - V) = \rho_0 (V - V_0)(D - V_0) \qquad [7.4]$$

7.1.2.3. *Conservation of energy*

Energy is the sum of the internal energy e and kinetic energy. Change over time in the elementary volume energy in question (dotted line in Figure 7.1) is caused by the power generated through the forces applied. This leads to formula [7.5]:

$$e - e_0 = \frac{1}{2}(p + p_0)\left(\frac{1}{\rho_0} - \frac{1}{\rho}\right) = \frac{1}{2}(p + p_0)(v_0 - v) \qquad [7.5]$$

We can deduce the change in enthalpy [7.6]:

$$h - h_0 = \frac{1}{2}(p - p_0)(v_0 + v) \qquad [7.6]$$

From the equation of assumed perfect state of gas, we can explain this change in enthalpy [7.7] (γ is the ratio of heat capacities of gas):

$$\frac{\gamma}{\gamma - 1}(p_0 v_0 - pv) = \frac{1}{2}(p - p_0)(v_0 + v) \qquad [7.7]$$

If combustion occurs as the jump passes, an amount of heat Q is contributed, and the formula becomes [7.8]:

$$\frac{\gamma}{\gamma - 1}(pv - p_0 v_0) + Q = \frac{1}{2}(p - p_0)(v_0 + v) \qquad [7.8]$$

Figure 7.2 shows a diagram of the state of pressure as a function of specific volume. Curve A, which corresponds to formula [7.7], is relative to a simple shock wave in the gas, without combustion. It is a hyperbola with horizontal and vertical asymptotes as specified in [7.9]:

$$\frac{p}{p_0} = -\frac{\gamma - 1}{\gamma + 1} \qquad \frac{v}{v_0} = \frac{\gamma - 1}{\gamma + 1} \qquad [7.9]$$

Curve B corresponds to formula [7.8], meaning that it is relative to gas after the contribution of heat Q. As the jump passes, the state will pass from a point on curve A, denoted by (p_0, v_0), to a point on curve B. By combining formulas [7.2] and [7.4], we obtain expression [7.10]:

$$\frac{p - p_0}{v - v_0} = -\rho_0^2 \left(D - V_0\right)^2 \qquad [7.10]$$

This means that one can only go from a point on curve A to a point on curve B through a line with negative slope. Thus, there are two possibilities. If at the passage of the combustion jump there is an increase in pressure and a decrease in specific volume, the system will undergo detonation. If at the passage of the combustion jump there is a decrease in pressure and an increase in the specific volume, the system will undergo deflagration. If the gas is initially at rest, formula [7.10] shows that the relationship between the slope of the line connecting the two states is proportional to the square of the jump propagation velocity. For maximum velocity, the state reached is called "Chapman–Jouguet" (p_{CJ} in Figure 7.2) [CHA 99, JOU 05].

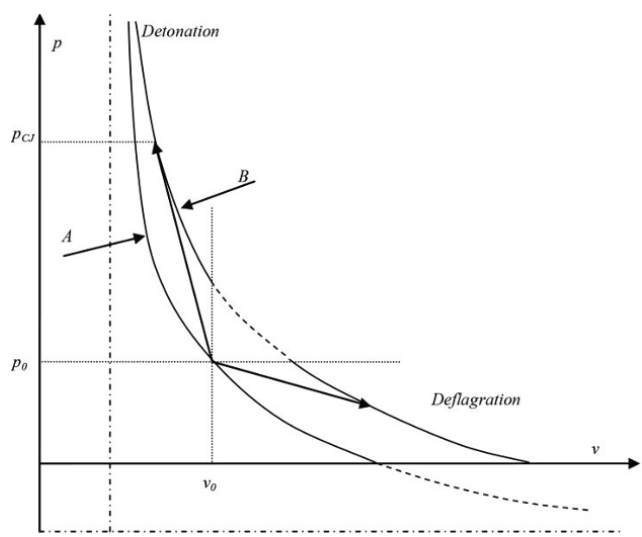

Figure 7.2. *Pressure state – specific volume diagram showing the two possibilities for state change at the passage of the combustion jump*

The explosion of a reactive gas mixture can therefore occur in two modes: detonation and deflagration. In free space, the characteristics of these two modes are described in Table 7.1. The detonation mode that corresponds to a supersonic jump velocity is very stable. It is also experimentally reproducible and insensitive to the environment. However, the deflagration mode is very unstable, and the combustion rate is strongly influenced by the environment in which the combustion propagates. Detonation of a gas mixture is produced by a chemical reaction that propagates into a gas cloud at a velocity that is supersonic relative to fresh gas (flame velocity can reach 3,000 m/s). The pressure behind the flame jump is high (Chapman–Jouguet pressure up to 5 MPa). This induces a shock wave in the surrounding space.

	Detonation	Deflagration
Flame jump velocity	1,800–3,000 m/s (stable)	0.01–100 m/s (unstable)
Combusted gas displacement	Same direction as the wave	Opposite direction of the wave
Pressure discontinuity	Large (# 5 MPa)	Weak (<< atmospheric pressure)
Expansion of reactive gases	No	Yes
External blast wave	Supersonic shock wave	Sonic blast wave

Table 7.1. *Comparison of the characteristics of detonation and deflagration regimes during the explosion of a gas cloud in free space*

7.1.2.4. *Energy*

We are only interested in external effects as detonation is mainly characterized by the energy it releases. This energy can be determined, *a priori*, from the enthalpies of formation for various reaction products. For example, for a cloud formed from a mixture of propane and oxygen, formula [7.11] shows the energy released at two different concentrations:

$$\begin{aligned} C_3H_8 + 5O_2 &\rightarrow 3CO_2 + 4H_2O \quad \text{9 966 kJ/kg or 15.26 kJ/kg} \\ C_3H_8 + 2{,}5O_2 &\rightarrow 2CO_2 + CO + 4H_2 \quad \text{6 389 kJ/kg or 10.19 kJ/kg} \end{aligned} \quad [7.11]$$

Detonation is fairly well known and described by models. There is a minimum initiation energy needed to produce detonation of a

reactive mixture. If the detonation of a homogeneous mixture occurs, only knowledge of the reaction products' enthalpies of formation and the geometric position of the center of the explosion are needed to define the pressure wave in any point in space. In practice, if we consider an accident, we can estimate the quantity of products likely to respond. Mixture of these products with air leads to the formation of an explosive cloud.

7.1.3. *Explosion with confinement*

For detonation of a gaseous mixture in a confined space, it is possible to estimate the value of the pressure over time. Existing models and measures are relative to homogeneous mixtures. As the chemical reaction is known, it is possible to determine the pressures following the initial conditions. The load imposed upon a building structure hosting the internal detonation results from pressure exerted by the gases from the detonation against the inner walls. The load is manifested by a pressure which, in the first tenths of a millisecond, is in the order of the Chapman–Jouguet pressure p_{CJ} and which, after several milliseconds, tends toward a so-called isochoric combustion pressure with half the magnitude of p_{CJ}. The pressure change is disturbed by peaks corresponding to multiple reflections off the internal walls of the structure. The pressure will decrease in a manner that depends on the presence, or not, of vents and their sizes.

7.2. *Pressure waves*

7.2.1. *External wave from a detonation*

7.2.1.1. *Characteristics*

The change in static pressure at a point in space at the passage of the blast wave after a gas explosion has the typical appearance of a shock wave in free space and is shown in Figure 7.3 with the parameters of pressure, pulse and duration.

The blast wave from an explosion introduces the parameters shown in Table 7.2.

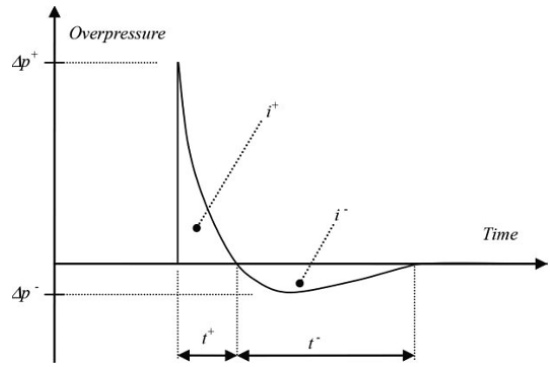

Figure 7.3. *Pressure change at the passage of a shock wave following detonation*

Δp^+ overpressure peak	t^+ duration of overpressure	i^+ positive pulse
Δp^- depression	t^- duration of depression	i^- negative pulse

Table 7.2. *Characteristic parameters of a shock wave following detonation*

7.2.1.2. *Rules of similarity*

A shock wave in free space is a physical phenomenon that follows the rules of similarities. It is possible to identify the dimensionless parameters by dimensional analysis. Table 7.3 lists the parameters and dimensions.

			"Exhibitors"		
	Variable	Dimension	M	L	T
t	Time	T	0	0	1
x	Distance	L	0	1	0
p	Pressure	$ML^{-1}T^{-2}$	1	−1	−2
E	Energy released by the explosion	ML^2T^{-2}	1	2	−2
p_0	Initial pressure (ambient)	$ML^{-1}T^{-2}$	1	−1	−2
c_0	Speed of sound in ambient air	LT^{-1}	0	1	−1
D	Wave velocity	LT^{-1}	0	1	−1
V	Particulate velocity	LT^{-1}	0	1	−1
ρ	Density (of gas)	ML^{-3}	1	−3	0

Table 7.3. *Parameters involved in the propagation of a shock wave after detonation, with their dimensions*

There are nine parameters and three physical dimensions (length, time and mass). The Vaschy–Buckingham theorem thus indicates that there are six dimensionless groups, which are shown in Table 7.4.

$\pi_1 = \frac{D}{c_0}$	$\pi_2 = x\left(\frac{p_0}{E}\right)^{1/3}$	$\pi_3 = \frac{p}{p_0}$
$\pi_4 = c_0 t \left(\frac{p_0}{E}\right)^{1/3}$	$\pi_5 = \frac{V}{a_0}$	$\pi_6 = \frac{\rho c_0^2}{p_0}$

Table 7.4. *Dimensionless parameters involved in the propagation of a shock wave following detonation*

7.2.1.3. *Sachs similarity*

To describe a shock wave, it is possible to use dimensionless parameters. The Sachs similarity involves expressing the values of dimensionless pressure, dimensionless pulse and dimensionless time, given in [7.12], depending on the value of dimensionless distance from that point to the center of the explosion [7.13]:

$$\overline{p} = \frac{p}{p_0} \quad \overline{i} = \frac{i\ c_0}{E^{1/3} p_0^{2/3}} \quad \overline{t} = c_0 t \left(\frac{p_0}{E}\right)^{1/3} \qquad [7.12]$$

$$\overline{R} = R \left(\frac{p_0}{E}\right)^{1/3} \qquad [7.13]$$

7.2.1.4. *Hopkinson's similarity*

The conditions of ambient air are invariable (pressure, speed of sound). By abandoning the dimensionless characteristic of parameters, we can write that pressure, reduced pulse and the reduced duration, as given in [7.14], are functions of the reduced source size and reduced distance λ, expressed in [7.15]:

$$p \frac{i}{E^{1/3}}, \frac{t}{E^{1/3}} \qquad [7.14]$$

$$\frac{R_0}{E^{1/3}}, \lambda = \frac{R}{E^{1/3}}, \qquad [7.15]$$

The Hopkinson similarity is often used either to correlate results from various experiments [BRO 85] or to conduct studies on a reduced scale [PRI 83, REN 88]. In the second case, Table 7.5 shows the scale for two experiments, respecting the Hopkinson similarity.

	Parameter	Scaling factors
p	Pressure	1
D, V	Speed and velocity	1
ρ	Density	1
i	Pulse	k
R	Lengths	k
t	Durations	k
E	Energy	k^3

Table 7.5. *Scaling factors for the parameters of a shock wave between a real situation and a reduced scale model*

Figure 7.4 illustrates the Hopkinson similarity situation.

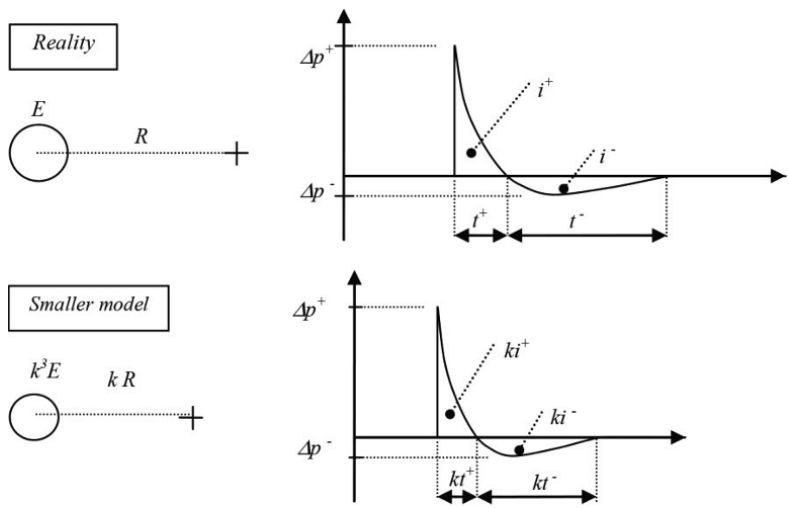

Figure 7.4. *Hopkinson similarity between a real explosion and reduced scale model*

With the usual conditions of ambient air (pressure, speed of sound), it is possible to make a link between the parameters of Hopkinson similarity, reduced distance, reduced pulse and reduced time, with the dimensionless parameters of distance, pulse and time [7.16]. For the reduced pulse and the reduced time, energy E is expressed in *MJ*:

$$\begin{aligned}
&\overline{R} = \lambda \left(\frac{p_0}{10^6}\right)^{1/3} \approx 0.4642\,\lambda \\
&\overline{i} = \left(\frac{i}{E^{1/3}}\right)\frac{c_0}{10^2\, p_0^{\,2/3}} \approx 0.1578\left(\frac{i}{E^{1/3}}\right) \\
&\overline{t} = \left(\frac{t}{E^{1/3}}\right)\frac{c_0\, p_0^{\,1/3}}{10^2} \approx 157.8\left(\frac{t}{E^{1/3}}\right)
\end{aligned} \qquad [7.16]$$

The characteristics of shock waves from gas explosions have been established by integrating a large number of experiments on different scales [BRO 85]. The formulas are presented in [7.17] as a function of dimensionless variables. Figure 7.5 shows the evolution of these features relative to dimensionless distance.

$$\begin{aligned}
&\ln\left(\frac{\Delta p^+}{p_0}\right) = -0.032\,\overline{X}^3 + 0.241\,\overline{X}^2 - 1.82\,\overline{X} + 0.356 \\
&\ln\left(\frac{\overline{i}^+}{0.1578}\right) = -0.0323\,\overline{X}^3 + 0.0648\,\overline{X}^2 - 0.94\,\overline{X} - 0.868 \\
&\ln\left(\frac{\overline{t}^+}{0.1578}\right) = -0.1118\,\overline{X}^2 + 0.676\,\overline{X} + 0.203 \\
&\overline{X} = \ln\frac{\overline{R}}{0.4642}
\end{aligned} \qquad [7.17]$$

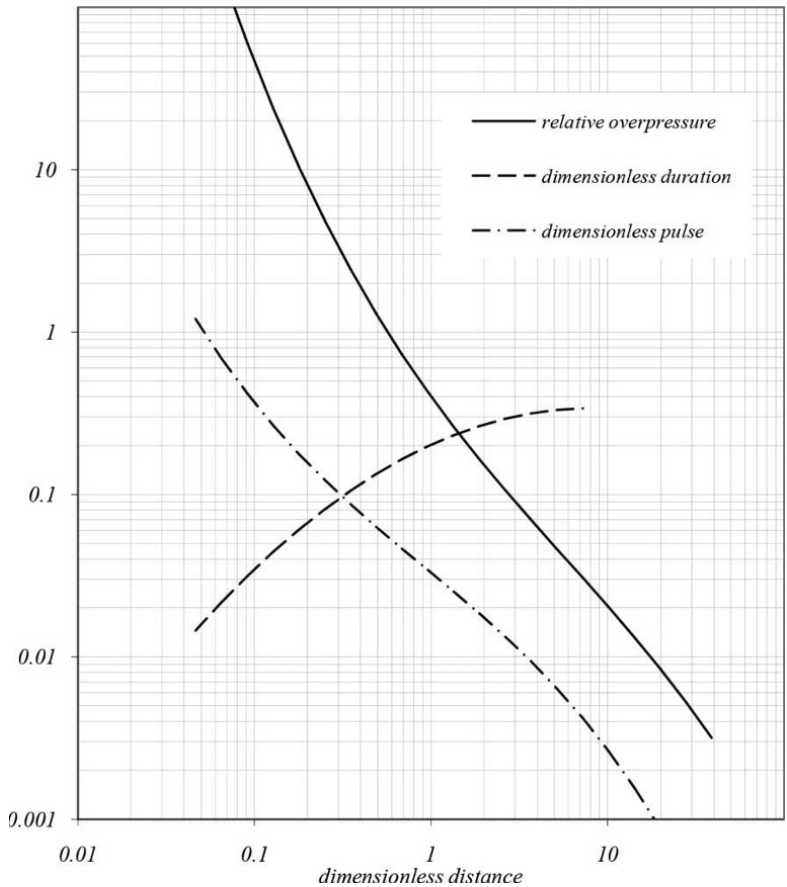

Figure 7.5. *Dimensionless characteristics of a shock wave after detonation of a gas mixture*

7.2.1.5. *The TNT reference*

When considering an accidental explosion, one method is to consider the "TNT equivalence" [MOU 99, LAN 84]. This consists of assessing the TNT mass (trinitrotoluene is a reference high explosive) that would have the same external effects as an accidental gas explosion. Determination of equivalence is difficult: on the one hand because the concepts of efficiency and energy equivalence are based on the choices of experts and, on the other hand, because shock waves

from gas or TNT explosions do not have exactly the same profile (Figure 7.3); thus, the equivalence of the external effect can only be done for a single characteristic, usually peak pressure or pulse. In Chapter 5, we saw that these two parameters are of equal importance and, therefore, only respecting one of them is questionable for the calculation of the mechanical response of structures. The energy produced by the explosion of 1 kg of TNT is shown in [7.18]:

$$E_{TNT} = 4.69\ MJ/kg \qquad [7.18]$$

To clarify the characteristics of the shock wave resulting from a TNT explosion, it is customary to consider a reduced distance Z. Formula [7.19] specifies the definition of Z, where m is the mass of TNT and d is the distance from the center of explosion. We also indicate the approximate ratio with reduced distance defined for gas explosions and dimensionless distance (calculated for ambient conditions):

$$Z = \frac{d}{\sqrt[3]{m}} \quad \left(m.kg^{-1/3} \right) \quad \lambda \approx 0.597\ Z \quad \bar{R} \approx 0.277\ Z \qquad [7.19]$$

There are many data on the characteristics of waves from TNT explosions [KIN 62, BAK 83]. We show one in [7.20]:

$$\frac{\Delta p^+}{p_0} = \frac{808\left(1+\left(Z/4.5\right)^{10}\right)}{\sqrt{1+\left(Z/0.048\right)^2}\sqrt{1+\left(Z/0.32\right)^2}\sqrt{1+\left(Z/1.35\right)^2}}$$
$$\frac{t^+}{\sqrt[3]{m}} = \frac{980\left(1+\left(Z/4.5\right)^2\right)}{\sqrt{1+\left(Z/0.02\right)^3}\sqrt{1+\left(Z/0.74\right)^6}\sqrt{1+\left(Z/6.9\right)^2}} \qquad [7.20]$$

Figure 7.6 shows the relative peak value of pressure relative to dimensionless distance for a gas explosion and TNT explosion. There are areas where the difference is significant.

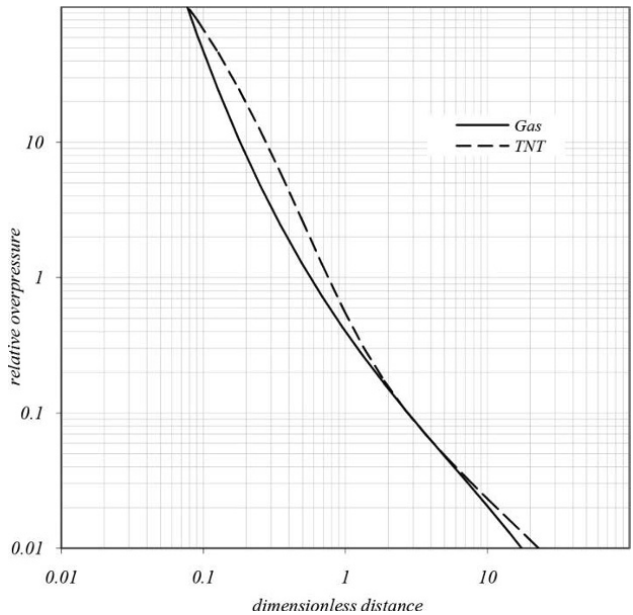

Figure 7.6. *Dimensionless characteristics of a shock wave after detonation of a gas mixture compared to that of an explosive solid (TNT)*

7.2.1.6. *Modeling*

The typical shape of pressure evolution can be modeled (Figure 7.3). Various possibilities exist, and in [7.21] we show the model proposed by [LAN 84]. All parameters of this expression can be determined as a function of dimensionless distance [BRO 88]:

$$\Delta p\left(t,\overline{R}\right)=\Delta p^{+}\frac{\sin\left(\pi\left(t-t^{+}\right)/t^{-}\right)}{\sin\left(-\pi t^{+}/t^{-}\right)}e^{-kt/t^{+}} \qquad [7.21]$$

7.2.2. *External wave after deflagration*

When considering an accidental explosion as a detonation, a deterministic study of its effects is possible. It is difficult to predict the combustion process that will occur, but it will depend on the external mechanical effect of the explosion, a pressure wave. The deflagration

process produces a pressure wave $\Delta p(r,t)$ which has a markedly random character and is difficult to model. At some point during the passage of a pressure wave, there will be an overpressure phase followed by a depression phase. There is no typical signal shape for detonation. In fact, for slow deflagrations, energy and fluid mechanics allow us to access the relationship between the evolution of combustion and the blast wave emitted $\Delta P(r,t)$. The spherical piston model represents the mechanical effect of combusted gas as these have a greater volume than fresh gas. The parameters for this are: r_0 radius of the spherical volume occupied by fresh gas, $r_f(t)$ radius of the flame, V_f flame velocity and V_P piston velocity. These last two parameters are specified in [7.22] (α being the expansion ratio or the ratio of combusted gas density to fresh gas density):

$$V_f = \frac{dr_f}{dt} \quad V_p = (1-\alpha)\frac{dr_f}{dt} \qquad [7.22]$$

An analytical solution can be obtained after integration of the Euler equations [DES 81]. It shows that for fields of overpressure $\Delta p(r,t)$ far from the flame, ($r>r_f$) is expressed as [7.23] (ρ_0 is the density of the gas mixture, and c_0 is the speed of sound):

$$\Delta p(r,t) = \frac{\rho_0(1-\alpha)}{r}\left(2r_f(\tau)\left(\frac{dr_f(\tau)}{d\tau}\right)^2 + r_f^2(\tau)\frac{d^2r_f(\tau)}{d\tau^2}\right) \qquad [7.23]$$
$$\left(\tau = t - \frac{r}{c_0}\right)$$

Combustion, and in particular velocity of the flame jump, is subjected to changes. We know the causes qualitatively, but these changes are difficult to predict and model. Indeed, any factor that may affect the flame jump can accelerate it. As the burning rate is clearly subsonic, geometry of the site and environment of the explosion will affect combustion. The presence of obstacles in the path of the flame jump disrupts combustion, increases the reaction surface by creating turbulence and finally accelerates, overall, the flame jump. In some cases, acceleration of the flame jump due to initial turbulence in fresh gas, obstacles, changes in concentration or interactions between the

flame and pressure waves from reflections becomes important. The flame velocity increases and the explosion regime then moves toward detonation. Methods exist for taking the risk of explosion in the deflagration mode into account [MOU 99]. The most used method is called the "multi-energy method" [VAN 84]. This evaluation method is based on expert analysis of the practical situation: nature and quantity of reagents, as well as the geometry and environment of the locations. This analysis leads to choosing an explosion violence index (1–10). The concept of violence is linked to the flame velocity value. As shown in equation [7.22], pressure effects are strongly related to this value and its variations. Based on this index, charts from calculations exist. These charts are used to determine the relative overpressure and dimensionless duration of overpressure at any point in the explosion environment. Figure 7.7 shows the three shapes used for the pressure wave (from left to right, with a higher index to a lower index). These models do not intend to account for a depression phase following overpressure. For deflagrations of low index, 1−3, this depression phase is of comparable amplitude to overpressure.

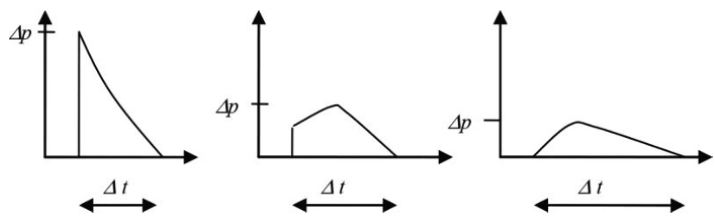

Figure 7.7. *Pressure wave shapes resulting from more or less violent deflagrations*

7.3. Action of an explosion on a structure

7.3.1. *Reflection of a shock wave*

A load imposed upon a structure results from the interaction of a pressure wave with a structure that obstructs its propagation. The aerodynamic phenomena involved are mainly wave reflection and diffraction. These phenomena are theoretically difficult to model. Simplified methods exist, the principle of which is expressed by certain regulations [UFC 08], and these are mainly derived from tests with highly explosive solids. The load on a structure is particularly

effective, or dangerous, if the structure opposes the passage of a wave and provokes its normal reflection. The surface perpendicular to propagation direction will support the reflected pressure from the shock wave. The reflection coefficient, i.e. the ratio between reflected overpressure and incident overpressure, is a "static" pressure as indicated by formula [7.24]. This coefficient tends toward 2 for weak overpressures and thus is close to a propagating wave in the acoustic model, and tends toward the value of 8 for very high overpressures:

$$\frac{\Delta p_r^+}{\Delta p_s^+} = \frac{8\Delta p_s^+ + 14 p_0}{\Delta p_s^+ + 7 p_0} \qquad [7.24]$$

If this reflected, overpressure is very high for a construction such as a concrete wall very close to the explosion (dimensionless distance less than 1) and it may result in a compression wave in the wall, as in a solid impact. If the overpressure has a value in the order of magnitude of the tensile strength of concrete, it can produce rupture through cracking [FRA 83, KOT 77]. If the structure surfaces are not perpendicular to wave propagation, there will be an oblique reflection of the shock wave. This oblique reflection can be regular, as in acoustics, or of the "Mach reflection" type [KIN 62, BAK 83]. We will not address this situation in this book.

7.3.2. *Response spectrum to a detonation*

The pressure reflected on the surface of a building is a distributed load (assuming the surface is perpendicular to the propagation of the shock wave). In Chapter 5, we discussed modeling a structure by a mechanical system with one degree of freedom. In this case, it is possible to find the response spectrum of such a system to a load from detonation for a unitary surface. The response of a structure is the solution of the equation formulated in [7.25]. The characteristics of the pressure signal can be determined as a function of dimensionless distance [BRO 88]:

$$m\ddot{x} + k\,x = f(t) = \Delta p_r^+ \frac{\sin\left(\pi\left(t - t^+\right)/t^-\right)}{\sin\left(-\pi t^+/t^-\right)} e^{-\kappa t/t^+} \qquad [7.25]$$

To generalize this result, this equation is written with dimensionless variables as given in [7.26]:

$$\ddot{x}^* + w^2 x^* = \frac{w^2}{2} e^{-\alpha\tau}\left(\cos\tau - \beta\sin\tau\right)$$
$$\tau = \frac{\pi t}{t^-} \quad w = \frac{\omega t^-}{\pi} \quad x^* = \frac{kx}{2\Delta P_r^+} \quad \alpha = \frac{\kappa t^-}{\pi t^+} \quad \beta = \frac{1}{\tan\left(\pi t^+ / t^-\right)} \qquad [7.26]$$

To calculate the spectrum, we consider a building located in the "far field", meaning a dimensionless distance greater than 1. The values of some parameters vary little in this field and are specified in [7.27]:

$$t^- \approx 4t^+ \quad \kappa \approx 0.6 \quad \alpha = 0.764 \quad \beta = 1 \qquad [7.27]$$

The solution to equation [7.26] with parameters [7.27] is explained in [7.28]:

$$x^*(\tau) = \frac{w}{2\left(2.5 - 0.83w^2 + w^4\right)} \begin{pmatrix} we^{-\alpha\tau}\left(\left(w^2 - 1.94\right)\cos\tau - \left(1.11 + w^2\right)\sin\tau\right) \\ +\left(1.76w^2 - 0.37\right)\sin w\tau \\ +w\left(1.94 - w^2\right)\cos w\tau \end{pmatrix} \qquad [7.28]$$

Figure 7.8 shows the response spectrum to a detonation (solid line). The dotted line shows the response spectrum calculated with a load only taking the overpressure phase into account. There is an area where the fact of considering only the overpressure phase does not lead to an upper bound of the response ($0.5 < w < 3$).

7.3.3. *Simplified model of an action on a structure*

The passage of a pressure wave around the obstacle that is a construction is a transient aerodynamic phenomenon. The load imposed on the construction corresponds to the sum of pressures applied when the shock wave strikes and then exceeds it. A first approach, as we have just discussed, is to consider the pressure reflected on a wall. In reality, diffraction phenomena will occur around the construction, which may affect the reflected pressure signal

to a greater or lesser degree [7.25]. There are simplified methods to address this diffraction phenomenon [BAK 83, KIN 62, UFC 08]. Calculation is also possible using powerful digital aerodynamic codes. To illustrate the simplified method, we consider a simply-shaped building hit by a shock wave (Figure 7.9).

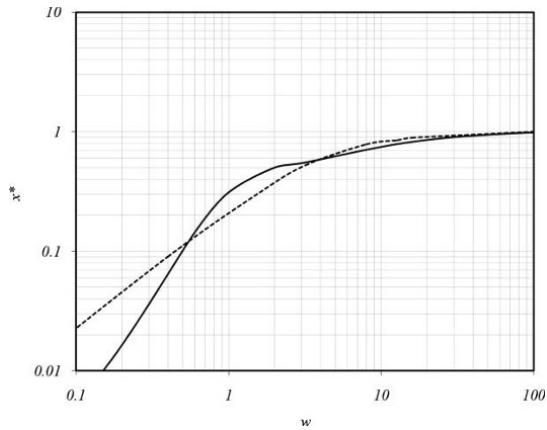

Figure 7.8. *Response spectrum to detonation: solid line, spectrum calculated with full signal; dotted line, spectrum calculated with the overpressure phase only*

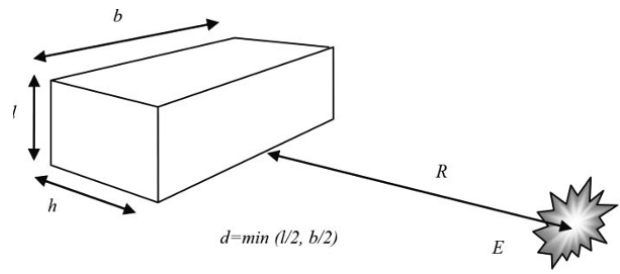

Figure 7.9. *Construction obstructing propagation of a shock wave*

Aerodynamic phenomena that occur are shown in Figure 7.10. We will use the following variables:

– p_0 atmospheric pressure;

– p_s static pressure;

– p_r reflected pressure;

– p_a stagnation pressure;

– p_t drag pressure;

– V particulate velocity behind the shock jump;

– C_x aerodynamic drag coefficient for the construction (≈2).

These values are functions of the amplitude of the shock wave [KIN 62, BAK 83]. Formulas [7.29] give the relationships between these variables.

$$p_a = p_s + \frac{1}{2}\rho V^2 \quad p_t = \frac{1}{2}C_x \rho V^2 \qquad [7.29]$$

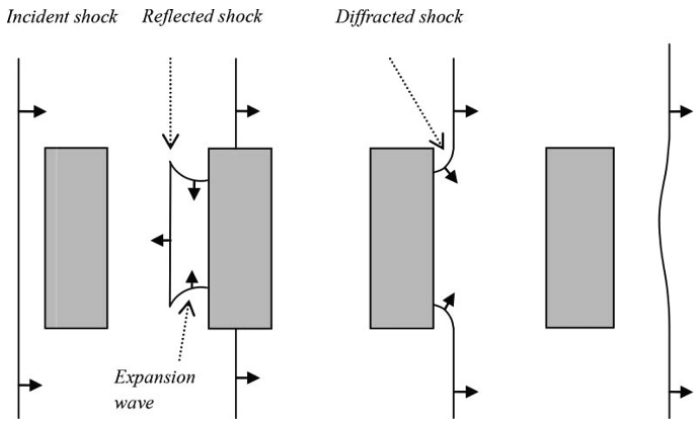

Figure 7.10. *Diffraction of a shock wave by a construction*

The wave is reflected on the face perpendicular to wave propagation. Diffraction occurs on the edges of the face. An expansion wave is propagated at the speed of sound from the edges. It arrives at the center of the face after a time d/c_0. After a delay estimated at $2d/c_0$, stagnation pressure is established. This stagnation pressure integrates dynamic pressure which is related to the flow behind the shock jump. The wave jump overtakes the construction and pressure builds up on the rear face. This pressure is in the order of the stagnation pressure decreased by aerodynamic drag and settles after a period estimated at $3d/c_0$. Figure 7.11 shows the sequence of different loading phases of

the construction. Figure 7.12 shows the changes in pressure on the face receiving the reflected pressure and its opposite face, called the rear face.

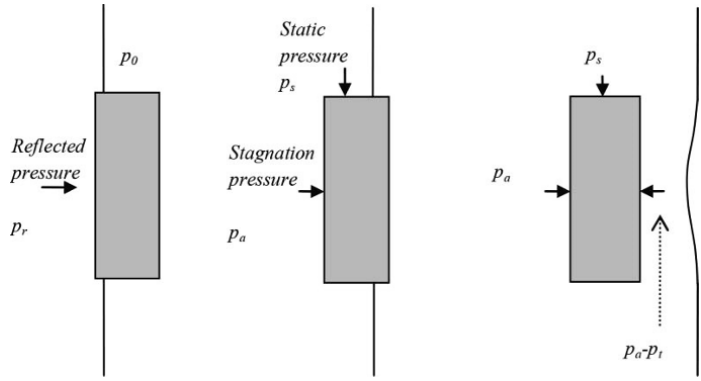

Figure 7.11. *Pressures applied on a construction at the passing of a shock wave: p_0 atmospheric pressure, p_s static pressure, p_r reflected pressure p_a stagnation pressure, p_t drag pressure*

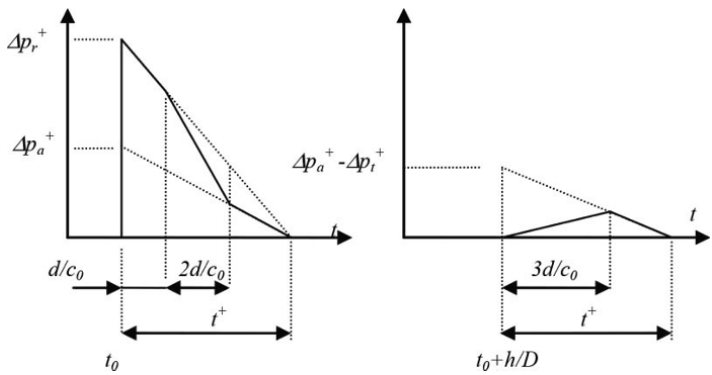

Figure 7.12. *Evolution of pressure on the front face of the structure, load on a construction at the passing of a shock wave*

EXAMPLE 7.1.– We consider a two-story building as shown in Figure 7.13. We want to find the load this structure would be subjected to if an explosion, representing a 700 MJ energy release, occurred at a distance of 25 m.

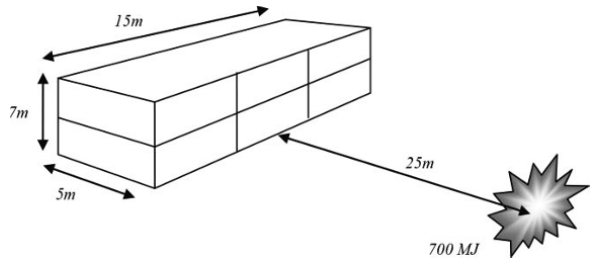

Figure 7.13. *Explosion near a construction*

The face has a surface normal to the direction of propagation of the shock wave. It is relatively easy to calculate the dimensionless distance and deduce, from charts, the shock wave characteristics that will reach this wall [7.30]:

$$\bar{R} = 1.3 \quad \Delta p_s^+ = 25\,kPa \quad t^+ = 13.10^{-3}\,s \quad i^+ = 141\,Pa.s \qquad [7.30]$$

The elements needed for definition of the load are deduced and shown in [7.31]:

$$\begin{aligned} &\Delta p_s^+ = 25\,kPa \quad Mach = 1.102 \quad V = 0.162\,c_0 \\ &\Delta p_r^+ = 55\,kPa \quad \Delta p_a^+ = 27.2\,kPa \quad \Delta p_t^+ = 4.4\,kPa \end{aligned} \qquad [7.31]$$

Calculation of the time delay for the relaxation waves to arrive to the middle of the wall gives $d/c_0 = 10^{-2}$ s. In this case, the expansion waves will not significantly alter the reflected pressure. We may consider the load as $\Delta p_r(t)$ [7.25].

7.4. Blast-structure coupling

7.4.1. *Coupling conditions*

The above considerations on load imposed upon a structure by a blast wave were made with the assumption that the building was a rigid obstacle relative to the movement of fluid. However, the structure is deformable and is displaced by the action of pressure exerted on its walls. This raises the question of a possible coupling between fluid flow that occurs behind the shock jump and movement of the structure. The elements required to answer this question are the

comparisons of characteristic time and characteristic displacement of fluid flow and motion of the structure. To establish these comparisons, the characteristic elements of fluid and shock waves in the air are shown in Table 7.6.

E	Explosion energy
R	Distance
Δp	Overpressure
t^+	Overpressure duration
V	Particulate velocity
Mach	Mach number
$Z_f = ((\gamma p_0)/(2c_0))$	Impedance of air (210 $kg.m^{-1}.s^{-2}$)

Table 7.6. *Variables characteristic of a blast wave in air*

The structure can be modeled by a system with degree of freedom (see Chapter 5). The characteristic features are shown in Table 7.7.

M_s	Mass
K_s	Stiffness
$\omega_S = \sqrt{K_S / M_S}$	Angular frequency
S_s	Exposed surface
$Z_s = \sqrt{K_s M_s} / S_s$	Surface impedance

Table 7.7. *Variables characteristic of a structure*

Two loading parameters follow: maximum load and impulse:

$$F = \Delta p_r^+ . S \qquad I \approx \frac{1}{2} F . t^+ \qquad [7.32]$$

The characteristic time of the wave is the duration of overpressure. The characteristic time of the structure is its half-period. An initial idea is thus to compare these two characteristic times. We first define a dimensionless parameter [7.33]:

$$\pi_t = \frac{\omega_s t^+}{\pi} \qquad [7.33]$$

If this parameter is very small compared to 1, the load can be considered impulsive. If it is very large, it approaches a quasi-static-type situation (which is rare). To estimate a possible coupling, the speed of sound V_s and the particle fluid velocity V_f must be compared. We then look at the value of the ratio of these two orders of variables [7.34]:

$$\pi_V = \frac{V_f}{V_s} \qquad \begin{cases} V_s \approx \dfrac{I}{M_s} & \left(if\ \pi_t < 1\right) \\ V_s \approx \dfrac{F}{\sqrt{K_s M_s}} & \left(if\ \pi_t \geq 1\right) \end{cases} \qquad [7.34]$$

If this dimensionless parameter is in the order of the unit, there is a reason to consider coupling between the motions of the fluid and the structure. If it is large compared to the unit, the structure displacements are negligible compared to the motion of the fluid and, thus, flow is unchanged. In this case, flow acts as if the structure was rigid.

EXAMPLE 7.2.– We consider the explosion previously defined in [7.30] and [7.31] and two types of structures: a tank on poles and a panel, also on poles, for which the characteristics are shown in Table 7.8.

	Tank	Panel
Mass	M_s = 20,000 kg	M_s = 200 kg
Stiffness	$K_s = 3.10^5$ N/m	K_s = 50,000 N/m
Angular frequency	$\omega_s = 3.87\ s^{-1}$	$\omega_s = 15\ s^{-1}$
Exposed surface	$S_s = 10\ m^2$	$S_s = 10\ m^2$
Surface impedance	$Z_s = 7{,}700\ kg.m^{-1}.s^{-2}$	$Z_s = 316\ kg.m^{-1}.s^{-2}$

Table 7.8. *Variables characteristic of the two structures*

The load parameters are calculated [7.35]:

$$F = 550\ \text{kN} \quad I = 3{,}500\ \text{N.s} \qquad [7.35]$$

For the first structure, with load time being 13.10^{-3} s, the time parameter is $\pi_t = 0.016$. The magnitude of the velocity of the structure can be estimated by the pulse response and we obtain $V_s = 0.17$ m/s. The particulate velocity behind the shock jump is $V_f = 54$ m/s;

therefore, the velocity parameter is $\pi_V = 300$. It seems reasonable in this case not to take coupling into account to determine the load. Fluid motion occurs as if the structure were fixed.

For the panel, the time parameter is $\pi_t = 0.06$. The magnitude of the velocity of the structure can be estimated at $V_s = 17.5$ m/s, and that of the fluid is $V_f = 54$ m/s. The displacement parameter is then $\pi_V = 3$. Taking coupling into account is relevant here. The velocity of the structure is high and it approaches fluid velocity because the structure is very light. Indeed, for a pulse load, the initial velocity depends only on the impulsion and mass of the structure. The surface impedance of the structure is the same order of magnitude as that of the fluid. We could imagine a situation where, for the same value of surface impedance, the time parameter would be in the order of the unit and the structure velocity would be high because its stiffness is very weak. This last situation does not occur in buildings.

7.4.2. *Linear approach to coupling*

Coupling between the movement of the fluid associated with a shock wave and that of a structure is a difficult problem. To see how this coupling affects load on the structure, we can deal with a very simplified approach. This is the problem of the uniaxial reflection movement of a wave on an elastic structure, assuming a linear behavior of the fluid. This is a strong assumption which can only concern waves of very small amplitude for which overpressure is small compared to atmospheric pressure. The linear model of compressible fluid is that of acoustics. We consider air as a perfect fluid and take the Euler equations as fundamental: continuity and fundamental law of dynamics. As we consider the problem to a single space parameter, the equations governing fluid motion are given in [7.36]:

$$\begin{cases} \dfrac{\partial \rho}{\partial t} + \dfrac{\partial \rho V}{\partial x} = 0 \\ \rho\left(\dfrac{\partial V}{\partial t} + v\dfrac{\partial V}{\partial x}\right) = -\dfrac{\partial p}{\partial x} \end{cases} \qquad [7.36]$$

We are considering small perturbations around the resting position. By only retaining the first-order terms, the linearized equations become [7.37]:

$$\begin{cases} \dfrac{\partial \rho'}{\partial t} + \rho_0 \dfrac{\partial V}{\partial x} = 0 \\ \rho_0 \dfrac{\partial V}{\partial t} + \dfrac{\partial p'}{\partial x} = 0 \end{cases} \quad \left(\rho' = \rho - \rho_0 \quad p' = p - p_0\right) \qquad [7.37]$$

We must add a thermodynamic relationship to this system. We consider an isentropic transformation. If we assume the gas is perfect, we get the relationship [7.38]:

$$\frac{\rho'}{\rho_0} = \frac{1}{\gamma}\frac{p'}{p_0} \text{ where } \rho' = \rho_0 K_f \, p' \qquad [7.38]$$

The system can then be written in terms of pressure and velocity [7.39]:

$$\begin{cases} \rho_0 K_f \dfrac{\partial p'}{\partial t} + \rho_0 \dfrac{\partial V}{\partial x} = 0 \\ \rho_0 \dfrac{\partial V}{\partial t} + \dfrac{\partial p'}{\partial x} = 0 \end{cases} \qquad [7.39]$$

By transformation of the system, we can separate the variables and obtain the equations of wave propagation [7.40]:

$$\begin{aligned} &\rho_0 K_f \frac{\partial^2 p'}{\partial t^2} - \frac{\partial^2 p'}{\partial x^2} = 0 \\ &\rho_0 K_f \frac{\partial^2 V}{\partial t^2} - \frac{\partial^2 V}{\partial x^2} = 0 \end{aligned} \qquad [7.40]$$

The general solution to these equations can be written as [7.41]:

$$V(x,t) = F_1\left(t - \frac{x}{c_0}\right) + F_2\left(t + \frac{x}{c_0}\right) \quad c_0 = \sqrt{\gamma \frac{p_0}{\rho_0}} \qquad [7.41]$$

where c_0 is the velocity of sound waves (or speed of sound). The displacement can also be written in the form [7.42]:

$$u(x,t) = f_1\left(t - \frac{x}{c_0}\right) + f_2\left(t + \frac{x}{c_0}\right) \quad \left(V = \frac{\partial u}{\partial t} \quad F_i = \frac{\partial f_i}{\partial t}\right) \qquad [7.42]$$

Overpressure is related to strain in the fluid. The pressure field is therefore [7.43]:

$$p'(x,t) = -\gamma p_0 \frac{\partial u}{\partial x} = -\gamma p_0 \left(-\frac{1}{c_0} f_1'\left(t - \frac{x}{c_0}\right) + \frac{1}{c_0} f_2'\left(t + \frac{x}{c_0}\right)\right) \qquad [7.43]$$

In this expression, incident pressure and reflected pressure [7.44] are recognized:

$$p'(x,t) = p_i(x,t) + p_r(x,t) \quad \begin{cases} p_i = \dfrac{\gamma p_0}{c_0} f_1'\left(t - \dfrac{x}{c_0}\right) \\ p_r = -\dfrac{\gamma p_0}{c_0} f_2'\left(t + \dfrac{x}{c_0}\right) \end{cases} \qquad [7.44]$$

Movement of the structure is a response to this pressure (at $x = 0$) [7.45]:

$$m_s \frac{\partial^2 u(0,t)}{\partial t^2} + k_s u(0,t) = p'(0,t) \qquad [7.45]$$

where m_s and k_s are the stiffness and weight per unit area. Introducing expressions [7.41] and [7.44] into this equation, we get expression [7.46]:

$$m_s\left(f_1''(t) + f_2''(t)\right) + k_s\left(f_1(t) + f_2(t)\right)u_0 = -\frac{\gamma p_0}{c_0}\left(-f_1'(t) + f_2'(t)\right) \qquad [7.46]$$

By alleviating writing, we obtain the formula [7.47]:

$$m_s f_2'' + \frac{\gamma p_0}{c} f_2' + k_s f_2 = -m_s f_1'' + \frac{\gamma p_0}{c} f_1' - k_s f_1 \qquad [7.47]$$

This equation, with image functions, is [7.48]:

$$\left(s^2 m_s + s\frac{\gamma p_0}{c} + k_s\right)\overline{f}_2(s) = \left(-s^2 m_s + s\frac{\gamma p_0}{c} - k_s\right)\overline{f}_1(s) \qquad [7.48]$$

We can then express the reflected wave as a function of the incident wave [7.49]:

$$\overline{f}_2(s) = -\left(\frac{s^2 - s\dfrac{\gamma p_0}{c_0 m_s} + \dfrac{k_s}{m_s}}{s^2 + s\dfrac{\gamma p_0}{c_0 m_s} + \dfrac{k_s}{m_s}} \right) \overline{f}_1(s) \qquad [7.49]$$

It is then possible to calculate reflected overpressure and total overpressure [7.50]:

$$\overline{p}_r(s) = \left(\frac{s^2 - s\dfrac{\gamma p_0}{c_0 m_s} + \dfrac{k_s}{m_s}}{s^2 + s\dfrac{\gamma p_0}{c_0 m_s} + \dfrac{k_s}{m_s}} \right) \overline{p}_i(s) \quad \overline{p}(s) = 2\left(\frac{s^2 + \dfrac{k_s}{m_s}}{s^2 + s\dfrac{\gamma p_0}{c_0 m_s} + \dfrac{k_s}{m_s}} \right) \overline{p}_i(s) \qquad [7.50]$$

The characteristic parameters of the problem are given in [7.51]:

$$\omega_s = \sqrt{\frac{k_s}{m_s}} \quad \alpha = \frac{\gamma p_0}{2 c_0 m_s} \quad et \quad \omega^2 = \left| \omega_s^2 - \alpha^2 \right| \qquad [7.51]$$

Two cases are to be considered depending on the value of impedance of the structure:

1) If $\sqrt{k_s m_s} > \dfrac{\gamma p_0}{2 c_0}$, the structure is said to be “stiff” and the operator is [7.52]:

$$\overline{p}(s) = 2\left(\frac{s^2 + \omega_s^2}{(s+\alpha)^2 + \omega^2} \right) \overline{p}_i(s) \qquad [7.52]$$

2) If $\sqrt{k_s m_s} < \dfrac{\gamma p_0}{2 c_0}$, the structure is said to be “supple” and the operator is [7.53]:

$$\overline{p}(s) = 2\left(\frac{s^2 + \omega_s^2}{(s+\alpha)^2 - \omega^2} \right) \overline{p}_i(s) \qquad [7.53]$$

To show the effect of coupling, let us take the example of an incident wave modeled by pressure discontinuity [7.54]:

$$p_i(t) = \Delta p\, H(t) \qquad \overline{p}_i = \Delta p \frac{1}{s} \qquad [7.54]$$

In the case of a "stiff" structure, the evolution of pressure will be [7.55], or if dimensionless [7.56]:

$$p'(t) = \Delta p\left(2 - \frac{4\alpha}{\omega} e^{-\alpha t} \sin \omega t\right) \qquad [7.55]$$

$$C = \frac{p'}{2\Delta p} = 1 - \frac{2\alpha}{\omega} e^{-\alpha \tau/\omega} \sin \tau \quad (\tau = \omega t) \qquad [7.56]$$

In the case of a "supple" structure, the evolution of pressure will be [7.57], or if dimensionless [7.58]:

$$p'(t) = \Delta p\left(2 - \frac{4\alpha}{\omega} e^{-\alpha t} \sinh \omega t\right) \qquad [7.57]$$

$$C = \frac{p'(t)}{2\Delta p} = 1 - \frac{2\alpha}{\omega} e^{-\alpha \tau/\omega} \sinh \tau \qquad [7.58]$$

Figure 7.14 shows these changes in pressure in the case of a "stiff" structure ($\alpha = \omega/2$) and a "supple" structure ($\alpha = 2\omega$).

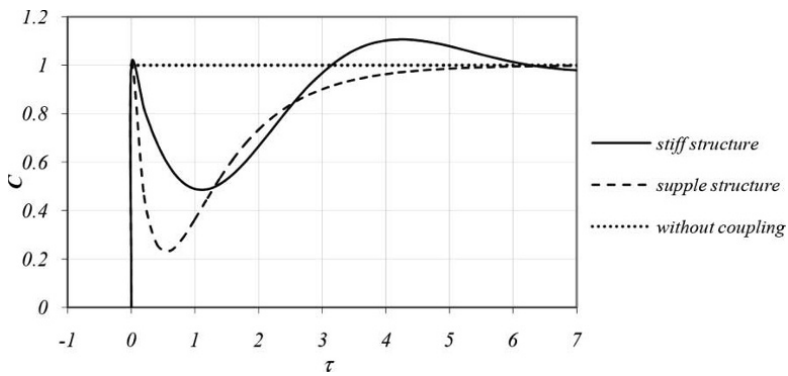

Figure 7.14. *Evolution of reflected pressure on a structure taking into account coupling with the movement of the structure*

The response of the structure can be calculated by solving [7.45]. In the case of a "stiff" structure ($\alpha = \omega/2$), the answer will be expressed as [7.59], or if dimensionless [7.60]:

$$u = \frac{2\Delta p}{k_s}\left(1 - e^{-\alpha t}\left(\frac{\alpha}{\omega}\sin \omega t + \cos \omega t\right)\right) \quad [7.59]$$

$$u^* = \frac{k_s u}{2\Delta p} = 1 - e^{-\alpha \tau/\omega}\left(\frac{\alpha}{\omega}\sin \tau + \cos \tau\right) \quad [7.60]$$

In the case of "supple" structure ($\alpha = 2\omega$), the response will be expressed as [7.61], or if dimensionless [7.62]:

$$u = \frac{2\Delta p}{k_s}\left(1 - e^{-\alpha t}\left(\frac{\alpha}{\omega}\sinh \omega t + \cosh \omega t\right)\right) \quad [7.61]$$

$$u^* = \frac{k_s u}{2\Delta p} = 1 - e^{-\alpha \tau/\omega}\left(\frac{\alpha}{\omega}\sinh \tau + \cosh \tau\right) \quad [7.62]$$

Figure 7.15 shows these responses. The case of the supple structure is unlikely to occur in buildings. The structure is said to be "stiff" because its surface impedance is greater than that of air. In reality, structures that have such low surface impedances are quite rare, and the effect of coupling is generally very low and, in practice, ignored.

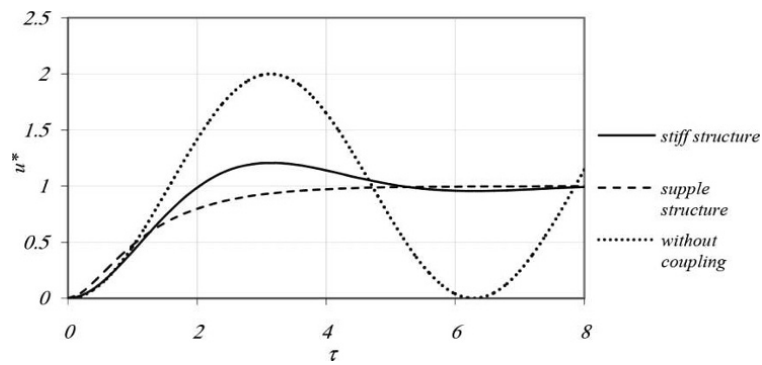

Figure 7.15. *Displacement of a structure under the action of an incident pressure jump, taking into account coupling with the movement of the fluid*

Chapter 8

Mechanical Response of Beams

When masses are spread over a structural element, it may be possible to use the beam model to represent mechanical behavior. The beam model is widely used by engineers for calculations of stresses and strains in structural elements under static loading, when these items have a "slim" geometry. It can also be used as a dynamic model. The mechanical response of a beam to an impact is studied here to highlight its specificities.

8.1. Dynamic beam models

8.1.1. *Notations*

There are three beam models that differ through the choice of representative kinematic strain [AXI 01b]. In the following, we present these three models in the framework of straight beams with an invariant section along its length, in the configuration of plane problems. Figure 8.1 shows a deformed beam.

We use the classical notations of beam theory or curved environments theory. A beam is defined by its axis (x) and a straight section (in the yz plane) with dimensions that are small compared to

the length, and for which the center is denoted by G. We denote the following:

– the kinematic variables:

- w (x,t): beam displacement (perpendicular to its x axis),

- Ω (x,t): rotation of a section (around z axis);

– the internal forces:

- $M(x,t)$: bending moment (around z axis),

- $V(x,t)$: shear force (according to y axis);

– the geometric characteristics of a section:

- S: beam section (constant),

- I: second moment of the section relative to the Gz axis (constant);

– the material characteristics:

- E: material strain module,

- ρ: material density.

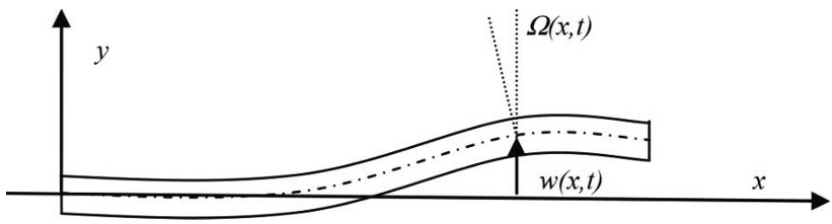

Figure 8.1. *Representation of a beam that is deformed in a plane, with transverse motion w and rotation of a section Ω*

If the beam is composite, linear density ρS and equivalent stiffness EI must be used. For beams with non-uniform sections along their length, the latter two elements are functions of x and solving the equations is generally not numerical.

8.1.2. *Bernoulli model*

The Bernoulli beam model (or Euler–Bernoulli) is a restriction of the curvilinear medium model in flexion where displacements are ignored, that is the strains associated with shear force. This assumption leads to a distinct simplification of the description of beam movement; in particular, the rotation of a section is equal to the slope of the displacement [8.1]:

$$\Omega = \frac{\partial w}{\partial x} \qquad [8.1]$$

The error from this assumption is negligible for beams with a "solid" section and large slenderness, or if considering long wavelengths. We will later discuss the limits imposed by this assumption. With the assumptions for modeling curvilinear media, equilibrium conditions for a single beam element allow us to write the relationships in [8.2]:

$$V(x,t) = -\frac{\partial M}{\partial x} \qquad f_y(x,t) = \frac{\partial V}{\partial x} \qquad [8.2]$$

where f_y is the linear density of force applied to the beam (in direction y axis). Therefore, we simply deduce equation [8.3], which reflects the balance:

$$\frac{\partial^2 M}{\partial x^2}(x,t) - f_y(x,t) = 0 \qquad [8.3]$$

In addition, the elastic behavior of the material leads us to write that the bending moment is proportional to the curvature of the beam [8.4]:

$$M(x,t) = EI\frac{\partial^2 w}{\partial x^2} \qquad [8.4]$$

This leads to equation [8.5] that governs the transverse displacements:

$$EI\frac{\partial^4 w}{\partial x^4}(x,t) - f_y(x,t) = 0 \qquad [8.5]$$

If we consider free vibrations in this model, the forces involved are the only inertial forces associated with transverse motion [8.6]:

$$f_y(x,t) = -\rho S\frac{\partial^2 w}{\partial t^2} \qquad [8.6]$$

The equation of motion can be written by formula [8.7]:

$$\frac{\partial^2 w}{\partial t^2} + c^2\frac{\partial^4 w}{\partial x^4} = 0 \quad \text{where} \quad c^2 = \frac{EI}{\rho S} \qquad [8.7]$$

This is a propagation equation, such as those seen in Chapter 1. Solutions to the propagation equation can be sought in the form of waves. It is interesting to consider the dispersion equation. If we give displacements a harmonic form [8.8]:

$$w = A\,e^{i(kx-\omega t)} \qquad [8.8]$$

we obtain the dispersion equation [8.9]:

$$EI\,k^4 - \rho S\,\omega^2 = 0 \quad \text{or} \quad C = \frac{2\pi}{\lambda}\sqrt{\frac{EI}{\rho S}} \qquad [8.9]$$

This dispersion equation gives a limit to the Bernoulli model to represent the movements of beams. Indeed, in an elastic bar, the waves cannot go faster than compression waves, for which the velocity is C_0. The Bernoulli model is only valid for sufficiently large wavelengths, as shown by condition [8.10]:

$$C_0 = \sqrt{\frac{E}{\rho}} \qquad C < C_0 \;\rightarrow\; \lambda > \frac{2\pi}{C_0}\sqrt{\frac{EI}{\rho S}} \quad \text{or} \quad \omega < C_0{}^2\sqrt{\frac{\rho S}{EI}} \qquad [8.10]$$

8.1.3. *Rayleigh model*

The Rayleigh beam model is based on the same kinematic assumption as the Bernoulli model, i.e. the rotation of a section is the same as the average slope of line [8.1]. Although the Bernoulli model only takes into account inertia forces due to transverse movements, the Rayleigh model introduces forces due to inertia that are associated with rotation of the sections. This leads to two equations of motion, one relative to displacement along the y axis and the other to the rotation around the z axis [8.11]:

$$\begin{cases} \rho S \dfrac{\partial^2 w}{\partial t^2} = \dfrac{\partial V}{\partial x} \\ \rho I \dfrac{\partial^2 \Omega}{\partial t^2} = \dfrac{\partial M}{\partial x} + V \end{cases} \qquad [8.11]$$

By eliminating the variables V, M and Ω, we obtain the equation of motion [8.12]:

$$\frac{\partial^2 w}{\partial t^2} - \frac{I}{S}\frac{\partial^4 w}{\partial x^2 \partial t^2} + c^2 \frac{\partial^4 w}{\partial x^4} = 0 \qquad [8.12]$$

The dispersion equation associated with this model is formulated as [8.13]:

$$c^2 k^4 - \omega^2 - \frac{I}{S}\omega^2 k^2 = 0$$

$$\text{or} \quad C = \sqrt{\frac{c^2}{I/S + \lambda^2/4\pi^2}} \quad \text{and} \quad \lim_{\lambda \to 0} C = \sqrt{\frac{E}{\rho}} \qquad [8.13]$$

If the wavelength decreases and tends toward 0, velocity tends toward a finite limit that, at lower frequencies, widens the description capacities of this model compared to the Bernoulli model.

8.1.4. *Timoshenko model*

A more comprehensive model that takes displacement deformations into account was introduced by Timoshenko [TIM 39]. Displacement γ, also called warping, corresponds to the difference between the rotation of the beam axis and rotation of a section as indicated by formula [8.14]:

$$\gamma = \frac{\partial w}{\partial x} - \Omega \qquad [8.14]$$

The transverse movements and rotations are then governed by equations [8.15]:

$$\begin{cases} \rho S \dfrac{\partial^2 w}{\partial t^2} = k'SG\left(\dfrac{\partial^2 w}{\partial x^2} - \dfrac{\partial \Omega}{\partial x}\right) \\ \rho I \dfrac{\partial^2 \Omega}{\partial t^2} = k'SG\left(\dfrac{\partial w}{\partial x} - \Omega\right) + EI\dfrac{\partial^2 \Omega}{\partial x^2} \end{cases} \qquad [8.15]$$

The first relationship reflects the consequence of the fundamental principle of dynamics in the transverse direction. The second relationship corresponds to the equation of moment. Internal forces, bending moment and shear force have the expressions [8.16]:

$$\begin{aligned} M &= -EI\frac{\partial \Omega}{\partial x} = EI\left(\frac{\partial^2 w}{\partial x^2} - \beta\frac{\partial^2 w}{\partial t^2}\right) \qquad \left(\beta = \frac{\rho}{k'G}\right) \\ V &= -k'SG\left(\frac{\partial w}{\partial x} - \Omega\right) \end{aligned} \qquad [8.16]$$

Coefficient k' is called Timoshenko's coefficient. This coefficient is introduced to connect displacement to shear force. Its value depends on the shape of the section and the Poisson coefficient of the material [FUN 68, BLE 79] ($k' = 0.8667$ for a solid steel section). The system of equation [8.15] can be used directly, or if the rotation variable is removed, we obtain a differential equation of motion [8.17]:

$$\frac{\partial^2 w}{\partial t^2} - \frac{I}{S}\left(1 + \frac{E}{Gk'}\right)\frac{\partial^4 w}{\partial x^2 \partial t^2} + \frac{\rho I}{GSk'}\frac{\partial^4 w}{\partial t^4} + c^2\frac{\partial^4 w}{\partial x^4} = 0 \qquad [8.17]$$

This model allows us to further increase the description capacities in the field of high frequencies and short wavelengths. This model is also necessary in the case of beams with displacement deformations that are non-negligible compared to flexion (this may be the case of composite beams or lattice beams). To write the Timoshenko model dispersion equation, we introduce parameter r that is the gyration radius of the section, and we consider the magnitude of the second coefficient term that is known for solid beam sections. Then, we obtain equation [8.18]:

$$-\omega^2 - 4r^2\,\omega^2 k^2 - 3\frac{r^2}{{C_0}^2}\,\omega^4 + {C_0}^2 r^2 k^4 = 0$$

where $r = \sqrt{\frac{I}{S}}$ and $\left(1 + \frac{E}{Gk'}\right) \approx 4$ [8.18]

or:

$$-C^2\left(1 + 16\frac{r^2}{\lambda^2}\pi^2 + 12\frac{r^2 C^2}{\lambda^2 {C_0}^2}\pi^2\right) + {C_0}^2 r^2 \frac{4\pi^2}{\lambda^2} = 0 \qquad [8.19]$$

If we introduce slenderness as the ratio of the wavelength to the gyration radius of the beam section $\ell = \lambda / r$, this dispersion equation takes the form [8.20]:

$$-C^2\left(\ell^2 + 16\pi^2 + 12\frac{C^2}{{C_0}^2}\pi^2\right) + 4\pi^2 {C_0}^2 = 0 \qquad [8.20]$$

We can compare dispersion relationships for the three models. The phase velocity as a function of the slenderness ratio is shown in Figure 8.2.

Formulas [8.21]–[8.23] recall the expression of phase velocity as a function of slenderness and its limit when slenderness, and hence the wavelength, tends toward zero:

– Euler Bernoulli:

$$\frac{C}{C_0} = \frac{2\pi}{\ell} \quad \lim_{\ell \to 0} C = \infty \qquad [8.21]$$

– Rayleigh:

$$\frac{C}{C_0} = \frac{1}{\sqrt{1 + \ell^2 / 4\pi^2}} \quad \lim_{\ell \to 0} C = C_0 \qquad [8.22]$$

– Timoshenko:

$$\frac{C}{C_0} = \sqrt{\frac{1}{24\pi^2}\left(\sqrt{\left(\ell^2 + 16\pi^2\right)^2 + 193\pi^4} - \left(\ell^2 + 16\pi^2\right)\right)} \qquad [8.23]$$

$$\lim_{\ell \to 0} C = 0,46\, C_0$$

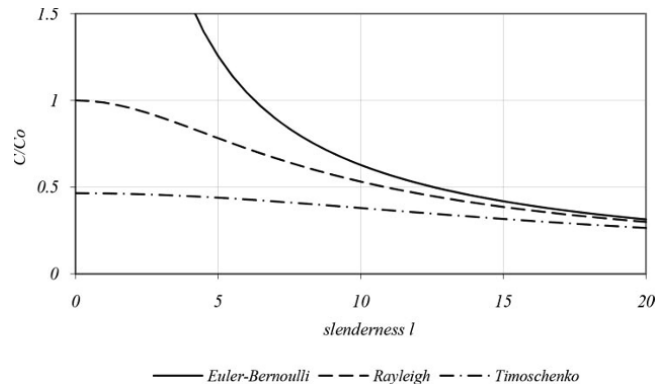

Figure 8.2. *Phase velocity as a function of slenderness*

The Euler–Bernoulli model is the most widely used model because of its simplicity. We can, with this model, use analytical formulas of solutions. Use of the Timoshenko model is rarer. If analytical solutions to this equation do exist [ORT 96], they are not very compact formulas. The Timoshenko model is used to represent the movement of a structure modeled as a beam with significant displacements. This is the case for composite beams and lattice systems or "scaling" structures. We may then need to use a numerical solution [REN 88].

8.2. Impacts on beams

8.2.1. *Adaptation of the model to a time scale*

8.2.1.1. *Introduction of the flexion*

An impact on a beam is a dynamic load that results in a transverse force for which intensity increases rapidly $F(t)$. This can be modeled by a point force or as a force distributed over an area that is small compared to the beam (Figure 8.3). The rapid application of this force generates a phenomenon that we call the mechanical response of the solid, which is the beam. Several phases can be considered for the description of the mechanical response. Each phase has a characteristic time scale. For each of these phases, modeling may differ.

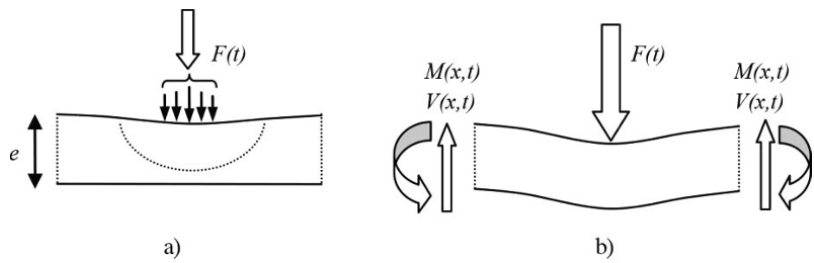

Figure 8.3. *Impact on a beam showing the two response phases: a) waves in a solid; b) flexion of a beam*

The first phase considers the first moments after impact and the area near the contact point (Figure 8.3(a)). The rapid application of load induces a compression wave that propagates through the solid, as described in Chapter 1. This compression wave will be reflected at the opposite side of the beam. This can eventually lead to rupture by spalling. A characteristic time for this phase is the duration of one round trip of waves in the transverse dimension of the solid. The order of magnitude of this time is $t_t = 2e/C_P$.

To describe what happens on this time scale, the beam model (one-dimensional) is, of course, not at all relevant. It is necessary to use a three-dimensional (or two-dimensional) model of the solid to

represent these waves and nonlinear effects that can potentially result if the stress levels are high enough. For example, for a 20 cm thick concrete beam, the characteristic time of this phase is about $t_t \approx 0.1$ ms.

The second phase considers times above time t_t (Figure 8.3(b)). On this time scale, waves have been reflected and diffracted several times in the solid. We can then consider motion across the beam structure. The movements have reached distances from the point of impact sufficient for the Saint-Venant hypothesis to be relevant. The average motion of the beam, i.e. its transverse displacements about its axis, can then be sought as a solution to the equations presented in the previous section.

8.2.1.2. *Influence of conditions at the limits*

Let us consider a beam on two supports, such as that shown in Figure 8.3. From a point of impact at the center, a movement propagates through the beam. We denote t_f the time required for transverse movements to propagate across a length equal to that of the half-beam. Below, we will specify the order of magnitude of this length. As long as movement does not reach the support, the transient motion of the beam is the same as if it were of infinite length. During this phase, support reactions are negligible. Beyond time t_f, support reactions appear and modify movement until a movement that can be described as a superposition of strain modes is achieved. We will first study the transient response of a long beam, which corresponds to the moments between t_t and t_f. In section 8.3, we will study movements by modal superposition, which is relevant for times that are much higher than t_f.

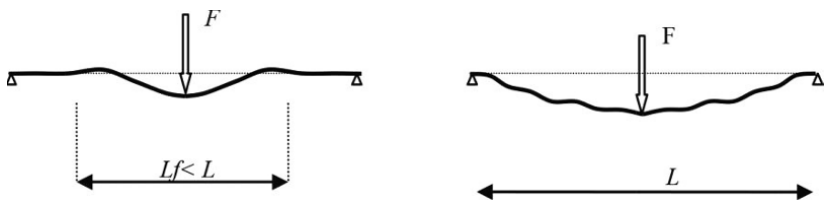

Figure 8.4. *Strains on the beam before movement has reached the supports, and at a time well beyond the arrival of movement on the supports*

8.2.2. *Impact at the center of a beam*

Let us study a beam by considering its length as very large. A point force is applied to its center. The origin of the coordinate is placed at this point. The equation governing transverse displacement w is given in [8.24]. We consider the Bernoulli model and, as there is symmetry, we only study a half-beam:

$$\frac{\partial^4 w}{\partial x^4} + 4\alpha^4 \frac{\partial^2 w}{\partial t^2} = 0 \qquad 4\alpha^4 = \frac{\rho S}{EI} \qquad x \in [\,0, +\infty\,[\qquad [8.24]$$

The boundary conditions at $x = 0$ are explained by relationships [8.25]. The displacement slope is zero by symmetry and the shear force is equal to half the point force applied:

$$\frac{\partial w}{\partial x}(0,t) = 0 \qquad \frac{\partial^3 w}{\partial x^3}(0,t) = \frac{1}{2EI} F(t) \qquad [8.25]$$

At the other end of the beam (to infinity), the transverse displacement remains zero. It is possible to find an analytical solution to this problem by using a Laplace transformation in time [DIT 79] [8.26]:

$$\frac{\partial^4 \overline{w}}{\partial x^4} + 4 s^2 \alpha^4 \overline{w} = 0 \qquad [8.26]$$

The image of the movement of the beam can be written as [8.27]:

$$\overline{w}(x,s) = e^{-\alpha x\sqrt{s}} \left(\overline{K}_1 \cos\left(\alpha x\sqrt{s}\right) + \overline{K}_2 \sin\left(\alpha x\sqrt{s}\right) \right) \qquad [8.27]$$

The following operators and time-associated functions [8.28] are posed:

$$\Omega_1(x,t) = \frac{1}{\sqrt{\pi t}} \cos\left(\frac{\alpha^2 x^2}{2t}\right) \qquad \overline{\Omega}_1(x,s) = \frac{1}{\sqrt{s}} e^{-\alpha x\sqrt{s}} \cos\left(\alpha x\sqrt{s}\right)$$

$$\Omega_2(x,t) = \frac{1}{\sqrt{\pi t}} \sin\left(\frac{\alpha^2 x^2}{2t}\right) \qquad \overline{\Omega}_2(x,s) = \frac{1}{\sqrt{s}} e^{-\alpha x\sqrt{s}} \sin\left(\alpha x\sqrt{s}\right) \qquad [8.28]$$

The response image is also expressed using these functions [8.29]:

$$\overline{w}(x,s) = \sqrt{s}\left(\overline{K}_1\overline{\Omega}_1 + \overline{K}_2\overline{\Omega}_2\right) \qquad [8.29]$$

Calculation of the partial derivatives with respect to x and consideration of boundary conditions at $x = 0$ leads to expressions [8.30]:

$$\frac{\partial \overline{w}}{\partial x}(0,s) = \alpha\sqrt{s}\left(\overline{K}_2 - \overline{K}_1\right) = 0 \rightarrow \quad \overline{K}_2 = \overline{K}_1 = \overline{K}$$

$$\frac{\partial^3 \overline{w}}{\partial x^3}(0,s) = 4\alpha^3 s\sqrt{s}\ \overline{K} = \frac{1}{2EI}\overline{F}(s) \rightarrow \quad \overline{K}(s) = \frac{1}{8\alpha^3 s\sqrt{s}EI}\overline{F}(s) \qquad [8.30]$$

Then, the response image is [8.31]:

$$\overline{w}(x,s) = \frac{1}{8s\alpha^3 EI}\overline{F}(s)\left(\overline{\Omega}_1 + \overline{\Omega}_2\right) \qquad [8.31]$$

First, we consider the case of pulse load: $F(t) = i\,\delta(t)\ \ \overline{F}(s) = i.$ The pulse response is formulated in [8.32]:

$$\begin{aligned} w(x,t) = {} & \frac{i}{8\alpha^3 EI}\sqrt{\frac{t}{\pi}}\left(\cos\left(\frac{\alpha^2 x^2}{2t}\right) + \sin\left(\frac{\alpha^2 x^2}{2t}\right)\right) \\ & + \frac{xi}{8\alpha^2 EI}\left(S_F\left(\frac{\alpha x}{\sqrt{\pi t}}\right) + C_F\left(\frac{\alpha x}{\sqrt{\pi t}}\right)\right) \end{aligned} \qquad [8.32]$$

This expression uses the Fresnel integrals [8.33]:

$$C_F(z) = \int_0^z \cos\left(\frac{\pi u^2}{2}\right)du \qquad S_F(z) = \int_0^z \sin\left(\frac{\pi u^2}{2}\right)du \qquad [8.33]$$

It is possible to represent the pulse response in a dimensionless manner using dimensionless variables [8.34]:

$$W = \frac{8\alpha^2 EI}{i}\frac{w}{x} \quad \eta = \frac{\alpha x}{\sqrt{t}} \qquad [8.34]$$

It may be noted that with this change of variables, equation [8.24] becomes an ordinary differential equation [8.35]:

$$\frac{d^4W}{d\eta^4} + \eta^2 \frac{d^2W}{d\eta^2} = 0 \qquad [8.35]$$

The solution is formulated in [8.36]:

$$W(\eta) = \frac{1}{\eta\sqrt{\pi}}\left(\cos\left(\frac{\eta^2}{2}\right) + \sin\left(\frac{\eta^2}{2}\right)\right) + \left(S_F\left(\frac{\eta}{\sqrt{\pi}}\right) + C_F\left(\frac{\eta}{\sqrt{\pi}}\right)\right) \qquad [8.36]$$

Figure 8.5 gives a representation of the solution.

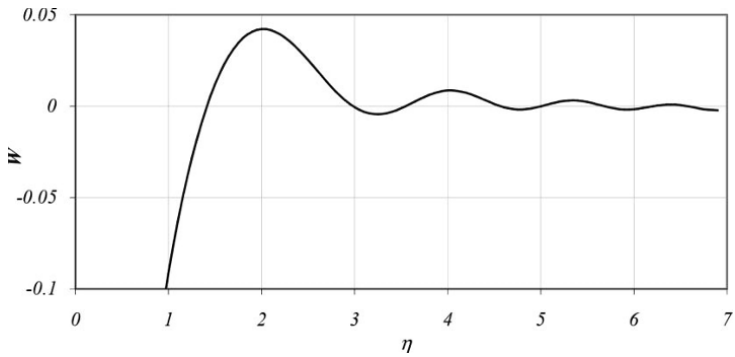

Figure 8.5. *Representation with dimensionless variables W(η) of the deflection of a beam under a specific pulse load*

The dimensionless character of curve $W(\eta)$ does not give an instantaneous image of the shape of the beam. However, we can notice that the effect of loading is relatively small beyond $\eta = 5$. The area with significant strain of both sides of the point of impact is of length *Lf* [8.37]:

$$Lf \approx 10\alpha\sqrt{t} \qquad [8.37]$$

It should be noted that flexion strain does not spread in the beam as a wave at constant velocity. This gives an order of magnitude of time

at which the supports will start to influence the movement of the beam [8.38]:

$$t_f \approx \left(\frac{L}{10\alpha} \right)^2 \qquad [8.38]$$

To give the engineer a more useful image of the transitional phase of flexion following an impact, it is best to consider load as the brutal application of a force that remains constant [8.39]. We can write the bending moments and shear forces in this beam:

$$F(t) = P\,H(t) \quad \bar{F}(s) = \frac{P}{s} \qquad [8.39]$$

The response image to this load is formulated in [8.40]:

$$\bar{w}(x,s) = \frac{P}{8s^2\alpha^3 EI}\left(\bar{\Omega}_1 + \bar{\Omega}_2\right) \qquad [8.40]$$

The transverse displacement can be calculated by formula [8.41] (* denoting the convolution product):

$$w(x,t) = \frac{Pt}{8\alpha^3 EI} * \left(\sqrt{\frac{1}{\pi t}} \left(\cos\left(\frac{\alpha^2 x^2}{2t} \right) + \sin\left(\frac{\alpha^2 x^2}{2t} \right) \right) \right) \qquad [8.41]$$

It is possible to calculate the bending moment and shear force and express it in a dimensionless manner [8.42]. The diagrams are shown in Figure 8.6. The maximum bending moment below the point of impact and its intensity varies as the square root of time:

$$v(\eta) = \frac{V}{2P} \quad m(\eta) = \frac{M\alpha}{P\sqrt{t}} \qquad [8.42]$$

8.2.3. *Beam acted upon by a blast*

Another case of rapid loading is that of the sudden application of a distributed force. This situation may arise under the action of a blast

wave. The equation that governs the transverse displacements w is then [8.43]:

$$EI\frac{\partial^4 w}{\partial x^4}+\rho S\frac{\partial^2 w}{\partial t^2}=p(t) \qquad [8.43]$$

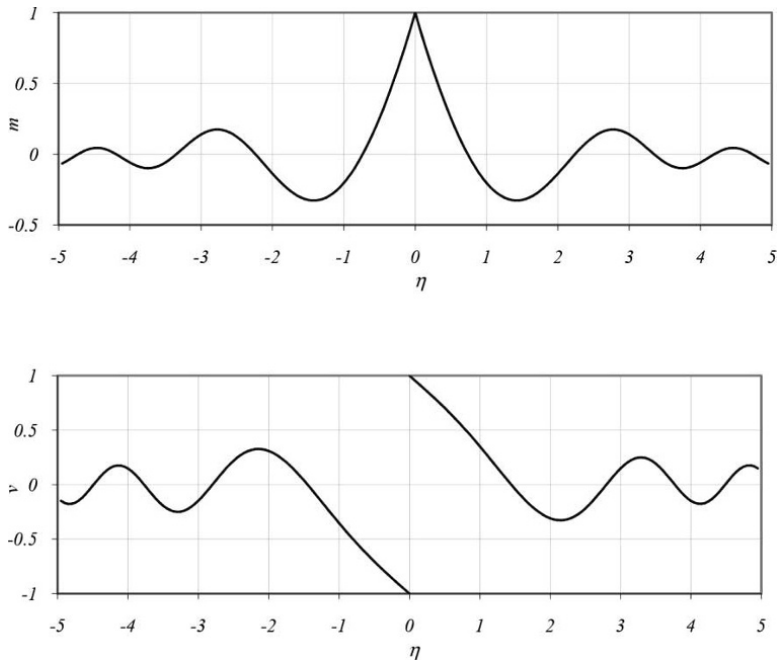

Figure 8.6. *Diagram of bending moment and shear force in a beam upon an impact*

Figure 8.7 represents this situation. In the first instants, the whole beam is displaced under the action of the blast. Flexion of the beam is initiated by the support, which requires a point force, and propagates toward the center of the beam.

To study movement in those first instants, it is useful to change the variable [8.44]. Then, we calculate the relative displacement of the support relative to the whole beam. During this phase, movement occurs as if the length of the beam was infinite. This assumption

becomes invalid as soon as the movement reaches the center of the beam:

$$w(x,t) = u(x,t) + v(t) \qquad x \in [\,0, +\infty\,[\qquad [8.44]$$

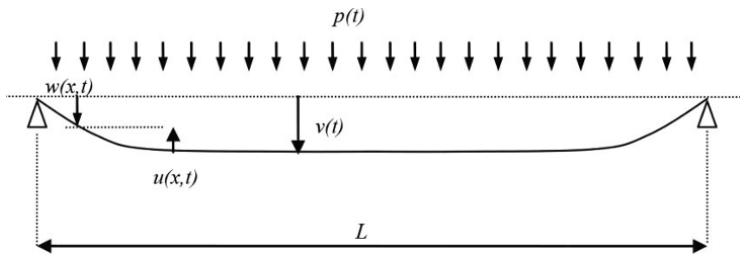

Figure 8.7. *Deformation of a beam under a distributed load applied suddenly*

The equations of the problem are formulated in [8.45]:

$$EI\frac{\partial^4 u}{\partial x^4} + \rho S\frac{\partial^2 u}{\partial t^2} = 0 \qquad \rho S\frac{\partial^2 v}{\partial t^2} = p(t) \qquad [8.45]$$

The boundary conditions at $x = 0$ are explained by relationships [8.46]. At the origin, a relative displacement is imposed. The bending moment, and therefore curvature, is zero:

$$\overline{u}(0,s) = \frac{\overline{p}}{s^2 \rho S} \qquad \frac{\partial^2 u}{\partial x^2}(0,t) = 0 \qquad [8.46]$$

At the other end of the beam (at infinity), the transverse displacement remains zero. It is possible to find an analytical solution to this problem. Using a Laplace transformation in time, the image of the movement of the beam is the shape [8.47]:

$$\overline{u}(x,s) = e^{-\alpha x\sqrt{s}}\left(\overline{K}_1 \cos\left(\alpha x\sqrt{s}\right) + \overline{K}_2 \sin\left(\alpha x\sqrt{s}\right)\right) \qquad [8.47]$$

Operators and associated time functions, as previously defined in [8.28], are used. The response image is also expressed using these functions. Calculation of the partial derivatives with respect to x and

taking into account the boundary conditions at $x = 0$ leads to expressions [8.48]:

$$\begin{aligned}
\overline{u}(x,s) &= \frac{2\alpha^2\,\overline{p}}{s^2\rho S}e^{-\alpha x\sqrt{s}}\sin\left(\alpha x\sqrt{s}\right)\\
\frac{\partial^2\overline{u}}{\partial x^2} &= \frac{2\alpha^2\,\overline{p}}{s\rho S}e^{-\alpha x\sqrt{s}}\sin\left(\alpha x\sqrt{s}\right)\\
\frac{\partial^3\overline{u}}{\partial x^3} &= \frac{2\alpha^3\,\overline{p}}{\sqrt{s}\rho S}e^{-\alpha x\sqrt{s}}\left(\cos\left(\alpha x\sqrt{s}\right)\text{-}\sin\left(\alpha x\sqrt{s}\right)\right)
\end{aligned} \qquad [8.48]$$

If we consider a pulse (i) as a load, we can explain the shear force and bending moment [8.49]:

$$\begin{aligned}
V &= \frac{i}{2\alpha\sqrt{\pi t}}\left(\cos\left(\frac{\eta^2}{2}\right)-\sin\left(\frac{\eta^2}{2}\right)\right)\\
M &= \frac{i}{2\alpha^2\sqrt{2}}\left(C_F\left(\frac{\eta}{\sqrt{\pi}}\right)-S_F\left(\frac{\eta}{\sqrt{\pi}}\right)\right)
\end{aligned} \qquad [8.49]$$

We can express this result with dimensionless parameters [8.50]:

$$v(\eta)=\frac{2\alpha V\sqrt{\pi t}}{i} \quad m(\eta)=\frac{4\sqrt{2}\,M\,\alpha^2}{i} \quad W(\eta)=\frac{w\rho S}{2it} \qquad [8.50]$$

The shear force, bending moment and displacement are represented in dimensionless form in Figure 8.8.

A more realistic situation is to consider the load as the sudden application of a distributed force of intensity P that remains constant [8.39]. We can write the bending moments in the beam as [8.51]:

$$M(x,t)=\frac{P}{2\alpha^2\sqrt{2}}\int_0^t\left(C_F\left(\frac{\alpha x}{\sqrt{\pi\tau}}\right)-S_F\left(\frac{\alpha x}{\sqrt{\pi\tau}}\right)\right)d\tau \qquad [8.51]$$

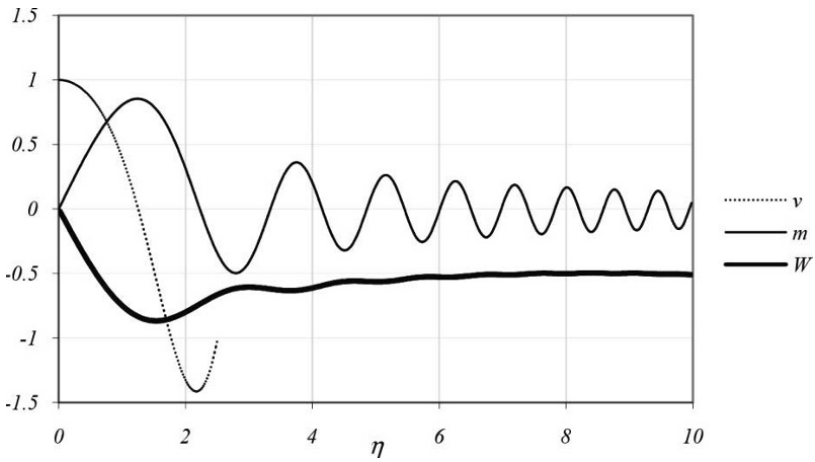

Figure 8.8. *Shear force (v), bending moment (m) and distorted line (W) near a support beam for a beam impulsively loaded by a blast (dimensionless parameters)*

By changing the variables, we obtain the expression [8.52]:

$$M = \frac{Px^2}{\sqrt{2}} \int_{\eta}^{\infty} \left(C_F\left(\frac{\beta}{\sqrt{\pi}}\right) - S_F\left(\frac{\beta}{\sqrt{\pi}}\right)\right) \frac{d\beta}{\beta^3} \qquad [8.52]$$

Dimensionless parameters [8.53] are used:

$$m(\eta) = \frac{M\alpha^2}{Pt} \quad \eta = \frac{\alpha x}{\sqrt{t}} \qquad [8.53]$$

The dimensionless bending moment diagram is shown in Figure 8.9.

As this case of loading is very representative of a real situation, it is interesting to investigate the value of the maximum bending moment and the location of this maximum. The dimensionless formula gives the result [8.54]:

$$M_{\max} = 0{,}11\frac{Pt}{\alpha^2} \quad x(M_{\max}) = 0{,}71\frac{\sqrt{t}}{\alpha} \qquad [8.54]$$

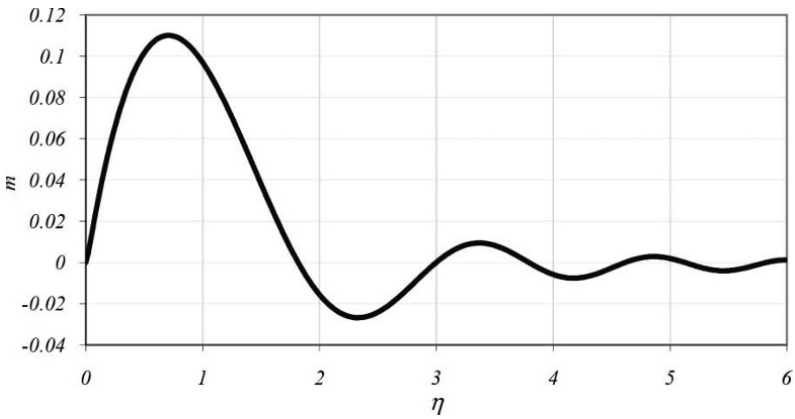

Figure 8.9. *Dimensionless bending moment, near a support, for a beam loaded by a pressure step*

If the bending moment is in practice limited by a maximum value M_p corresponding to plasticizing (or rupture), we can estimate position x_p of the plastic zone (or fissure) [8.55]:

$$x_p = 2{,}14\sqrt{\frac{P}{M_p}} \qquad [8.55]$$

8.2.4. *Solicitation in a section of a beam under impact*

The above examples show that the shear force and bending moment do not evolve according to the same time functions. To understand the consequences, we consider the elementary section of the beam located at the point of impact. This is the central section ($x = 0$) of the problem seen in section 8.2.2. The internal forces in this section are then determined as a function of any force $F(t)$ by relationships [8.56]:

$$\bar{M}(0,s) = \frac{1}{4\alpha\sqrt{s}}\bar{F}(s) \qquad \bar{V}(0,s) = \frac{1}{2}\bar{F}(s)$$

$$M(0,t) = \frac{1}{2\alpha}\int_0^t \frac{1}{\sqrt{\pi(t-\tau)}} F(\tau)\,d\tau \qquad V(0,t) = \frac{1}{2}F(t) \qquad [8.56]$$

To highlight the role of load velocity, let us consider that force is applied at a certain velocity [8.57]:

$$F(t) = \beta t \quad \bar{F}(s) = \frac{\beta}{s^2} \qquad [8.57]$$

We deduce the bending moment rate of change [8.58]:

$$\bar{M}(0,s) = \frac{\beta}{4\alpha s^2\sqrt{s}} \qquad M(0,t) = \frac{\beta t^{3/2}}{3\alpha\sqrt{\pi}} \qquad [8.58]$$

The difference between a quasi-static load and dynamic load is not only the strain rate. It is also linked to the loading path characterized by the evolution of the two loading parameters: shear force and bending moment. Figure 8.10 schematically shows the two types of rupture.

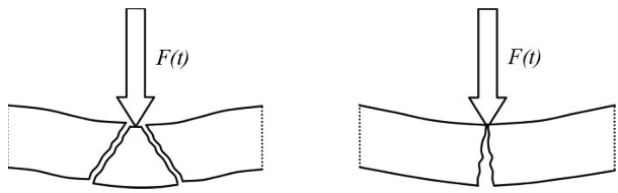

Figure 8.10. *Rupture patterns in "shear" and in "bending"*

In a quasi-static load, the two loading parameters are functions of the applied force and their ratio remains constant. To the central section of a rectangular beam, the path will be given by formula [8.59]:

$$M = \frac{FL}{4} \quad V = \frac{F}{2} \qquad [8.59]$$

Impact on a beam, especially if it is made of brittle material, can lead to several types of rupture (cratering, spalling, perforation, etc.). If the shock is of the "soft" type, there are two main mechanisms. The first is rupture by flexion, and the second is rupture through shearing. Shear rupture is not usually observed in quasi-static loading.

The material rupture criteria and the dynamic response of the test body are what will determine the type of rupture that will occur. For a brittle material, the simplest criterion is the Rankine criterion. This criterion states that rupture occurs when the greatest principal stress reaches a threshold f_t [8.60]:

$$Sup\left\{\sigma_I, \sigma_{II}, \sigma_{III}\right\} < f_T \qquad [8.60]$$

The rupture plane is then orthogonal to the corresponding principal direction map. A load on a beam section is described by two parameters, the bending moment M and the shear force V. Modeling provides these two parameters, and it is possible to express the Rankine criterion based on them. In beam theory, a stress plane state defined by relationships [8.61] is assumed (the stress σ_{11} is the normal tensile stress or compression and σ_{12} is the shear stress, y is the ordinate in the transverse direction):

$$\underline{\underline{\sigma}} = \begin{pmatrix} \sigma_{11} & \sigma_{12} \\ \sigma_{12} & 0 \end{pmatrix} \quad \sigma_{11} = y\frac{M}{I} \qquad \sigma_{12} = \frac{V}{2I}\left(\frac{e^2}{4} - y^2\right) \qquad [8.61]$$

To show dimensionless load parameters, we adopt the notation [8.62]:

$$z = \frac{2y}{e} \quad V_T = \frac{8I}{e^2} f_T \quad M_T = \frac{2I}{e} f_T \quad \mu = \frac{M}{M_T} \quad \upsilon = \frac{V}{V_T} \qquad [8.62]$$

The stresses are expressed as a function of load parameters [8.63]:

$$\sigma_{11} = z\,\mu\, f_t \qquad \sigma_{12} = \upsilon\, f_t\left(1 - z^2\right) \qquad [8.63]$$

The maximum principal stress is then expressed as [8.64]:

$$\sigma_I = \frac{1}{2}\left(\sigma_{11} + \sqrt{{\sigma_{11}}^2 + 4{\sigma_{12}}^2}\right)$$

$$= \frac{1}{2} f_T \left(z\mu + \sqrt{\left(z\mu\right)^2 + 4\upsilon^2\left(1 - z^2\right)^2} \right) \qquad [8.64]$$

The Rankine criterion is expressed in terms of the two load parameters [8.65]:

$$\max_{z\in[0,1]}\left\{ z\mu+\sqrt{(z\mu)^2+4\upsilon^2\left(1-z^2\right)^2}\right\} < 2 \qquad [8.65]$$

It is also possible to use the Saint-Venant criterion that indicates that rupture occurs when the largest principal strains reach a limit value [8.66]. In practice, this criterion is very similar to the Rankine criterion:

$$\begin{aligned} &Sup\left\{\varepsilon_I,\varepsilon_{II},\varepsilon_{III}\right\} < \frac{f_T}{E} \\ &\max_{z\in[0,1]}\left\{ z(1-\nu)\mu+(1+\nu)\sqrt{(z\mu)^2+4\upsilon^2\left(1-z^2\right)^2}\right\} < 2 \end{aligned} \qquad [8.66]$$

Figure 8.11 shows the Rankine criterion in the plane of load parameters. It has two parts:

– if rupture occurs because the load parameters are such that (μ = 1 and 0 < ν < 0.92), there will be flexion rupture and the rupture plane will be normal to the axis of the beam;

– if the parameters become the coordinates of a point of the second part (0 < μ <1 and 0.92 < ν < 1), there will be a shear rupture, and the rupture plane will be inclined on the axis of the beam at an angle close to 45°.

The terms “flexion” and “shear” associated with rupture are common but inaccurate because, in both cases, rupture of the material occurs under tension. In the plane of Figure 8.11, if the loading path is quasi-static, it is a line with a slope greater than 10 (if L > 5) [8.67]:

$$\frac{\mu}{\upsilon}=\frac{2L}{e} \qquad [8.67]$$

We note that only flexion rupture is possible. For dynamic loads, change in both parameters depends on the load application velocity [8.68]:

$$M=\frac{\beta t\sqrt{t}}{3\alpha\sqrt{\pi}} \qquad V=\frac{\beta t}{2} \qquad [8.68]$$

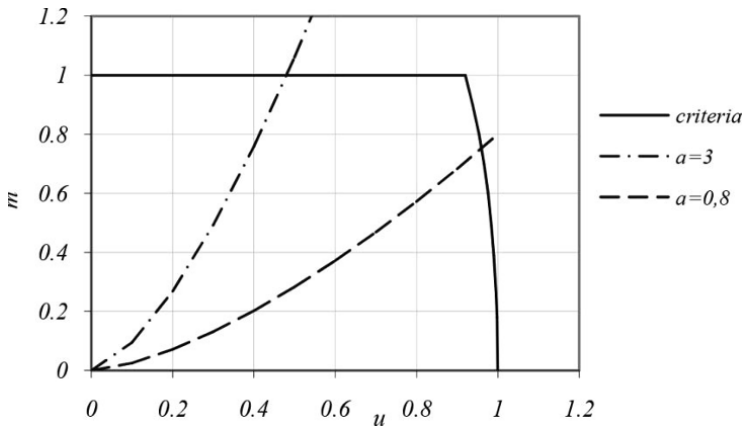

Figure 8.11. *Rupture criterion for a beam of quasi-brittle material. Different load paths at different strain rates*

The load path is then described by equation [8.69]:

$$\mu = a\,\upsilon^{3/2} \quad \left(a = \frac{32}{3\alpha e^2}\sqrt{\frac{If_t}{\pi\beta}} \right) \qquad [8.69]$$

Depending on the value of load velocity β, it is possible to observe either of the two modes of rupture. The load velocity that corresponds to the transition between the two modes is called β_{tr} [8.70]:

$$\beta_{tr} = \frac{30\,I\,f_T}{\alpha^2\,e^4} \qquad [8.70]$$

For a rectangular beam section, we obtain the expression [8.71]:

$$\beta_{tr} \approx 1.7\;\; f_t\sqrt{\frac{E}{\rho}} \qquad [8.71]$$

Several loading paths are shown in Figure 8.11, with different values for the relative load velocity.

8.3. Calculation by modal superposition

8.3.1. *Eigenmodes of displacement*

For times that are significantly higher than t_f, it is possible to use the modal superposition method to represent the mechanical response of a beam. This method requires us, as a first step, to calculate the eigenmodes of the beam, and as a second step, to project the equation of motion on these modes. To find the eigenmodes, we seek a solution in the form $w(x,t)=\phi(x)\psi(t)$. Its introduction into the partial differential equation allows us to write [8.72]:

$$\frac{EI}{\rho S}\frac{1}{\phi}\frac{d^4\phi}{dx^4}=-\frac{1}{\psi}\frac{d^2\psi}{dt^2}=\omega^2 \qquad [8.72]$$

This will separate the variables and obtain two ordinary differential equations. For the time function, we have the classical equation [8.73]:

$$\frac{d^2\psi}{dt^2}+\omega^2\psi=0 \qquad \psi(t)=A\cos\omega t+B\sin\omega t \qquad [8.73]$$

The equation governing the function of space is [8.74]:

$$\frac{d^4\phi}{dx^4}-k^4\phi=0 \qquad k^4=\omega^2\frac{\rho S}{EI} \qquad [8.74]$$

If the distributions of mass and stiffness of the beam are constant (uniform beam section), the solution can be written as follows [8.75]:

$$\phi(x)=a\cos kx+b\sin kx+c\cosh kx+d\sinh kx \qquad [8.75]$$

The constants must be determined using boundary conditions. Three types of condition meet at the extremity of a beam and are presented in Table 8.1.

Fixed extremity	Hinged or simply supported extremity	Free extremity
$\phi = 0 \quad \frac{d\phi}{dx} = 0$	$\phi = 0 \quad \frac{d^2\phi}{dx^2} = 0$	$\frac{d^2\phi}{dx^2} = 0 \quad \frac{d^3\phi}{dx^3} = 0$

Table 8.1. *Conditions imposed on the deformed function at the extremity of the beam*

As a beam has two extremities, the boundary conditions provide four linear equations linking the four constants. This system is non-trivial, i.e. admits solutions other than zero, if its determinant is zero. This provides the "pulses equation". The solutions to this equation determine an infinite sequence of eigenfrequencies ω_n. Therefore, there exist an infinite number of modes $\phi_n(x)$ with which we associate just as many time functions $\psi_n(t)$ [8.76]:

$$\phi_n(x) = a_n \cos k_n x + b_n \sin k_n x + c_n \cosh k_n x + d_n \sinh k_n x$$
$$\psi_n(t) = A_n \cos \omega_n t + B_n \sin \omega_n t \quad \left(k_n{}^4 = \omega_n{}^2 \frac{\rho S}{EI} \right) \qquad [8.76]$$

The solution of the equation of free vibration is [8.77]:

$$w(x,t) = \sum_{n=1}^{\infty} \psi_n(t)\, \phi_n(x) \qquad [8.77]$$

The eigenmodes are mutually orthogonal in the sense of scalar products incorporating mass and stiffness distributions. This can be seen by projecting the equation of space variable for mode *n* onto another mode *m*, and then projecting the equation of space variable for mode *m* onto mode *n* [8.78]:

$$\int_0^L \phi_m EI \frac{d^4\phi_n}{dx^4}\, dx - \omega_n^2 \int_0^L \phi_m \rho S\, \phi_n\, dx = 0$$
$$\int_0^L \phi_n EI \frac{d^4\phi_m}{dx^4}\, dx - \omega_m^2 \int_0^L \phi_n \rho S\, \phi_m\, dx = 0 \qquad [8.78]$$

The difference of the two equations gives [8.79]:

$$\int_0^L \phi_m EI \frac{d^4\phi_n}{dx^4}\, dx - \int_0^L \phi_n EI \frac{d^4\phi_m}{dx^4}\, dx + \left(\omega_n^2 - \omega_m^2\right) \int_0^L \phi_m \rho S\, \phi_n\, dx = 0 \qquad [8.79]$$

– $EI \frac{d^4\phi_n}{dx^4} = f_y^n$ is the load that must be imposed upon the beam such that its displacement is mode n;

– $\int_0^L \phi_m EI \frac{d^4\phi_n}{dx^4}\, dx$ represents the work load n for mode m displacements;

– $\int_0^L \phi_n EI \frac{d^4\phi_m}{dx^4}\, dx$ represents the work load m for mode n displacements.

The Maxwell–Betti reciprocity theorem allows us to express that the sum of the first two terms of [8.79] is zero. Therefore, we deduce [8.80]:

$$\left(\omega_n^2 - \omega_m^2\right) \int_0^L \phi_n \rho S\, \phi_m\, dx = 0 \qquad [8.80]$$

This gives the orthogonality relationship [8.81]:

$$\text{if } n \neq m \quad \int_0^L \phi_n \rho S\, \phi_m\, dx = 0 \qquad [8.81]$$

8.3.2. *Modal base projection*

To introduce load into these equations, we must project it onto the modal base. We must be able to separate the variables in the formula for transverse load on the beam [8.82]:

$$Q(x,t) = p(t)\, q(x) \qquad [8.82]$$

We try to write the spatial distribution of this load as [8.83]:

$$q(x) = \sum q_n \phi_n(x) \qquad [8.83]$$

The coefficients of this decomposition are obtained through the projection of load onto the mode, taking into account the orthogonality of eigenmodes [8.84]:

$$\int_0^L \phi_n(x) q(x)\, dx = \int_0^L \sum_{m=1}^{\infty} q_m \phi_m(x) \phi_n(x)\, dx = \int_0^L q_n \phi_n^2(x)\, dx = 0 \qquad [8.84]$$

We deduce the value of each coefficient q_n [8.85]:

$$q_n = \frac{\int_0^L \phi_n(x)\, dx}{\int_0^L \phi_n{}^2(x)\, dx} \qquad [8.85]$$

If a point force $F(t)$ is placed at $x = \alpha$, this expression becomes [8.86]:

$$Q(x,t) = F(t)\, \delta(x-\alpha) \qquad q_n = \frac{\phi_n(\alpha)}{\int_0^L \phi_n{}^2(x)\, dx} \qquad [8.86]$$

Each modal equation is [8.87]:

$$\ddot{\psi}_n + \omega_n{}^2 \psi = \frac{q_n}{\rho S}\, p(t) \qquad [8.87]$$

As the $p(t)$ function is known, we can solve each modal equation. To do this, the pulse response can be used [8.88]:

$$\psi_{n\delta}(t) = \frac{1}{\omega_n} \sin(\omega_n t) \qquad [8.88]$$

The response to an imposed load can be expressed as the convolution product of the load with pulse response (Duhamel integral) [8.89]:

$$\psi_n(t) = \int_0^t \frac{q_n}{\rho S} \psi_{n\delta}(t-\tau)\ p(\tau)\ d\tau \qquad [8.89]$$

Then, we restore the total response by superposition [8.90]:

$$w(x,t) = \sum \psi_n(t)\ \phi_n(x) \qquad [8.90]$$

In practice, we only do the sum of a finite number of modal responses, so there is a truncation error. To choose the number of modes to take into account in order to obtain a good response estimate, we may consider the following points:

– we must not forget a mode for which the q_n coefficient is not negligible;

– the load spectrum usually has a significant amplitude within a certain range of frequencies; these are the modes for which the frequency is in the range that will be important for the response.

8.3.3. *Example of a blast against a wall*

As an example of calculation by modal superposition, we consider a vertical beam (the wall) embedded at the base and free at the top. The load can be a distributed action, for example the action of a blast (Figure 8.11). The search for eigenmodes is facilitated by writing the function of space as [8.91]:

$$\begin{aligned}\phi(x) = {} & \alpha(\cos kx + \cosh kx) + \beta(\cos kx - \cosh kx) \\ & + \gamma(\sin kx + \sinh kx) + \delta(\sin kx - \sinh kx)\end{aligned} \qquad [8.91]$$

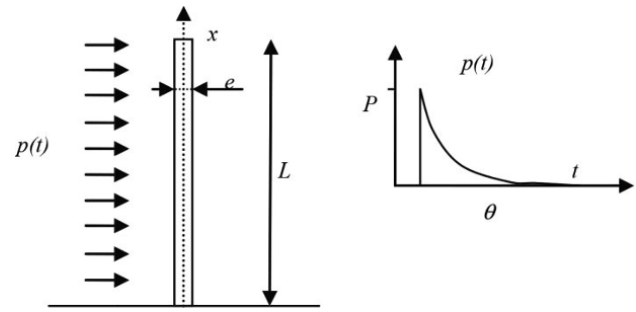

Figure 8.12. *Embedded beam receiving a transitional distributed load*

The conditions for perfect embedding at $x = 0$ and free extremity at $x = L$ can be written as [8.92]:

$$\phi(0)=0 \quad \left(\frac{d\phi}{dx}\right)_0=0 \quad \left(\frac{d^2\phi}{dx^2}\right)_L=0 \quad \left(\frac{d^3\phi}{dx^3}\right)_L=0 \qquad [8.92]$$

– the first two conditions impose: $\alpha = 0$ and $\gamma = 0$;

– the following two are expressed by the system [8.93]:

$$\begin{cases} \beta(\cos kL+\cosh kL)+\delta(\sin kL+\sinh kL)=0 \\ \beta(\cosh kL-\sin kL)+\delta(\cos kL+\cosh kL)=0 \end{cases} \qquad [8.93]$$

This system is non-trivial if the determinant is zero, i.e. if $z = \cos kL \cosh kL = -1$, which we call the "pulses equation". Solutions are found numerically. We note that for higher order modes $k_nL \approx \pi(n-1/2)$. These values are used to find the ω_n values and we can write the modes as [8.94]:

$$\begin{aligned} &\phi_n(x)=\beta_n(\cos k_nx-\cosh k_nx)+\delta_n(\sin k_nx-\sinh k_nx) \\ &\delta_n=-\beta_n\frac{\cos k_nL+\cosh k_nL}{\sin k_nL+\sinh k_nL} \end{aligned} \qquad [8.94]$$

If the load is uniformly distributed [8.95], the characteristic parameters of the first six modes are summarized in Table 8.2. The modal displacements of the first six modes are shown in Figure 8.13:

$$Q(x,t)=q(x)\,p(t) \quad q(x)=1 \quad p(t)=Pe^{-t/\theta}$$
$$q_n=\frac{\int_0^L \phi_n(x)\,dx}{\int_0^L \phi_n{}^2(x)\,dx} \qquad [8.95]$$

No.	$\xi_n=\frac{\omega_n}{\omega_1}$	k_nL	β_n	δ_n	$\int_0^L \phi_n(x)dx$	$\int_0^L \phi_n^2(x)dx$	q_n
1	1	1.8751	1	– 0.7341	– 0.8335	1.1023	– 0.7561
2	6.2667	4.6940	1	– 1.018	– 0.3879	1.0998	– 0.3590
3	17.547	7.8547	1	0.9999	– 0.1540	0.9646	– 0.1597
4	34.389	10.996	1	–1	– 0.2455	0.9842	– 0.2466
5	56.842	14.137	1	–1	– 0.09864	0.9957	– 0.0991
6	84.916	17.279	1	–1	– 0.1149	1.0037	– 0.1145

Table 8.2. *Parameters of the first six eigenmodes of a cantilever beam*

The response of the beam is calculated by superimposing the first six modal responses [8.96]:

$$w(x,t)=\sum_{n=1}^{6}\psi_n(t)\,\phi_n(x) \qquad [8.96]$$

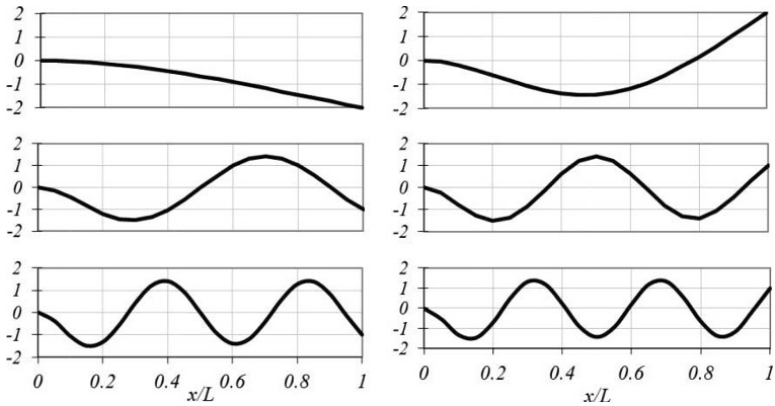

Figure 8.13. *First six eigenmodes of the cantilever beam*

A dimensionless time and relative load duration are introduced [8.97]:

$$p(t) = Pe^{-t/\theta} \quad p(\tau) = Pe^{-\tau/\lambda} \quad \tau = \omega_1 t \quad \lambda = \omega_1 \theta \tag{8.97}$$

Each modal response can be expressed [8.98]:

$$\psi_n(\tau) = \frac{P}{\rho S} \frac{q_n}{\omega_n^2 \left(1 + \left(1/\lambda\xi_n\right)^2\right)} \left(e^{-\tau/\lambda} + \left(1/\lambda\xi_n\right)\sin\xi_n\tau - \cos\xi_n\tau\right) \tag{8.98}$$

To represent a result relating to the strength of the structure, we consider the embedding time of the beam. The embedding curvature is [8.99]:

$$\frac{\partial^2 w}{\partial x^2} = \sum_{n=1}^{6} \psi_n \left(\frac{\partial \phi_n}{\partial x}\right)_0 = -2\sum_{n=1}^{6} \beta_n k_n^2 \psi_n \tag{8.99}$$

The embedding moment can be expressed dimensionlessly [8.100]:

$$\begin{aligned} M^* &= \frac{M(0,t)}{PL^2} = \frac{EI}{PL^2}\frac{\partial^2 w}{\partial x^2} \\ &= \sum_{n=1}^{6} \frac{-2\beta_n q_n}{k_n^2 L^2 \left(1 + \left(1/\lambda\xi_n\right)^2\right)} \left(e^{-\tau/\lambda} + \left(1/\lambda\xi_n\right)\sin\xi_n\tau - \cos\xi_n\tau\right) \end{aligned} \tag{8.100}$$

We describe two examples of solutions:

– in the case of Figure 8.14, the load duration is in the same order of magnitude as the first natural period. The solution is very close to the solution of single mode 1. Contribution from other modes is very small and could be neglected;

– in the case of Figure 8.15, the load duration is much shorter. The contribution of modes 2 and 3 is significant.

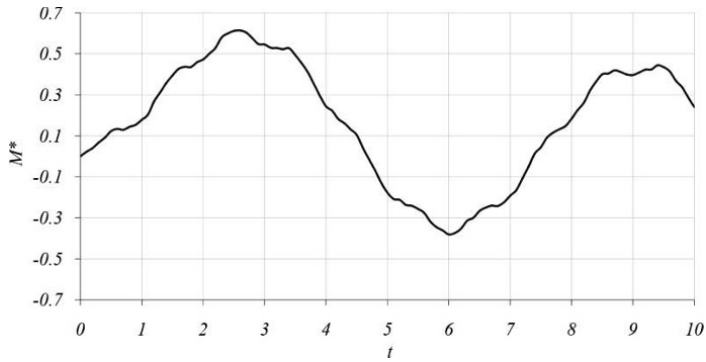

Figure 8.14. *Response to a load duration relative to* $\lambda = \pi$

To represent the response of the beam as a function of load duration, a response spectrum is used. The maximum amplitude attained by the dimensionless embedment moment M^* is shown as a function of the relative load duration w^*. The relative duration is determined with respect to the natural period of the first mode [8.101]:

$$w^* = \frac{\theta \omega_1}{\pi} \qquad [8.101]$$

This spectrum is shown in Figure 8.16 with the sum of the first six modes. The response spectra of modes 1 and 2 are also shown. For the latter, we find the typical shape of the spectrum of a system with one degree of freedom. In the range of explored load durations, it is mainly modes 1 and 2 that contribute to the response of the beam. For relatively long loads ($w^* > 1$), mode 1 provides a good estimate of the response of the beam. For shorter loads, contribution from mode 2 is

no longer negligible. It may be noted that, as the two modes are clearly separated, meaning that their eigenpulse ratio is not close to 1 (it is 6.267), the amplitude obtained by superposition is close to the sum of the maximum amplitudes for each mode.

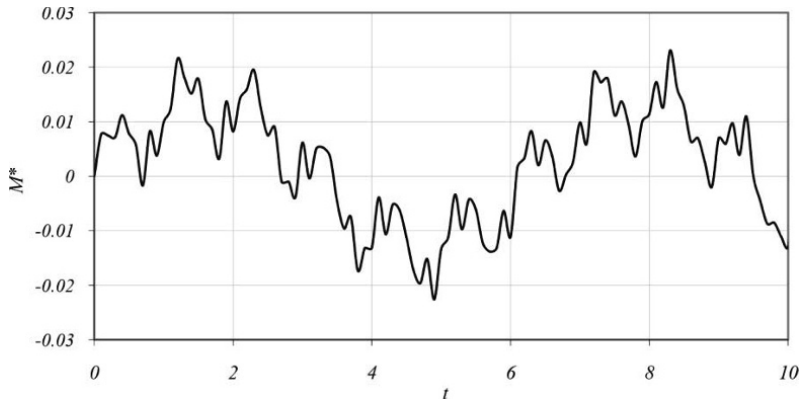

Figure 8.15. *Response to a load duration relative to* $\lambda = \pi/100$

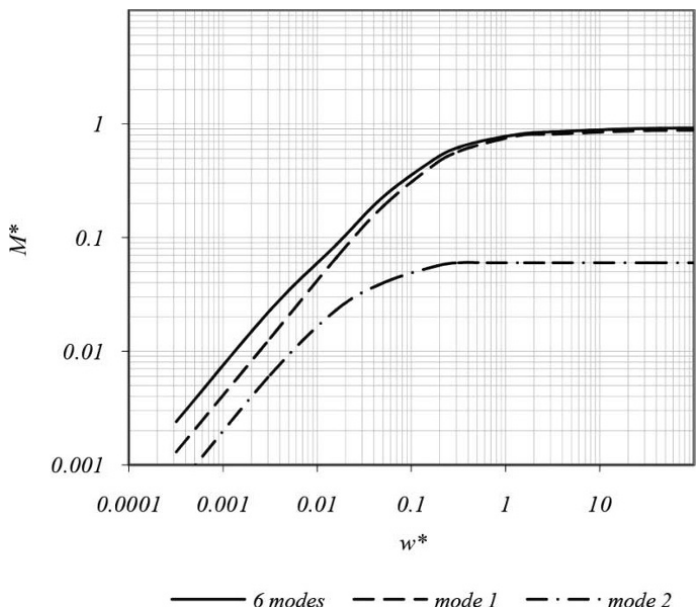

Figure 8.16. *Beam response spectra to dynamic loading*

This can also be represented in an "iso-damage" diagram, which here will be an "iso-embedding moment" diagram. The parameters used to construct the curves are made dimensionless by referring to the parameters of the first mode [8.102]:

$$P^* = \frac{PL^2}{M_{\max}} \quad I^* = \frac{P\theta L^2}{M_{\max}}\omega_1 \qquad [8.102]$$

Figure 8.17 presents two curves. For the curve of moment calculated by only using the first mode, we obtain the classic shape of a hyperbolic system with one degree of freedom. The curve of moment calculated using the six superposition modes takes on a different appearance. Indeed, in the area of impulsive loading, the curve does not tend toward a horizontal asymptote. This is due to the important role that successive modes take when the load duration weakens.

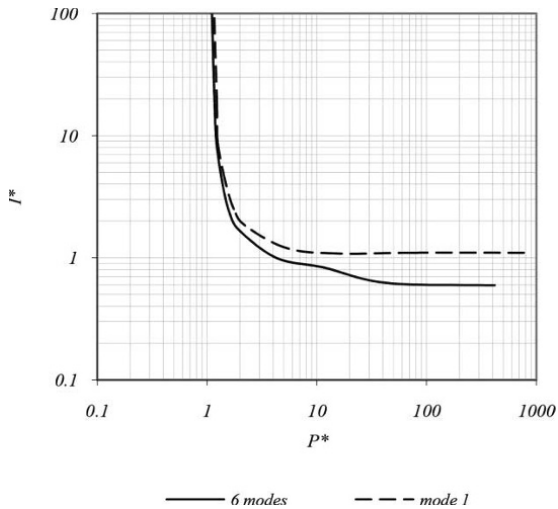

Figure 8.17. *"P-I" curves indicating the load parameters that give the same embedding moment*

To locate the position of a real case in Figure 8.16, we can take the example of a concrete wall, 3 m high and 20 cm thick. The load comes from an explosion located 7 m from the wall, releasing 1.1 MJ of

energy. The overpressure is 270 kPa, the overpressure duration is 3 ms. The natural period of the first mode is 0.1 s and the relative load duration is $w^* = 0.06$. This is a situation where inclusion of the first mode only is insufficient.

8.3.4. *Transfer function through a bending element*

When a blast wave hits a structure, the load begins as pressure, mainly reflected, on front panel or siding type walls. These walls are associated with resistant building structure and behave, more often, as beams on two supports. Therefore, we consider a beam of length L whose eigenmodes are written according to expression [8.103]:

$$\phi_n(x) = a_n \cos k_n x + b_n \sin k_n x + c_n \cosh k_n x + d_n \sinh k_n x \quad [8.103]$$

The boundary conditions are written at each end [8.104]:

$$\phi_n(0) = 0 \quad \left(\frac{\partial^2 \phi_n}{\partial x^2}\right)_0 = 0 \quad \phi_n(L) = 0 \quad \left(\frac{\partial^2 \phi_n}{\partial x^2}\right)_L = 0 \qquad [8.104]$$

These boundary conditions require that the shape of the modes be [8.105]:

$$\phi_n(x) = \sin\frac{n\pi x}{L} \qquad [8.105]$$

Each modal equation is expressed as [8.106]:

$$\ddot{\psi}_n + \omega_n^2 \psi_n = \frac{q_n}{\rho S} p(t) \qquad \left(\omega_n = \frac{n^2\pi^2}{L^2}\sqrt{\frac{EI}{\rho S}}\right) \qquad [8.106]$$

The modal load coefficient is [8.107]:

$$q_n = \frac{\int_0^L \phi_n(x)\,dx}{\int_0^L \phi_n{}^2(x)\,dx} \quad \begin{cases} q_n = \dfrac{4}{n\pi} \ (n \ odd) \\ q_n = 0 \ (n \ even) \end{cases} \qquad [8.107]$$

We consider the load as the sudden application of pressure [8108]:

$$p(t) = P\,H(t) \qquad [8.108]$$

Then, the movement of the beam is [8.109]:

$$w(x,t) = \sum_{n\ odd} \frac{4P}{n\pi\rho S}\frac{1}{\omega_n^2}\left(1-\cos\omega_n t\right)\sin\frac{n\pi x}{L} \qquad [8.109]$$

The load to be transmitted to the rest of the structure corresponds to the support reaction that is equal to the shear force at the end of the beam [8.110]:

$$V(0,t) = -EI\left(\frac{\partial^3 w}{\partial x^3}\right)_0 \qquad V(0,t) = \sum_{n\ odd}\frac{4PL}{n^2\pi^2}\left(1-\cos\omega_n t\right) \qquad [8.110]$$

Figure 8.18 shows the evolution of this shear force with variables [8.111]:

$$\tau = \omega_1 t \quad V^* = \frac{V(0,t)}{PL} \qquad [8.111]$$

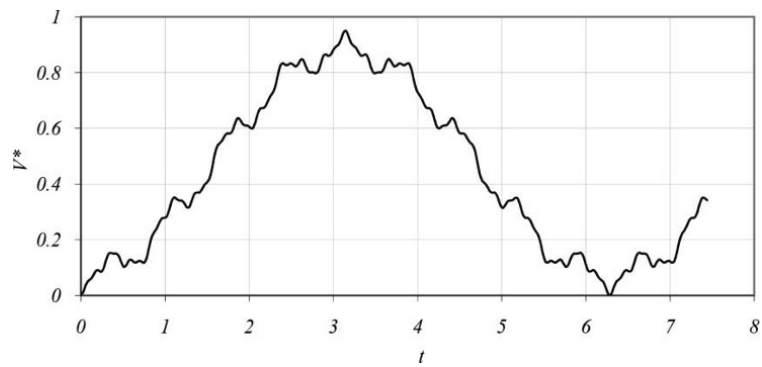

Figure 8.18. *Support reaction for a load level (Heaviside)*

In the case of a short load, we can do the calculation. As in the previous section, we introduce dimensionless time and a relative load duration [8.112]:

$$p(t) = Pe^{-t/\theta} \quad p(\tau) = Pe^{-\tau/\lambda} \quad \tau = \omega_1 t \quad \lambda = \omega_1\theta \qquad [8.112]$$

If the relative load time is not too short, the strain will be estimated with the first eigenmode. The response of this mode is [8.113]:

$$\psi_1(\tau) = \frac{P}{\rho S}\frac{q_1}{\omega_1^2\left(1+(1/\lambda)^2\right)}\left(e^{-\tau/\lambda}+(1/\lambda)\sin\tau-\cos\tau\right) \qquad [8.113]$$

Shear force at the extremity is [8.114]:

$$V^* = \frac{V(0,t)}{PL} = \frac{4}{\pi^2\left(1+(1/\lambda)^2\right)}\left(e^{-\tau/\lambda}+(1/\lambda)\sin\tau-\cos\tau\right) \quad [8.114]$$

Figure 8.19 shows the load and support reaction for two relative durations of different loads.

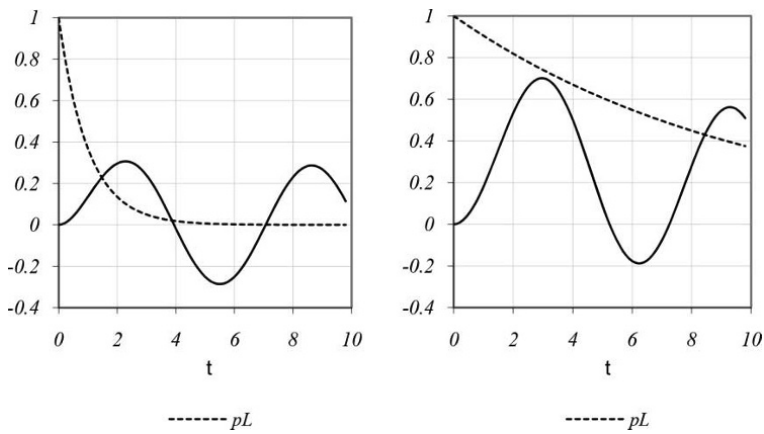

Figure 8.19. *Load on the beam (pL) and support reactions (V*) (left $\lambda = 1$, right $\lambda = 10$)*

8.4. Dynamic buckling

8.4.1. *Equation of motion for elastic buckling*

Buckling has already been discussed in Chapter 6. This was the case of very rapid loading following a solid impact. Strain in buckling mode begins at the same time as the pressure wave generated by the leading shock. Here, we consider loads that are possibly less violent in

intensity, but of longer duration θ. The purpose is to calculate the buckling behavior, knowing that inertia opposes buckling strain and allows compression to significantly exceed the critical value given by the Euler theory in quasi-staticity. To study dynamic buckling behavior, it is assumed that there is an initial deformation of the beam that the buckling phenomenon amplifies. Figure 8.20 shows a non-perfect straight beam subjected to a compressive force.

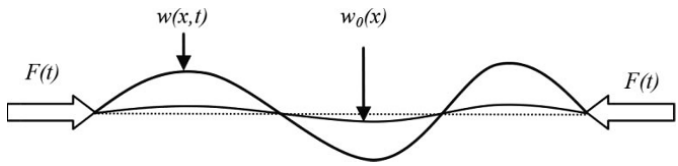

Figure 8.20. *Schematic of the buckling strain of an initially distorted beam*

The bending moment in the beam is explained in [8.115]. The total displacement of the beam is the sum of the initial displacement w_0 and displacement created by flexion w_1:

$$M\left(x\right)=-F\,w=-F\left(w_0+w_1\right) \qquad [8.115]$$

The equation of motion of the beam is shown in formula [8.116]:

$$EI\frac{\partial^4 w_1}{\partial x^4}+\rho S\frac{\partial^2 w_1}{\partial t^2}+F\left(t\right)\frac{\partial^2 w}{\partial x^2}=0 \qquad [8.116]$$

The problem is that we do not know the original displacement. We can decide to write it as a Fourier series, as the sum of sinusoidal functions respecting boundary conditions. The strain created by flexion is written in the same way [8.117]:

$$w_0=\sum a_{n0}\sin\left(\frac{n\pi x}{L}\right)\quad w_1\left(t\right)=\sum a_{n1}\left(t\right)\sin\left(\frac{n\pi x}{L}\right) \qquad [8.117]$$

Given this decomposition of functions, equation [8.116] leads to the formulation of *n*-type equations [8.118]:

$$EI\frac{n^4\pi^4}{L^4}a_{n1}\left(t\right)+\rho S\,\ddot{a}_{n1}\left(t\right)-\frac{n^2\pi^2}{L^2}F\left(t\right)a_{n1}\left(t\right)=\frac{n^2\pi^2}{L^2}F\left(t\right)a_{n0} \qquad [8.118]$$

These equations are rewritten using the amplitude amplification of each strain mode as variable [8.119]:

$$\rho S\, \ddot{a}_n(t) + \left(EI \frac{n^4\pi^4}{L^4} - \frac{n^2\pi^2}{L^2} F(t) \right)$$
$$a_n(t) = -\frac{n^2\pi^2}{L^2} F(t) \quad \left(a_n = \frac{a_{n1}}{a_{n0}} \right) \qquad [8.119]$$

In making the Euler critical force appear, we obtain formula [8.120]. Moreover, we note that if we consider a static situation, instability corresponding to an infinite value of amplification is obtained for the critical Euler force. The risk of instability exists when the a_n coefficient is positive, so for modes such as $n^2 < F/F_c$:

$$\rho S\, \ddot{a}_n + \frac{n^2\pi^2}{L^2}\left(n^2 F_c - F\right) a_n(t) = -\frac{n^2\pi^2}{L^2} F \quad \left(a_n = \frac{a_{n1}}{a_{n0}} \right) \qquad [8.120]$$

8.4.2. *Response to a pulse*

A calculation method for response to loading is to estimate the maximum amplification caused by this load. We do not know, *a priori*, the mode n that will best represent the response of the beam. Then, we calculate the amplification coefficient of modes that can be activated, and retain as most probable the one that is amplified the most with the given load. For example, for a load of slot type [8.121], we will calculate the amplification for all modes such that $n^2 < F/F_c$:

$$F(t) = F\left(H(t) - H(t-\theta)\right) \qquad \theta >> \frac{L}{C_0} \qquad [8.121]$$

For this load, we can do the calculation. Equation [8.120] becomes [8.122]:

$$0 < t < \theta \quad \rho S\, \ddot{a}_n - \frac{n^2\pi^2}{L^2}\left(F - n^2 F_c\right) a_n = -\frac{n^2\pi^2}{L^2} F$$
$$t > \theta \qquad \rho S\, \ddot{a}_n + \frac{n^4\pi^2}{L^2} F_c\, a_n = 0 \qquad [8.122]$$

Resolution gives solution [8.123] during the application of force and [8.124] after the end of loading:

$$a_n(t) = \frac{F}{F - n^2 F_c}\left(-1 + \cosh\left(\frac{n\pi t}{L}\sqrt{\frac{F - n^2 F_c}{\mu}}\right)\right) \qquad [8.123]$$

$$a_n(t) = \frac{F}{F - n^2 F_c}\left(\begin{array}{l}\left(-1 + \cosh\left(\frac{n\pi\theta}{L}\sqrt{\frac{F - n^2 F_c}{\mu}}\right)\right)\cos\left(\frac{n\pi(t-\theta)}{L}\sqrt{\frac{F_c}{\mu}}\right) + \\ \left(\sqrt{\frac{F - n^2 F_c}{F_c}}\sinh\left(\frac{n\pi\theta}{L}\sqrt{\frac{F - n^2 F_c}{\mu}}\right)\right)\sin\left(\frac{n\pi(t-\theta)}{L}\sqrt{\frac{F_c}{\mu}}\right)\end{array}\right) \qquad [8.124]$$

The maximum amplification is obtained during the second phase and its value is given by expression [8.125]:

$$a_n^{\max} = \frac{F}{F - n^2 F_c}\sqrt{\begin{array}{l}\left(-1 + \cosh\left(\frac{n\pi\theta}{L}\sqrt{\frac{F - n^2 F_c}{\mu}}\right)\right)^2 + \\ \frac{F - n^2 F_c}{F_c}\left(\sinh\left(\frac{n\pi\theta}{L}\sqrt{\frac{F - n^2 F_c}{\mu}}\right)\right)^2\end{array}} \qquad [8.125]$$

It is possible to formulate this result with dimensionless parameters [8.126]. We obtain expression [8.127]:

$$f^* = \frac{F}{F_c} \quad w^* = \frac{\omega\theta}{\pi} \qquad \left(\omega = \frac{\pi^2}{L}\sqrt{\frac{F_c}{\mu}} = \frac{\pi^3}{L^2}C_0\sqrt{\frac{I}{S}}\right) \qquad [8.126]$$

$$a_n^{\max} = \frac{f^*}{f^* - n^2}\sqrt{\begin{array}{l}\left(-1 + \cosh\left(nw^*\sqrt{f^* - n^2}\right)\right)^2 \\ +\left(f^* - n^2\right)\left(\sinh\left(nw^*\sqrt{f^* - n^2}\right)\right)^2\end{array}} \qquad [8.127]$$

The assumption on the duration of loading is expressed as a reduced duration [8.128]:

$$\theta >> \frac{L}{C_0} \quad \rightarrow \quad w^* > \frac{\pi^2}{L}\sqrt{\frac{I}{S}} \qquad [8.128]$$

The acceptable limit for a beam can be formulated by a maximum permissible value for a specific amplification coefficient in the considered work [LIN 83] (this parameter is based on expert knowledge that may rely on feedback and test results). For example, to present the method, we arbitrarily take an amplification coefficient of 1,000 as the limit. We can then find the characteristics, intensity and duration that can lead to this value. The higher the force, the greater the number of modes to be considered. Figure 8.21 combines the results for six different loads. For each load, calculation of amplification modes such as $n^2 < f^*$ was done. Note that for higher forces, the most amplified mode is also of a high order. This is consistent with experimental observations. Therefore, we retained the most amplified mode as probable.

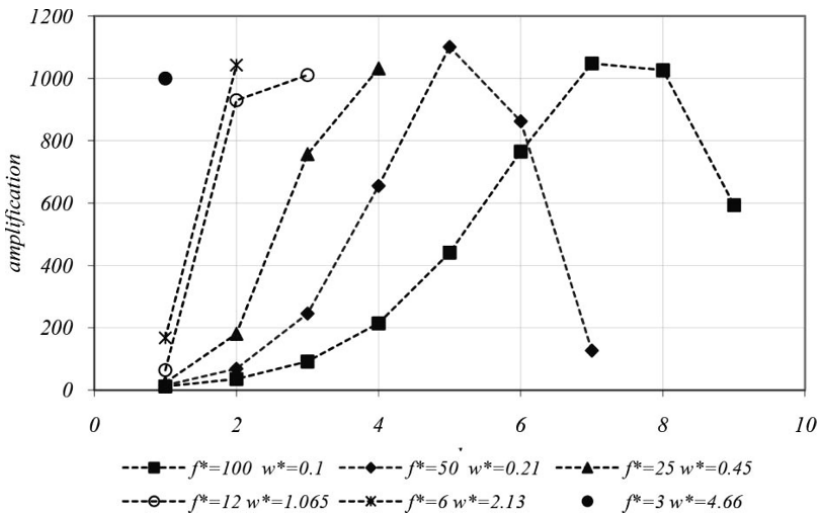

Figure 8.21. *Amplification relative to buckling modes for different loads*

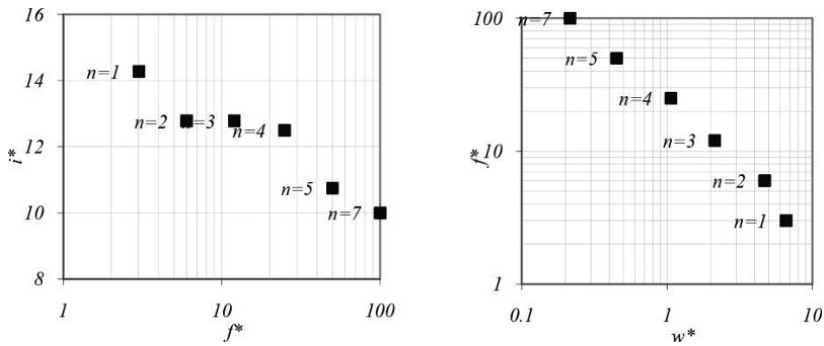

Figure 8.22. *Representations of "iso-damage" points in a diagram of force duration and momentum (dimensionless parameters)*

We logically note that the higher the intensity of a load, the more brief the application duration must be, for a fixed amplification limit. Figure 8.22 shows the "iso-damage" points in a diagram of force duration and momentum, with dimensionless parameters. There is no simple curve as we have seen for simple linear systems, since here each point is relative to a different mode. We may consider that the set of points form a curve that delimits two areas. There is an area under the curve where the coordinates of points are parameters that do not lead to the fixed criterion (here, arbitrarily). There is another area above the curve where the coordinates of points are parameters that lead to exceedence of the fixed criterion.

Chapter 9

Responses of Multiple Degree of Freedom Structures

A building structure can be modeled by a number of mechanical systems with multiple degrees of freedom. An analytical solution for equations of motion is possible by using the modal superposition method. The movement of a structure may be coupled to the movement of fluids, which is the case for reservoirs.

9.1. Modeling through a discrete system

9.1.1. *Equations of motion*

A structure can be modeled by a set of masses concentrated at points connected by deformable elements. This type of modeling is widely used to study the movement of structures such as multi-story buildings. Methods for calculating the response of these structures to dynamic loads, including earthquakes, have been widely developed [GOU 80, BAT 87, SCH 91, PAU 05, RAK 09]. To describe the motion of a structure to multiple degrees of freedom, consisting of n number of nodes identified by their number i, we define the following parameters:

– m_i: mass concentrated at node i;

– x_i: displacement of node i in a given direction (scalar);

– F_i: component of force applied at node i (scalar);

– $\underline{X}$: set of displacements (vector);

– $\underline{F}$: set of forces (vector).

An example of such a structure is shown in Figure 9.1. The search for equations begins by studying the static structure. A structure shows linear behavior if there is a linear mapping between the forces and displacements. This results in a linear system of equations [9.1]:

$$\underline{X} = \underline{\underline{A}}\,\underline{F}\left(x_i = a_{ij}F_j\right) \qquad \underline{F} = \underline{\underline{K}}\,\underline{X}\left(F_i = k_{ij}x_j\right)\underline{\underline{K}} = \underline{\underline{A}}^{-1} \qquad [9.1]$$

The terms in matrix A, a flexibility matrix, can be calculated using a method based on the curvilinear media theory if the structure is made up of beams. By choosing different unitary loads, we can calculate displacements of all nodes corresponding to elements of the flexibility matrix (a_{ij} is also called the influence coefficient; it is the displacement of node i for a unitary force placed at node j). The stiffness matrix is the inverse of the flexibility matrix. The Maxwell–Betti reciprocity theorem allows us to say that $a_{ij} = a_{ji}$, and the matrix is symmetrical.

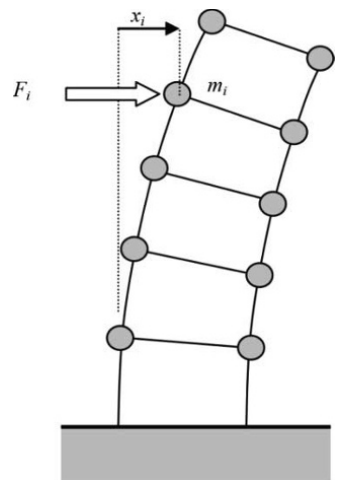

Figure 9.1. *Model of a multiple degree of freedom structure. Identification of masses, forces and displacements*

If vibration is studied, forces are the forces of inertia and external forces [9.2]. The mass matrix appears as:

$$F_i = -m_i \ddot{x}_i \quad + F_i^e \qquad \underline{F} = -\underline{\underline{M}}\,\underline{\ddot{X}} + \underline{F}^e \qquad [9.2]$$

When writing linear behavior, we obtain the system of equations governing movement of the structure [9.3]:

$$m_{ij} \ddot{x}_j + k_{ij} x_j = F_i^e \qquad \underline{\underline{M}}\,\underline{\ddot{X}} + \underline{\underline{K}}\,\underline{X} = \underline{F}^e \qquad [9.3]$$

We may notice that the kinetic energy and the elastic strain energy of the system can be written as [9.4]:

$$E_c = \frac{1}{2} \underline{\dot{X}}^t \underline{\underline{M}}\,\underline{\dot{X}} = \frac{1}{2} \dot{x}_i m_{ij} \dot{x}_j \quad E_e = \frac{1}{2} \underline{X}^t \underline{\underline{K}}\,\underline{X} = \frac{1}{2} x_i k_{ij} x_j \qquad [9.4]$$

9.1.2. *Search for eigenmodes*

Vibration eigenmodes are sought by considering the free movement of a structure without loading. To do this, displacement is written as [9.5]:

$$\underline{X} = \psi(t)\,\underline{\phi} \qquad [9.5]$$

$\underline{\phi}$ is a modal vector representing eigendisplacement. The equations of motion take the form [9.6]:

$$\ddot{\psi}\, m_{ij} \phi_j + \psi\, k_{ij} \phi_j = 0 \qquad \ddot{\psi}\, \underline{\underline{M}}\,\underline{\phi} + \psi\, \underline{\underline{K}}\,\underline{\phi} = \underline{0} \qquad [9.6]$$

By multiplying the left by the modal vector, we obtain a scalar equation [9.7]:

$$\left(\phi_i m_{ij} \phi_j\right) \ddot{\psi} + \left(\phi_i k_{ij} \phi_j\right) \psi = 0 \qquad \left(\underline{\phi}^t \underline{\underline{M}}\,\underline{\phi}\right) \ddot{\psi} + \left(\underline{\phi}^t \underline{\underline{K}}\,\underline{\phi}\right) \psi = 0 \; [9.7]$$

The coefficients of this equation are quadratic. The separation of variables leads to the relationship [9.8]:

$$\omega^2 = -\frac{\ddot{\psi}}{\psi} = \frac{\underline{\phi}^t \underline{\underline{K}} \underline{\phi}}{\underline{\phi}^t \underline{\underline{M}} \underline{\phi}} = \frac{\phi_i k_{ij} \phi_j}{\phi_i m_{ij} \phi_j} \quad [9.8]$$

The modal vector is defined by [9.9]:

$$\left(\underline{\underline{K}} - \omega^2 \underline{\underline{M}} \right) \underline{\phi} = 0 \quad [9.9]$$

This system is non-trivial if the matrix is singular [9.10]:

$$\det \left(\underline{\underline{K}} - \omega^2 \underline{\underline{M}} \right) = 0 . \quad [9.10]$$

This equation, called "pulses equation", is of n degree in ω^2; the solutions are called eigenfrequencies. A discrete system has as many eigenfrequencies as degrees of freedom. For each eigenfrequency ω_i, we calculate the eigenmode $\underline{\phi}^i$. All eigenvectors form the modal matrix [9.11]:

$$\underline{\underline{\Phi}} = \left(\underline{\phi}^1 .... \underline{\phi}^n \right) \quad \Phi_{ij} = \phi_j^i \quad [9.11]$$

The solution of the initial system can be written as [9.12]:

$$\underline{X} = \psi_i \, \underline{\phi}^i = \sum_{i=1}^{n} \alpha_i \cos\left(\omega_i t + \theta_i \right) \underline{\phi}^i \quad [9.12]$$

Eigenmodes are mutually orthogonal with respect to the mass matrix and the stiffness matrix, which results in relationships [9.13]:

$$\begin{cases} \underline{D}_i^t \underline{\underline{M}} \underline{D}_j = 0 \quad si \quad i \neq j \\ \underline{D}_i^t \underline{\underline{K}} \underline{D}_j = 0 \quad si \quad i \neq j \end{cases} \quad [9.13]$$

Indeed, if $\underline{\phi}^i$ and $\underline{\phi}^j$ are two modes, they are solutions of [9.14]:

$$\begin{cases} \underline{\underline{K}} \, \underline{\phi}^i - \omega_i^2 \underline{\underline{M}} \, \underline{\phi}^i = \underline{0} \\ \underline{\underline{K}} \, \underline{\phi}^j - \omega_j^2 \underline{\underline{M}} \, \underline{\phi}^j = \underline{0} \end{cases} \text{or} \begin{cases} \underline{\phi}^j \underline{\underline{K}} \, \underline{\phi}^i - \omega_i^2 \underline{\phi}^j \underline{\underline{M}} \, \underline{\phi}^i = 0 \\ \underline{\phi}^i \underline{\underline{K}} \, \underline{\phi}^j - \omega_j^2 \underline{\phi}^i \underline{\underline{M}} \, \underline{\phi}^j = 0 \end{cases} \quad [9.14]$$

If the mass and stiffness matrices are symmetrical, the difference of the two equations leads to [9.15]:

$$\left(\omega_i^2 - \omega_j^2\right) {}^t\underline{\phi}^i \underline{\underline{M}}\, \underline{\phi}^j = 0 \qquad [9.15]$$

We see that if $i \neq j$, we show [9.16]:

$$\omega_i \neq \omega_j \qquad {}^t\underline{\phi}^i \underline{\underline{M}}\, \underline{\phi}^j = 0 \text{ and } {}^t\underline{\phi}^i \underline{\underline{K}}\, \underline{\phi}^j = 0 \qquad [9.16]$$

It may be interesting to write the equations in the eigenbase. Modal masses and modal stiffnesses [9.17] can be calculated. We can "normalize" the modal vectors such that the modal masses are equal to the unit:

$${}^t\underline{\phi}^i \underline{\underline{M}}\, \underline{\phi}^i = \tilde{m}_i \text{ and } {}^t\underline{\phi}^i \underline{\underline{K}}\, \underline{\phi}^i = \tilde{k}_i \qquad [9.17]$$

Alternatively, using the modal matrix, we define the modal mass and stiffness matrices which are diagonal matrices [9.18]:

$$\underline{\underline{\Phi}}^t \underline{\underline{M}}\, \underline{\underline{\Phi}} = \underline{\underline{\tilde{M}}} \text{ and } \underline{\underline{\Phi}}^t \underline{\underline{K}}\, \underline{\underline{\Phi}} = \underline{\underline{\tilde{K}}} \qquad [9.18]$$

In the modal base, the system of equations becomes [9.19], which is a system of n independent or decoupled equations:

$$\underline{\underline{\tilde{M}}}\, \underline{\ddot{\tilde{X}}} + \underline{\underline{\tilde{K}}}\, \underline{\tilde{X}} = 0 \qquad [9.19]$$

9.2. Resolution by modal superposition

9.2.1. *Projection on a modal base*

We will now consider a dynamic load imposed on the structure, represented by the forces applied to the nodes of the structure. If the actual load does not appear in this form, for example as pressure on a wall, it will need to be modeled. The system of equations then contains a second member [9.20]:

$$m_{ij}\ddot{x}_j + k_{ij}x_j = F_i^e \qquad \underline{\underline{M}}\, \underline{\ddot{X}} + \underline{\underline{K}}\, \underline{X} = \underline{F}^e \qquad [9.20]$$

Solutions are sought using modal vectors [9.21]:

$$x_i = \psi_k \phi_i^k \qquad \underline{X} = \psi_k \, \underline{\phi}^k \tag{9.21}$$

This leads to system [9.22]:

$$m_{ij} \, \phi_k^j \ddot{\psi}_k + k_{ij} \phi_k^j \psi_k = F_i^e \qquad \underline{\underline{M}} \, \underline{\underline{\Phi}} \, \underline{\ddot{\psi}} + \underline{\underline{K}} \, \underline{\underline{\Phi}} \, \underline{\psi} = \underline{F}^e \tag{9.22}$$

By multiplying the left by the modal matrix, we obtain [9.23]:

$$\phi_i^l m_{ij} \, \phi_k^j \ddot{\psi}_k + \phi_i^l k_{ij} \phi_k^j \psi_k = \phi_i^l F_i^e \qquad {}^t\underline{\underline{\Phi}} \, \underline{\underline{M}} \, \underline{\underline{\Phi}} \, \underline{\ddot{\psi}} + {}^t\underline{\underline{\Phi}} \, \underline{\underline{K}} \, \underline{\underline{\Phi}} \, \underline{\psi} = {}^t\underline{\underline{\Phi}} \, \underline{F}^e \tag{9.23}$$

As seen in the previous section, eigenmodes are orthogonal to mass and stiffness matrices. The system is then composed of *n* independent equations [9.24]:

$$\phi_i^k m_{ij} \, \phi_j^k \ddot{\psi}_k + \phi_i^k k_{ij} \phi_j^k \psi_k = \phi_i^k F_i^e \qquad {}^t\underline{\phi}^k \, \underline{\underline{M}} \underline{\phi}^k \, \underline{\ddot{\psi}} + {}^t\underline{\phi}^k \, \underline{\underline{K}} \, \underline{\phi}^k \, \underline{\psi} = {}^t\underline{\phi}^k \, \underline{F}^e \tag{9.24}$$

In each equation, the eigenfrequency of the considered mode appears and the second member is the projection of load onto the mode [9.22]:

$$\omega_k^2 = \frac{\phi_i^k k_{ij} \phi_j^k}{\phi_i^k m_{ij} \phi_j^k} = \frac{{}^t\underline{\phi}^k \, \underline{\underline{K}} \, \underline{\phi}^k}{{}^t\underline{\phi}^k \, \underline{\underline{M}} \, \underline{\phi}^k} \qquad Q_k^e = \frac{\phi_i^k F_i^e}{\phi_i^k m_{ij} \phi_j^k} = \frac{{}^t\underline{\phi}^k \, \underline{F}^e}{{}^t\underline{\phi}^k \, \underline{\underline{M}} \, \underline{\phi}^k} \tag{9.25}$$

Each modal equation is, therefore simply formulated as [9.26]:

$$\ddot{\psi}_k + \omega_k^2 \psi_k = Q_k^e \tag{9.26}$$

The solution can be written as [9.27]:

$$\psi_k(t) = \frac{1}{\omega_k} \int_0^t Q_k^e(\tau) \sin \omega_k (t - \tau) \, d\tau \tag{9.27}$$

The complete response is obtained by superimposing the modal responses [9.21]. In some cases, if careful, we can use the load response spectrum. If the load can be expressed at any point by the

same time function [9.28] (this can be the case for a blast wave load), each modal load component uses this function [9.29]:

$$\underline{F}^e = \underline{q}\, f(t) \quad F_i^e = q_i\, f(t) \qquad [9.28]$$

$$Q_k^e = \frac{\phi_i^k q_i}{\phi_i^k m_{ij} \phi_j^k} f(t) = \frac{{}^t\underline{\phi}^k\, \underline{q}}{{}^t\underline{\phi}^k\, \underline{\underline{M}}\, \underline{\phi}^k} f(t) = q_k f(t) \qquad [9.29]$$

If the load has a characteristic application time of θ and we know the response spectrum to this load f, $x^*(w^*)$, we can use it to estimate the amplitude of each modal response [9.30]:

$$\psi_k^{\max} = \frac{2q_k}{\tilde{k}_k} x^*\left(\frac{\omega_k \theta}{\pi}\right) \qquad [9.30]$$

It is then possible to estimate an upper bound on the response by superimposing the maximums of modal responses.

9.2.2. *Example*

To illustrate the method, we consider the two-story building from Chapter 7 (see Figure 9.2) and calculate its response to loading from the planned explosion. The supporting structure of the building consists of cross-beams made up of metal columns embedded in a concrete slab. The repetitive nature of the cross-beam structure, every 5 m, allows us to address this problem as the study of the motion of a cross-beam in its plane. The latter is then modeled by a structure with two degrees of freedom. The reinforced concrete floors are considered to be solid and rigid elements. Steel columns (HEA steel profile) are the flexible elements and their own mass is negligible compared to the floors. The degrees of freedom are the horizontal displacements of the floors. Static structure calculations have clarified the stiffnesses to be considered. The load will be modeled by point forces applied at the floor level. Figure 9.3 shows the model structure and its characteristics.

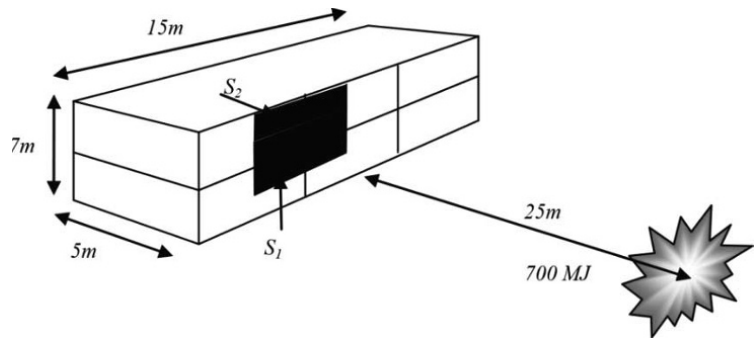

Figure 9.2. *A building face receives the effects of an explosion*

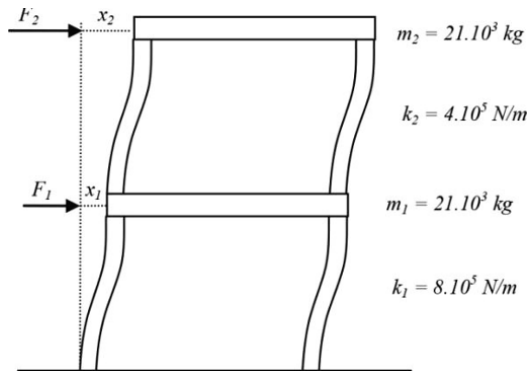

Figure 9.3. *A building structure modeled by a system with two degrees of freedom*

When applied successively to both constituted masses of floors, the fundamental principle of dynamics provides equations [9.31]:

$$\begin{aligned} m_1\ddot{x}_1 + k_1x_1 - k_2\left(x_2 - x_1\right) &= F_1 \\ m_2\ddot{x}_1 + k_2\left(x_2 - x_1\right) &= F_2 \end{aligned} \qquad [9.31]$$

These equations can be put into matrix form by introducing a mass matrix and a stiffness matrix [9.32]:

$$\begin{pmatrix} m_1 & 0 \\ 0 & m_2 \end{pmatrix}\begin{pmatrix} \ddot{x}_1 \\ \ddot{x}_2 \end{pmatrix} + \begin{pmatrix} k_1 + k_2 & -k_2 \\ -k_2 & k_2 \end{pmatrix}\begin{pmatrix} x_1 \\ x_2 \end{pmatrix} = \begin{pmatrix} F_1 \\ F_2 \end{pmatrix} \qquad [9.32]$$

The system is simplified by considering $m_1 = m_2, = m$, $k_1 = 2k$ and $k_2 = k$ [9.33]:

$$\begin{pmatrix} m & 0 \\ 0 & m \end{pmatrix}\begin{pmatrix} \ddot{x}_1 \\ \ddot{x}_2 \end{pmatrix}+\begin{pmatrix} 3k & -k \\ -k & k \end{pmatrix}\begin{pmatrix} x_1 \\ x_2 \end{pmatrix}=\begin{pmatrix} F_1 \\ F_2 \end{pmatrix} \quad [9.33]$$

The eigenfrequencies are solutions of equation [9.34]:

$$\det\left(\underline{\underline{K}}-\omega^2\underline{\underline{M}}\right)=\begin{vmatrix} 3k-\omega^2 m & -k \\ -k & k-\omega^2 m \end{vmatrix}= m^2\omega^4-4km\omega^2+2k^2 \quad [9.34]$$

Eigenfrequencies and eigenperiods have the values [9.35]:

$$\underline{\underline{M}}\,\underline{\ddot{X}}+\underline{\underline{K}}\,\underline{X}=\underline{0} \quad [9.35]$$

The eigenvectors are the solutions to systems [9.36]:

$$\underline{\underline{M}}\,\underline{\ddot{X}}+\underline{\underline{K}}\,\underline{X}=\underline{0}$$

$$\left(\underline{\underline{K}}-\omega_2^2\underline{\underline{M}}\right)\underline{\phi}^2=\begin{pmatrix} 3k-\omega_2^2 m & -k \\ -k & k-\omega_2^2 m \end{pmatrix}\begin{pmatrix} \phi_1^2 \\ \phi_2^2 \end{pmatrix}=\begin{pmatrix} 0 \\ 0 \end{pmatrix} \quad \Rightarrow \quad 0.41\phi_1^2+\phi_2^2=0 \quad [9.36]$$

We choose [9.37] as eigenvectors:

$$\underline{\phi}^1=\begin{pmatrix} 1 \\ 2.41 \end{pmatrix} \quad \underline{\phi}^2=\begin{pmatrix} 1 \\ -0.41 \end{pmatrix} \quad [9.37]$$

The modal forms associated with these eigenvectors and eigenfrequencies are shown in Figure 9.4.

The solution of the equations of motion can be deduced from the solutions of the system of independent modal equations [9.38]:

$$\begin{pmatrix} x_1 \\ x_2 \end{pmatrix}=\psi_1\,\underline{\phi}^1+\psi_2\,\underline{\phi}^2 \quad \begin{cases} \ddot{\psi}_1+\omega_1^2\psi_1=\dfrac{F_1+2.41F_2}{6.8\,m} \\ \ddot{\psi}_2+\omega_2^2\psi_2=\dfrac{F_1-0.41F_2}{1.2\,m} \end{cases} \quad [9.38]$$

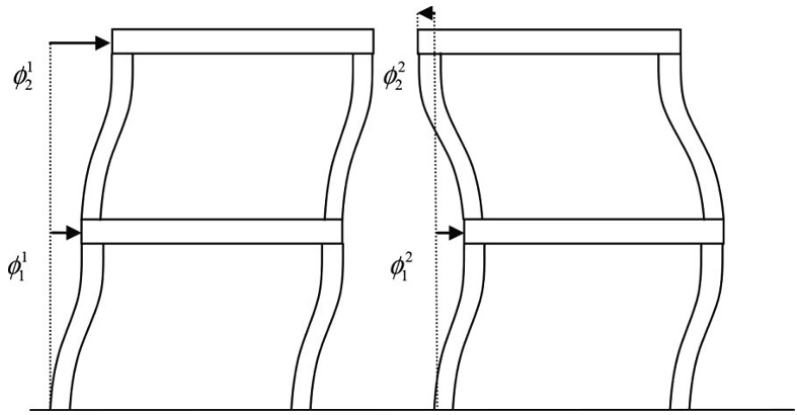

Figure 9.4. *Visualization of two eigenmodes of deformation of a structure modeled by a system with two degrees of freedom*

The force on a node is the integral of pressures applied to a part of the face that is based on that node (Figure 9.2). The two forces can be formulated according to expressions [9.39], *p(t)* being the pressure exerted on the face at the reflection of the shock wave:

$$\begin{aligned} F_1 &= S_1 \quad p(t) = 5 \times 3.5 \times p(t) \\ F_2 &= S_2 \quad p(t) = 5 \times 1.75 \times p(t) \end{aligned} \qquad [9.39]$$

The characteristics of the reflected pressure are given in [9.40]:

$$\overline{R} = 1.3 \;\; \Delta p_r^+ = 55 \;\; kPa \;\; t^+ = 13 \;\; \times 10^{-3} s \;\; i_r^+ = 310 \;\; Pa.s \qquad [9.40]$$

Load duration (t^+) is very short compared to the eigenperiods of the structure [9.35]. We can estimate each modal response as a response to a pulse [9.41]:

$$\begin{cases} \ddot{\psi}_1 + \omega_1^2 \psi_1 = \dfrac{5.67}{m} p(t) \\ \ddot{\psi}_2 + \omega_2^2 \psi_2 = \dfrac{11.6}{m} p(t) \end{cases} \qquad \begin{cases} \psi_1 = \dfrac{5.67 \; i_r^+}{m \omega_1} \sin \omega_1(t) \\ \psi_2 = \dfrac{11.6 \; i_r^+}{m \omega_2} \sin \omega_2(t) \end{cases} \qquad [9.41]$$

We then obtain the complete expression of the response [9.42]:

$$x_1(t) = \frac{i_r^+}{m}\left(\frac{5.67}{\omega_1}\sin\omega_1(t) + \frac{11.6}{\omega_2}\sin\omega_2(t)\right)$$
$$x_2(t) = \frac{i_r^+}{m}\left(\frac{2.41\times 5.67}{\omega_1}\sin\omega_1(t) - \frac{0.41\times 11.6}{\omega_2}\sin\omega_2(t)\right) \qquad [9.42]$$

An upper bound of the displacements amplitude can be estimated from the maximums of modal responses [9.43]:

$$\begin{cases} x_1^{\max} \le \psi_1^{\max} + \psi_2^{\max} & x_1^{\max} \le 0.046\ m \\ x_2^{\max} \le 2.41\psi_1^{\max} + 0.41\psi_2^{\max} & x_2^{\max} \le 0.069\ m \end{cases} \qquad [9.43]$$

9.3. Fluid–structure coupling

9.3.1. *Small movements of fluids*

There exist various situations of coupling between the movement of a fluid and that of a solid. Each coupling contains a relevant model [DEL 01, AXI 01c]. Small movements of a fluid, in the absence of flow, can be coupled with the movement of a solid or structures if there are one or several surfaces of contact between the fluid and the solid. There are two areas where this coupling comes into play: high frequency (>100 Hz), where fluid movements are of the acoustic type and related to fluid compressibility, and low frequency (<10 Hz), where fluid movements are convective in nature, usually with a free surface. The second case is especially important to consider if one is interested in the overall response of a structure. The first case is used to consider a shock on the wall of a reservoir (plate or shell) in order to study the local response of this element (which is beyond the scope of this book). Therefore, we are interested in fluid movements in the absence of flow, that is to say movements around an equilibrium position that corresponds to a resting fluid state. The velocity field is, *a priori*, written in an Eulerian manner based on the current coordinates. For small movements, one can confuse the latter with the initial positions as in a Lagrangian description [9.44]:

$$\underline{V}(\underline{x},t) \approx \underline{V}(\underline{X},t) \qquad [9.44]$$

To write the equations of fluid motion simply, we show that pressure p_t (total) is the sum of hydrostatic pressure p_0 at rest and fluctuating pressure p [9.45]:

$$p_t = p_0 + p \qquad [9.45]$$

The equations governing small fluid movements are derived from the writing of conservation of mass in an incompressible fluid and conservation of momentum [9.46]:

$$\begin{aligned} &div\underline{V} = 0 \\ &\rho_F \frac{\partial \underline{V}}{\partial t} = -\rho_F g\, \underline{e}_z - \underline{grad}\, p_t \end{aligned} \qquad [9.46]$$

These equations are simplified because they are only functions of fluctuating pressure [9.47]:

$$\begin{aligned} &div\, \underline{V} = 0 \\ &\rho_F \frac{\partial \underline{V}}{\partial t} = -\underline{grad}\, p \end{aligned} \qquad [9.47]$$

We seek velocity and pressure fields from modal forms [9.48]:

$$\begin{aligned} &\underline{V}(\underline{X},t) = \dot{\psi}(t)\, \underline{grad}\, \Phi(\underline{X}) \\ &p(\underline{X},t) = -\rho_F\, \ddot{\psi}(t)\, \Phi(\underline{X}) \end{aligned} \qquad [9.48]$$

For the fluid, the problem comes back to seeking function Φ such that [9.49]:

$$\Delta\Phi = 0 \qquad [9.49]$$

From these equations, we can consider two types of practical problems. First, the case of partially or totally submerged structures: pile bridge, pillar supporting a quay or a platform, etc. In this case, it is the concept of added mass that will take the presence of fluid into account. Second, there is the case of structures supporting, or containing, a reservoir. In this case, it is the convective motions of the

fluid, the sloshing modes, which will be coupled to the movement of the structure.

9.3.2. *Concept of added mass*

If a structure is immersed in a fluid, expression of fluid and solid coupling movement originates from the conditions imposed on the communal surface, called interface, of the two elements (Figure 9.5).

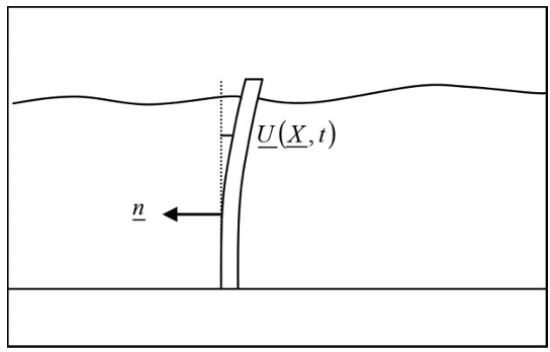

Figure 9.5. *Movement of a solid submerged in a fluid*

At a solid–fluid interface, there is equality of normal velocities and forces [9.50]:

$$\underline{V}.\underline{n} = \frac{\partial \underline{U}}{\partial t}.\underline{n}$$
$$-p\underline{n} = \underline{T} \qquad [9.50]$$

If a modal approach is adopted for the structure, motion of the solid is described using a single time-dependent parameter [9.51]:

$$\underline{U}(\underline{X},t) = \psi(t)\,\underline{\phi}(\underline{X}) \qquad [9.51]$$

The velocity condition at the interface is then reflected as [9.52]:

$$\underline{V}.\underline{n} = \dot{\psi}\,\underline{\phi}.\underline{n} \qquad [9.52]$$

or by using the potential function for fluid [9.53]:

$$\underline{grad}\,\Phi.\underline{n} = \underline{\phi}.\underline{n} \qquad [9.53]$$

The force condition becomes [9.54]:

$$\rho_F\,\ddot{\psi}\,\Phi\,\underline{n} = \underline{T} \qquad [9.54]$$

Projection onto the mode of force exerted by the fluid onto the solid gives expression [9.55]:

$$F_{FS} = \int_s -p\,\underline{n}.\underline{\phi}\,ds = \rho_F\,\ddot{\psi}\int_s \Phi\,\underline{n}.\underline{\phi}\,ds \qquad [9.55]$$

This force is proportional to acceleration. The proportional coefficient can, therefore, be interpreted as a mass, called the added mass [9.56]:

$$M_a = \rho_F \int_s \Phi\,\underline{n}.\underline{\phi}\,ds \qquad [9.56]$$

Movement of the structure that was governed, outside of the fluid, by equation [9.57]:

$$M_e\,\ddot{\psi} + K_e\,\psi = 0 \quad \omega_e = \sqrt{\frac{K_e}{M_e}} \qquad [9.57]$$

becomes [9.58] if the solid is submerged in a fluid:

$$(M_e + M_a)\ddot{\psi} + K_e\,\psi = 0 \qquad [9.58]$$

The effect of this added mass reduces the eigenfrequency of the structure [9.59]:

$$\omega = \frac{\omega_e}{\sqrt{1+\dfrac{M_a}{M_e}}} \qquad [9.59]$$

The presence of fluid also adds a damping on the movement of the structure. This is usually not taken into account during the search for responses to loads of short duration. A simple example is the bending of a beam in a fluid. If the fluid volume is large compared to the volume of the submerged structure, the added mass can be only determined from the shape of the beam. The simplest case is that of the beam with a circular cross section of radius R. Its movement in a fluid is obtained by considering a linear added mass of $\rho_F \pi R^2$.

9.3.3. *Sloshing mode*

Sloshing is a form of fluid oscillation associated with convective movements of a fluid mass contained in a reservoir and with a free surface (Figure 9.6) [DEA 91].

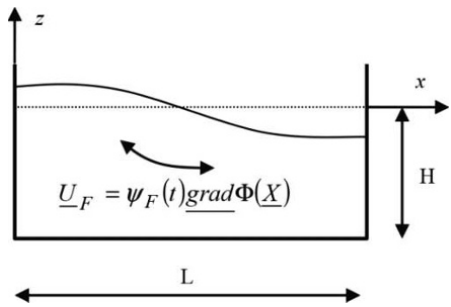

Figure 9.6. *Sloshing mode of fluid in a reservoir*

Description of motion is sought modally [9.60]:

$$\begin{aligned} \underline{V}(\underline{X},t) &= \dot{\psi}_F(t)\,\underline{grad}\,\Phi(\underline{X}) \\ p(\underline{X},t) &= -\rho_F \ddot{\psi}_F(t)\,\Phi(\underline{X}) \end{aligned} \qquad [9.60]$$

The potential [9.61] respects the different boundary conditions of the fluid domain (the altitude measured from the free surface at rest is called z):

$$\Phi(x,z) = A_k \cos kx \frac{\cosh k(H+z)}{\cosh kH} \qquad k = \frac{n\pi}{L} \qquad [9.61]$$

If the A_k coefficient has the dimension of a length, then this is also the case for the time function [9.62]:

$$\psi_F(t) = a_k \sin(\omega_k t + \theta_k) \quad [9.62]$$

The free surface condition results in a relationship between pressure at $z = 0$ and vertical displacement at this same level [9.63]:

$$-p(x,0) + \rho_F g U_{Fz}(x,0) = 0 \quad [9.63]$$

The equation governing modal motion is obtained by projecting the free surface condition onto the modal pressure field (B is the width of the reservoir) [9.64]:

$$B\int_0^L -p(x,0)\Phi(x,0)dx + \rho_F g B\int_0^L U_{Fz}(x,0)\Phi(x,0)dx = 0 \quad [9.64]$$

Taking the modal form of pressure and displacement [9.60] into account, we obtain equation [9.65]:

$$\rho_F \ddot{\psi}_F B\int_0^L \Phi^2(x,0)dx + \rho_F g \psi_F B\int_0^L \Phi(x,0)\frac{\partial \Phi}{\partial z}(x,0)dx = 0 \quad [9.65]$$

The modal elements are [9.66]:

$$\Phi(x,0) = A_k \cos kx \quad \frac{\partial \Phi}{\partial z}(x,0) = kA_k \cos kx \tanh kH \quad [9.66]$$

The modal equation of motion is then [9.67]:

$$\frac{1}{2}\rho_F BL A_k^2 \ddot{\psi}_F + \frac{1}{2}\rho_F BLgk A_k^2 \tanh kH \psi_F = 0 \quad [9.67]$$

We find the eigenfrequency of a sloshing mode [9.68]:

$$\omega_k^2 = gk \tanh kH \quad [9.68]$$

We can give the coefficients of this equation the usual dimensions. The coefficient of acceleration has the dimension of a mass and displacement has that of stiffness [9.69]:

$$\rho_F\left(\frac{BL}{2k\tanh kH}\right)\ddot{\psi}_F+\rho_F\left(\frac{BLg}{2}\right)\psi_F=0 \qquad [9.69]$$

The equivalent mass and equivalent stiffness describing a sloshing mode are thus defined as [9.70]:

$$M_{ef}\,\ddot{\psi}_F+K_{ef}\,\psi_F=0 \qquad [9.70]$$

Moreover, for the potential function coefficient, which has the dimension of a length, it is possible to choose [9.71]:

$$A_k=\frac{g}{\omega_k^2} \qquad [9.71]$$

The time function has the dimension of a length that represents the height of waves. For example, the first mode $k=\pi/L$ and the free surface has equation [9.72]:

$$U_{Fz}(x,0)=\psi_F(t)\left(\frac{\partial\Phi}{\partial z}\right)(x,0)=\psi_F(t)\cos\left(\frac{\pi x}{L}\right) \qquad [9.72]$$

9.3.4. *Coupling with a structure*

The most common case of coupling of a fluid sloshing mode and a structure is that of a reservoir supported by a structure (Figure 9.7). We will consider a structure represented by a system with one degree of freedom, taking into account the concepts of equivalent mass and stiffness as defined in Chapter 5. Only the first sloshing mode will be considered.

Free movement of the structure, when the reservoir is empty, is governed by the following equation [9.73]:

$$M_S\ddot{U}_S+K_SU_S=0 \qquad [9.73]$$

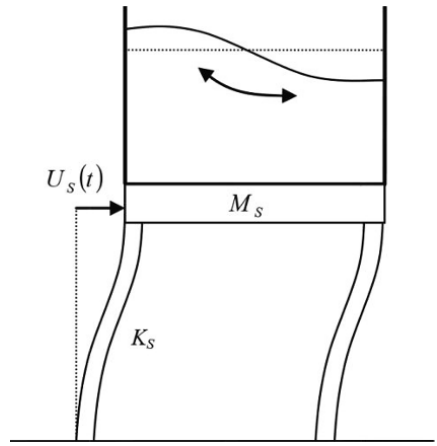

Figure 9.7. *A structure supporting a reservoir*

The interface used here consists of the two vertical walls of the reservoir. On these planes, the kinematic interface condition is written as [9.74]:

$$\underline{V}.\underline{e}_1 = \dot{U}_S \quad \text{or} \quad -\frac{1}{\rho_F}\frac{\partial p}{\partial x} = \ddot{U}_S \qquad [9.74]$$

To satisfy this condition, we must add a term to the previously defined pressure field [9.75]:

$$p = \rho_F \ddot{\psi}_F \Phi - x\rho_F \ddot{U}_S \qquad [9.75]$$

The displacement of the fluid is then formulated as [9.76]:

$$\underline{U}_F = -\psi_F \underline{grad}\,\Phi + U_S \underline{e}_1 \qquad [9.76]$$

The equation governing fluid motion is obtained by projecting the free surface condition onto the mode [9.77]:

$$\int_0^L -p(x,0)\Phi(x,0)dx + \rho_F g \int_0^L U_{Fz}(x,0)\Phi(x,0)dx = 0 \qquad [9.77]$$

In this case, it gives equation [9.78]:

$$\rho_F \ddot{\psi}_F \int_0^L \Phi^2(x,0)\,dx + \rho_F g \psi_F \int_0^L \Phi(x,0)\frac{\partial \Phi}{\partial z}(x,0)\,dx = \\ = \rho_F \ddot{U}_S \int_0^L x\Phi(x,0)\,dx \quad [9.78]$$

or by giving the equation of motion coefficients the usual dimensions [9.79]:

$$\rho_F \left(\frac{BL^2}{2\pi \tanh(\pi H/L)}\right)\ddot{\psi}_F + \rho_F \left(\frac{BLg}{2}\right)\psi_F = -\rho_F \left(\frac{2BL^2}{\pi^2}\right)\ddot{U}_S \quad [9.79]$$

Coupling is reflected in the fluid equation of motion as the presence of a second member dependent on the acceleration of the solid [9.80]:

$$M_{ef}\,\ddot{\psi}_F + K_{ef}\,\psi_F = -M_{SF}\ddot{U}_S \quad [9.80]$$

The factor affecting acceleration is called the solid–fluid coupling mass [9.81]:

$$M_{SF} = \rho_F \frac{2BL^2}{\pi^2} \quad [9.81]$$

To find structure movement, we calculate the force exerted by the fluid on the vertical walls at $x = 0$ and $x = L$ [9.82]:

$$F_{FS} = B\int_{-H}^{0} -p(0,z)\,dz + B\int_{-H}^{0} p(L,z)\,dz \quad [9.82]$$

or:

$$F_{FS} = -\rho_F B\ddot{\psi}_F \left(\int_{-H}^{0} \Phi(0,z)\,dz - \int_{-H}^{0} \Phi(L,z)\,dz\right) - \rho_F \ddot{U}_S BL\int_{-H}^{0} dz \quad [9.83]$$

Two terms appear in this force. One is proportional to the acceleration of the fluid and the other is proportional to that of the structure [9.84]:

$$F_{FS} = -M_{FS}\,\ddot{\psi}_F - M_F \ddot{U}_S \qquad [9.84]$$

The coefficients have the dimension of masses. The first is called solid–fluid coupling mass and the second is called the total mass of the fluid [9.85]:

$$M_{FS} = \rho_F \frac{2BL^2}{\pi^2} \qquad M_F = \rho_F BHL \qquad [9.85]$$

The equations governing the motion of the structure and the fluid, taking coupling into account, are [9.86]:

$$\begin{aligned} M_{ef}\,\ddot{\psi}_F + K_{ef}\,\psi_F &= -M_{SF}\ddot{U}_S \\ M_S\ddot{U}_S + K_S U_S &= -M_{FS}\ddot{\psi}_S - M_F\ddot{U}_S \end{aligned} \qquad [9.86]$$

or, in matrix form [9.87]:

$$\begin{pmatrix} M_{ef} & M_{SF} \\ M_{FS} & M_S + M_F \end{pmatrix} \begin{pmatrix} \ddot{\psi}_F \\ \ddot{U}_S \end{pmatrix} + \begin{pmatrix} K_{ef} & 0 \\ 0 & K_S \end{pmatrix} \begin{pmatrix} \psi_F \\ U_S \end{pmatrix} = \begin{pmatrix} 0 \\ 0 \end{pmatrix} \qquad [9.87]$$

Coupling results in non-diagonal terms in the masses' matrix. Coupled movements give, *a priori*, non-diagonal and non-symmetric masses' matrices. In this particular case, the choice of modal mass for motion of fluid and the fact that the stiffness matrix is diagonal lead to a symmetrical masses' matrix. This system is formally equivalent to that of an oscillator coupled to a pendulum. Calculations of equivalent masses and coupling masses were made for different reservoir geometries (cylindrical, conical, etc.) [DOD 66].

EXAMPLE 9.1.– The search for system eigenmodes goes through calculation of the determinant [9.88]:

$$\begin{vmatrix} K_{ef} - \omega^2 M_{ef} & -\omega^2 M_{SF} \\ -\omega^2 M_{FS} & K_S - \omega^2 \left(M_S + M_F \right) \end{vmatrix} = 0 \qquad [9.88]$$

This gives the pulses equation [9.89]:

$$\begin{aligned} &\left(M_{ef} \left(M_S + M_F \right) - M_{FS}^2 \right) \omega^4 \\ &-\left(K_S M_{ef} + K_{ef} \left(M_S + M_F \right) \right) \omega^2 + K_{ef} K_S = 0 \end{aligned} \qquad [9.89]$$

The characteristics of the structure are the following:

– structure: "HEA 240" poles, 5 m in height;

$M_S = 40 \times 10^3$ kg; $K_S = 6.26 \times 10^6$ N/m;

– reservoir: $L = 1$ m;

– for a water height of 3 m, $M_F = 40 \times 10^3$ kg;

$M_{ef} = 20.8 \times 10^3$ kg; $K_{ef} = 0.122 \times 10^6$ N/m; $M_{FS} = 25.3 \times 10^3$ kg.

Figure 9.8 shows the variation of eigenperiods according to the water level in the reservoir. For comparison, the structure and fluid eigenperiods that would be obtained without considering coupling are also shown in the figure.

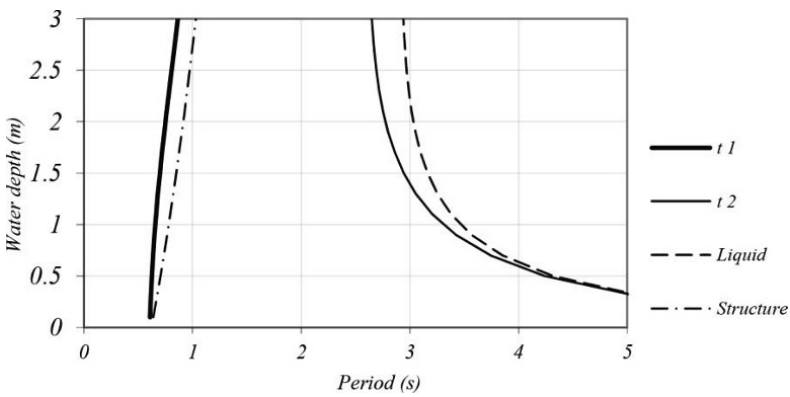

Figure 9.8. *Variation of vibration eigenperiods according to the water level in the reservoir (t1 and t2). For comparison, the structure and fluid eigenperiods without considering coupling are shown*

For a water depth of 3 m, there are two eigenmodes [9.90]. Displacements associated with these two modes are shown in Figure 9.9:

$$\underline{\boldsymbol{\phi}}^1 = \begin{pmatrix} 0.76 \\ 1 \end{pmatrix} \quad \underline{\boldsymbol{\phi}}^2 = \begin{pmatrix} -35 \\ 1 \end{pmatrix} \qquad [9.90]$$

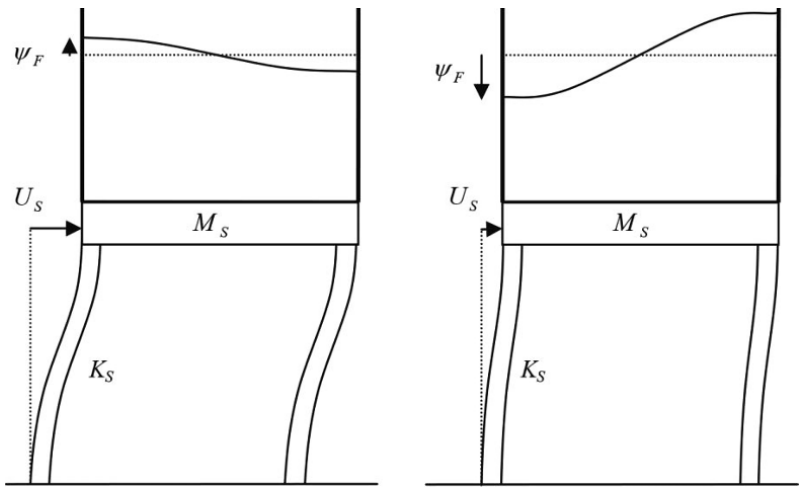

Figure 9.9. *Representation of two eigenmodes*

Chapter 10

Response of a Nonlinear Structure

In this chapter, we consider the nonlinear behavior of structures made up of beams. First, we present nonlinear metallic structure behaviors and then reinforced concrete structure behaviors. Then, we discuss the inclusion of nonlinear behavior in the modeling of a structure with one degree of freedom. To conclude, we discuss the structural response of an elastoplastic beam to impact.

10.1. Nonlinear behavior of structures

We speak of nonlinear behavior of a structure when the movement of a structure cannot be described by one or more linear differential equations, as discussed in Chapters 5, 8 and 9. There are two origins for the introduction of nonlinear equations. The first origin is geometric in nature. Linear equations are obtained by approximation to small displacements. If the amplitude of structure movements or relevant description of physical mechanisms cannot maintain this hypothesis, the equation of motion will be nonlinear. The second origin is the consequence of the structure on the behavior when taking the nonlinear behavior of a material into account, i.e. of different linear elasticity or viscoelasticity. These nonlinear material behaviors were discussed on the level of waves in solids in Chapter 3. A combination of these two types of nonlinearities can also occur.

10.1.1. *Metallic structures*

Different plasticizing mechanisms can occur in a metal beam depending on the state of stress. Plasticization is the main mechanism that defines the ultimate state of resistance of a structure [AFN 93]. If the bending stress is predominant, a plastic hinge is produced. The shear force can be predominant and lead to plasticization by yielding. If a beam supports a normal force and bending moment, a plastic hinge can be formed, and in this case the normal plastic force and the plastic moment that this hinge can support are linked. Generally, determination of plasticization conditions for a beam as a function of stress (normal force, shear force and bending moment) can be quite complex and require the use of limit analysis methods [SAL 01]. Nonlinear behavior can combine plasticization and the effect of large beam displacements. This situation occurs when the beam is fixed at both extremities and strain induces a significant stretching in the midline of the beam.

10.1.1.1. *Plastic hinge*

For a beam in flexion, behavior is elastic as long as the maximum stress is below the elasticity limit. Figure 10.1 shows the stress diagram in a section of a beam in flexion. If the elastic limit is reached in the section, the corresponding bending moment is called M_e (a1). If solicitation increases, a plastic hinge is formed. The section is then partially plasticized (a2). If the section is fully plasticized (a3), the bending moment reaches the M_P value that cannot be exceeded, although the strain of the beam can be increased. Figure 10.1(b) shows the elastoplastic behavior of a beam, i.e. the bending moment change according to curvature. For a rectangular section (width b and height h), these moments are given by formulas [10.1]:

$$M_e = \frac{2I\sigma_e}{h} = \frac{bh^2\sigma_e}{6} \quad M_P = \frac{bh^2\sigma_e}{4} \qquad [10.1]$$

The ratio between moment M_P and moment M_e depends on the shape of the section of the beam. This ratio is 1.5 for a rectangular section and approximates to 1 in sections in *I*. To simplify the calculations, we can ignore the intermediate phase and only consider

two phases of behavior, the elastic phase and plastic phase, where the moment is M_P.

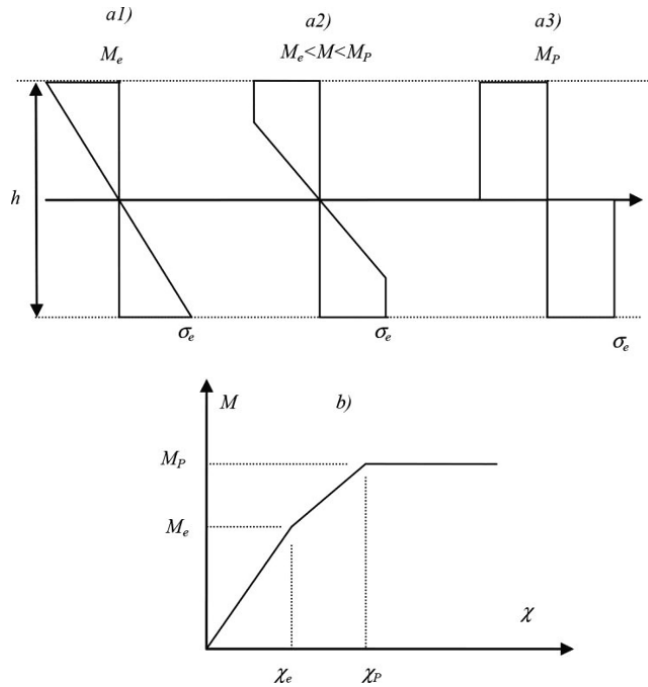

Figure 10.1. *Elastoplastic behavior in a beam section. Distribution of stresses: (a1) elastic section; (a2) partially plasticized section; (a3) fully plasticized section; (b) changes in moment according to curvature*

10.1.1.2. *Plasticization by shear force*

As discussed in Chapter 9, during a dynamic load, shear force increases much faster than bending moment. This situation can lead to plasticization mainly due to shear stresses created by shear force, although stresses due to flexion are still weak. This situation is very rare in staticity. For a compact section, an estimate of the shear force causing plasticization is given by [10.2]:

$$V_P \approx \frac{S\sigma_e}{2} \qquad [10.2]$$

If the shear force and bending moment coexist in a beam section, a plasticization condition connects these two solicitations [DRU 56, HOD 57]. We will not detail this coupling. In practice, for metal beams for which the section is in *I*, it can be assumed that the shear stresses due to shear force are significant in the "web" of the beam (S_a section) and stresses due to the bending moment are significant in the "flange" (S_s section). We do not consider coupling between shear force and bending moment in the plasticity condition, and the plastic limit values are given in [10.3]:

$$V_P \approx \frac{S_a \sigma_e}{2} \quad M_P \approx \frac{h S_s \sigma_e}{2} \qquad [10.3]$$

10.1.1.3. *Plasticization in flexion and tension or compression*

There are a number of situations in many structures where a beam supports a bending moment and a normal force: for example, a post supporting a compressive force to which flexion, due to an action such as a lateral impact, can be added. Another example is that of beams supporting a cladding or roofing element that, if fixed at their extremities, can undergo tension due to large displacements caused by flexion. Plasticization results in the formation of a plastic hinge. Figure 10.2 shows the graphs of stress distribution in a plastic hinge when there is a normal force and bending moment. As discussed previously, if the normal force is zero, plasticization is only due to the moment and the stress distribution as shown in (a1). If the bending moment is zero, the stress distribution is homogeneous in the section as shown in (a3). In the presence of two solicitations, the stress distribution in the section is shown in (a2). In the latter case, and for a rectangular section, the normal force and bending moment are given by expressions [10.4]:

$$\begin{aligned} M &= \alpha b h^2 \sigma_e (1-\alpha) = 4 M_P \alpha (1-\alpha) \\ N &= bh\sigma_e (2\alpha - 1) = N_P (2\alpha - 1) \end{aligned} \qquad [10.4]$$

By removing the α parameter, we obtain formula [10.5], which connects the normal force and bending moment. This relationship, given here for a rectangular section and shown in the graph in

Figure 10.2(b), depends on the shape of the section and may not have a simple analytical expression:

$$\frac{M}{M_P}+\left(\frac{N}{N_P}\right)^2-1=0 \qquad [10.5]$$

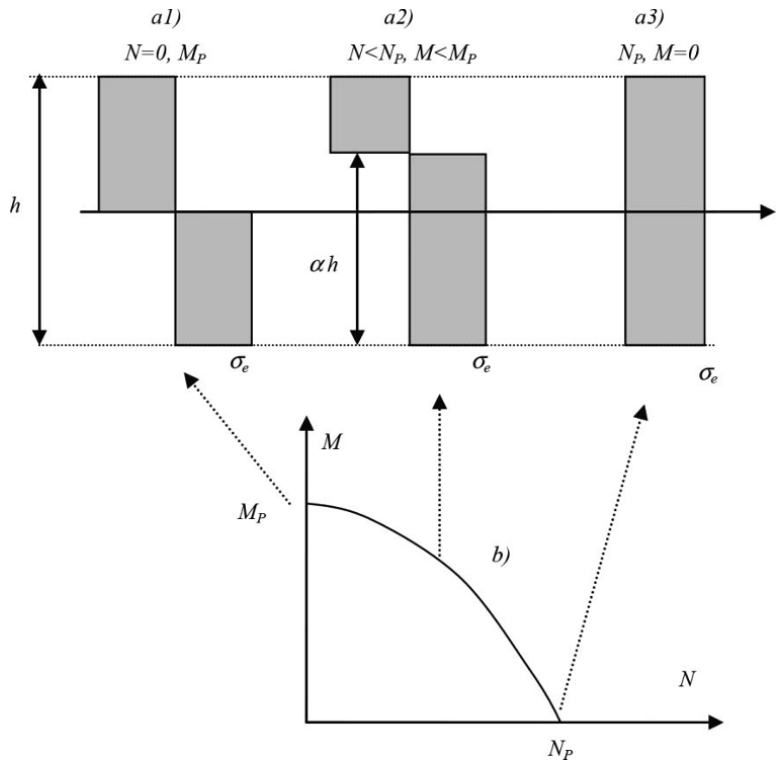

Figure 10.2. *Ultimate plastic states for a beam section. Stress distribution: (a1) flexion without normal force; (a2) tension and flexion; (a3) tension only; (b) final plastic states coupling M and N*

10.1.2. *Reinforced concrete structures*

For reinforced concrete structures, we focus on material nonlinearities. The manifestations of these material nonlinearities can be modeled as plasticity, at the beam section scale, to determine the

ultimate resistance states of a reinforced concrete element [AFN 92]. The usual values for "yield" and "ultimate limit" states of steel and concrete materials used in reinforced concrete structures are shown in Table 10.1. A plastic hinge results from many nonlinear mechanisms in materials, such as steel plasticity, damage and cracking of concrete, and landslides. Determination of the conditions for hinge formation according to stresses that are the normal force, shear force and bending moment can prove to be quite a complex problem, depending on the level of elaboration of the model used to represent the behavior of materials. This can be done using analytical methods such as limit analysis [KOE 07], or digital and experimental methods. Numerous studies on this subject exist (for example [MAI 05, ZIN 07]). We will consider the most common situation, which is the formation of a plastic hinge in the presence of a normal force and bending moment. Coupling between the shear force and bending moment has been studied by Sheridan and Cowdey [SHE 92]. Figure 10.6 schematically shows a reinforced concrete beam section. Steels are represented by two sets of sections, A and A'.

	Steel	Concrete compression	Concrete tension
Module	$E_A = 2\times10^{11}$ Pa	$E_B = 2\times10^{10}$ Pa	$E_B = 2\times10^{10}$ Pa
Elastic limit Stress Strain	$\sigma_A{}^e = 3.5\times10^8$ Pa $\varepsilon_A{}^e = 1.8\times10^{-3}$	$\sigma_B{}^e = 3.5\times10^7$ Pa $\varepsilon_B{}^e = 2\times10^{-3}$	$\sigma_B{}^T = 0.6 + 0.06\ \sigma_B{}^u$ (MPa)
Ultimate limit Stress Strain	$\sigma_A{}^u = 3.5\times10^8$ Pa $\varepsilon_A{}^u = 1.0\times10^{-2}$	$\sigma_B{}^u = 3.5\times10^7$ Pa $\varepsilon_B{}^u = 2\times10^{-3}$ (or 3.5)	

Table 10.1. *Characteristic values for "elasticity limit" and "ultimate limit" states of steel and concrete materials*

An assumption of reinforced concrete is the perfect adherence between steel and concrete. Therefore, we locally have relationships

[10.6] between stresses and strains (index A for steel and index B for concrete). A coefficient of equivalence n is defined as:

$$\varepsilon_A = \varepsilon_B \quad \Rightarrow \quad \frac{\sigma_A}{E_A} = \frac{\sigma_B}{E_B} \qquad \sigma_A = n\,\sigma_B \quad n = \frac{E_A}{E_B} \qquad [10.6]$$

The concrete section is $B = bh$ and steel sections are A and A' ($B >> A$). We define an equivalent section as [10.7]:

$$S_0 = B + n\left(A + A'\right) \qquad [10.7]$$

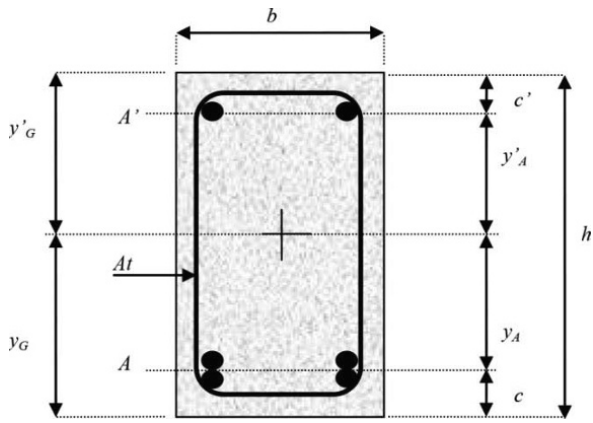

Figure 10.3. *Schematic section of a reinforced concrete beam*

The center of this section is the point G defined by its position [10.8]:

$$y_G = \frac{hB + n\left(c'A' + \left(h - c\right)A\right)}{2\left(B + n\left(A + A'\right)\right)} \qquad [10.8]$$

Under flexion, this section has a quadratic moment [10.9]:

$$I_0 = B\left(\frac{h^2}{3} - y_G y'_G\right) + y'^2_A\,A' + y_A^2 A \qquad [10.9]$$

Ultimate limit states associated with a plastic hinge are defined by strain limit states [AFN 92] that are shown in Figure 10.7 (in the case of a positive bending moment). The definition of these states is based on the fact that the strain diagram, assumed to be linear, rests at a point called the "pivot". Table 10.2 specifies the definition of the three pivots. The search for a criterion, depending on the normal force and bending moment stresses, is based on the calculation of the resultant force and resultant moment of stress states compatible with strain limits states. This calculation, which is often carried out and completed digitally, leads to a criterion that has a shape such as that shown in Figure 10.4 (dotted line). We can see this criterion very schematically as a quadrilateral that can specify the position of the four peaks (I, II, III and IV, see Figure 10.5).

Pivot A	Zone 1	$\varepsilon_{st} = 10 \times 10^{-3}$	Simple tension, tension + flexion Simple flexion
Pivot B	Zone 2	$\varepsilon_{bct} = 3.5 \times 10^{-3}$	Compound flexion
Pivot C	Zone 3	$2 \times 10^{-3} \leq \varepsilon_{bc} \leq 3.5 \times 10^{-3}$	Compound flexion Simple compression

Table 10.2. *The three "pivots" determining the ultimate limit states of a reinforced concrete beam section*

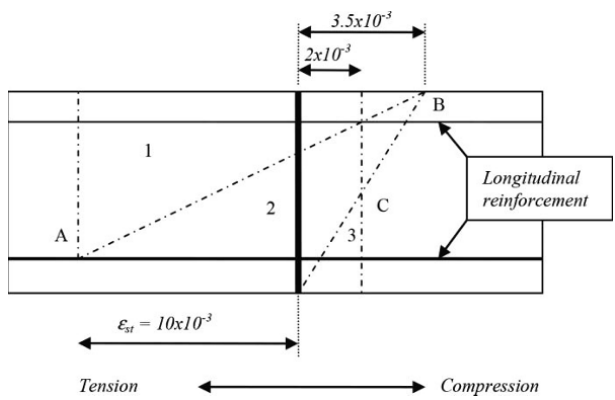

Figure 10.4. *Final states of strain in a reinforced concrete beam section*

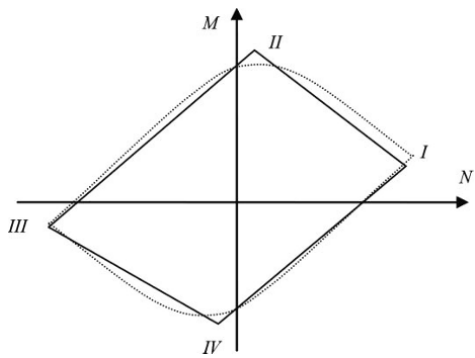

Figure 10.5. *Conditions for plastic hinge formation in a reinforced concrete beam supporting a normal force and a bending moment (dotted line: schematic form of the criterion; solid line: simplified representation)*

In Figure 10.5, point I corresponds to a state where the steel is plasticized when under tension. The section is fully extended. The coordinates of this point are given in [10.10]:

$$\begin{cases} N_I = \sigma_A^e \, S_A \\ M_I = \sigma_A^e \left(A y_A - A' y'_A \right) \end{cases} \qquad [10.10]$$

Point II corresponds to a state where inferior steels are plasticized under tension and the concrete is plasticized under compression (it is also assumed that the compressed steels are very close to plasticizing). The compression zone is defined by distance d, and the coordinates of this point are given by [10.11]:

$$\begin{cases} N_{II} = \sigma_A^e \left(A - A' \right) - \dfrac{1}{2} \sigma_B^e \, bd \\ M_{II} = \sigma_A^e \left(A y_A + A' y'_A \right) + \dfrac{1}{2} \sigma_B^e \, bd \left(y'_G - \dfrac{d}{3} \right) \end{cases} \qquad d = \frac{-\left(y_A + y'_G \right) \varepsilon_B^e}{\varepsilon_A^e - \varepsilon_B^e} \quad [10.11]$$

Point III corresponds to a state where the concrete is plasticized under compression (it is also assumed that the compressed steels are very close to the plasticizing). The coordinates of this point are given by [10.12]:

$$\begin{cases} N_{III} = -\sigma_A^e \left(A + A'\right) - \sigma_B^e \; B = -\sigma_B^e \; S_0 \\ M_{III} = -\sigma_A^e \left(Ay_A - A'y'_A\right) \end{cases} \quad [10.12]$$

Point IV corresponds to a state where high-quality steels are plasticized under tension and concrete is plasticized under compression (it is also assumed that the compressed steels are very close to the plasticizing). This is the equivalent of point II in the case of negative curvature. The compression zone is defined by d'. The coordinates of this point are given by [10.13]:

$$\begin{cases} N_{IV} = \sigma_A^e \left(A - A'\right) - \dfrac{1}{2}\sigma_B^e \; bd' \\ M_{IV} = -\sigma_A^e \left(Ay_A + A'y'_A\right) - \dfrac{1}{2}\sigma_B^e \; bd' \left(y_G - \dfrac{d'}{3}\right) \end{cases} \quad d' = \frac{-\left(y'_A + y_G\right)\varepsilon_B^e}{\varepsilon_A^e - \varepsilon_B^e} \quad [10.13]$$

The size of the hinge is length (L_{pl}) of the beam, which can be attributed to the plasticization state defined above. This length is determined empirically from experimental observations. A formula proposed by Paulay and Priestley [PAU 92] is shown in [10.14]:

$$L_{pl} = a_{st}\left(0.08 \;\; L_v + 0.022 \;\; f_s d_{bl}\right) \;\; (\text{mm}) \quad [10.14]$$

– a_{st}: coefficient of steel grade:

- $a_{st} = 0.8$ if $(f_t/f_s) < 1.15$;

- $a_{st} = 1$ if $(f_t/f_s) > 1.15$;

– L_v: shear extent $L_v = M/V$ (mm);

– f_s: elasticity limit of the longitudinal reinforcements (MPa);

– f_t: resistance of longitudinal reinforcements (MPa);

– d_{bl}: diameter of longitudinal reinforcements.

10.1.2.1. *Limit state for shear force*

In a reinforced concrete beam, resistance to shear force stress is provided by the transverse reinforcement in the form of frames (Figure 10.3). Faced with this solicitation, the reinforced concrete beam functions as a truss (in N). The vertical bars of the lattice are the

transverse reinforcement, which are in a state of tension, and the diagonal bars, which are in compression, correspond to an area of compressed concrete called the "compression link", as shown in Figure 10.6. The stress in the frames or transverse reinforcement is, according to assumptions [AFN 92], determined by formula [10.15]:

$$\sigma = \frac{V\ st}{0.9\ z\ A_t} \qquad [10.15]$$

– V is the shear force;

– st is the spacing of frames;

– z is the height ($y'_G + y_A$);

– A_t is the cross section of steel.

The ultimate shear force associated with plasticization of transverse reinforcements is then determined by formula [10.16]:

$$V_U = \frac{0.9\ z\ A_t \sigma_A^e}{st} \qquad [10.16]$$

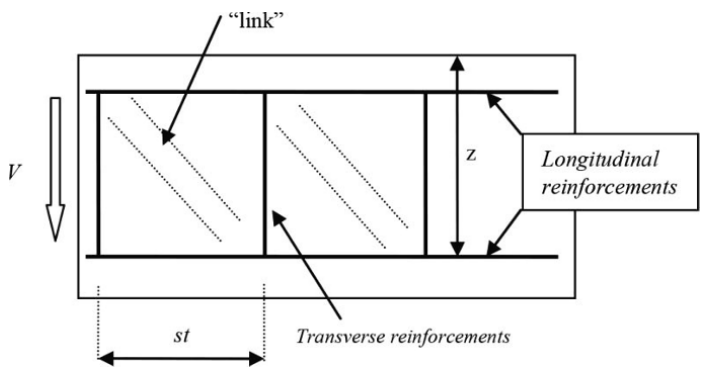

Figure 10.6. *A reinforced concrete beam element supporting a shear force, lattice diagram of N*

As discussed in Chapter 8 (section 8.2.4), with dynamic loading, the shear force stress may be the critical solicitation for the strength of a beam. The extreme value of shear force is in the impact area that

may be located at any point along the beam. Therefore, in beams dimensioned to withstand impacts, we find significantly higher amounts of transverse reinforcement than those currently in the literature. For violent actions generating high shear forces, there is even the provision of specific frames, called "lacing", consisting of bars forming a "W" lattice [UFC 08, WHI 55].

10.1.3. *Flexion and extension in large displacements*

We have just seen the consequence of the material nonlinearity that is plasticity in a beam section. On another level, the structural behavior of a beam can be nonlinear. Figure 10.7 shows a localized force applied in the middle of an elastoplastic beam. Under the action of force, the beam bends. The value of the force may increase until the appearance of a plastic hinge at its center (this value is $F = 2M_P/L$). If the beam is fixed at its extremities, the value of the force can be further increased, which has the effect of creating a normal force linked to the extension of the midline of the beam. The midline extension strain is estimated by formula [10.17]. We only take into account the strains that are due to expansion and ignore those that are due to bending:

$$\frac{\Delta \ell}{\ell} \approx \frac{2}{L}\left(\sqrt{\frac{L^2}{4}+x^2}-\frac{L}{2}\right) \approx \frac{2x^2}{L^2} \quad (x \ll L) \qquad [10.17]$$

The normal force linked to this extension is [10.18]:

$$N = ES\frac{2x^2}{L^2} \qquad [10.18]$$

The beam balance provides the relationship between applied force, displacement, normal force and bending moment [10.19]:

$$F = \frac{4x}{L}N + \frac{2}{L}M \qquad [10.19]$$

In the plastic hinge, the normal force and bending moment are connected by a criterion that is characteristic of the beam section (see,

for example, Figure 10.2 for a rectangular section steel bar or Figure 10.5 for a reinforced concrete beam). If we continue the calculation for the example of a steel beam with rectangular section, the criterion is given by formula [10.5]. We can then deduce the nonlinear relationship between force and displacement [10.20]:

$$F = \frac{8ES}{L^3}x^3 + \frac{2}{L}M_P\left(1 - \left(\frac{2ESx^2}{N_P L^2}\right)^2\right) \qquad [10.20]$$

As displacement x increases, the second term decreases until it becomes negligible. Expression of force tends toward cubic proportionality of displacement [10.21]:

$$F \approx \frac{8ES}{L^3}x^3 \qquad [10.21]$$

When the plasticity threshold is reached under tension across the beam, force takes expression [10.22]:

$$x \geq L\sqrt{\frac{\sigma_e}{2E}} \quad F \approx \frac{4N_P}{L}x \qquad [10.22]$$

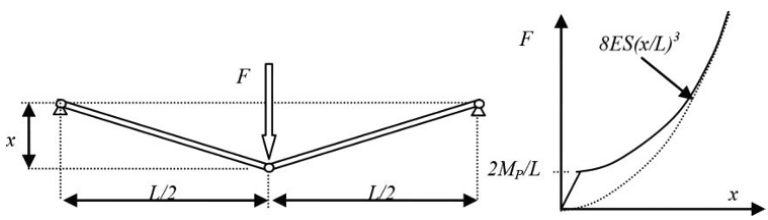

Figure 10.7. *Elastoplastic strain of a beam articulated at its two extremities. Behavior taking into account the normal force of traction subsequent to large displacement*

Another example of a nonlinear structure behavior associated with large displacement is that of a flexible wall, such as a metal siding, under the action of pressure. Flexion of a siding, which has the geometry of a pleated or corrugated metal sheet, only supports bending in one direction. The behavior of an element of unitary width

is comparable to that of a beam. A siding element under pressure deforms to become a cylindrical surface. Figure 10.8 illustrates this situation. If the strain becomes large, the stresses due to bending become negligible compared to those due to extension. This extension is linked to the extension of the center line of the beam and is estimated by formula [10.23]:

$$x = R(1-\cos\theta) \qquad \frac{\Delta\ell}{\ell} = \frac{2R\theta}{L} - 1 \qquad [10.23]$$

The tensile stress is estimated to be that of a cylinder of small thickness under pressure [10.24]:

$$\sigma = P\frac{h}{R} = E\left(\frac{2R\theta}{L} - 1\right) \qquad [10.24]$$

If we express pressure and displacement in a dimensionless manner, according to expressions [10.25], the nonlinear relationship between force and displacement is as shown in Figure 10.9:

$$x^* = \frac{2x}{L} = \frac{1}{\zeta}\left(1-\sqrt{1-\zeta^2}\right) \quad \left(\zeta = \sin\theta = \frac{L}{2R}\right)$$
$$P^* = \frac{2Ph}{EL} = \frac{1}{\zeta}\left(\frac{1}{\zeta}\arcsin\zeta - 1\right) \qquad [10.25]$$

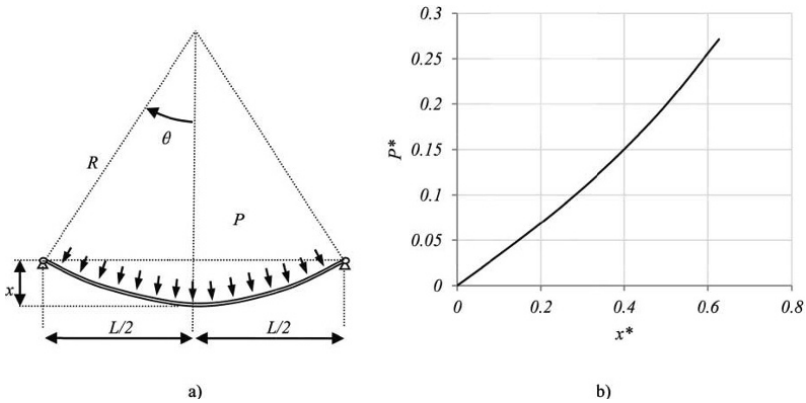

Figure 10.8. *a) Deformation of a wall under the action of pressure (membrane effect); b) associated nonlinear behavior*

10.2. Nonlinear system with one degree of freedom

10.2.1. *Formula*

We have just discussed the mechanisms, mainly related to plasticity, that lead to the nonlinear behavior of a structure. If the structure is modeled as a mechanical system with one degree of freedom, it should be noted that resistance R that opposes the load $F(t)$ is expressed as a nonlinear function of the displacement x of the latter. The movement results in an equation of the form [10.26]:

$$m\ddot{x} = F(t) - R(x) \qquad [10.26]$$

The work of the resisting force structure is $W(x)$ [10.27]:

$$W(x) = \int_0^x R(y)\,dy \qquad [10.27]$$

In general, an equation of type [10.26] is not analytically integrable. It is then possible to use digital resolution.

Structure response begins with an elastic phase. It is possible to express the conditions under which the elastic limit is reached. This is similar to the determination of conditions leading to the iso-damage curves discussed in section 5.3. For example, let us consider a load of "rectangular pulse" type, that is a constant force P, applied for duration θ. The elastic response of the structure (mass m and stiffness k) has the expressions given in [10.28]. There are two cases, depending on whether we consider time t during loading or after:

$$\begin{aligned} &0 < t < \theta \qquad x = \frac{P}{k}(1 - \cos\omega t) \qquad \dot{x} = \frac{P}{\sqrt{km}}\sin\omega t \\ &\theta < t \qquad x = \frac{1}{\omega}\dot{x}(\theta)\sin\omega t + x(\theta)\cos\omega t \end{aligned} \qquad [10.28]$$

The elasticity limit is reached in the first phase under conditions [10.29]:

$$P > \frac{R}{2} \text{ and } \theta > \frac{\pi}{\omega} \qquad [10.29]$$

If these conditions are not met, the maximum amplitude during the second phase is expressed as [10.30]:

$$x_{\max} = \sqrt{\frac{1}{\omega^2}\dot{x}(\theta)^2 + x(\theta)^2} = \frac{P}{k}\sqrt{2-\cos\omega\theta} \qquad [10.30]$$

The plasticity threshold will be exceeded during the second phase under conditions [10.31]:

$$P > \frac{R}{\sqrt{2}} \text{ and } \theta > \frac{1}{\omega}\arccos\left(2-\zeta^2\right)\left(\zeta = \frac{R}{P}\right) \qquad [10.31]$$

10.2.2. *Pulse load*

A situation in which estimation of the nonlinear response of a structure is analytically possible is that of load pulse. The load is considered impulsive or short term within the meaning given in section 5.1.2 if the duration is small compared to the eigenperiod of the structure ($\theta << \pi/\omega$). With this condition, the elasticity limit cannot be reached during loading. We consider that after loading, the structure has barely moved. The effect of loading was to provide the structure with a velocity. The momentum gained by the structure at the end of loading is equal to the pulse it receives [10.32]:

$$m\dot{x}(\theta) = \int_0^{\theta}(F-R)\,dt \qquad [10.32]$$

As the displacement of the structure is negligible, we can ignore the resistance force R relative to load F [10.33]:

$$\dot{x}(\theta) \approx \frac{1}{m}\int_0^{\theta} F\,dt \approx \frac{i}{m} \qquad [10.33]$$

Once charging is complete, we can estimate the velocity of the structure using the kinetic energy theorem [10.34]:

$$\begin{aligned} \dot{x}^2(t) &= \dot{x}^2(\theta) - \frac{2}{m}\int_{x(\theta)}^{x(t)} R(y)\,dy \\ \dot{x}(t) &\approx \frac{1}{m}\sqrt{i^2 - 2m\,W(x)} \end{aligned} \qquad [10.34]$$

When the velocity of the structure cancels out, the displacement reaches its maximum value. An estimation of the maximum displacement is possible from the pulse and resistance [10.35]. This is illustrated in Figure 10.9:

$$W\left(x_{\max}\right)=\frac{i^2}{2m} \qquad [10.35]$$

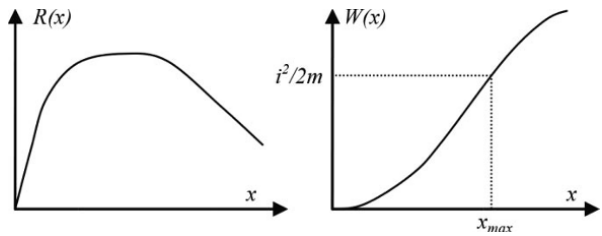

Figure 10.9. *Resistance curve of a structure and energy dissipated versus displacement; determination of the maximum displacement depending on the load pulse*

10.2.3. *Plastic rigid approach*

Another situation allowing rapid assessment of the response is that the behavior of the structure can be considered as "plastic rigid". This assumption is relevant if the elastoplastic structure is plasticized from the first moment of loading. Let us consider a load of amplitude P and duration θ if time t_e marks reaching the elasticity threshold such that $t_e << \theta$. At the end of loading, the velocity and position of the structure are shown in [10.36]:

$$\dot{x}(\theta)=\frac{\theta}{m}(P-R) \qquad x(\theta)=\frac{\theta^2}{2m}(P-R) \qquad [10.36]$$

After the end of loading, the movement is slowed and the maximum displacement is reached when velocity is zero [10.37]:

$$x_{\max}=\frac{\theta^2}{2m}(P-R)+\frac{m}{2R}\left(\frac{\theta(P-R)}{m}\right)^2 \qquad [10.37]$$

The maximum displacement can be expressed in terms of the pulse load [10.38]:

$$x_{\max} = \frac{i^2}{2m}\frac{(P-R)}{PR} \qquad [10.38]$$

If we define an x_{max} value that is not to be exceeded for a structure, we can try to represent the loading conditions that can lead to the displacement limit. This leads to an iso-damage curve equivalent to the "pressure pulse" diagram seen for elastic structures. We will use dimensionless pulse i^* and the ζ parameter that characterizes the relative amplitude of the load. The condition is formulated in [10.39] and is shown in the graph in Figure 10.10:

$$i^* = \frac{i}{\sqrt{2mRx_{\max}}} = \frac{1}{\sqrt{1-\zeta}} \quad \left(\frac{R}{P} = \zeta\right) \qquad [10.39]$$

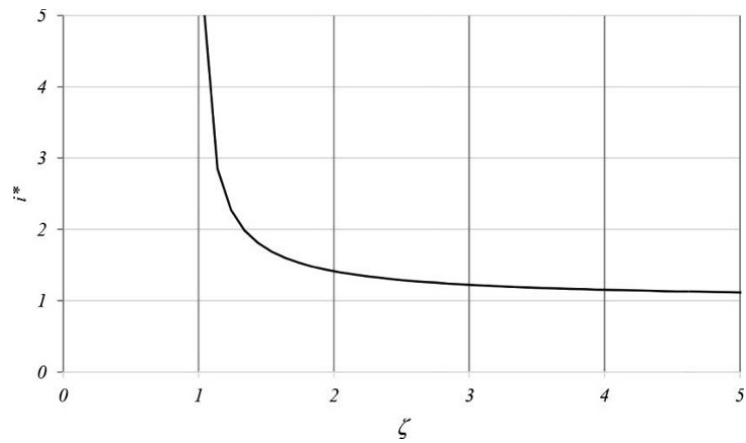

Figure 10.10. *Iso-damage curve for a rigid plastic structure*

10.3. The case of elastoplastic behavior

10.3.1. *Pulse load*

To further estimate the response of a nonlinear structure, we will consider the case of perfect elastoplastic behavior, which is one of the most used models. Before considering a more general case, we will

study the case where the pulse load hypothesis is valid. The elastoplastic behavior model is shown in Figure 10.11. It indicates the resistance of the structure according to the displacement as well as the work of this force, which is also explained in [10.40]:

$$\begin{aligned} x < x_e \quad & W(x) = \frac{1}{2} K x^2 \\ x > x_e \quad & W(x) = R\left(x - x_e/2\right) \end{aligned} \qquad [10.40]$$

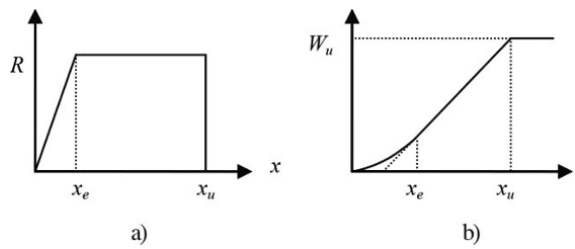

Figure 10.11. *a) Resistance curve of an elastoplastic structure; b) work as a function of displacement*

On the basis of considerations of section 10.2.2 and formula [10.35], the elastic limit is exceeded if the value of the pulse exceeds value [10.41]:

$$i > \frac{R}{\omega} \qquad [10.41]$$

The maximum displacement can be calculated on the basis of pulse [10.42]:

$$x_{\max} = \frac{i^2}{2mR} + \frac{x_e}{2} \qquad [10.42]$$

For nonlinear systems, we take the ratio of maximum displacement to displacement corresponding to the elasticity limit as the dimensionless response [10.43]:

$$x^* = \frac{x_{\max}}{x_e} = \frac{k P^2 \theta^2}{2mR^2} + \frac{1}{2} \qquad [10.43]$$

The dimensionless response can be expressed in terms of dimensionless parameters relative to loading time (w^*) and relative resistance of the structure (ζ) [10.44]:

$$x^* = \frac{\pi^2 w^{*2}}{2\zeta^2} + \frac{1}{2} \quad \left(w^* = \frac{\omega\theta}{\pi} \quad \zeta = \frac{R}{P} \right) \qquad [10.44]$$

Expression [10.44] is only valid if the load is impulsive and if plasticity is achieved, which results in condition [10.45]:

$$\zeta\pi < w^* << 1 \qquad [10.45]$$

Figure 10.12 shows the response spectra of a nonlinear system under pulse loading. Condition [10.45] indicates that this situation occurs for loads of short duration, but amplitude is much greater than resistance of the structure.

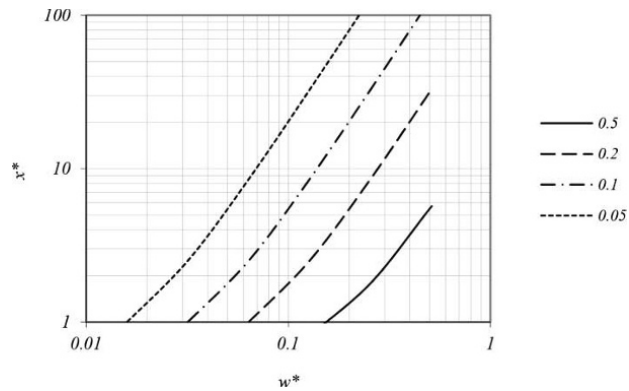

Figure 10.12. *Nonlinear response spectrum for a pulse load with different load amplitudes ($\zeta = 0.5$, $\zeta = 0.2$, $\zeta = 0.1$, $\zeta = 0.05$)*

10.3.2. *Nonlinear response spectrum*

More generally, the response spectrum of a structure with nonlinear behavior can be sought for a given load. Let us take the example of a structure with elastoplastic behavior, as presented in the previous section. The considered load is a slot of amplitude P and duration θ. Plasticization occurs if at least one of the conditions [10.29] and [10.31] is not checked. This case being excluded, there

are five possible situations to describe the different phases of structure response (Figure 10.13):

– Cases shown under Figure 10.13(a) correspond to loads with an amplitude below the plasticity threshold.

– In case a1, loading ends when the behavior is still elastic, but the free movement of the structure in the moments after the end of the loading leads it to the plasticity threshold.

– In case a2, the structure reaches the plastic phase during loading. In the plastic phase, movement is decelerated and loading is ended before the maximum displacement is reached.

– Case a3 is similar to the previous case, except that the maximum displacement is achieved when loading has yet to be finished.

When the load amplitude exceeds the structure plasticization threshold, only two situations are possible:

– In case b1, the relatively brief load ends as the structure is still in the elastic phase.

– In case b2, loading continues even though plasticization has started.

The case where maximum displacement is reached and loading continues is not possible if the load amplitude exceeds the plasticity threshold. If the end of loading occurs while the structure is still elastic ($t_e > \theta$) (case a1 and b1), the loading phase ends at time θ, and an elastic phase without loading and a plastic phase without loading follow. At the end of loading, the position and velocity parameters are given as [10.46]:

$$x(\theta) = \frac{P}{k}(1 - \cos\omega\theta) \qquad \dot{x}(\theta) = \frac{P}{\sqrt{km}}\sin\omega\theta \qquad [10.46]$$

In the elastic phase following completion of loading, movement is governed by equation [10.47]:

$$\theta < t < t_e \qquad x = \frac{P}{k}\left(\cos\omega(t-\theta) - \cos\omega t\right) \qquad [10.47]$$

Plasticity is reached at time t_e set by [10.48]:

$$\cos\omega\left(t_e-\theta\right)-\cos\omega t_e=\zeta \qquad [10.48]$$

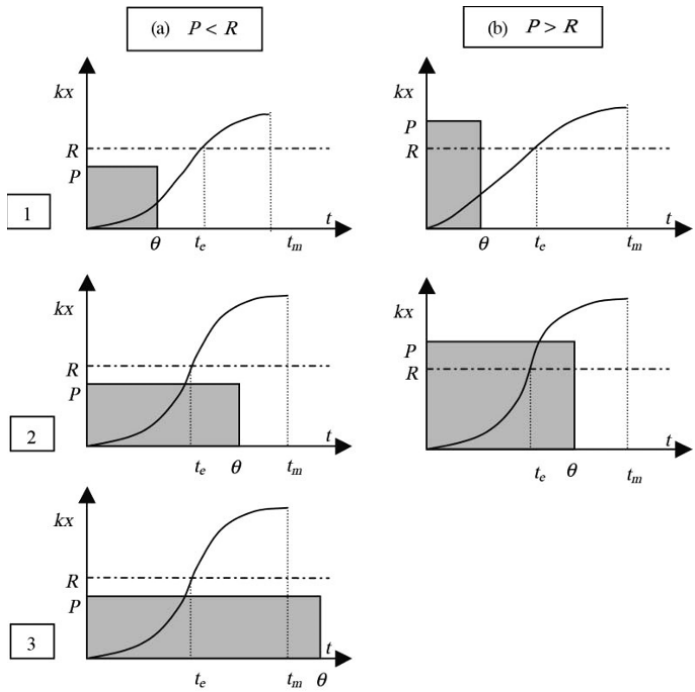

Figure 10.13. *The five possible situations for the elastoplastic response of a structure to a "rectangular" type load*

After this time, movement is uniformly decelerated and displacement reaches the maximum value [10.49]:

$$x_m=x_e+\frac{1}{2R}\dot{x}\left(t_e\right)^2 \qquad [10.49]$$

If plasticization appears before the end of loading (cases a2, a3 and b2), the elastic phase ends at time t_e ($t_e < \theta$). The end of the elastic phase is characterized by parameters [10.50]:

$$t_e=\frac{\alpha}{\omega} \qquad \alpha=\arccos\left(1-\zeta\right) \qquad \dot{x}\left(t_e\right)=\frac{P\omega}{k}\sin\alpha=\frac{P\xi}{\sqrt{km}} \qquad [10.50]$$

Then, there will be a plastic phase in the presence of loading. This movement is described by expressions [10.51]:

$$t_e < t < \theta \qquad x = \frac{P-R}{2m}\left(t-t_e\right)^2 + \frac{P\xi\left(t-t_e\right)}{\sqrt{km}} + x_e \qquad [10.51]$$

This phase ends either because maximum displacement is reached (which can happen if $R > P$, as in case a3), or because loading is finished, followed by a plastic stopping phase without charge (as in cases a2 and b2). In case a3, maximum displacement is reached when velocity is zero and its expression is specified as in [10.52]:

$$\begin{aligned} &R > P \qquad \dot{x}\left(t_m\right) = 0 \quad \left(t_m - t_e\right) = \frac{mP\xi}{\left(R-P\right)\sqrt{km}} = \frac{\xi}{\left(\zeta-1\right)\omega} \\ &x_m = -\frac{R-P}{2m}\left(\frac{\xi}{\left(\zeta-1\right)\omega}\right)^2 + \frac{P\xi}{\sqrt{km}}\left(\frac{\xi}{\left(\zeta-1\right)\omega}\right) + x_e \end{aligned} \qquad [10.52]$$

In cases a2 and b2, the movement ($t_m > \theta$) continues after loading with positional parameters [10.53]:

$$\begin{aligned} t = \theta \qquad x\left(\theta\right) &= \frac{P-R}{2m}\left(\theta-t_e\right)^2 + \frac{P\xi\left(\theta-t_e\right)}{\sqrt{km}} + x_e \\ \dot{x}\left(\theta\right) &= \frac{P-R}{m}\left(\theta-t_e\right) + \frac{P\xi}{\sqrt{km}} \end{aligned} \qquad [10.53]$$

The movement is then described by equation [10.54]:

$$\theta < t < t_m \quad x = -\frac{R}{2m}\left(t-\theta\right)^2 + \dot{x}\left(\theta\right)\left(t-\theta\right) + x\left(\theta\right) \qquad [10.54]$$

Phase (c) ends when velocity is zero, that is at moment t_m indicated in [10.55]:

$$t_m = \theta + \frac{m}{R}\dot{x}\left(\theta\right) = \theta + \frac{1-\zeta}{\zeta}\left(\theta-t_e\right) + \frac{\xi}{\zeta\omega} \qquad [10.55]$$

Maximum displacement is reached at this moment and is set by the value explained in [10.56]:

$$x_m = -\frac{R}{2m}\left(t_m - \theta\right)^2 + \dot{x}\left(\theta\right)\left(t_m - \theta\right) + x\left(\theta\right)$$

$$x_m = -\frac{R}{2m}\left(\frac{1-\zeta}{\zeta}\left(\theta - \frac{\alpha}{\omega}\right) + \frac{\xi}{\zeta\omega}\right)^2 + \left(\frac{P-R}{m}\left(\theta - \frac{\alpha}{\omega}\right) + \frac{P\xi}{\sqrt{km}}\right)\left(\frac{1-\zeta}{\zeta}\left(\theta - \frac{\alpha}{\omega}\right) + \frac{\xi}{\zeta\omega}\right) + \frac{P-R}{2m}\left(\theta - \frac{\alpha}{\omega}\right)^2 + \frac{P\xi}{\sqrt{km}}\left(\theta - \frac{\alpha}{\omega}\right) + x_e \quad [10.56]$$

The set of expressions thus found allows us to calculate the maximum displacement in all cases and represent the nonlinear response spectrum for a "rectangular" type load. As in the previous section, we define the dimensionless response as the ratio of maximum displacement to that corresponding to the elasticity limit ($x^* = x_{max}/x_e$). Figure 10.14 shows the response spectrum, i.e. the dimensionless response as a function of the relative duration of loading ($w^* = \omega\theta/\pi$). Similarly, we can construct the response spectrum for triangular-type loading [UFC 08].

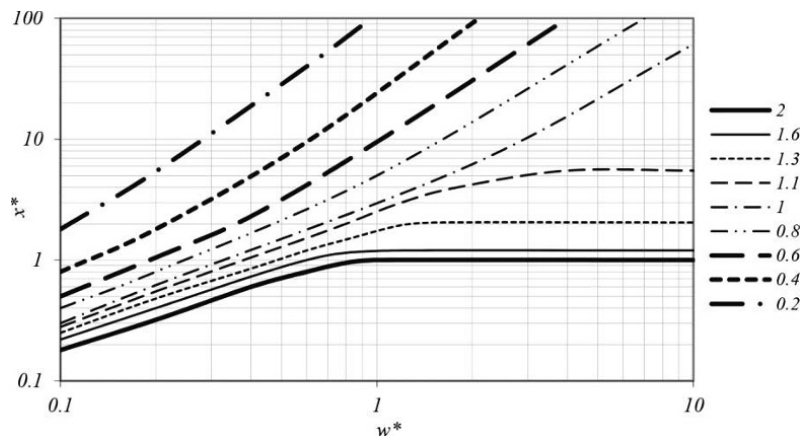

Figure 10.14. *Response spectrum of a nonlinear system for a rectangular-type load (curves according to the R/P ratio)*

10.3.3. *Equivalent system*

Replacing a real structure with a system with one degree of freedom is based on a concept of equivalence. The concepts of equivalent force, representative of loading, and equivalent displacement, representative of deformation of the structure, do not change compared to those defined for elastic structures in Chapter 5. For example, for a beam supporting a point force as shown in Figure 10.15, the equivalent force is the actual force and the equivalent displacement may be the displacement of the center of the beam. There is no equivalent stiffness, but we must respect the equivalent load resistance force. In the example, with M_P being the momentum in the plastic hinge, the equivalent reaction is $R_e = 4M_P/L$. If plasticity occurs in a structure, displacements related to elastic behavior quickly become negligible compared to those related to the plastic strain mechanism. For an elastic structure, the equivalence requires that the eigenfrequency of the structure, according to the representative mode, be the same as that of the equivalent system. This condition determines the choice of equivalent mass to give the simple system. Once the structure is plasticized, this equivalence has no more meaning because the eigenfrequency is a characteristic of linear elastic behavior. Then, we must find another equivalence condition to determine mass. In a nonlinear structure, in plasticity, and for loads of short duration, dissipated energy is the main parameter determining the maximum displacement amplitude. We can therefore find an equivalent energy. The equivalent mass M_e can be sought by explaining the kinetic energy equivalence of the structure and the equivalence of the system with one degree of freedom. For the example in Figure 10.16, this equivalence is formulated as [10.57]:

$$\frac{1}{2}M_e\dot{X}_e^2 = \frac{1}{2}\int_0^{L/2}\rho S u^2(x)\,dx = \rho S\dot{X}_e^2\int_0^{L/2}\left(\frac{2x}{L}\right)^2 dx = \frac{\rho SL}{6}\dot{X}_e^2 \quad [10.57]$$

We deduce that the equivalent mass should be one-third of the total mass. However, when the beam had an elastic behavior, the equivalent mass was about half of the total mass (see section 5.4). Therefore, when the beam plasticizes, we reduce the value of the equivalent mass. If the valuation of the maximum displacement of a plasticized

beam is worked out with the equivalent mass determined for elastic behaviour, the result will be underestimated. This mistake is not in the interests of safety.

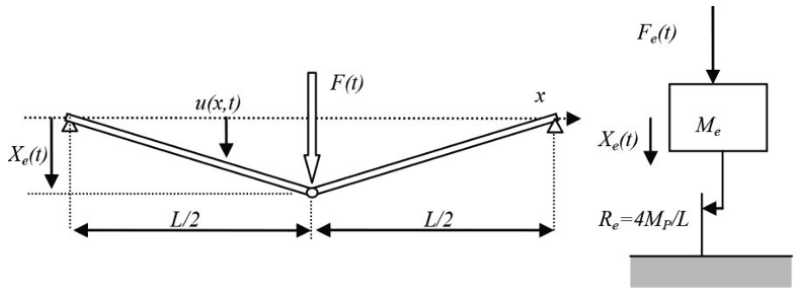

Figure 10.15. *Elastoplastic strain of a beam and equivalent system*

10.4. Approach of response to a violent impact

10.4.1. *Shock on a beam*

Previous studies on the response of nonlinear structures assumed that the displacement mode shape of the structure under dynamic loading was the same as in quasi-static loading. We discussed the limits of this hypothesis in Chapter 8 (section 8.2) when the structure was elastic. These considerations remain relevant if the elasticity limit is reached. Under the effect of a violent impact, plasticization may appear before the movement is propagated enough for the effect of boundary conditions, the supports, to influence structure response. Different cases were studied by Jones [JON 89]. To illustrate this, we consider the impact on a beam. In section 8.2.2, we discussed the development of a bending moment diagram that is, for some time, independent of the boundary conditions that are the supports or embeddings. If the load has sufficient amplitude, plasticization may appear during this phase. This situation is shown in Figure 10.16 and we will discuss it with an approximate method that involves metal beams. A plastic hinge is formed at the point of impact, as well as two other hinges at a distance α from that point. As we have already assumed, when plasticization occurs, displacements due to elastic strains are negligible compared to

those due to plastic strains. Under this assumption, the velocity field can be formulated with expression [10.58]:

$$\dot{u}(x,t) = \dot{u}(0,t)\left\langle 1 - \frac{x}{\alpha} \right\rangle \qquad [10.58]$$

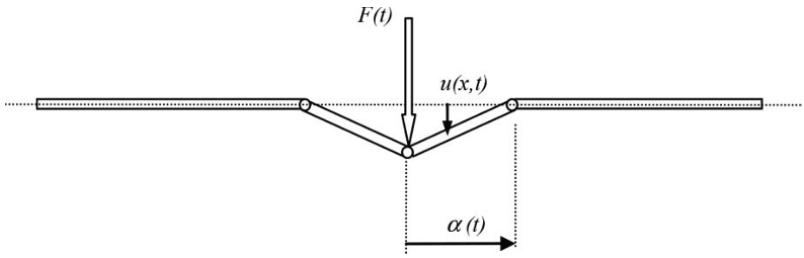

Figure 10.16. *Impact on a beam with formation of plastic hinges*

Expression of the fundamental principle of dynamics, by projecting the resultant onto the vertical axis and projecting the moment along the normal to the face, leads to the system of equations [10.59]. It is assumed that the shear force is zero at the location of plastic hinges, which is the location of the maximum bending moment:

$$\begin{aligned} &\int_0^{\alpha} \rho S\, \ddot{u}(x,t)\, dx = \frac{1}{2} F(t) \\ &\int_0^{\alpha} \rho S\, x \ddot{u}(x,t)\, dx = 2M_P \end{aligned} \qquad [10.59]$$

Acceleration of transverse motion of the beam can be expressed by formula [10.60]:

$$\ddot{u}(x,t) = \ddot{u}(0,t)\left(1 - \frac{x}{\alpha}\right) + \frac{x\dot{\alpha}}{\alpha^2}\dot{u}(0,t) \qquad 0 < x < \alpha \qquad [10.60]$$

This therefore provides, by replacement in [10.59], equations [10.61]:

$$\begin{aligned} &\frac{\rho S}{2}\left(\alpha \ddot{u}_0 + \dot{\alpha}\dot{u}_0\right) = \frac{1}{2} F(t) \\ &\frac{\rho S}{6}\left(\alpha^2 \ddot{u}_0 + 2\alpha\dot{\alpha}\dot{u}_0\right) = 2M_P \end{aligned} \qquad [10.61]$$

These equations can also be written in the form [10.62]:

$$\frac{d}{dt}\left(\alpha \dot{u}_0\right) = \frac{1}{\rho S} F(t)$$
$$\frac{d}{dt}\left(\alpha^2 \dot{u}_0\right) = \frac{12}{\rho S} M_P \qquad [10.62]$$

By integrating, we obtain expressions [10.63]:

$$\alpha \dot{u}_0 = \frac{1}{\rho S} i(t) \quad i(t) = \int_0^t F(\tau) d\tau$$
$$\alpha^2 \dot{u}_0 = \frac{12}{\rho S} M_P t \qquad [10.63]$$

From these expressions, we extract those that give the length α affected by the movement associated with plastic hinges and the displacement of the beam at the point of impact [10.64]:

$$\alpha(t) = 12 M_P \frac{t}{i(t)} \qquad u_0 = \frac{1}{12 \rho S M_P} \int_0^t \frac{i^2(\tau)}{\tau} d\tau \qquad [10.64]$$

We note that if the load is of constant amplitude (Heaviside function), α stays constant and the hinge is fixed. Quite often, as discussed in Chapter 6 with the Riera formula, force is a decreasing function of time and, therefore $\alpha(t)$ is an increasing function of time. If the mobile hinge reaches the limit of the beam, the above model is no longer relevant and we obtain a structure like that seen in section 10.3.3. An example of a violent impact is a solid mass m hitting a beam with an impact velocity V_i. This is a hard shock, according to the classification given in Chapter 6. The projection of the fundamental principle onto the vertical axis in this case provides formula [10.65]:

$$\int_0^{\alpha} \rho S \ddot{u}(x,t) dx = -\frac{1}{2} m \ddot{u}_0 \qquad [10.65]$$

The use of the acceleration field [10.60] leads to expression [10.66]:

$$\frac{d}{dt}\left(\alpha \dot{u}_0\right) = -\frac{m}{\rho S}\ddot{u}_0 \qquad [10.66]$$

By integrating, taking the initial condition of impact velocity V_i into account, expression [10.67] is obtained:

$$\alpha \dot{u}_0 = \frac{m}{\rho S}\left(V_i - \dot{u}_0\right) \qquad [10.67]$$

System [10.63] takes, in this case, the form [10.68]:

$$\begin{aligned} &\left(\alpha + \frac{m}{\rho S}\right)\dot{u}_0 = \frac{m}{\rho S}V_i \\ &\alpha^2 \dot{u}_0 = \frac{12}{\rho S}M_P t \end{aligned} \qquad [10.68]$$

By removing the point of impact velocity from these expressions, we get equation [10.69]:

$$mV_i\alpha^2 - 2M_P t\alpha - 12\frac{m}{\rho S}M_P t = 0 \qquad [10.69]$$

Then, we get an expression of the law of evolution of the area affected by the movement associated with the plastic hinges [10.70]:

$$\alpha(t) = \frac{6M_P}{mV_i}t + \sqrt{M_P t\left(\frac{36M_P t}{m^2 V_i^2} + \frac{12}{\rho S V_i}\right)} \qquad [10.70]$$

This kind of approach can also be conducted by taking into account a shearing plasticization due to shear force, if the latter occurs [JON 89].

10.4.2. *Impact of a distributed load*

Another example of a violent load imposed on a beam is that imposed by a distributed load that is applied suddenly. This may be

the effect of pressure subsequent to an explosion in a confined space or the interaction of a shock wave with a wall, as discussed in Chapter 7. We consider the case where the structure is modeled by a beam in flexion. We have already discussed this type of loading for an elastic beam (section 8.2.3). Once a load is applied, a shear force occurs near the supports providing a bending moment diagram that has its maximum near the supports. The primary cause of rupture is related to the ability of the beam section to resist this shear force. If rupture by shearing does not occur and the intensity of the load is sufficient, plastic hinges may appear near the support, as shown in Figure 10.17. We approach the study of nonlinear response in the first moments of the response by an approximate calculation to estimate the position of the plastic hinges. Here, we do not take into account the effect of large displacements and tension of the beam.

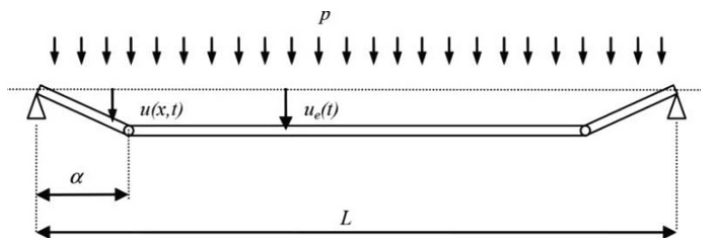

Figure 10.17. *Impact of a distributed force on a beam with formation of plastic hinges*

By only considering displacements due to plastic strains, the velocity field can be approximated by formula [10.71]. We assume, in this case, that the intensity of pressure is constant and the plastic hinge is fixed:

$$\dot{u}(x,t)=\frac{x}{\alpha}\dot{u}_e(t) \quad (0<x<\alpha) \quad \dot{u}(x,t)=\dot{u}_e(t) \quad (\alpha<x<L-\alpha) \text{ [10.71]}$$

We will use the kinetic energy theorem. The estimation of this energy is made by formula [10.72]:

$$E_C=\frac{1}{2}\int_0^L \rho S\dot{u}^2(x,t)\,dx=\int_0^L \rho S\left(\frac{x}{\alpha}\dot{u}_e\right)^2 dx+\frac{1}{2}\rho S(L-2\alpha)\dot{u}_e^2 \text{ [10.72]}$$

Calculation of this gives expression [10.73]:

$$E_C = \rho S\left(\frac{L}{2} - \frac{2\alpha}{3}\right)\dot{u}_e^2 \qquad [10.73]$$

The power of external forces, distributed load and the internal forces, plastic moments, can be connected through formula [10.74]:

$$\begin{aligned} \Pi &= \int_0^L p\,\dot{u}(x,t)\,dx - 2M_P\frac{\dot{u}_e}{\alpha} \\ &= 2\int_0^L p\frac{x}{\alpha}\dot{u}_e dx + (L-2\alpha)\,p\dot{u}_e - 2M_P\frac{\dot{u}_e}{\alpha} \end{aligned} \qquad [10.74]$$

Calculation of this gives expression [10.75]:

$$\Pi = (L-\alpha)\,p\dot{u}_e - 2M_P\frac{\dot{u}_e}{\alpha} \qquad [10.75]$$

The kinetic energy theorem leads to formula [10.76]:

$$2\rho S\left(\frac{L}{2} - \frac{2\alpha}{3}\right)\ddot{u}_e = (L-\alpha)\,p - \frac{2M_P}{\alpha} \qquad [10.76]$$

Moreover, the fundamental principle of dynamics applied to the central part of the beam that undergoes translational motion gives formula [10.77]. It is assumed that the shear force is zero at the location of plastic hinges, which is the location of a bending moment maximum:

$$\rho S(L-2\alpha)\ddot{u}_e = (L-2\alpha)\,p \qquad [10.77]$$

From these two expressions, we can deduce the expression giving the position of the plastic hinge [10.78]:

$$\alpha = 2{,}45\sqrt{\frac{M_P}{p}} \qquad [10.78]$$

We can compare this value of the plastic hinge position to that, very close, calculated in [8.55] from the elastic behavior of the beam. It may be noted that when the hinge is in the middle, the linear force is equal to three times the value, causing static plasticization. If we want to take into account a variable pressure p and a mobile hinge, the approximate method above leads to equations [10.79], for which digital resolution should be considered:

$$\begin{aligned} &2\rho S\left(\frac{L}{2}-\frac{2\alpha}{3}\right)\ddot{u}_e-\frac{2}{3}\rho S\dot{\alpha}\dot{u}_e=(L-\alpha)\,p-\frac{2M_P}{\alpha} \\ &\rho S(L-2\alpha)\ddot{u}_e-\rho S\dot{\alpha}\dot{u}_e=(L-2\alpha)\,p \end{aligned} \qquad [10.79]$$

Bibliography

[ACH 93] ACHENBACH J.D., *Wave Propagation in Elastic Solids*, Elsevier, Amsterdam, 1993.

[AFN 92] AFNOR EUROCODE 2, *Calcul des structures en béton*, AFNOR, La Plaine Saint-Denis, 1992.

[AFN 93] AFNOR EUROCODE 3, *Calcul des structures en acier*, AFNOR, La Plaine Saint-Denis, 1993.

[AFN 98] AFNOR EUROCODE 8, *Calcul des structures pour leur résistance aux séismes*, AFNOR, La Plaine Saint-Denis, 1998.

[ARC 04] ARCADY V., BROGLIATO B., Coefficients de restitution et efforts aux impacts; revue et comparaison des estimations analytiques, INRIA Research Report No. 5401, INRIA, Rocquencourt, December 2004.

[AXI 01a] AXISA F., *Modélisation des systèmes mécaniques: systèmes discrets*, vol. 1, Hermès, Paris, 2001.

[AXI 01b] AXISA F., *Modélisation des systèmes mécaniques: systèmes continus*, vol. 2, Hermès, Paris, 2001.

[AXI 01c] AXISA F., *Modélisation des systèmes mécaniques: interaction fluide structure*, vol. 3, Hermès, Paris, 2001.

[BAK 83] BAKER W.E., COX P.A., WESTINE P.S., *et al.*, *Explosion Hazard and Evaluation,* Elsevier, Amsterdam, 1983.

[BAN 41] BANCROFT D., "The velocity of longitudinal waves in cylindrical bars", *Physical Review*, vol. 59, pp. 588–593, 1941.

[BAN 09] BANGASH M.Y.H., *Shock, Impact and Explosion: Structural Analysis and Design*, Springer, Berlin, Heidelberg, 2009.

[BAT 87] BATA M., PLACHY V., *Analysis of Dynamic Effects on Engineering Structures*, Elsevier, Amsterdam, 1987.

[BIG 64] BIGGS J.M., *Introduction to Structural Dynamics*, McGraw-Hill, New York, 1964.

[BIS 91] BISHOFF P.H., PERRY S.H., "Compressive behaviour of concrete at high strain rates", *Materials and Structures*, vol. 24, pp. 245–450, 1991.

[BLA 93] BLANC R.H., "Transient wave propagation methods for determining the viscoelastic properties of solids", *Journal of Applied Mechanics*, vol. 60, pp. 763–768, 1993.

[BLE 79] BLEVINS R.D., *Natural Frequencies and Modal Chapes*, Van Norstrand Reinhold, New York, 1979.

[BOD 75] BODNER S.R., PARTOM Y., "Constitutives equations for elastic viscoplastic strain hardening materials", *Journal of Applied Mechanics*, *Transactions of the ASME*, vol. 42, pp. 385–389, 1975.

[BRO 85] BROSSARD J., LEYER J.C., DESBORDES D., *et al.*, "Air blast unconfined gaseous detonations", *Progress in Astronautics and Aeronautics*, *AIAA*, vol. 94, pp. 556–566, 1985.

[BRO 88] BROSSARD J., BAILLY P., DESROSIER C., *et al.*, "Overpressures imposed by a blast wave", *Progress in Astronautics and Aeronautics*, *AIAA*, vol. 114, pp. 389–400, 1988.

[BUI 78] BUI H.D., *Mécanique de la rupture fragile*, Masson, Paris, 1978.

[BUR 01] BURLION N., PIJAUDIER-CABOT G., DAHAN N., "Experimental analysis of compaction of concrete and mortar", *International Journal for Numerical and Analytical Methods in Geomechanics*, vol. 25, pp. 1467–1486, 2001.

[CEB 88] COMITÉ EURO INTERNATIONAL DU BÉTON, Concrete structures under impact and impulsive loading, Synthesis Report, bull. 187, 1988.

[CHA 99] CHAPMAN D.L., *Philosophical Magazine*, 213, series 5, vol. 47, pp. 90–104, 1899.

[CHR 89] CHREE C., "The equations of an isotropic elastic solid in polar and cylindrical co-ords, their solutions and applications", *Transactions of the Cambridge Philosophical Society*, vol. 14, pp. 250–369, 1889.

[CLO 75] CLOUGH R.H., PENZIEN J., *Dynamic of Structures*, McGraw-Hill, New York, 1975.

[DAR 95] DARVE F., *Les géomatériaux: théorie, expériences et modèles*, Hermès, Paris, 1995.

[DAV 48] DAVIES R.M., "A critical study of the Hopkinson pressure bar", *Philosophical Transactions of the Royal Society, A*, vol. 240, pp. 375–457, 1948.

[DAV 63] DAVIES E.D.H., HUNTER S.C., "The dynamic compression testing of solids by the method of the split Hopkinson pressure bar", *Journal of the Mechanics and Physics of Solids*, vol. 11, pp. 155–179, 1963.

[DEA 91] DEAN R.G., DALRYMPLE R.A., *Water Waves Mechanics for Engineers and Scientists*, World Scientific Publishing, Singapore, 1991.

[DE 01] DE LANGRE E., *Fluides et solides*, Presses Ecole Polytechnique editions, Palaiseau, France, 2001.

[DEN 00] DENOUAL C., HILD F., "A damage model for the dynamic fragmentation of brittle solids", *Computer Method in Applied Mechanics and Engineering*, vol. 183, pp. 247–258, 2000.

[DES 81] DESHAIES B., Les flammes sphériques, propagation divergente et combustion stationnaire, Thesis, University of Poitiers, 1981.

[DIT 79] DITKINE V., PROUDNIKOV A., *Operational Calculus*, Editions MIR, Moscow, 1979.

[DNA 83] DEFENSE NUCLEAR AGENCY, *Dynamic Pulse Buckling, Theory and Experiment*, SRI International, Menio Park, CA, 1983.

[DOD 66] DODGE F.T., *The Dynamic Behaviour of Liquids in Moving Containers,* Southwest Research Institute, San Antonio, TX, 2000.

[DRU 52] DRUCKER D.C., PRAGER W., "Soil mechanics and plastic analysis or limit design", *Quartely of Applied Mathematics*, vol. 10, pp. 157–175, 1952.

[DRU 56] DRUCKER D.C., "The effect of shear on the plastic bending of beams", *Journal of Applied Mechanics*, vol. 23, pp. 509–514, 1956.

[FOL 83] FOLLANSBEE P.S., FRANZ C., "Wave propagation in the split Hopkinson pressure bar", *Journal of Engineering Materials and Technology*, vol. 105, pp. 61–66, 1983.

[FRA 83] FRANCH T., "Strain in the interior of concrete caused by blast impact", *Concrete Structure under Impact and Impulsive Loading*, *RILEM Symposium Proceedings*, Federal Institute for Material Testing, Berlin, pp. 623–634, 1983.

[FRA 95] FRANÇOIS D., PINEAU A., ZAOUI A., *Comportement mécanique des matériaux*, Hermès, Paris, 1995.

[FRA 01] FRANÇOIS D., *Essais mécaniques et loi de comportement*, Hermès, Paris, 2001.

[FUN 68] FUNG Y.C., *Foundations of Solids Mechanics*, Prentice Hall, Upper Saddle River, NJ, 1968.

[GAR 93] GARY G., ZHAO H., "Inverse methods for the dynamic study of non-linear materials with a split Hopkinson bar", *Proceedings of IUTAM*, Victoria, Canada, 1993.

[GAR 97] GARY G., KLEPACZKO J.R., ZHAO H., "On the use of a viscoelastic split Hopkinson pressure bar", *International Journal of Impact Engineering*, vol. 19, pp. 319–330, 1997.

[GÉR 96] GÉRADIN M., RIXEN D., *Théorie des vibrations, application à la dynamique des structures*, Masson, Paris, 1996.

[GOL 01] GOLDSMITH W., *Impact: The Theory and Physical Behaviour of Colliding Solids*, Dover Publications, London, 2001.

[GON 90] GONG J.C., MALVERN L.E., JENKINS D.A., "Dispersion investigation in the split Hopkinson pressure bar", *Journal of Engineering Material Technology*, vol. 112, pp. 309–314, 1990.

[GOU 80] GOULD P.L., ABU-SITTA S.H., *Dynamic Response of Structures to Wind and Earthquake Loading*, Pentech Press, Plymouth, 1980.

[GRA 75] GRAFF K.F., *Wave Motion in Elastic Solids*, Ohio State University Press, 1975.

[GUR 77] GURSON A.L., "Continuum theory of ductile rupture by void nucleation and growth: part 1 – yield criteria and flow rules for porous ductile media", *Engineering Materials and Technology*, vol. 99, pp. 2–15, 1977.

[HAN 85] HAN D.J., CHEN W.F., "A nonuniform hardening plasticity model for concrete materials", *Mechanics of Materials*, vol. 4, pp. 283–302, 1985.

[HER 69] HERMAN W., "Constitutive equation for the dynamic compaction of ductile porous materials", *Journal of Applied Physics*, vol. 40, no. 6, pp. 2490–2500, 1969.

[HOD 57] HODGES P.G., "Interaction curves for shear and bending of plastic beams", *Journal of Applied Mechanics*, vol. 24, pp. 453–456, 1957.

[HØI 92] HØISETH K.V., "Response of reinforced structure exposed to transient loading", in BULSON P. (ed.), *Structure under Shock and Impact II*, Computational Mechanics Publications, Southampton, Boston, pp. 247–258, 1992.

[HOL 93] HOLMQUIST T.J., JOHNSON G.R., COOK W.H., "Computational constitutive model for concrete subjected to large strains, high strain rates, and high pressures", *14th International Symposium on Ballistics*, Québec, Canada, September 1993.

[HOP 14] HOPKINSON B., "A method of measuring the pressure in the deformation of high explosive by impact of bullets", *Philosophical Transactions of the Royal Society of London*, vol. A213, pp. 437–452, 1914.

[HUN 60] HUNTER S.C., "Viscoelastic waves", in SNEDDON N., HILL R. (eds), *Progress in Solid Mechanics*, vol. 1, Amsterdam, The Netherlands, North Holland Publishing Company, pp. 1–57, 1960.

[JON 89] JONES N., *Structural Impact,* Cambridge University Press, Cambridge, 1989.

[JOU 05] JOUGUET E., *Journal of Pure and Applied Mathematics*, vol. 70, no. 6, pp. 347–425, 1905.

[KIN 62] KINNEY J.F., *Explosive Shock in Air*, Macmillan, London, 1962.

[KOE 07] KOECHLIN P., Modélisation de comportement membrane flexion et critère de perforation pour l'analyse de structures minces en béton armé sous choc mou, PhD Thesis, University of Paris VI, 2007.

[KOL 49] KOLSKY H., "An investigation of mechanical properties of materials at very high strain rates of loading", *Proceedings of the Physical Society of London*, vol. B62, pp. 676–700, 1949.

[KOL 56] KOLSKY H., "The propagation of stress pulses in viscoelastic solids", *Philosophical Magazine*, vol. 1, no. 8, pp. 693–710, 1956.

[KOT 77] KOT C.A., "Spalling of concrete walls under blast load", *SMIRT 4,* J10/5, Nuclear Engineering and Design, San Francisco, CA, 1977.

[LAL 99] LALANNE C., *Vibrations et chocs mécaniques: chocs mécaniques*, vol. 2, Hermès, Paris, 1999.

[LAM 07] LAMON J., *Mécanique de la rupture fragile et de l'endommagement, approches statistiques et probabilistes*, Hermès, Paris, 2007.

[LAN 84] LANNOY A., "Analyse des explosions air hydrocarbure en milieu libre", *Bulletin de la direction des études et recherche d'EDF*, no. 4, 1984.

[LAT 01] LATAILLADE J.L., "Essais dynamiques", in FRANÇOIS D. (ed.), *Essais mécaniques et lois de comportement*, Hermès, Paris, pp. 249–317, 2001.

[LEE 65] LEE J.H., The propagation of shocks and blast waves in a detonation gas, Report No. 65-1, McGill University, M.E.R.L., Montreal, Canada, 1965.

[LEM 09] LEMAITRE J., CHABOCHE J.L., BENALLAL A., *et al*., *Mécanique des matériaux solides*, 3rd ed., Dunod, 2009.

[LIN 83] LINDBERG H.E., FLORENCE A.L., Dynamic pulse buckling, theory and experiment, Report No. 6503H, Defense Nuclear Agency, 1983.

[LOR 87] LORET B., "Application de la théorie des multimécanismes au comportement des sols", *Manuel de rhéologie de géomatériaux*, Presses ENPC Editions, Paris, 1987.

[MAI 05] MAI I.M., CHEN Y., OWEN D.R.J., *et al.*, "Experimental testing and finite element simulation of the behaviour of reinforced concrete beams under impact loading", *8th International Conference on Computational Plasticity*, CIMNE, Barcelona, 2005.

[MAL 51] MALVERN L.E., "The propagation of longitudinal waves of plastic deformation in a bar of material exhibiting a strain rate effect", *Journal of Applied Mechanics*, vol. 18, pp. 203–208, 1951.

[MAL 86] MALINOWSKI J.Z., KLEPACZKO J.R., "A unified analytic and numerical approach to specimen behaviour in split Hopkinson pressure bar system", *International Journal of Mechanical Sciences*, vol. 28, pp. 381–391, 1986.

[MAZ 04] MAZARS J., MILLARD A., *Comportement dynamique des bétons et génie parasismique*, Hermès, Paris, 2004.

[MCQ 70] MCQUEEN R.G., MARSH S.P., TAYLOR J.W., *et al.*, "The equation of state of solids from shock wave studies", *High Velocity Impact Phenomena*, Academic Press, New York, 1970.

[MIM 96] MIMURA K., TANIMURA S., HOGASHI K., "A strain rate and temperature dependant constitutive model with unified parameters for various materials", *IUTAM Symposium*, Kawata & Shiori, Springer, Tokyo, pp. 69–76, 1996.

[MIN 60] MINDLIN R.D., MCNIVEN H.D., "Axially symmetric waves in elastic rods", *Journal of Applied Mechanic*, vol. 27, pp. 145–151, 1960.

[MOR 06] MORY Y., *Chocs mécaniques et application au matériel*, Hermès, Paris, 2006.

[MOU 99] MOUILLEAU Y., Guide des méthodes d'évaluation des effets d'une explosion de gaz à l'air libre, INERIS Report No. 20433, Nancy, 1999.

[ORT 96] ORTNER N., WAGNER P., "Solution of the initial-boundary value problem for the simply supported semi-infinite Timoshenko beam", *Journal of Elasticity*, vol. 42, pp. 217–241, 1996.

[PAU 92] PAULAY T., PRIESTLEY J.N.M., *Seismic Design of Reinforced Concrete and Masonery Building*, John Wiley, New York, 1992.

[PAU 05] PAULTRE P., *Dynamique des structures,* Hermès, Paris, 2005.

[PER 63] PERZYNA P., "The constitutive equations for rate sensitive plastic materials", *Quarterly Applied Mechanics*, vol. 20, no. 4, pp. 312–332, 1963.

[PER 69] PERSOZ B., *La Rhéologie*, Masson, Paris, 1969.

[POC 76] POCHHAMMER L., "Uber die fortpflanzungsgeschwindigkeiten kleiner schwingungen in einem unbergrenzten isotropen kreiszylinder", *Journal für die Reine und Angewande Mathematic*, vol. 81, pp. 324–336, 1876.

[PRI 83] PRITCHARD D.R., "An experimental and theoretical study of blast effects on a simple structure", *4th International Symposium on Loss Prevention and Safety in the Process Industries*, London, 1983.

[RAK 09] RAKOTOMANANA L.R., *Eléments de dynamique des solides et structures déformables,* PPRU, EPFL Press, Lausanne, 2009.

[REN 88] RENARD J., DESROSIER C., BAILLY P., *et al.*, "Réponses dynamiques de structures du génie civil", *Matériaux-Mécanique-Electricité*, vol. 427, pp. 60–64, 1988.

[RIE 68] RIERA J., "On the stress analysis of structures subjected to aircraft impact forces", *Nuclear Engineering and Design*, vol. 8, no. 4, pp. 415–428, 1968.

[SAA 07] SAARENHEIMO, TUOMALA M., HAKOLA I., *et al.*, "Impact of deformable missiles on reinforced concrete walls", *International Conference on Concrete under Severe Conditions*, LCPC, France, pp. 1381–1388, 2007.

[SAL 01] SALENÇON J., *Elastoplasticité et calcul à la rupture*, Presses Ecole Polytechnique editions, Palaiseau, France, 2001.

[SAN 76] SANDLER I.S., DI MAGGIO F.L., BALADI G.Y., "Generalized CAP model for geological materials", *Journal of the Geotechnical Engineering Division*, vol. GT7, pp. 683–699, 1976.

[SCH 63] SCHANZ M., *Wave Propagation in Viscoelastic and Poroelastic Continua*, Springer, Berlin, 1963.

[SCH 91] SCHUELLER G.I., *Structural Dynamics: Recent Advances*, Springer-Verlag, Berlin, 1991.

[SCI 86] SCILLY N.F., HIGH W.G., "The blast effects of explosions", *5th International Symposium Congress*, Cannes, 1986.

[SHE 92] SHERIDAN A.J., COWDEY C.A., "An analysis of shear/flexure coupling – applied to the failure of reinforced concrete structures", in BULSON P. (ed.), *Structure under Shock and Impact II*, Computational Mechanics Publications, Southampton, Boston, pp. 189–197, 1992.

[SMI 94] SMITH P.D., HETHERINGTON J.G., *Blast and Ballistic Loading of Structures*, Butterworth Heinemann, Oxford, 1994.

[SOK 48] SOKOLOWSKY V.V., "The propagation of elastic viscous plastic waves in bars", *Prikladnaia Matematika i Meckhanika*, vol. 12, pp. 261–280, 1948.

[STE 89] STEINBERG D.J., LUND C.M., "A constitutive model for strain rates from 10^{-4} to 10^{6} s^{-1}", *Journal of Applied Physics*, vol. 65, pp. 1528–1533, 1989.

[SUA 84] SUARIS W., SHAH S., "Rate sensitive damage theory for brittle solids", *Journal of Engineering Mechanics*, vol. 110, no. 6, pp. 985–997, 1984.

[TAN 92] TANG T., MALVERN L.E., JENKINS D.A., "Rate effects in uniaxial dynamic compression of concrete", *Journal of Engineering Mechanics*, vol. 118, pp. 108–124, 1992.

[TIL 86] TILLY G.P., *Dynamic Behaviour of Concrete Structures*, Elsevier, Amsterdam, 1986.

[TIM 39] TIMOSCHENKO S., *Théorie des vibrations*, Librairie Polytechnique C. Beranger editions, Paris, 1939.

[UFC 08] UFC-3-340-02, Structure to resist the effect of accidental explosions, Department of Defense, technical manual, USA, 2008.

[VAN 84] VAN DEN BERG A.C., The multi-energy method, a framework for vapour cloud explosion blast prediction, Report PML C-72, TNO Prins Maurits Laboratory, 1984.

[WEE 07] WEERHEIJM J., MEDIAVILLA J., VAN DOORMAAL J.C.A.M., "Damage assessment for impulsively loaded concrete structures", *Concrete under Severe Conditions*, LCPC, France, pp. 1323–1330, 2007.

[WHI 55] WHITNEY C.S., ANDERSON B.G., COHEN E., "Design of blast resistant construction for atomic explosion", *Journal of American Concrete Institute*, vol. 26, no. 7, pp. 580–683, 1955.

[YOK 93] YOKOYAMA T., "Determination of dynamic fracture-initiation toughness using a novel impact bend test procedure", *Journal of Pressure Vessel Technology*, vol. 115, pp. 389–397, 1993.

[ZHA 95] ZHAO H., GARY G., "A three dimensional analytical solution of the longitudinal wave propagation in an infinite linear viscoelastic cylindrical bar. Application to experimental technique", *Journal of Mechanics and Physics of Solids*, vol. 43, pp. 1335–1348, 1995.

[ZHA 96] ZHAO H., GARY G., "On the use of SHPB technique to determine the dynamic behavior of the materials in the range of small strains", *International Journal of Solids & Structures*, vol. 33, pp. 3363–3375, 1996.

[ZHA 06] ZHANG Y., Analyse et dimensionnement d'ouvrages de protection contre les chutes de blocs, PhD Thesis, School of Civil Engineering, Champs-sur-Marne, 2006.

[ZIN 07] ZINN R., STANGENBERG F., BORGERHOFF M., *et al.*, "Nonlinear behaviour of concrete structures under severe impact", *Concrete under Severe Conditions*, LCPC, France, pp. 1357–1364, 2007.

[ZUK 90] ZUKAS J.A., *High Velocity Impact Dynamics*, Wiley-Interscience, Bognor Regis, 1990.

Index